

(12) **United States Patent**  
**Wang et al.**

(10) **Patent No.:** US 10,439,517 B2  
(45) **Date of Patent:** Oct. 8, 2019

(54) **TRIBOELECTRIC NANOGENERATOR FOR HARVESTING ENERGY FROM WATER**

(71) Applicant: **Georgia Tech Research Corporation**, Atlanta, GA (US)

(72) Inventors: **Zhong Lin Wang**, Atlanta, GA (US); **Zong-Hong Lin**, Hsinchu (TW); **Gang Cheng**, Atlanta, GA (US)

(73) Assignee: **Georgia Tech Research Corporation**, Atlanta, GA (US)

(\* ) Notice: Subject to any disclaimer, the term of this patent is extended or adjusted under 35 U.S.C. 154(b) by 550 days.

(21) Appl. No.: **15/006,865**

(22) Filed: **Jan. 26, 2016**

(65) **Prior Publication Data**  
US 2016/0218640 A1 Jul. 28, 2016

**Related U.S. Application Data**  
(60) Provisional application No. 62/107,855, filed on Jan. 26, 2015, provisional application No. 62/128,757, filed on Mar. 5, 2015.

(51) **Int. Cl.**  
**H02N 1/04** (2006.01)

(52) **U.S. Cl.**  
CPC ..... **H02N 1/04** (2013.01)

(58) **Field of Classification Search**  
CPC ..... H02N 1/00-12  
See application file for complete search history.

(56) **References Cited**

U.S. PATENT DOCUMENTS

2014/0246950 A1 9/2014 Wang et al.  
2014/0246951 A1 9/2014 Wang et al.  
2014/0292138 A1 10/2014 Wang et al.

(Continued)

FOREIGN PATENT DOCUMENTS

CN 103825489 A 5/2014  
CN 104682767 A 6/2015

(Continued)

OTHER PUBLICATIONS

Ahmad, M. A. et al., Electronically Droplet Energy Harvesting Using Piezoelectric Cantilevers, *Electron. Lett.* 2012, 48, 11, 2 pages.

(Continued)

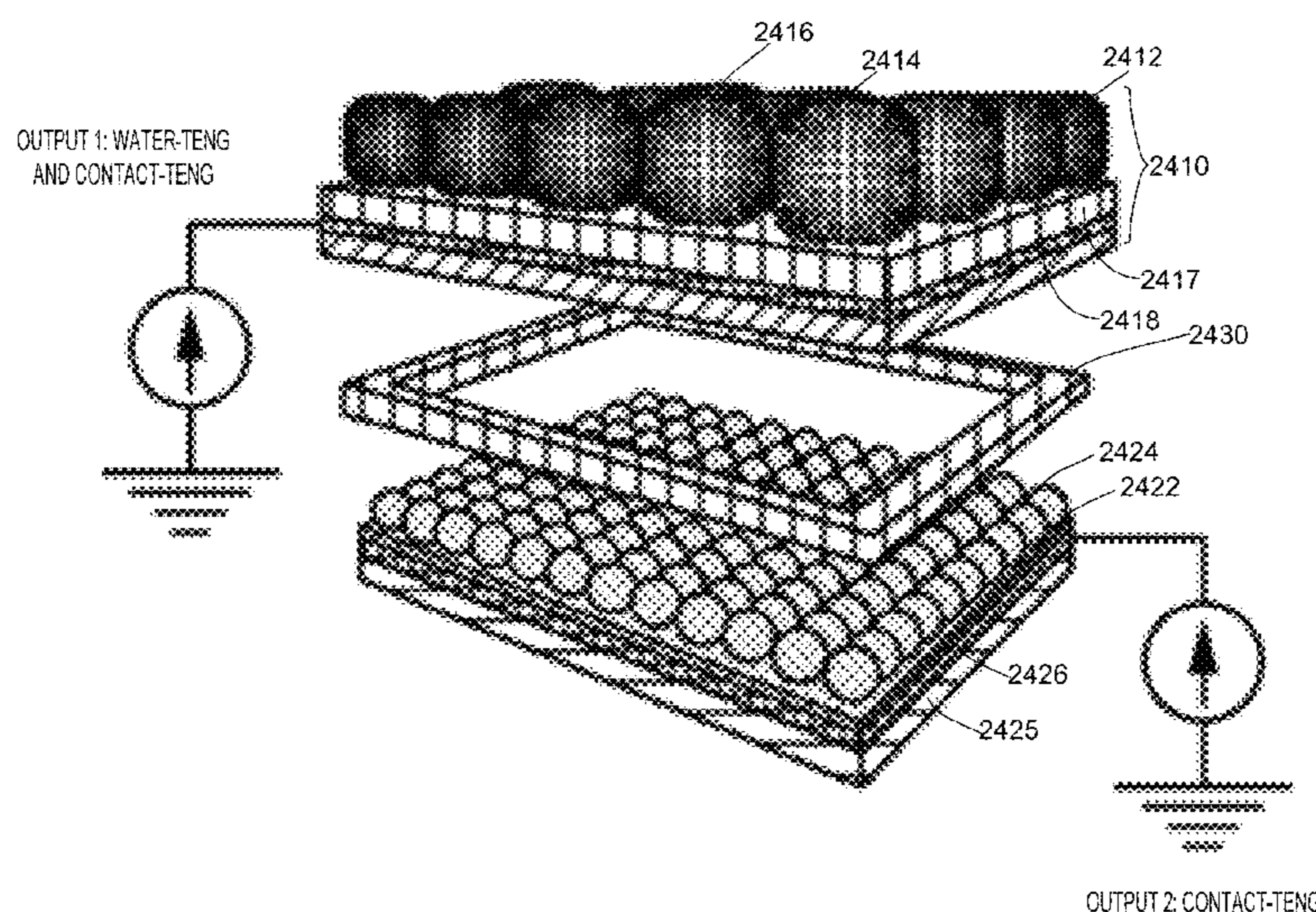
*Primary Examiner* — Ramon M Barrera

(74) *Attorney, Agent, or Firm* — Troutman Sanders LLP; Ryan A. Schneider

(57) **ABSTRACT**

A generator for harvesting energy from flowing water is disclosed. The generator harvests electrostatic energy as well as mechanical kinetic energy from the flowing water. In one aspect, the generator includes a plurality of blades arranged in a radially outward fashion. Each blade includes an electrode and a surface layer for receiving flowing water carrying triboelectric charges. The flowing water affects a flow of electrons between the electrode and ground. In another aspect, the generator includes a first member with a first electrode, and a second member coupled to the first member about an axis. The second member includes a second electrode, and a surface layer between the first electrode and the second electrode. The second member is rotatable with respect to the axis to change triboelectric charges on the electrodes, and to affect a flow of electrons between the electrodes.

**10 Claims, 58 Drawing Sheets**



(56)

## References Cited

## U.S. PATENT DOCUMENTS

2014/0033845 A1 11/2014 Wang et al.  
2015/0031880 A1 11/2015 Zhang et al.

## FOREIGN PATENT DOCUMENTS

WO 2014154092 A1 10/2014  
WO 2015154693 A1 10/2015

## OTHER PUBLICATIONS

Akyildiz, I. F. et al., Electromagnetic Wireless Nanosensor Networks, *Nano Commun. Networks*, 2010, 1, 3-19.  
Bai, P. et al., Cylindrical Rotating Triboelectric Nanogenerator, *ACS Nano*, 2013, 7, 7, 6361-6366.  
Banerji, S. K. et al., Electric Charges on Rain Drops, *Nature*, 3296, 130, 1932, 998-999.  
Baytekin, B.; et al., What Really Drives Chemical Reactions on Contact Charged Surfaces?, *J. Am. Chem. Soc.* 2012, 134, 7223-7226.  
Beeby, S. P. et al., A Micro Electromagnetic Generator for Vibration Energy Harvesting, *J. Micromech. Microeng.* 2007, 17, 1257-1265.  
Beeby, S. P. et al., Energy Harvesting Vibration Sources for Microsystems Applications, *Meas. Sci. Technol.*, 2006, 17, R175-R195.  
Burgo, T. A. L. et al., Triboelectricity: Macroscopic Charge Patterns Formed by Self-Arrayed Ions on Polymer Surfaces, *Langmuir*, 2012, 28, 7407-7416.  
Castle, G. S. P., Contact Charging Between Insulators, *J. Electrostat.* 1997, 40-41, 13-20.  
Chang, C. E. et al., Direct-Write Piezoelectric Polymeric Nanogenerator with High Energy Conversion Efficiency, *Nano Lett.*, 2010, 10, 726-731.  
Chen, F. et al., Correlation of Photocatalytic Bactericidal Effect and Organic Matter Degradation of TiO<sub>2</sub> Part I: Observation of Phenomena, *Environ. Sci. Technol.*, 2009, 43, 1180-1184.  
Chen, X. et al., 1.6 V Nanogenerator for Mechanical Energy Harvesting Using PZT Nanofibers, *Nano Lett.*, 2010, 10, 2133-2137.  
Chen, X. et al., Titanium Dioxide Nanomaterials: Synthesis, Properties, Modifications, and Applications, *Chem. Rev.*, 2007, 107, 2891-2959.  
Cheng, G. et al., Increase Output Energy and Operation Frequency of a Triboelectric Nanogenerator by Two Grounded Electrodes Approach, *Adv. Funct. Mater.*, 2014, 24, 2892-2898.  
Cheng, G. et al., Simultaneously Harvesting Electrostatic and Mechanical Energies from Flowing Water by a Hybridized Triboelectric Nanogenerator, *ACS Nano*, 2014, 8, 2, 1932-1939.  
Cheng, G. et al., Pulsed Nanogenerator with Huge Instantaneous Output Power Density, *ACS Nano* 2013, 7, 8, 7383-7391.  
Choi, D. et al., Spontaneous Electrical Charging of Droplets by Conventional Pipetting, *Sci. Rep.*, 2013, 3, 2037, 7 pages.  
Deng, L. et al., Integrated Self-Powered Microchip Biosensor for Endogenous Biological Cyanide, *Anal. Chem.*, 2010, 82, 4283-4287.  
Fan, F. R. et al., Flexible Triboelectric Generator!, *Nano Energy*, 2012, 1, 328-334.  
Fan, F. R. et al., Transparent Triboelectric Nanogenerators and Self-Powered Pressure Sensors Based on Micropatterned Plastic Films, *Nano Lett.*, 2012, 12, 3109-3114.  
Feng, X. et al., The Fabrication and Switchable Superhydrophobicity of TiO<sub>2</sub> Nanorod Films, *Angew. Chem., Int. Ed.*, 2005, 44, 5115-5118.  
Gu, L. et al., Flexible Fiber Nanogenerator with 209 V Output Voltage Directly Powers a Light-Emitting Diode, *Nano Lett.*, 2013, 13, 91-94.  
Guigon, R. et al., Harvesting Raindrop Energy: Experimental Study, *Smart Mater. Struct.* 2008, 17, 015039, 6 pages.

Hoang, S. et al., Chemical Bath Deposition of Vertically Aligned TiO<sub>2</sub> Nanoplatelet Arrays for Solar Energy Conversion Applications, *J. Mater. Chem. A*, 2013, 1, 4307-4315.

Hosono, E. et al., Growth of Submicrometer-Scale Rectangular Parallelepiped Rutile TiO<sub>2</sub> Films in Aqueous TiCl<sub>3</sub> Solutions under Hydrothermal Conditions, *J. Am. Chem. Soc.*, 2004, 126, 7790-7791.

Hu, Y. et al., Replacing a Battery by a Nanogenerator with 20 V Output, *Adv. Mater.*, 2012, 24, 110-114.

Jiang, P. et al., Single-Crystal Colloidal Multilayers of Controlled Thickness, *Chem. Mater.*, 1999, 11, 2132-2140.

Katz, E. et al., Self-Powered Enzyme-Based Biosensors, *J. Am. Chem. Soc.*, 2001, 123, 10752-10753.

Lee, M. et al., Self-Powered Environmental Sensor System Driven by Nanogenerators, *Energy Environ. Sci.* 2011, 4, 3359-3363.

Lee, S. et al., Artificial Lotus Leaf Structures Made by Blasting with Sodium Bicarbonate, *Curr. Appl. Phys.* 2011, 11, 800-804.

Lee, S. et al., Tens of Centimeter-Scale Flexible Superhydrophobic Nanofiber Structures Through Curing Process, *Lab Chip* 2009, 9, 2234-2237.

Lin, L. et al., Segmentally Structured Disk Triboelectric Nanogenerator for Harvesting Rotational Mechanical Energy, *Nano Lett.* 2013, 13, 2916-2923.

Lin, Z.-H. et al., A Self-Powered Triboelectric Nanosensor for Mercury Ion Detection, *Angew. Chem. Int. Ed.*, 2013, 52, 5065-5069.

Lin, Z.-H. et al., Enhanced Triboelectric Nanogenerators and Triboelectric Nanosensor Using Chemically Modified TiO<sub>2</sub> Nanomaterials, *ACS Nano*, 2013, 7, 5, 4554-4560.

Lin, Z.-H. et al., Harvesting Water Drop Energy by a Sequential Contact-Electrification and Electrostatic-Induction Process, *Adv. Mater.*, 2014, DOI: 10.1002/adma.201400373.

Lin, Z.-H. et al., BaTiO<sub>3</sub> Nanotubes-Based Flexible and Transparent Nanogenerators, *J. Phys. Chem. Lett.* 2012, 3, 3599-3604.

Lin, Z.-H., Dual-Mode Triboelectric Nanogenerator for Harvesting Water Energy and as a Self-Powered Ethanol Nanosensor, *ACS Nano*, 2014, 10.1021/nm501983s.

Lin, Z.-H. et al., Triboelectric Nanogenerator as an Active UV Photodetector, *Adv. Funct. Mater.* 2014, 28, 2810-2816.

Lin, Z.-H. et al., Water-Solid Surface Contact Electrification and its Use for Harvesting Liquid-Wave Energy, *Angew. Chem. Int. Ed.*, 2013, 52, 12545-12549.

Liu, C. Y. et al., Chemical Redox Reactions Induced by Cryptoelectrons on a PMMA Surface, *J. Am. Chem. Soc.* 2009, 131, 6397-6401.

Liu, C. Y. et al., Electrostatic Electrochemistry at Insulators, *Nat. Mater.* 2008, 7, 505-509.

Ma, M. et al., Bio-Inspired Polymer Composite Actuator and Generator Driven by Water Gradients, *Science*, 2013, 339, 186-189.

Ma, X. et al., Selective Discharge of Electrostatic Charges on Electrets Using a Patterned Hydrogel Stamp, *Angew. Chem. Int. Ed.* 2010, 122, 5669-5672.

Mazza, T. et al., Raman Spectroscopy Characterization of TiO<sub>2</sub> Rutile Nanocrystals, *Phys. Rev. B*, 2007, 75, 045416-1 to 045416-5.

McCarty, L. S. et al., Electrostatic Charging Due to Separation of Ions at Interfaces: Contact Electrification of Ionic Electrets, *Angew. Chem. Int. Ed.* 2008, 47, 2188-2207.

Mitcheson, P. D. et al., Energy Harvesting from Human and Machine Motion for Wireless Electronic Devices, *Proc IEEE*, 2008, 96, 9, 1457-1486.

Mitcheson, P. D. et al., MEMS Electrostatic Micropower Generator for Low Frequency Operation, *Sens. Actuators, A* 115, 2004, 115, 523-529.

Moon, J. K. et al., Electrical Power Generation by Mechanically Modulating Electrical Double Layers, *Nat. Commun.*, 2013, 4, 1-6.

Naruse, Y. et al., Electrostatic Micro Power Generation from Low-Frequency Vibration such as Human Motion, *J. Micromech. Microeng.*, 2009, 19, 094002, 5 pages.

Nguyen, V. et al., Effect of Humidity and Pressure on the Triboelectric Nanogenerator, *Nano Energy*, 2013, 2, 604-608.

Pai, D. M. et al., Physics of Electrophotography, *Rev. Mod. Phys.* 1993, 65, 1, 163-211.

(56)

## References Cited

## OTHER PUBLICATIONS

- Park, K. L. et al., Flexible Nanocomposite Generator Made of BaTiO<sub>3</sub> Nanoparticles and Graphitic Carbons, *Adv. Mater.*, 2012, 24, 2999-3004.
- Qin, Y. et al., Microfiber-Nanowire Hybrid Structure for Energy Scavenging, *Nature*, 2008, 451, 809-813.
- Ravelo, B. et al., Demonstration of the Triboelectricity Effect by the Flow of Liquid Water in the Insulating Pipe, *J. Electrostat.*, 2011, 69, 473-478.
- Roundy, S. et al., A Piezoelectric Vibration Based Generator for Wireless Electronics, *Smart Mater. Struct.* 2004, 13, 1131-1142.
- Santos, L. P. et al., Corona-Treated Polyethylene Films Are Macroscopic Charge Bilayers, *Langmuir*, 2013, 29, 892-901.
- Snyder, G. J. et al., Complex Thermoelectric Materials, *Nature Mater.* 2008, 7, 105-114.
- Stöber, W. et al., Controlled Growth of Monodisperse Silica Spheres in the Micron Size Range, *J. Colloid Interface Sci.*, 1968, 26, 62-69.
- Su, Y. et al., Hybrid Triboelectric Nanogenerator for Harvesting Water Wave Energy and as a Self-Powered Distress Signal Emitter, *J. Nano En.*, 2014, DOI: 10.1016.
- Takahashi, T., Measurement of Electric Charge of Cloud Droplets, Drizzle, and Raindrops, *Rev. Geophys. and Space Physics*, 1973, 11, 4, 903-924.
- Taylor, G. W. et al. The Energy Harvesting Eel: A Small Subsurface Ocean/River Power Generator, *IEEE J. Oceanic Eng.* 2001, 26, 4, 539-547.
- Thomson, S. W., On a Self-Acting Apparatus for Multiplying and Maintaining Electric Charges, with Applications to Illustrate the Voltaic Theory, *Proc. R. Soc. London* 1867, 16, 67-72.
- Tian, B. et al., Coaxial Silicon Nanowires as Solar Cells and Nanoelectronic Power Sources, *Nature*, 2007, 449, 885-890.
- Wang, R. et al., Studies of Surface Wettability Conversion on TiO<sub>2</sub> Single-Crystal Surfaces, *J. Phys. Chem. B*, 1999, 103, 2188-2194.
- Wang, S. H. et al., Nanoscale Triboelectric-Effect-Enabled Energy Conversion for Sustainably Powering Portable Electronics, *Nano Lett.* 2012, 12, 6339-6346.
- Wang, S. H. et al., Sliding-Triboelectric Nanogenerators Based on In-Plane Charge-Separation Mechanism, *Nano Lett.*, 2013, 13, 2226.
- Wang, Z. L. et al., Nanotechnology-Enabled Energy Harvesting for Self-Powered Micro-Nanosystems, *Angew. Chem., Int. Ed.*, 2012, 51, 11700-11721.
- Wang, Z. L. et al., Piezoelectric Nanogenerators Based on Zinc Oxide Nanowire Arrays, *Science* 2006, 312, 242-246.
- Wang, Z. L. et al., Progress in Nanogenerators for Portable Electronics, *Mater. Today* 2012, 15, 12, 532-543.
- Wang, Z. L., Self-Powered Nanosensors and Nanosystems, *Adv. Mater.*, 2012, 24, 280-285.
- Wang, Z. L., Self-Powered Nanotech Nanosize Machines Need Still Tinier Power Plants, *Sci. Am*, 2008, 298, 82-87.
- Wang, Z. L., Triboelectric Nanogenerators as New Energy Technology for Self-Powered Systems and as Active Mechanical and Chemical Sensors, *ACS Nano*, 2013, 7, 9533-9557.
- Wen, D. et al., Self-Powered Sensor for Trace Hg<sup>2+</sup> Detection, *Anal. Chem.*, 2011, 83, 3968-3972.
- Wiles, J. A. et al., A Tool for Studying Contact Electrification in Systems Comprising Metals and Insulating Polymers., *Anal. Chem.*, 2003, 75, 4859-4867.
- Williams, C. B. et al., Development of an Electromagnetic Micro-Generator, *Proc IEEE Circ. Dev. Syst.*, 2001, 148, 6, 337-342.
- Xie, Y. et al., Rotary Triboelectric Nanogenerator Based on a Hybridized Mechanism for Harvesting Wind Energy, *ACS Nano* 2013, 7, 7119-7125.
- Xu, S. et al., Self-Powered Nanowire Devices, *Nat. Nanotechnol.*, 2010, 5, 366-373.
- Yang, Y. et al., A Single-Electrode Based Triboelectric Nanogenerator as Self-Powered Tracking System, *Adv. Mater.*, 2013, 25, 6594-6601.
- Yang, Y. et al., Human Skin Based Triboelectric Nanogenerators for Harvesting Biomechanical Energy and as Self-Powered Active Tactile Sensor System, *ACS Nano*, 2013, 7, 10, 9213-9222.
- Yang, Y. et al., Nanowire-Composite Based Flexible Thermoelectric Nanogenerators and Self-Powered Temperature Sensors, *Nano Res.*, 2012, 5, 12, 888-895.
- Yang, Y. et al., Silicon-Based Hybrid Energy Cell for Self-Powered Electrodegradation and Personal Electronics., *ACS Nano*, 2013, 7, 3, 2808-2813.
- Yang, Y. et al., Single-Electrode-Based Sliding Triboelectric Nanogenerator for Self-Powered Displacement Vector Sensor System, *ACS Nano*, 2013, 7, 8, 7342-7351.
- Yang, Y. et al., Triboelectric Nanogenerator for Harvesting Wind Energy and as Self-Powered Wind Vector Sensor System, *ACS Nano* 2013, 7, 10, 9461-9468.
- Zhang, J. et al., UV Raman Spectroscopic Study on TiO<sub>2</sub>. I. Phase Transformation at the Surface and in the Bulk, *J. Phys. Chem. B*, 2006, 110, 2, 927-935.
- Zhang, X. S. et al., Frequency-Multiplication High-Output Triboelectric Nanogenerator for Sustainably Powering Biomedical Microsystems., *Nano Lett.*, 2013, 13, 1168-1172.
- Zhang, X.-S. et al., High-Performance Triboelectric Nanogenerator with Enhanced Energy Density Based on Single-Step Fluorocarbon Plasma Treatment, *Nano Energy*, 2014, 4, 123-131.
- Zhao, D. et al., Patterning of Electrostatic Charge on Electrets Using Hot Microcontact Printing, *Angew. Chem. Int. Ed.*, 2009, 48, 6699-6703.
- Zheng, L. et al., Silicon-Based Hybrid Cell for Harvesting Solar Energy and Raindrop Electrostatic Energy, *Nano Energy*, 2014, 9, 291-300.
- Zhu, G. et al., Linear-Grating Triboelectric Generator Based on Sliding Electrification, *Nano Lett.* 2013, 13, 2282-2289.
- Zhu, G. et al., Toward Large-Scale Energy Harvesting by a Nanoparticle-Enhanced Triboelectric Nanogenerator, *Nano Lett.*, 2013, 13, 847-853.
- Zhu, G. et al., Triboelectric-Generator-Driven Pulse Electrodeposition for Micropatterning, *Nano Lett.* 2012, 12, 4960-4965.

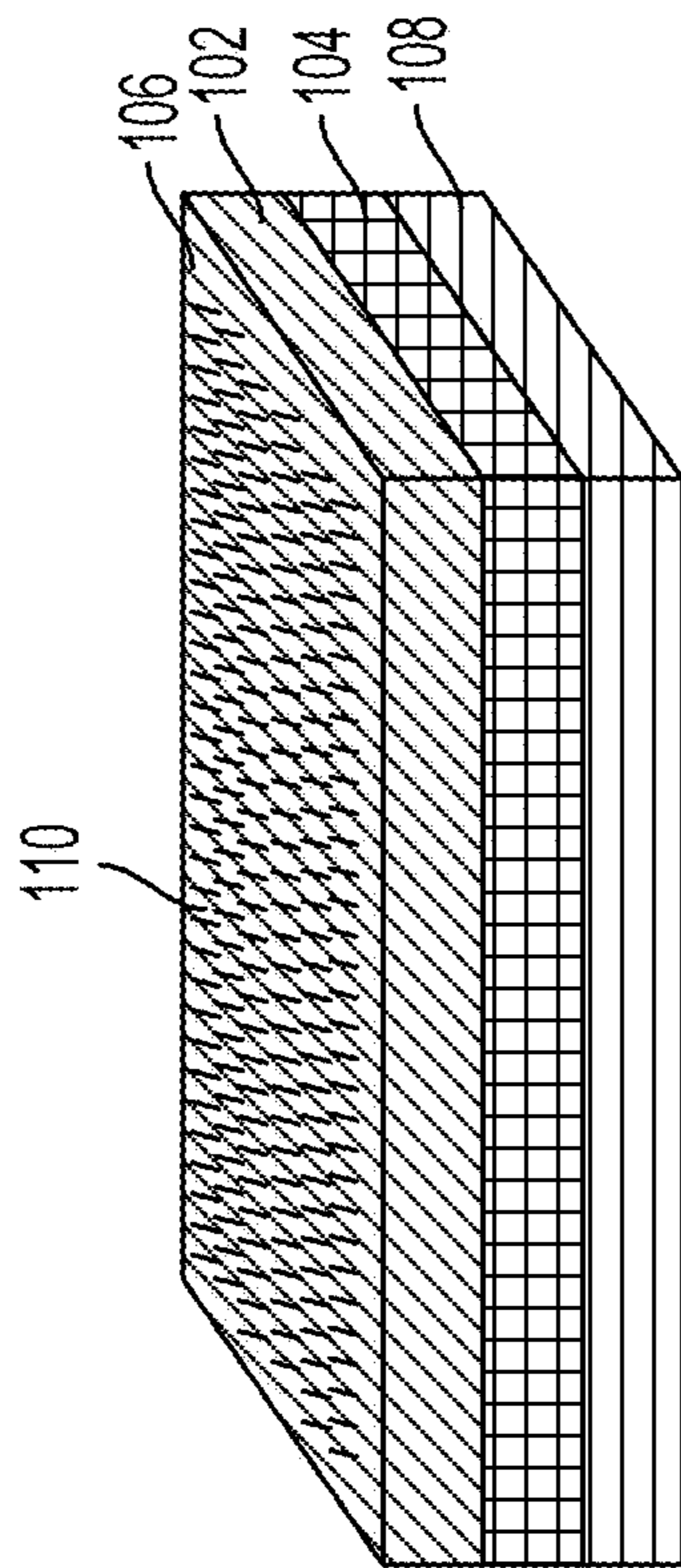


FIG. 1

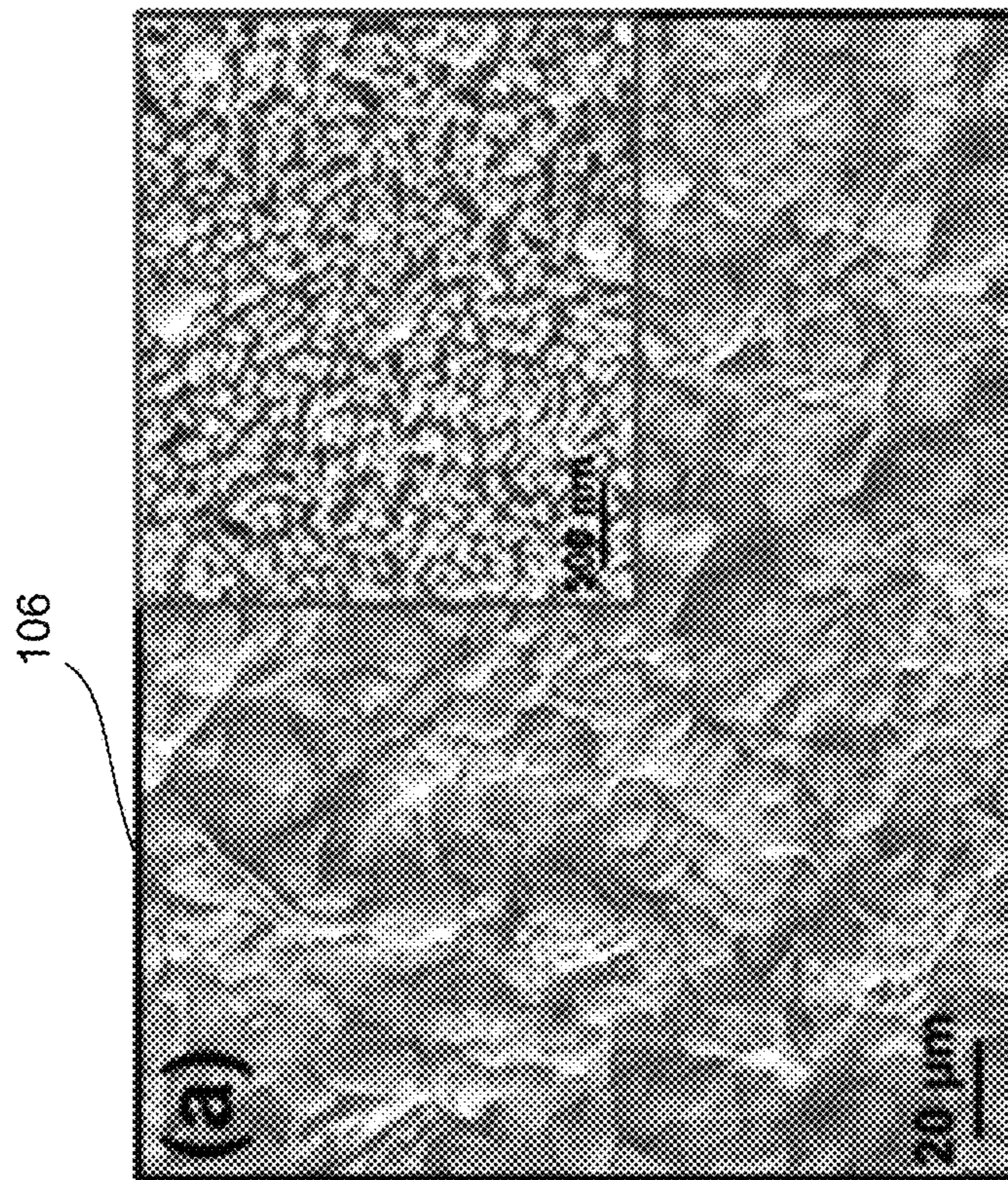


FIG. 2A

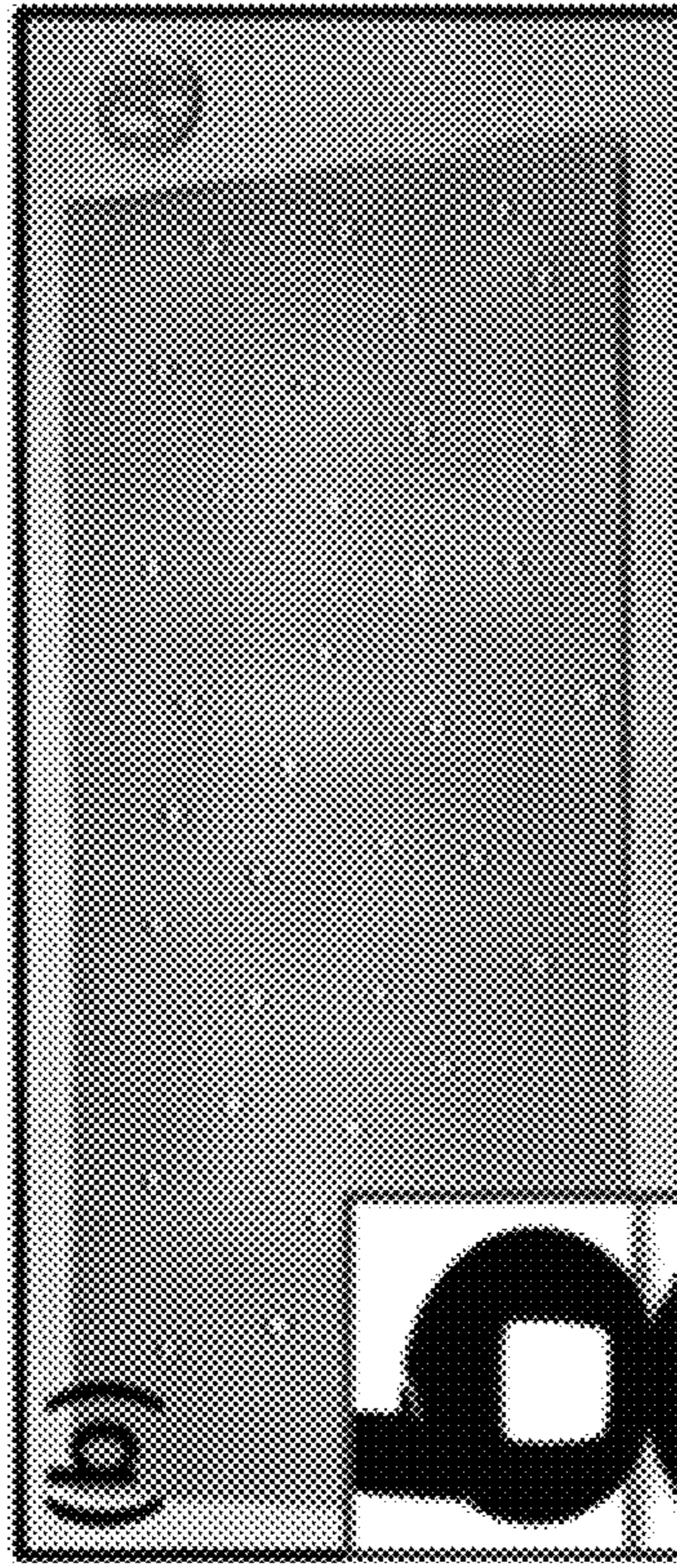


FIG. 2B

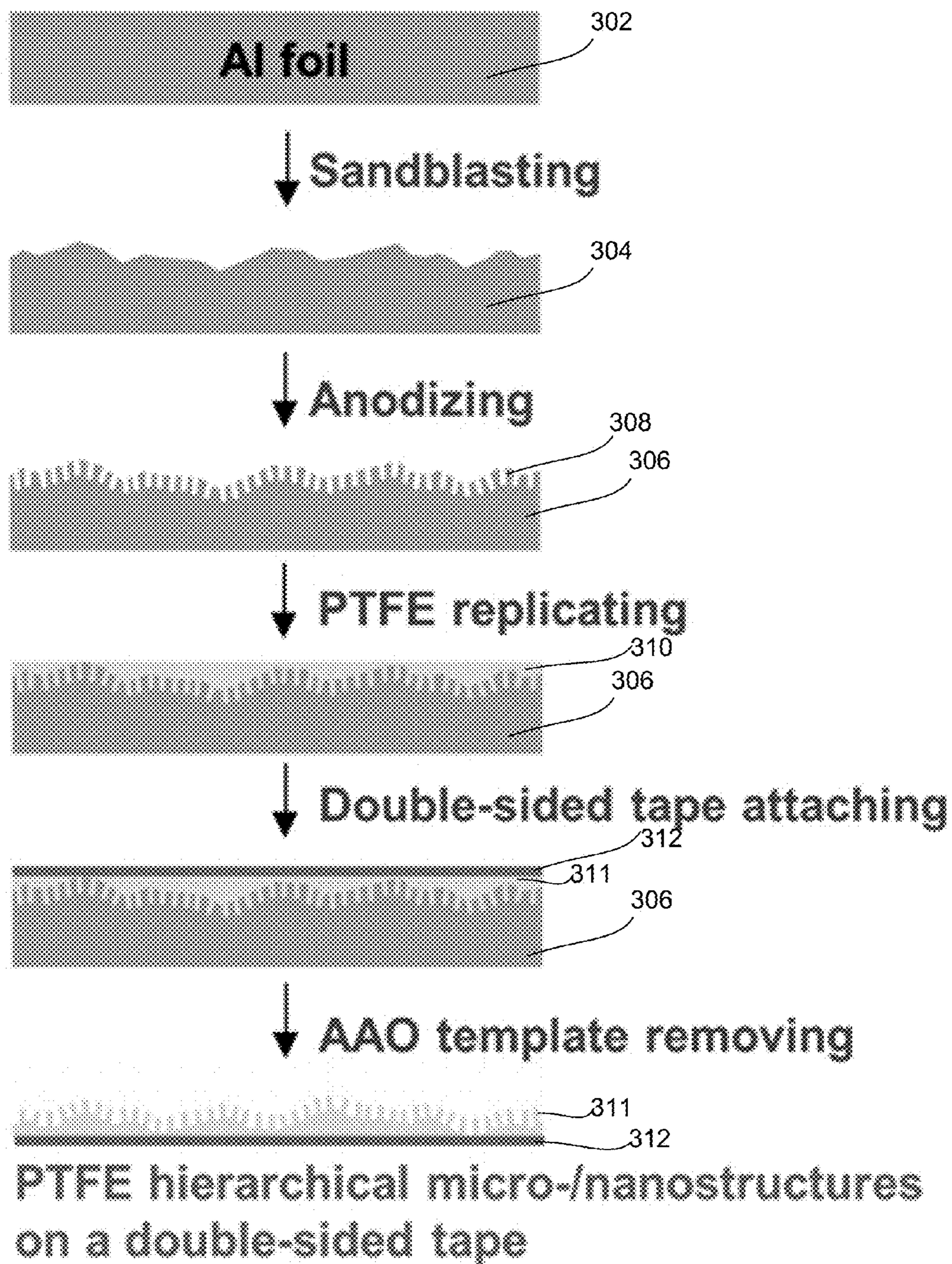


FIG. 3

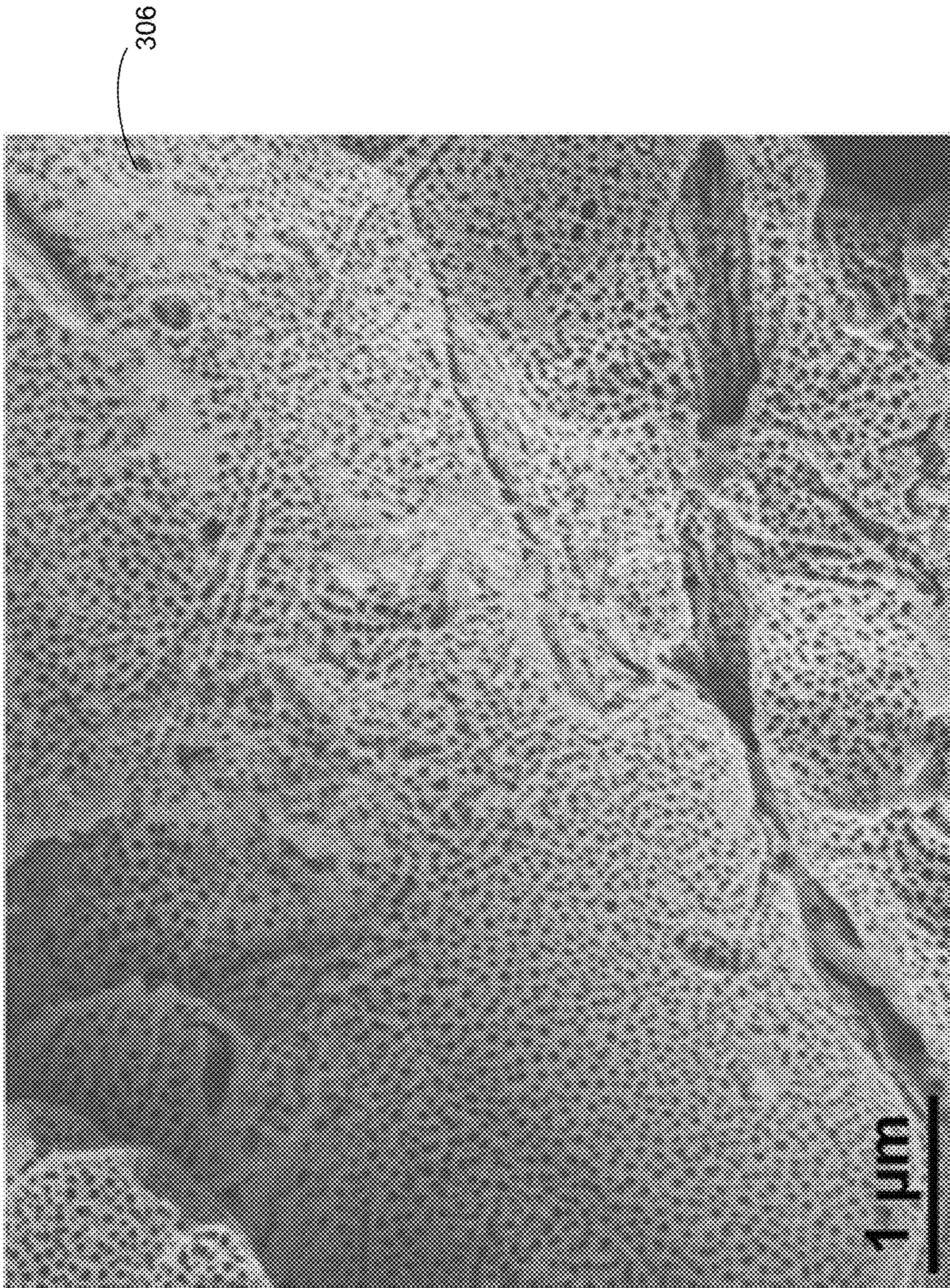


FIG. 4

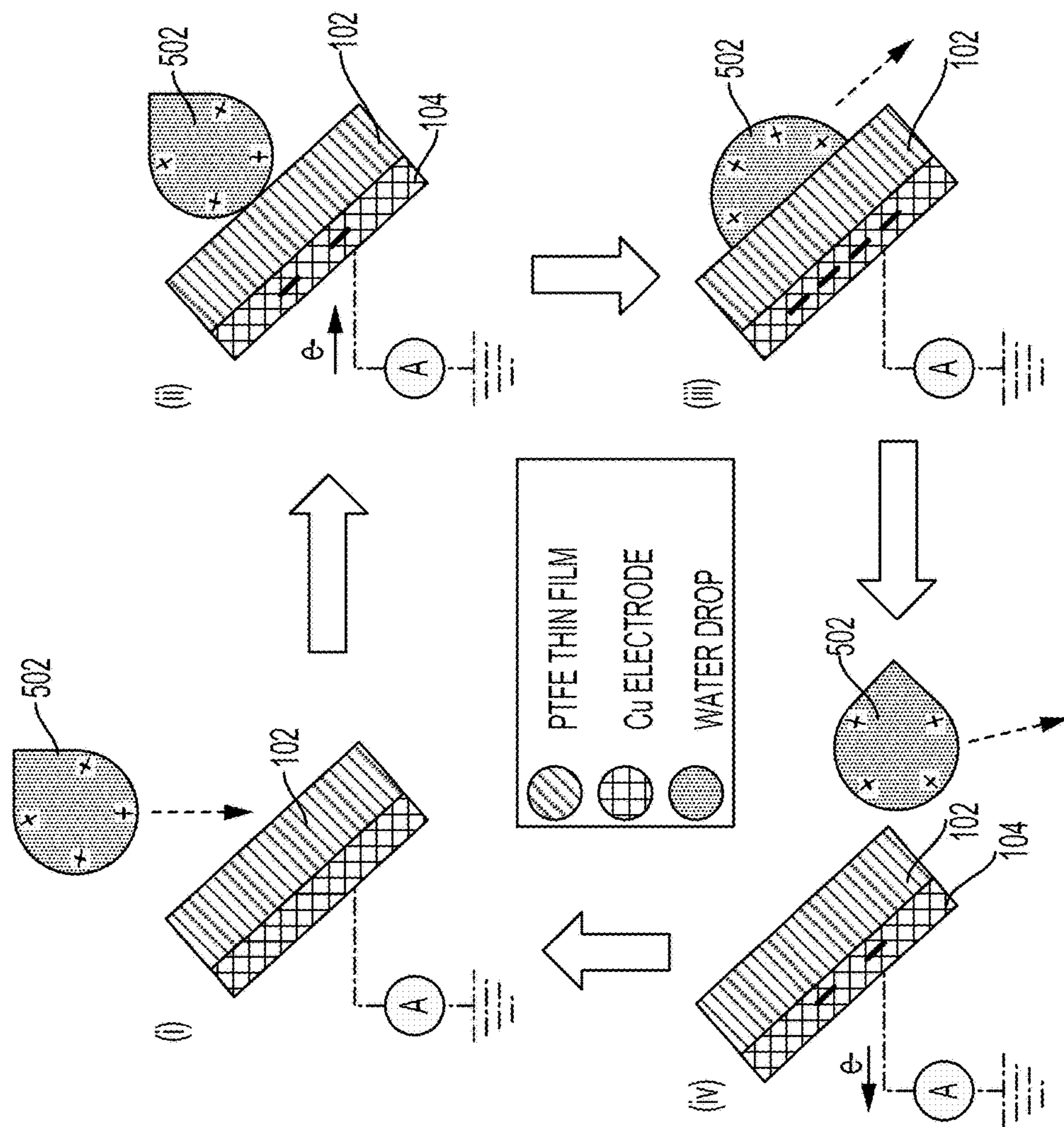


FIG. 5



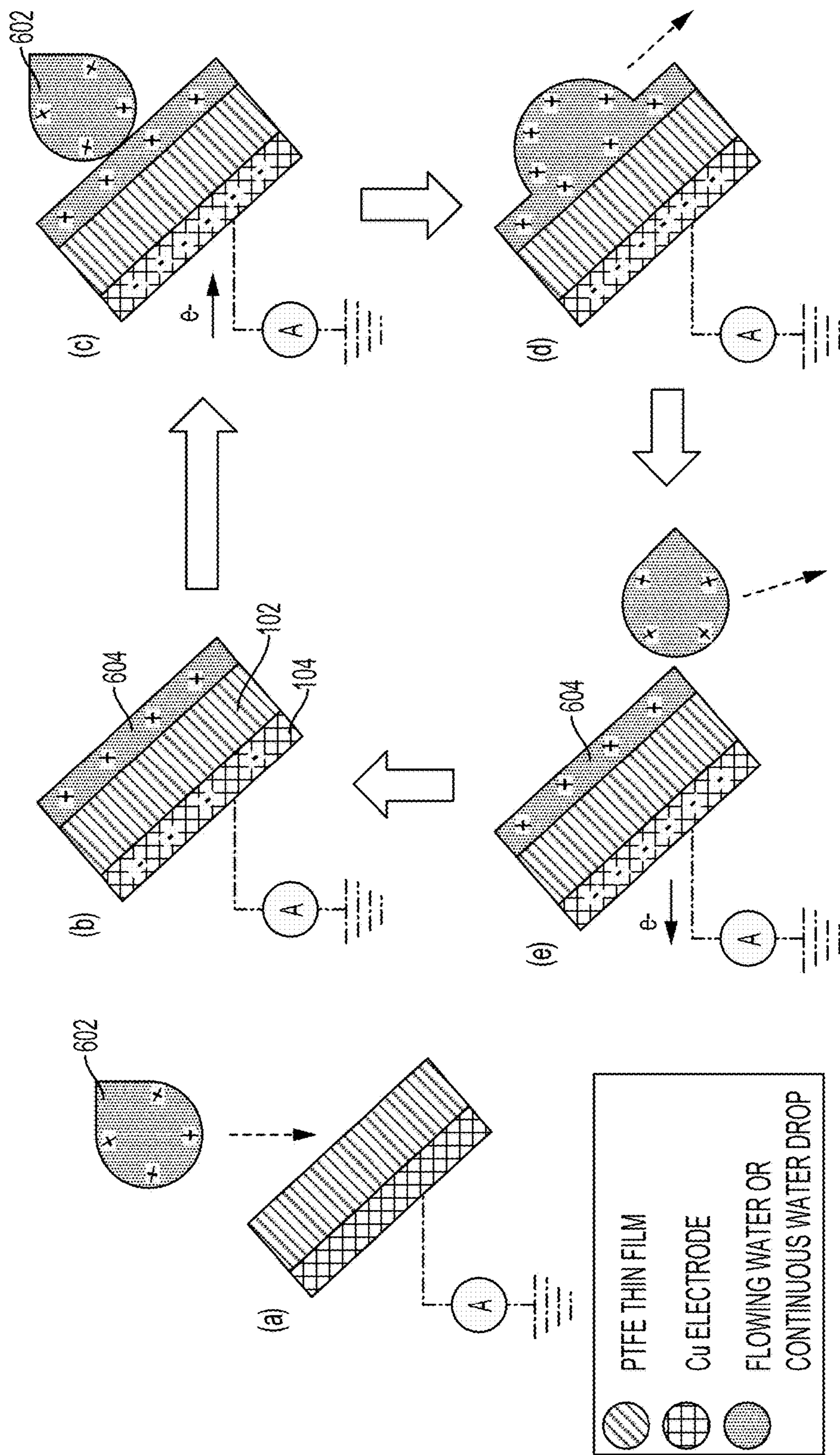


FIG. 6

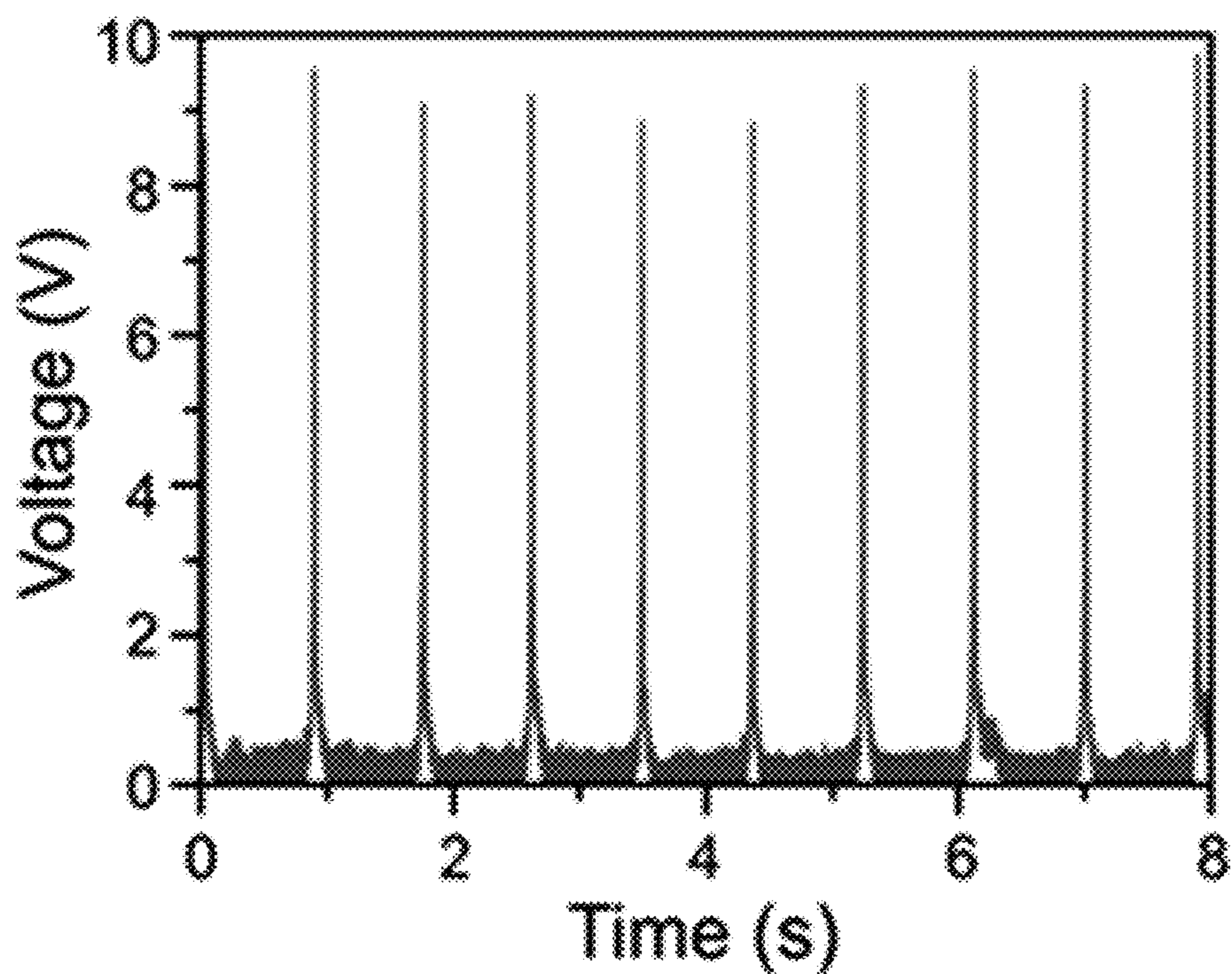


FIG. 7A

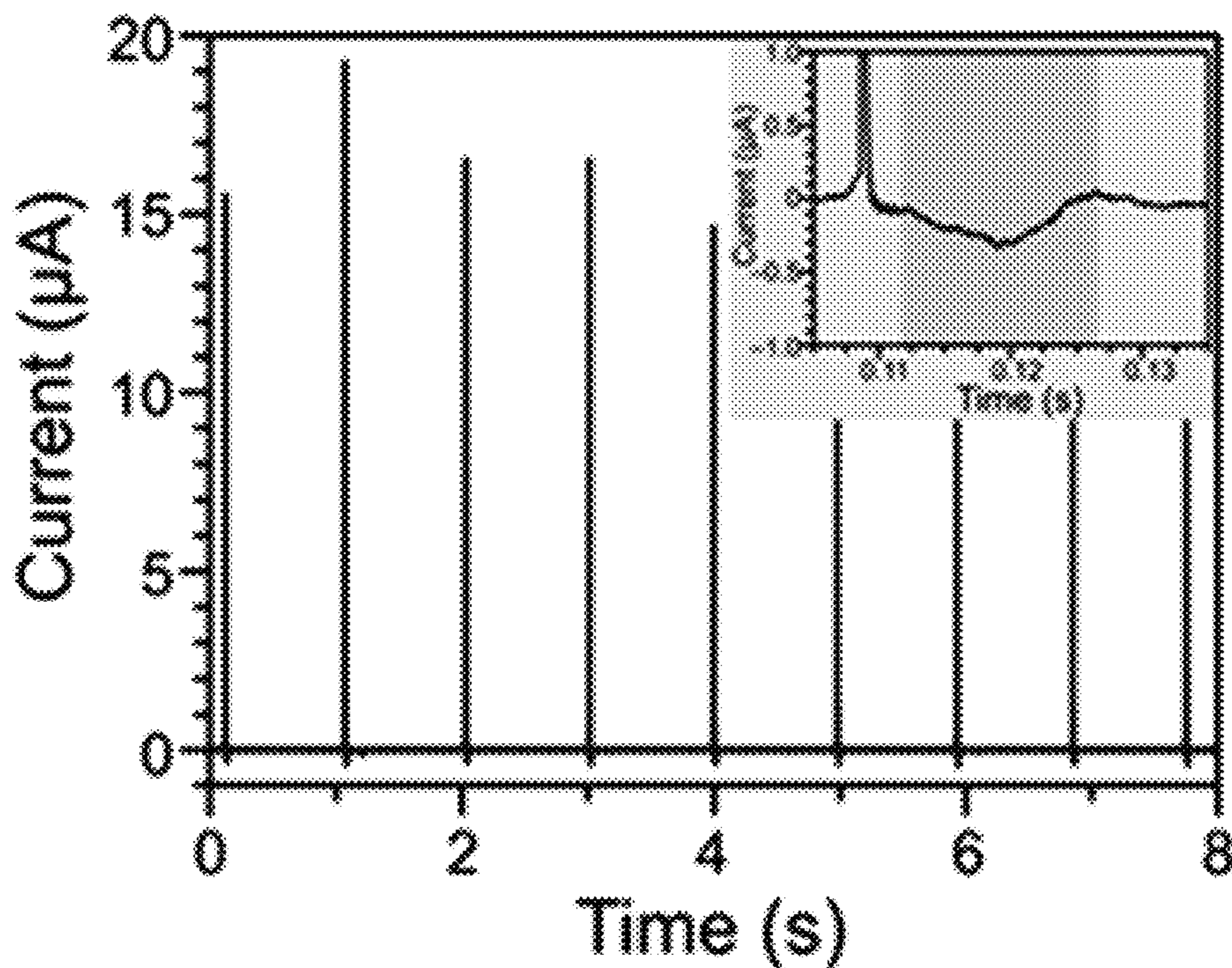


FIG. 7B

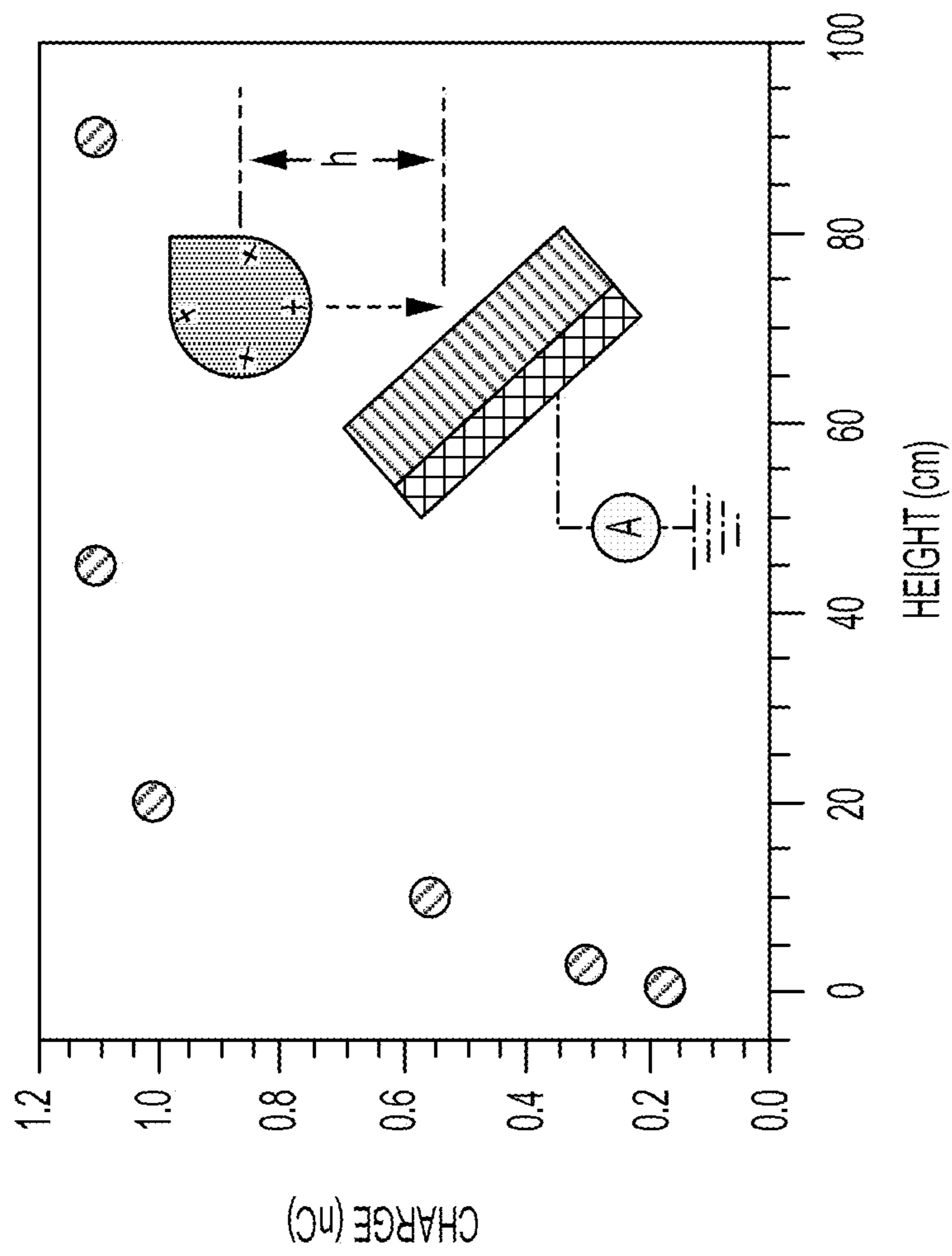


FIG. 7C

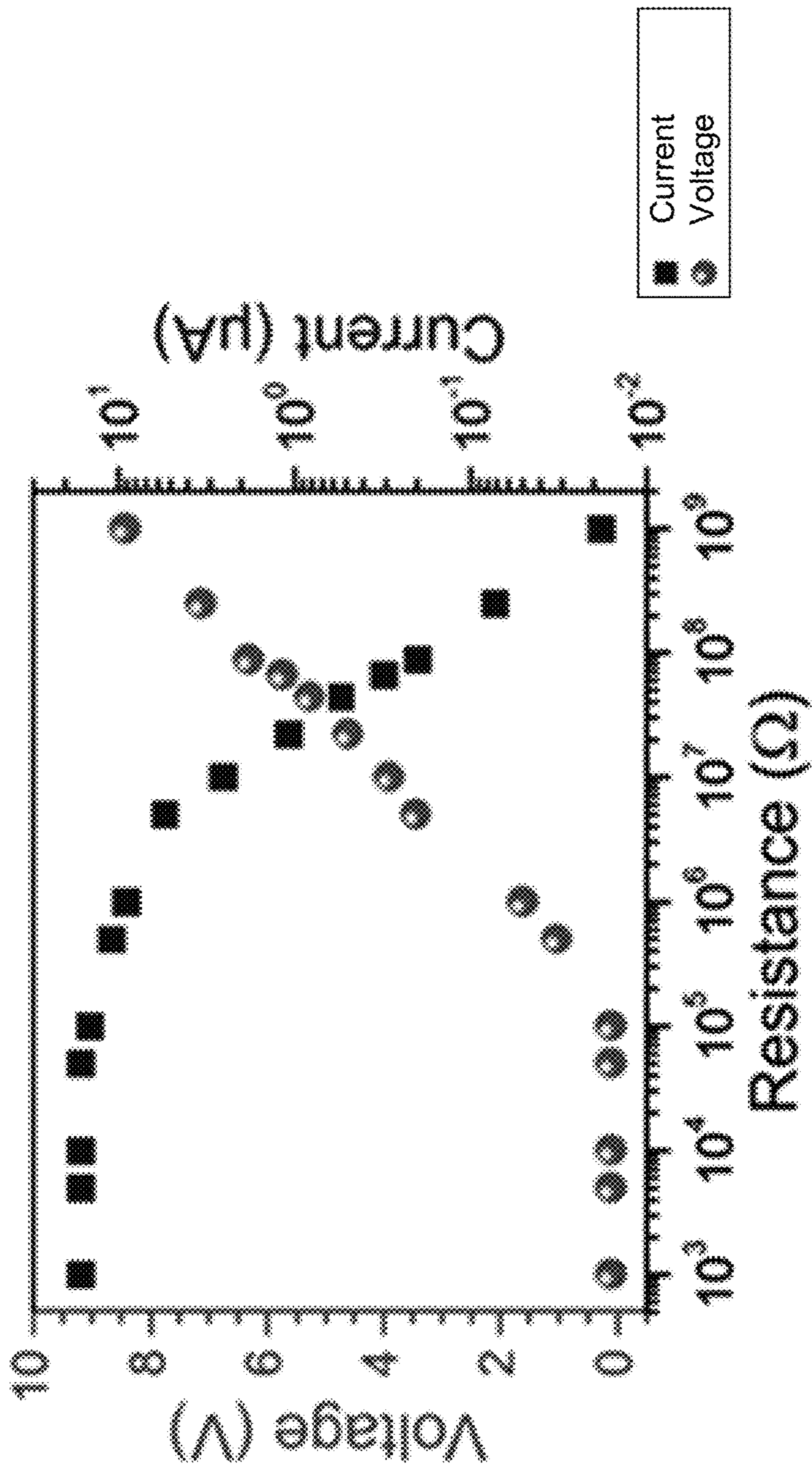


FIG. 7D

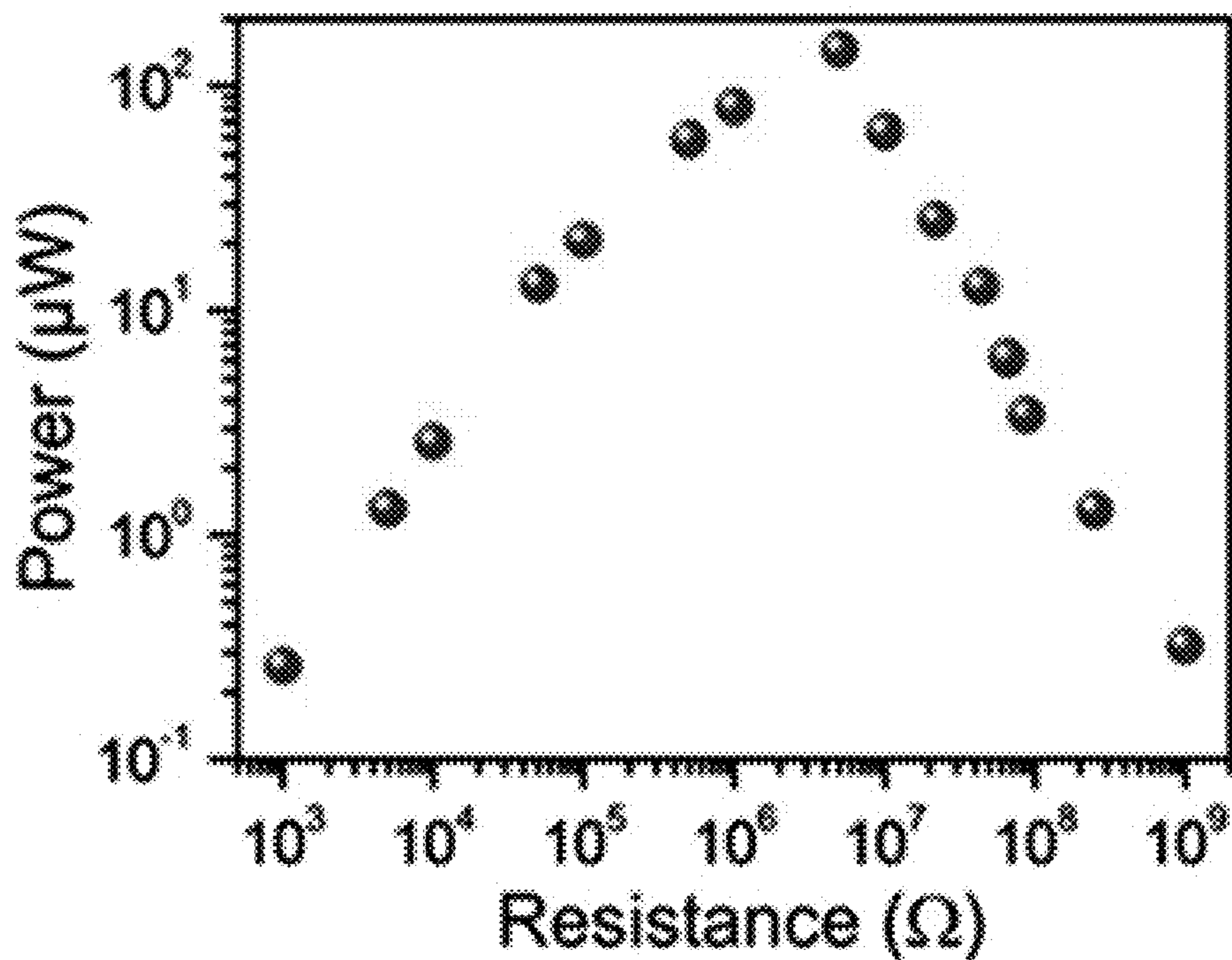


FIG. 7E

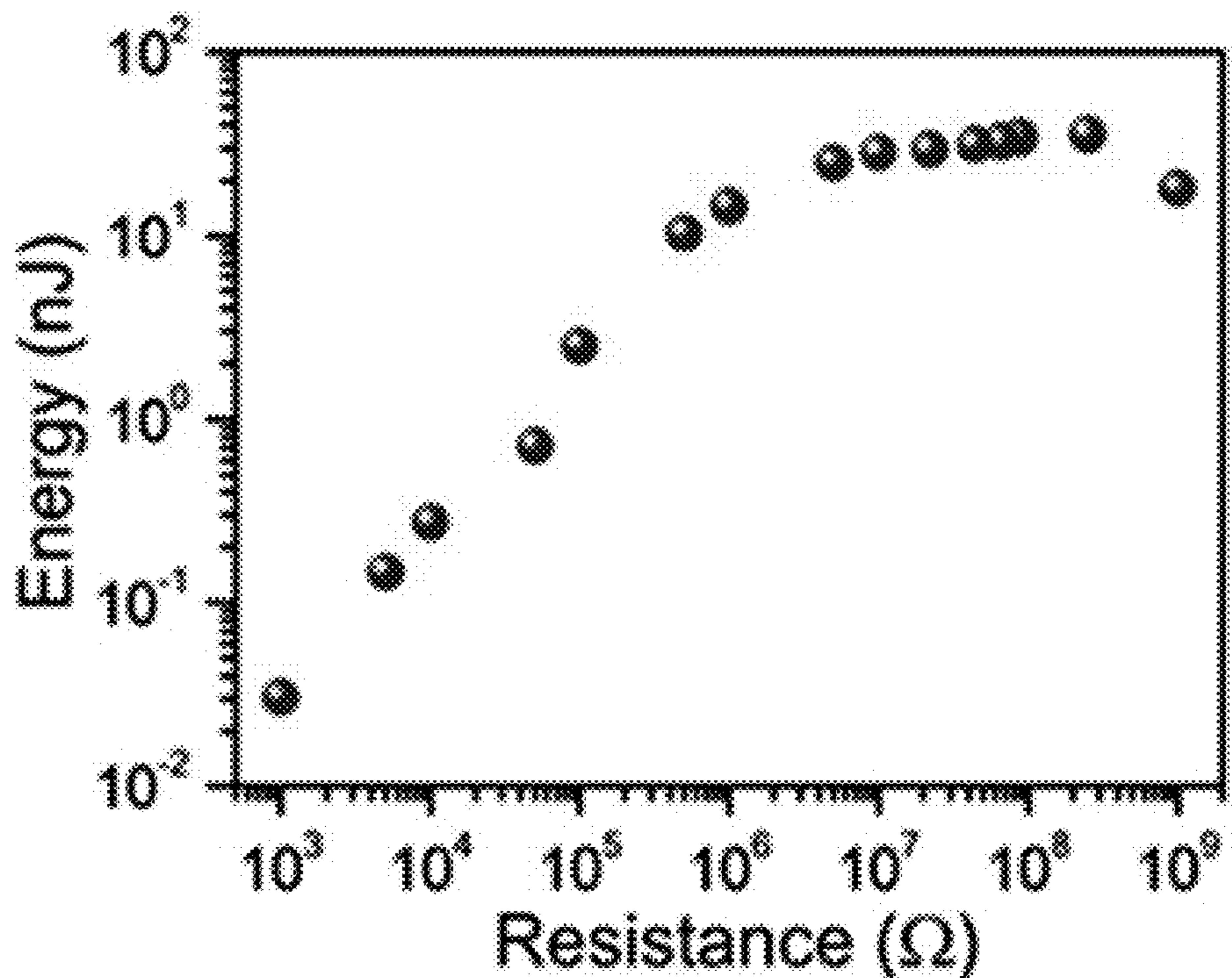


FIG. 7F

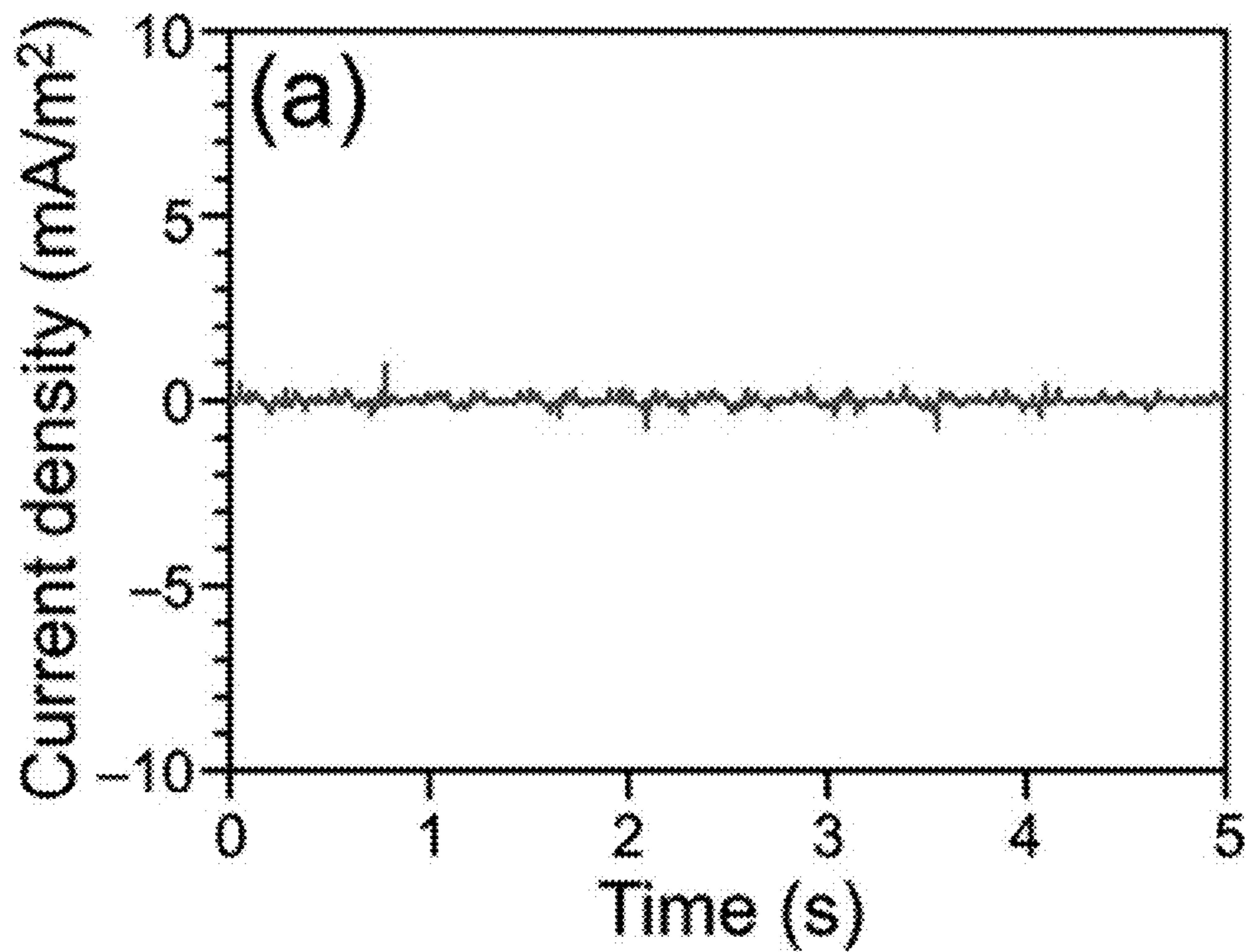


FIG. 8A

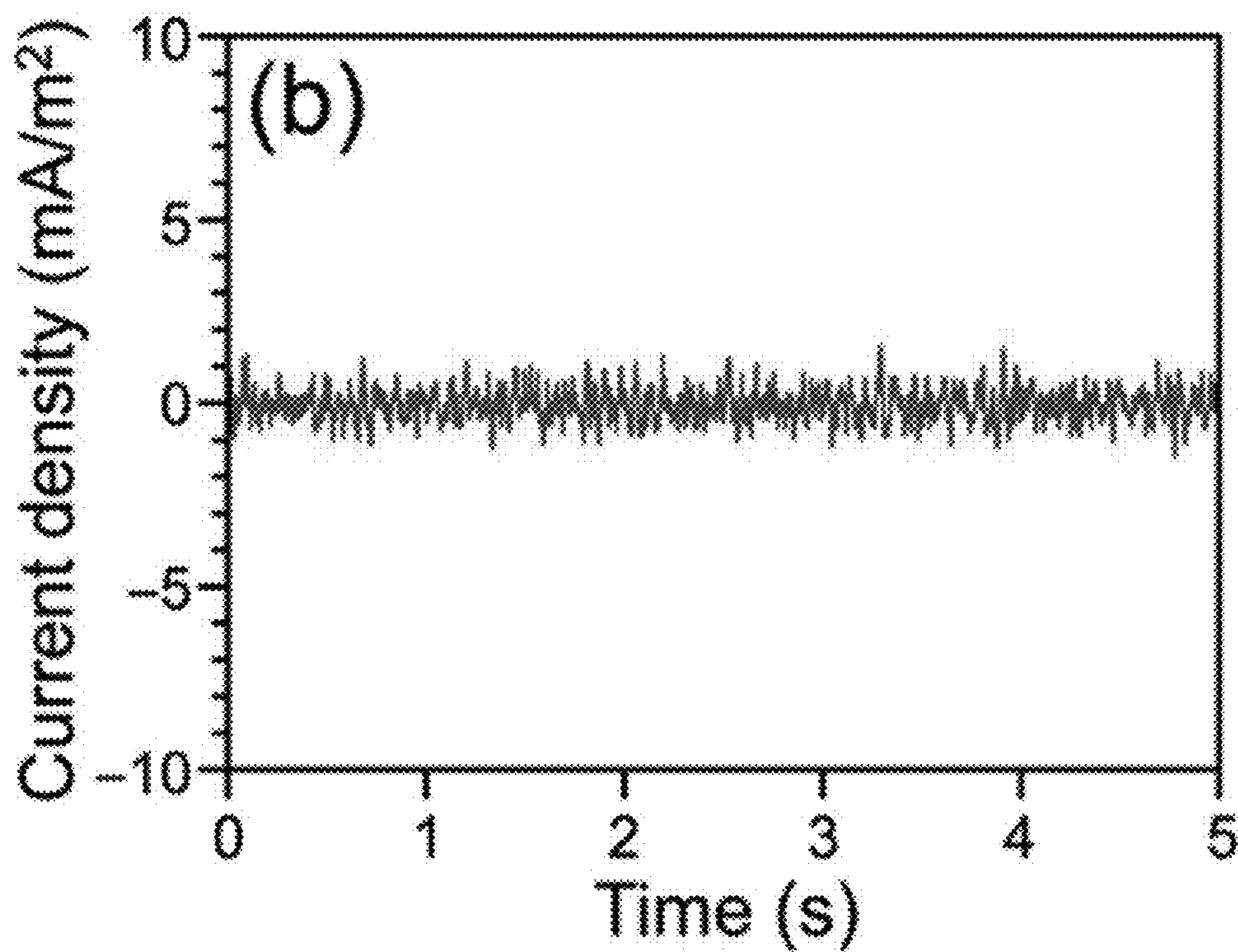


FIG. 8B

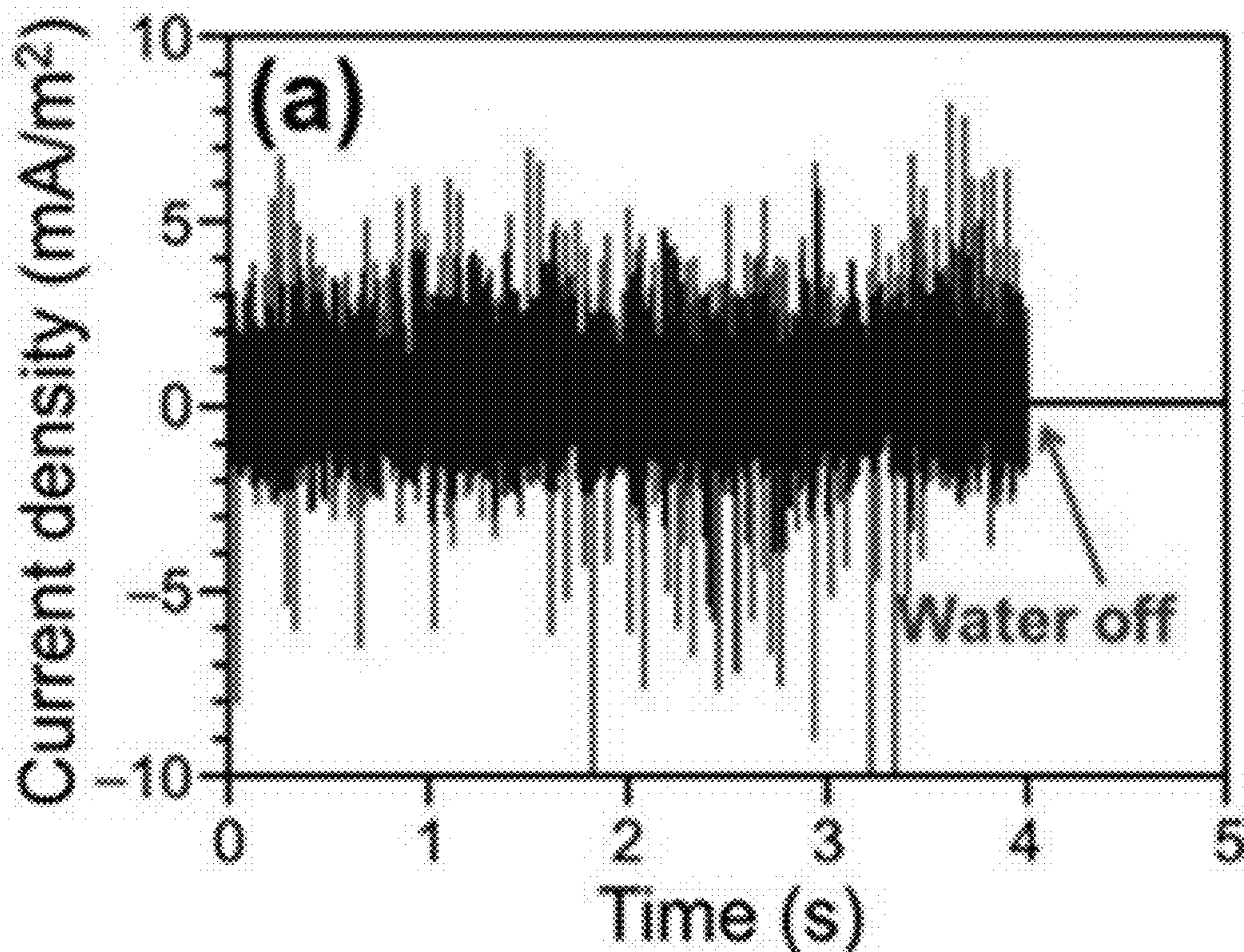


FIG. 9A

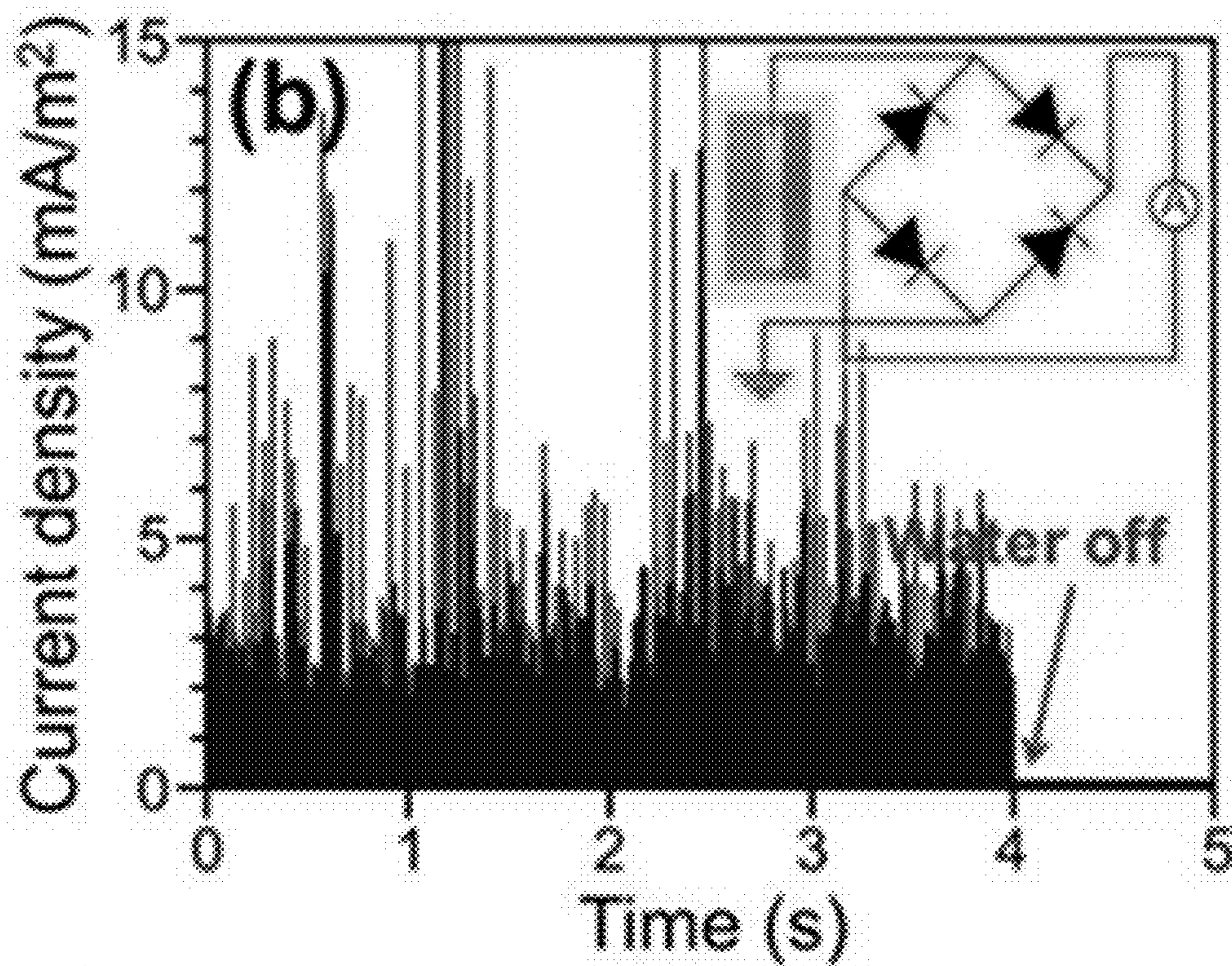


FIG. 9B

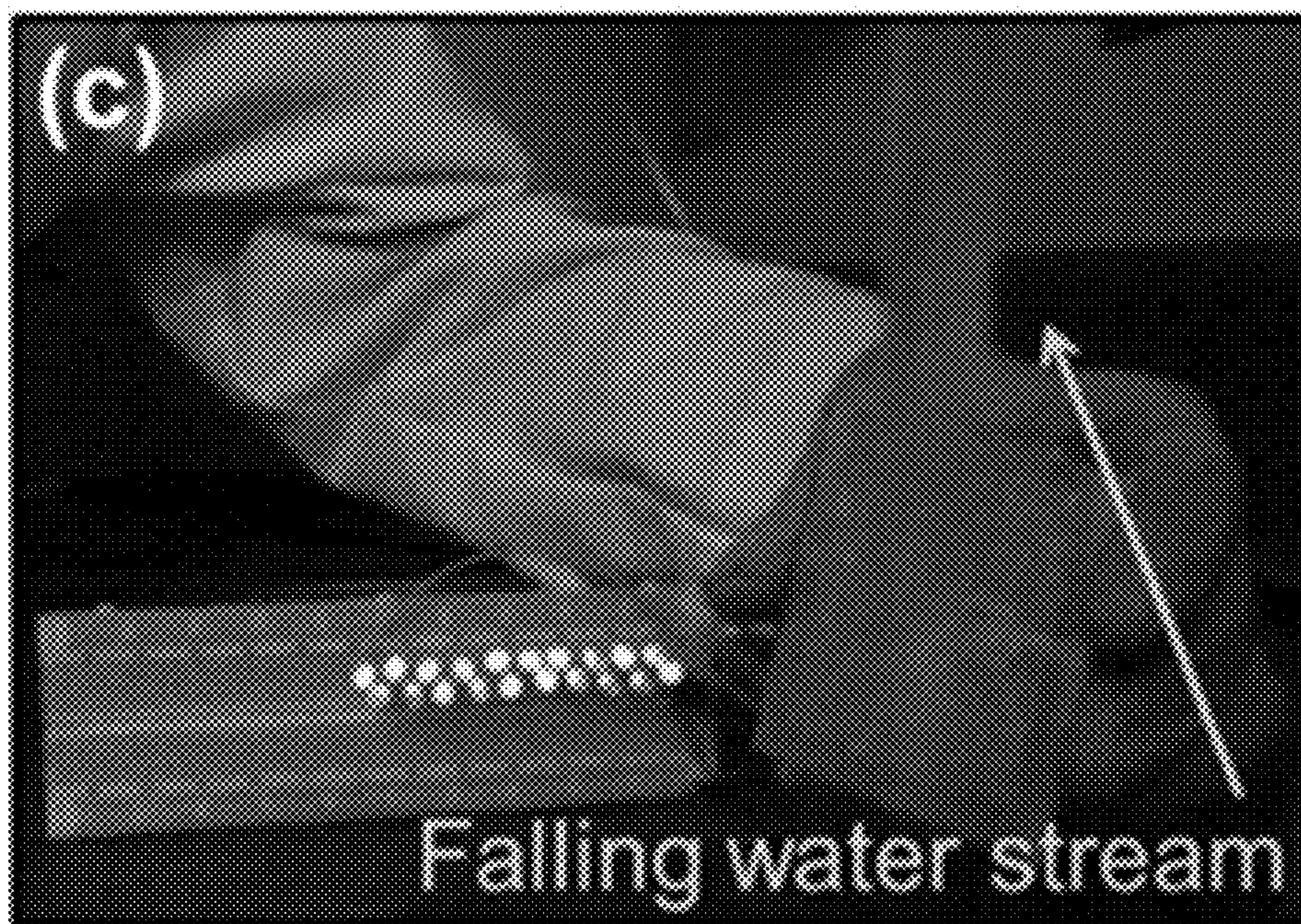


FIG. 9C

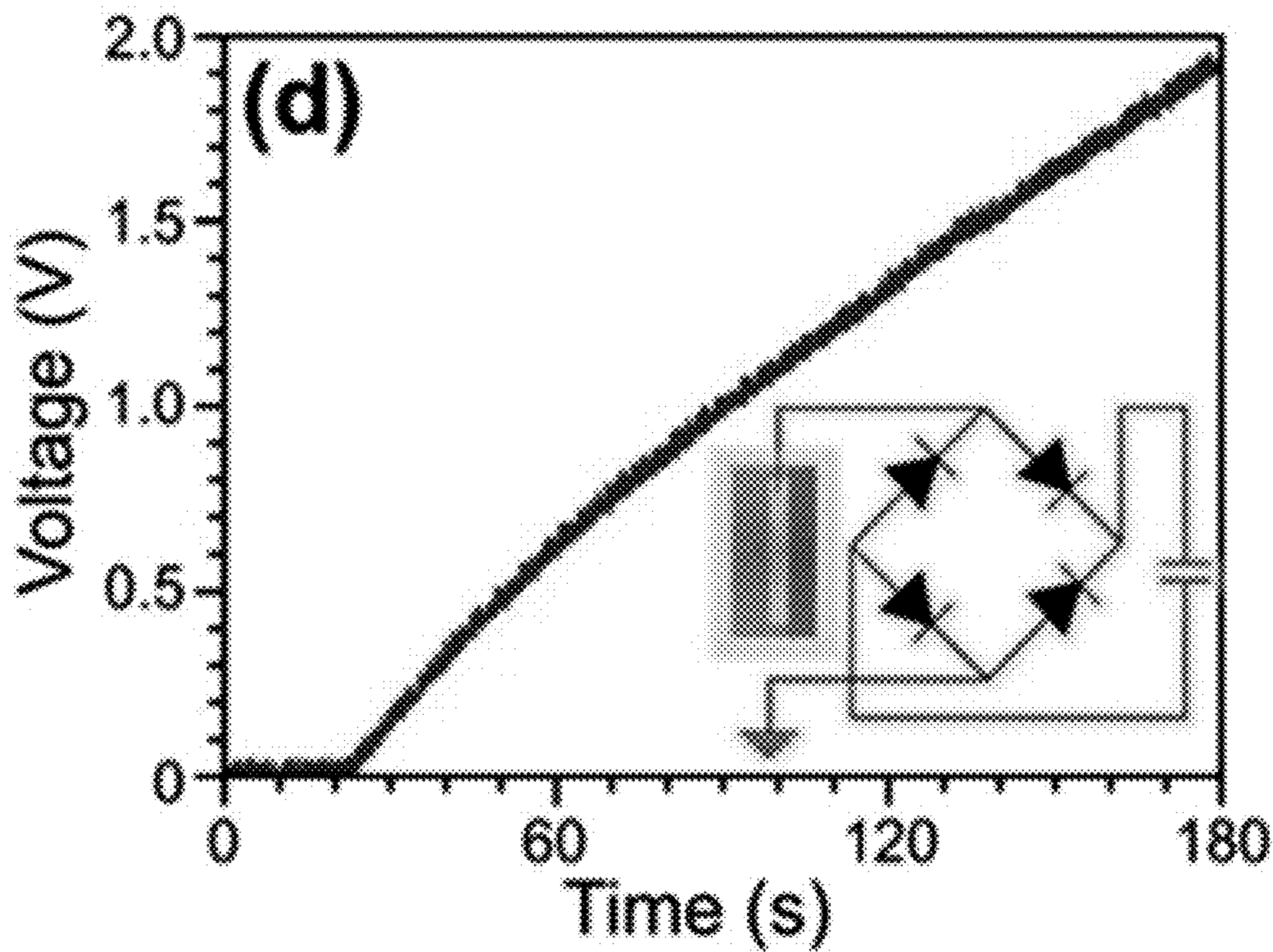


FIG. 9D



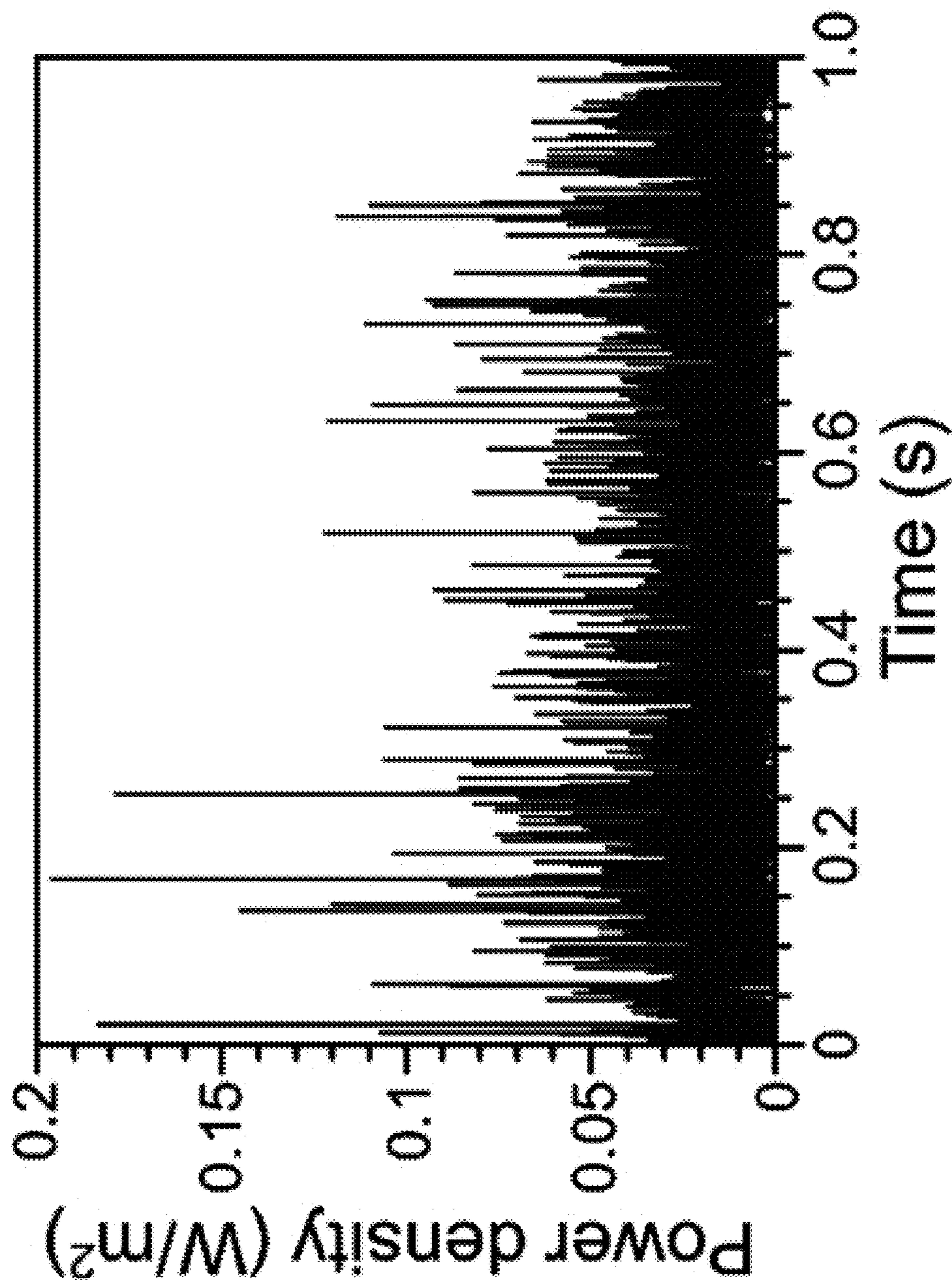


FIG. 9E

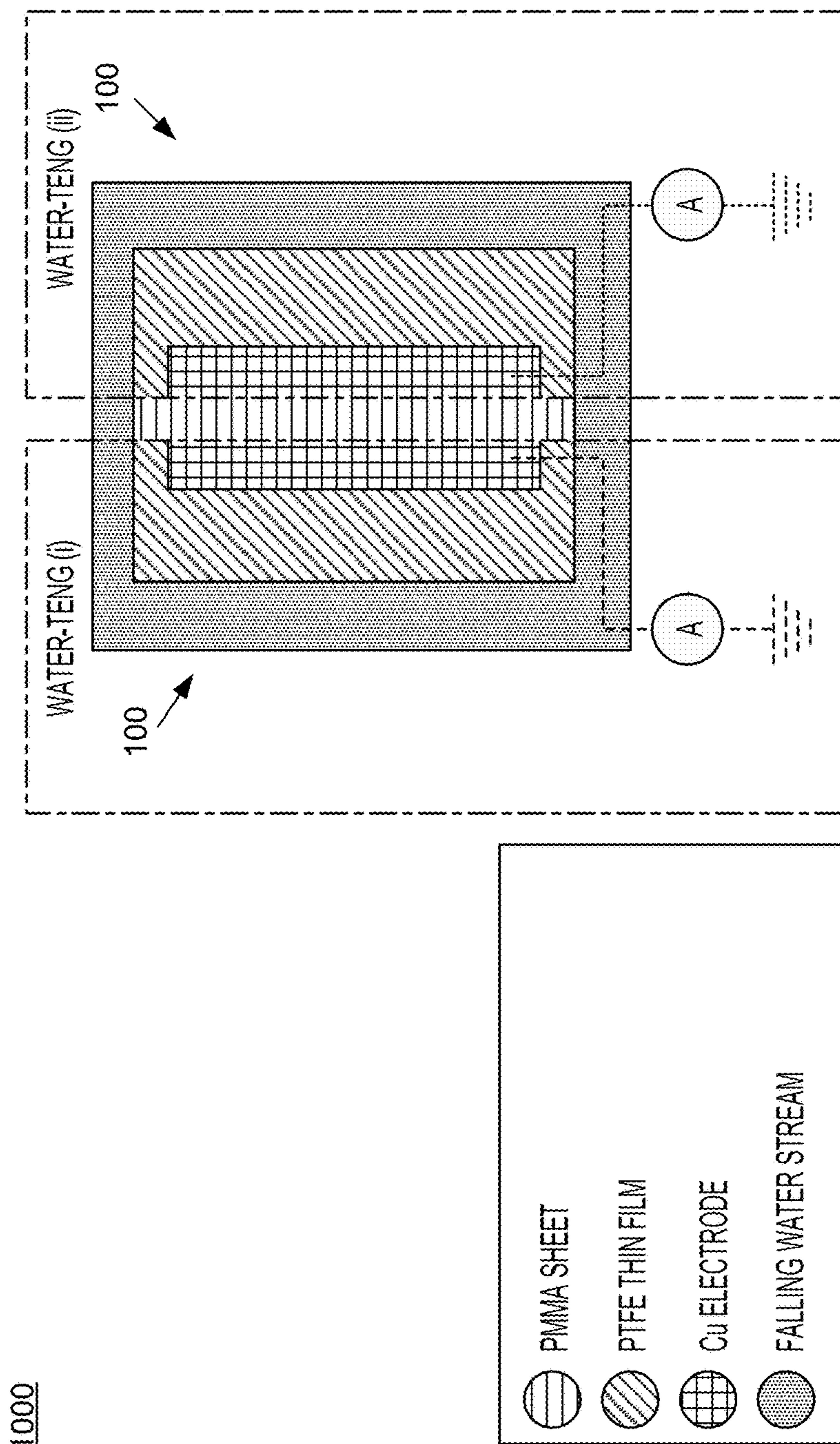


FIG. 10A

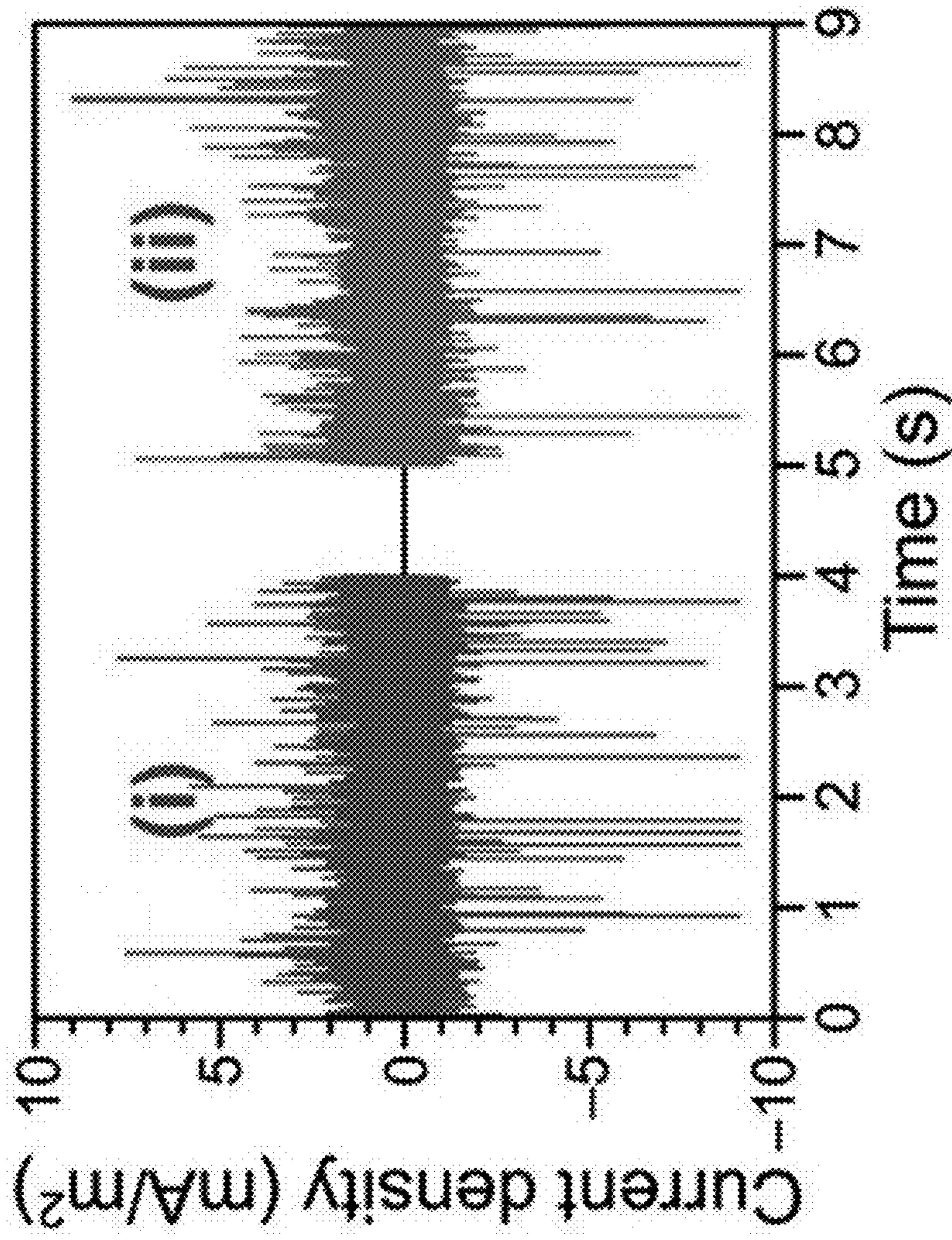


FIG. 10B

1100

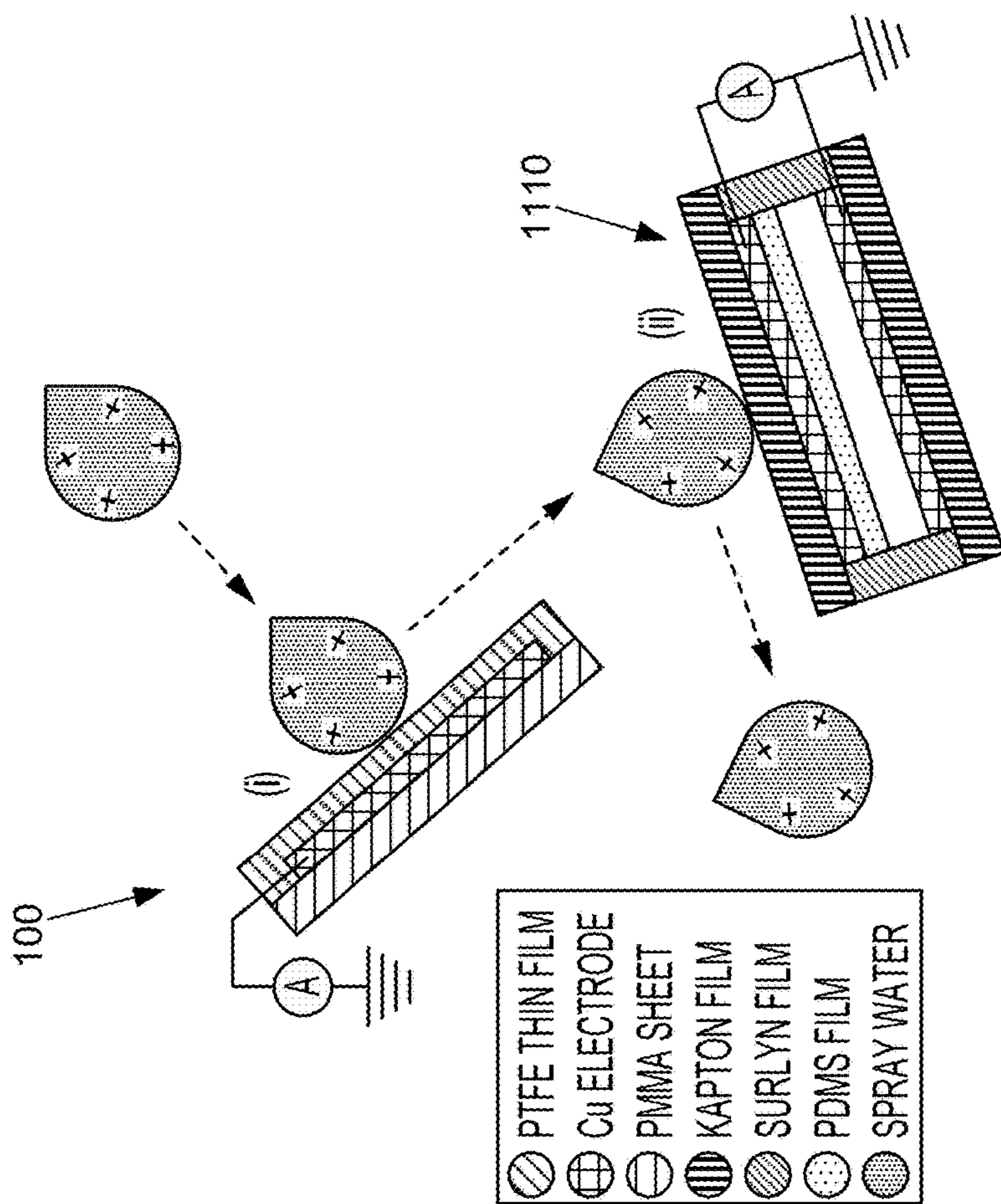


FIG. 11A

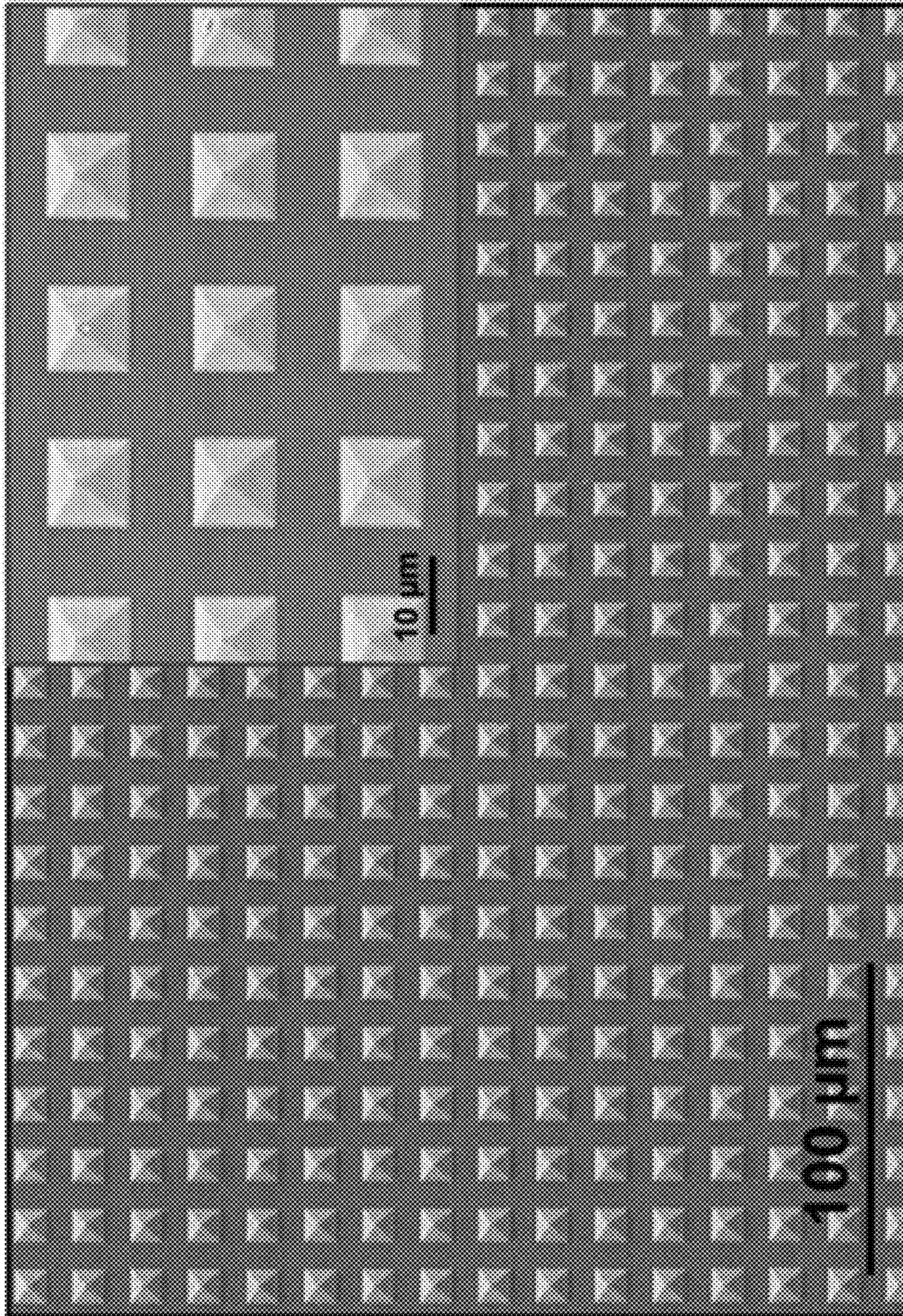


FIG. 11B

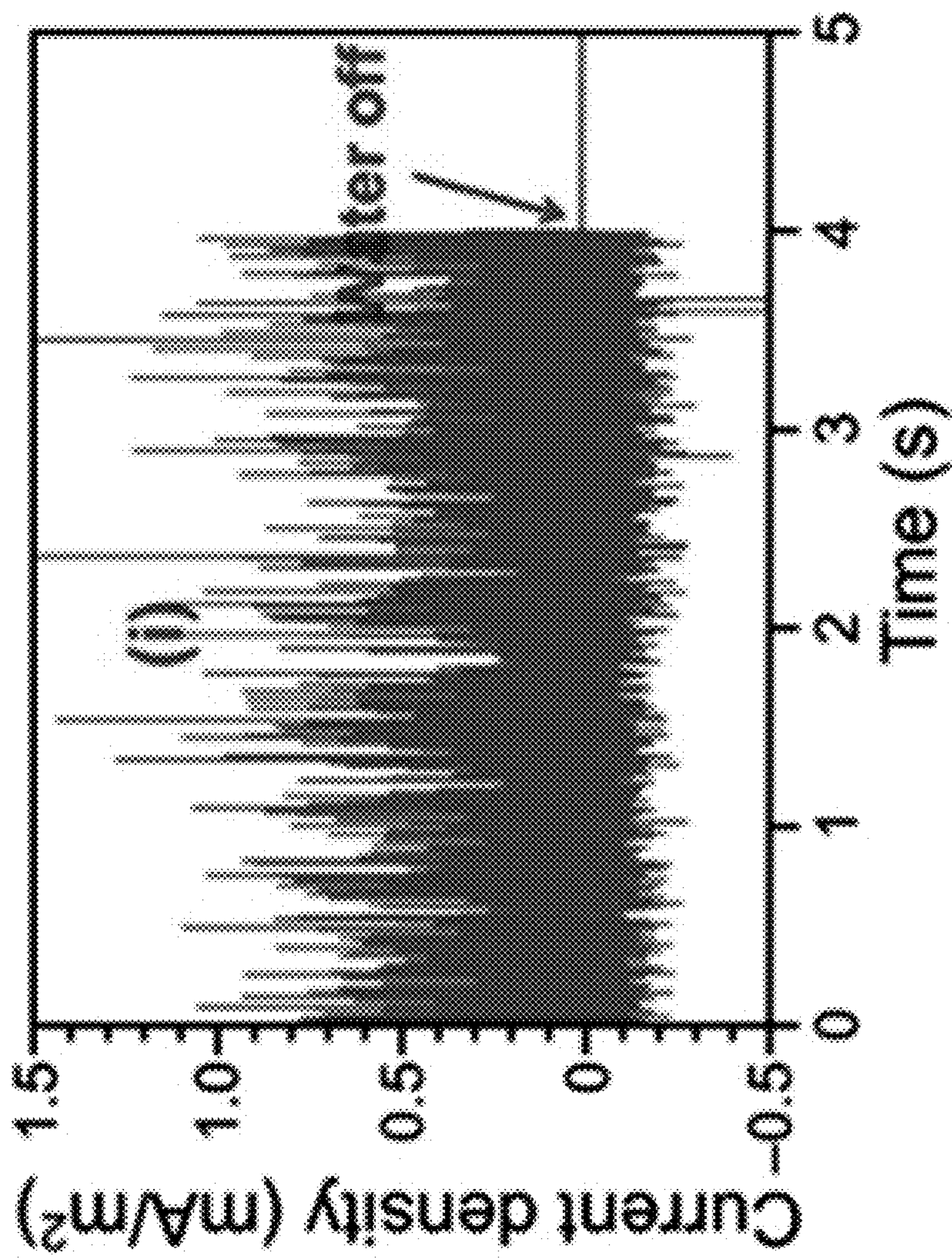


FIG. 11C

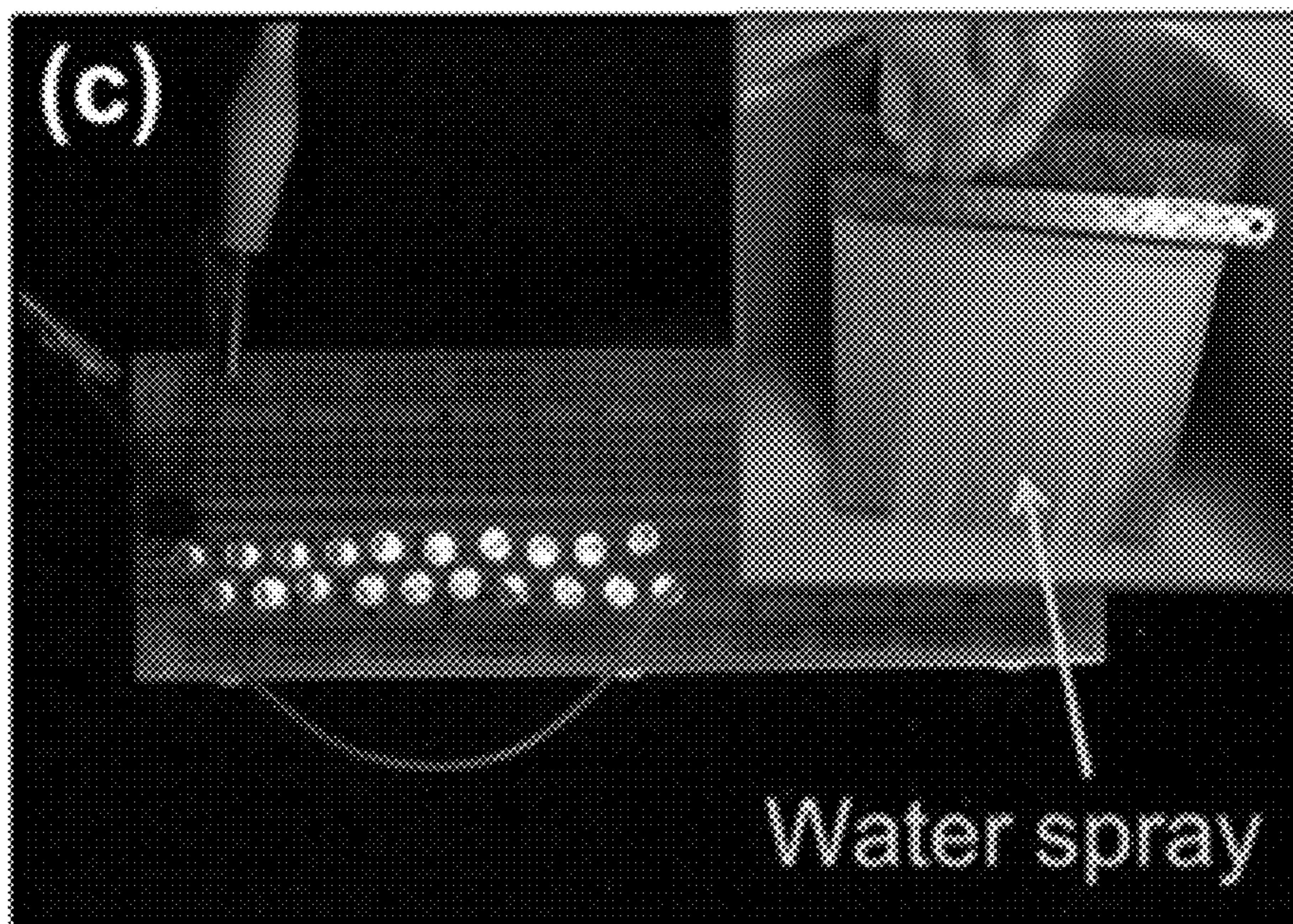


FIG. 11D

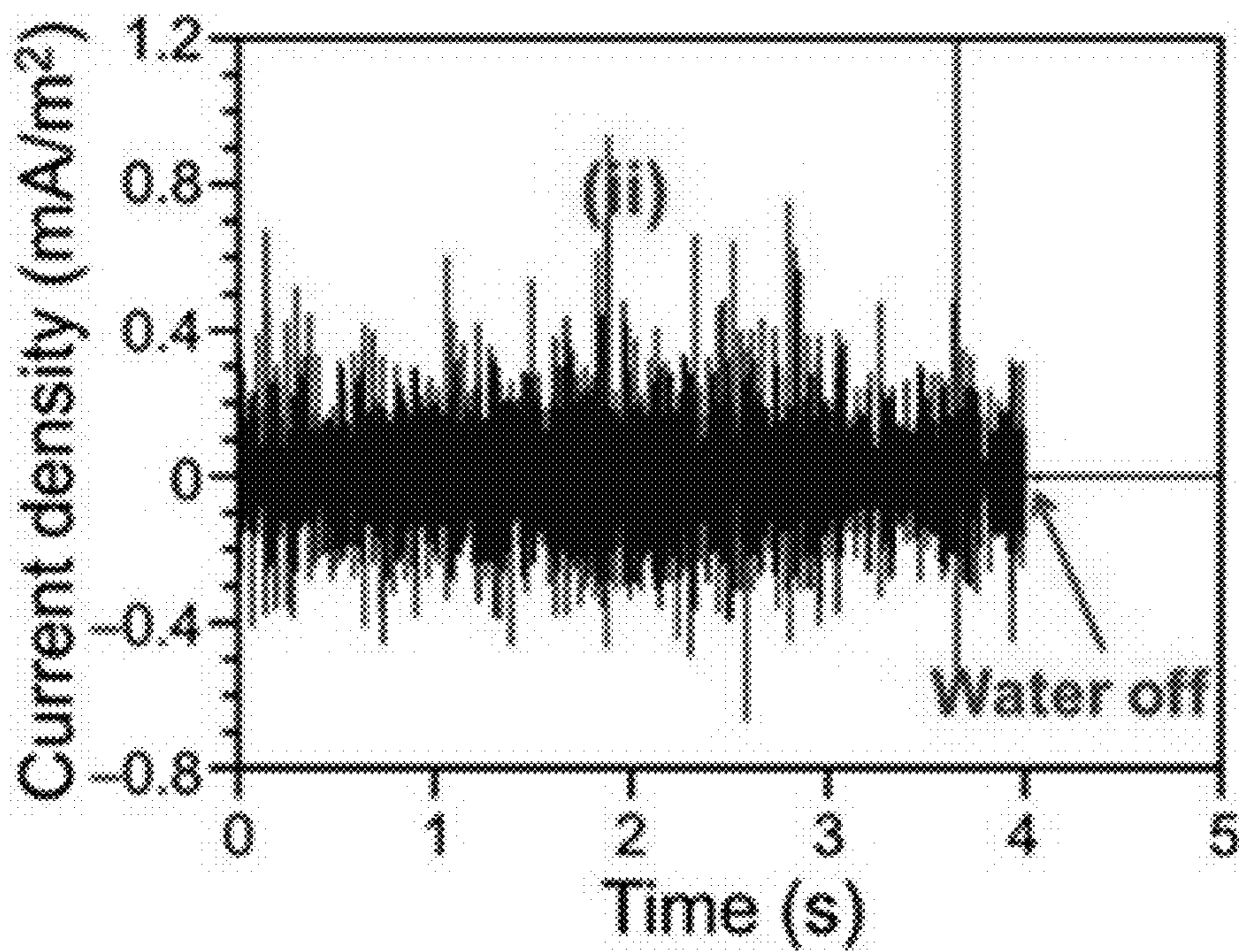


FIG. 11E

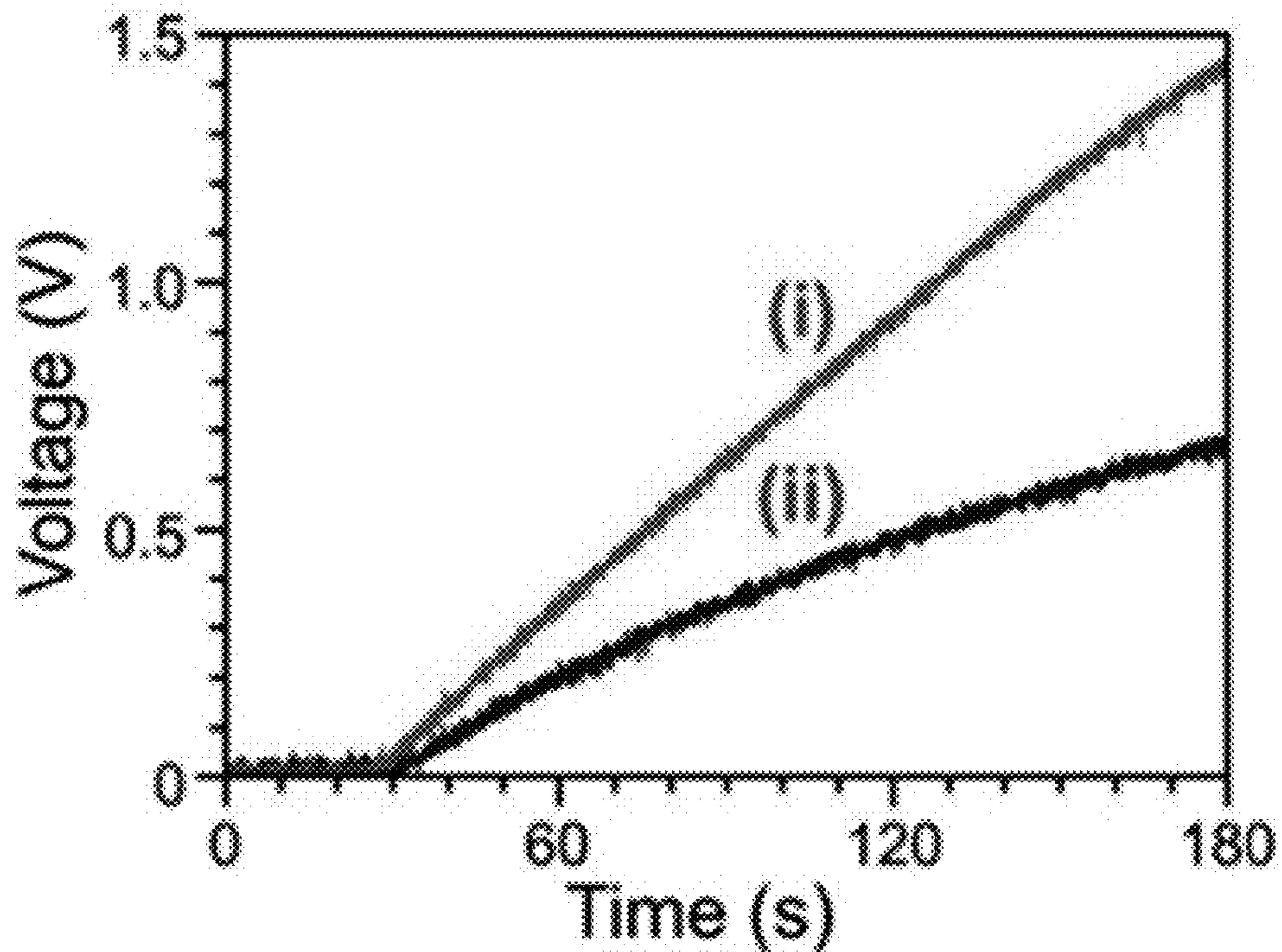


FIG. 11F

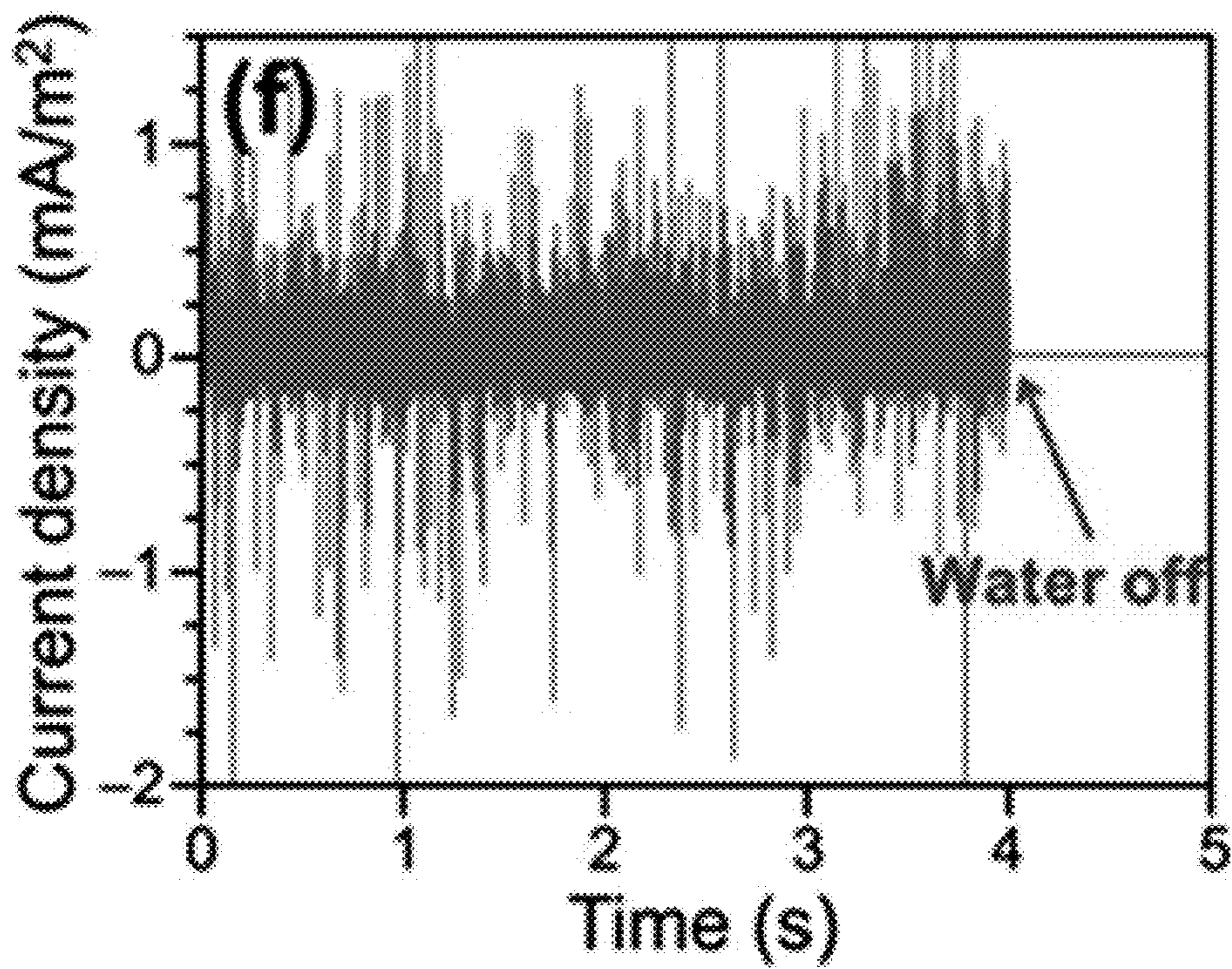


FIG. 11G



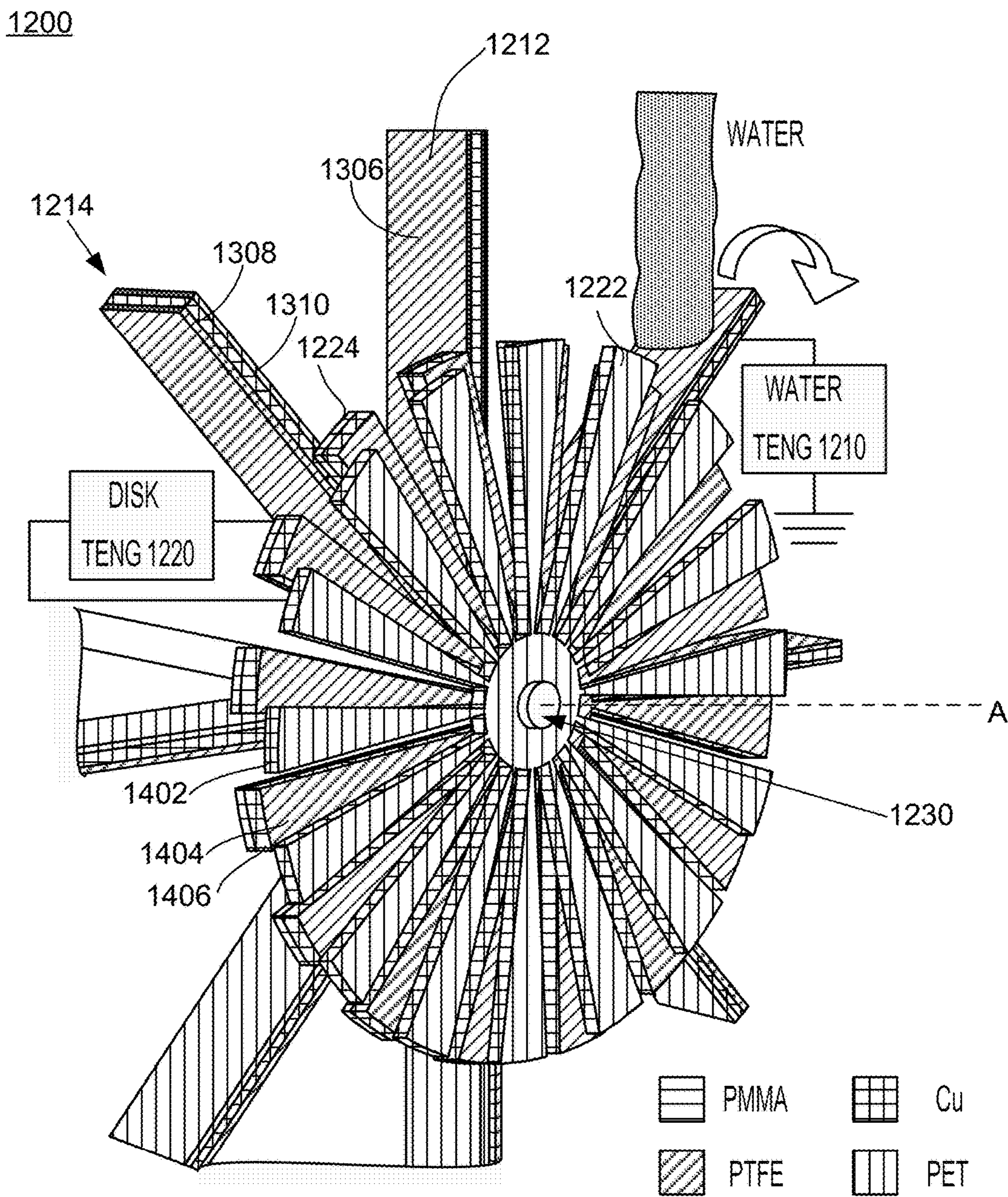


FIG. 12A

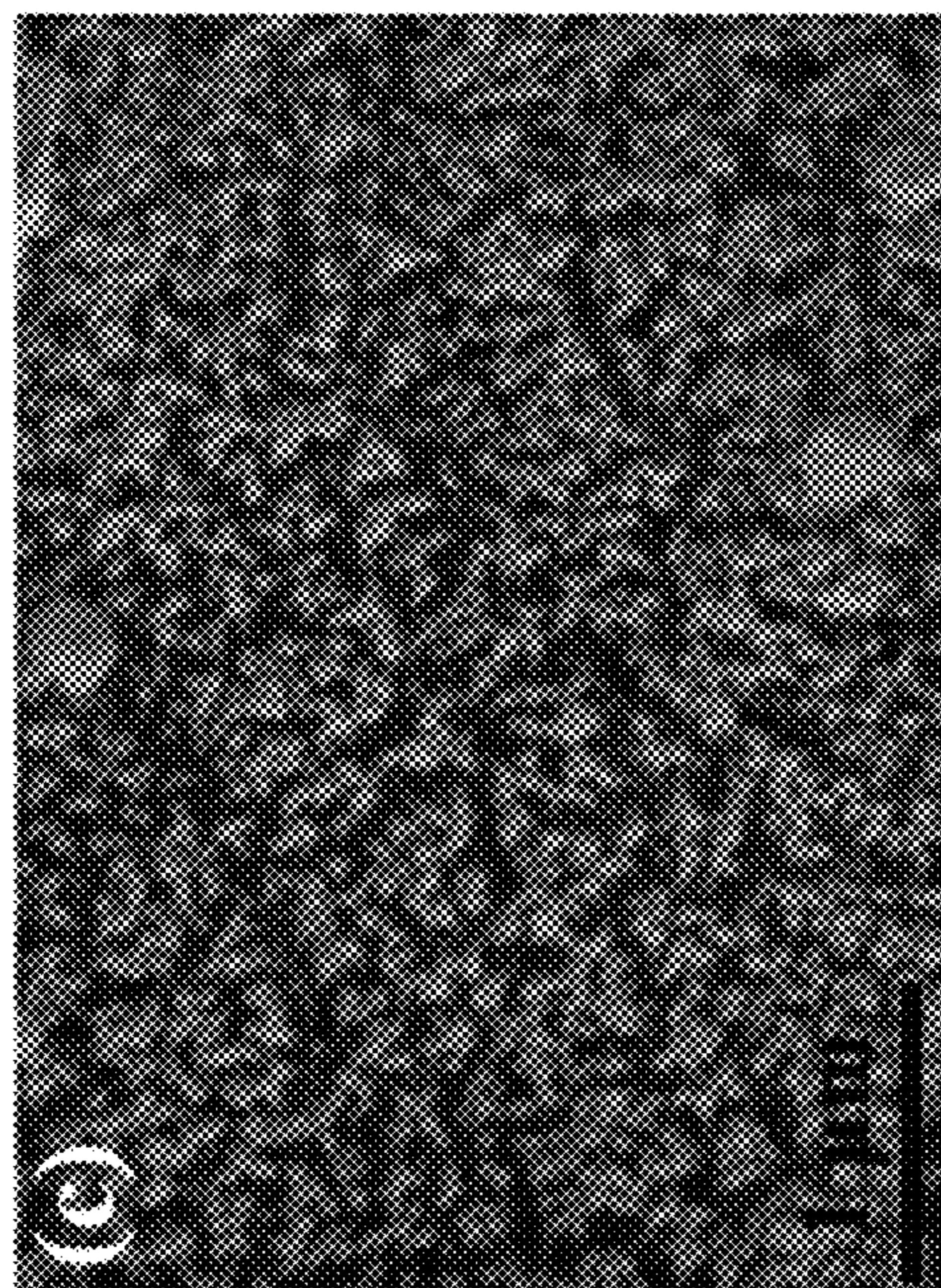
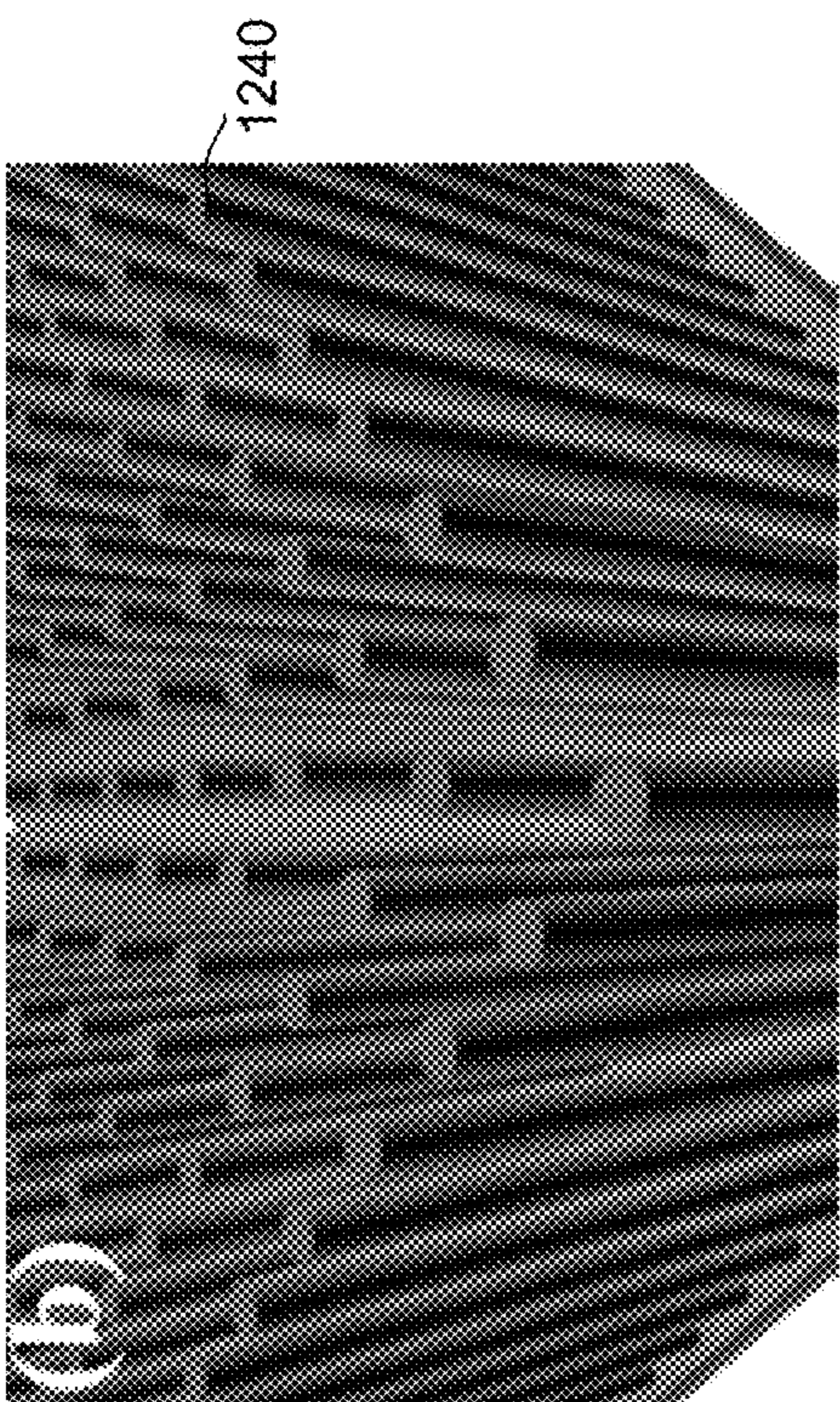


FIG. 12B

FIG. 12C

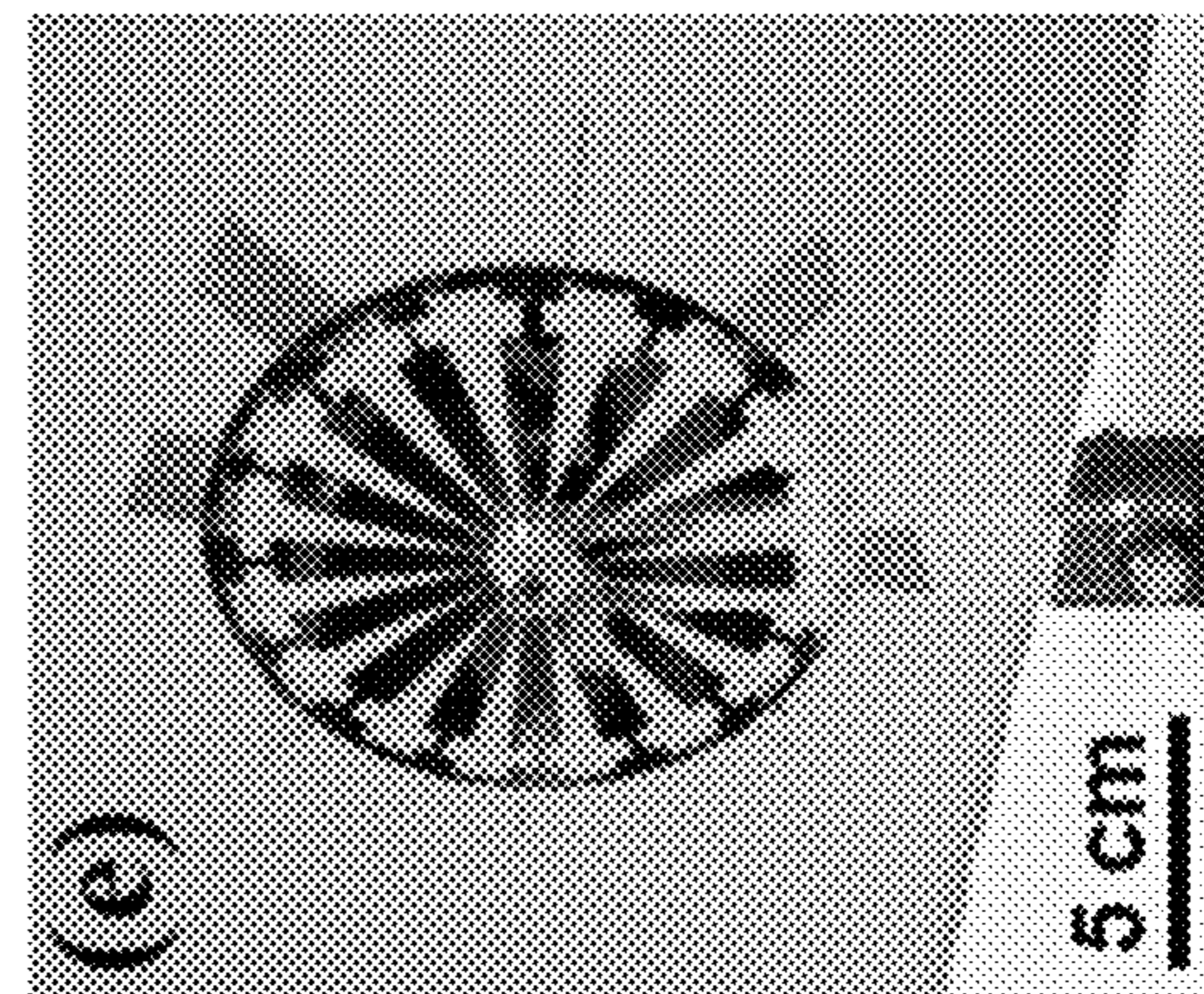
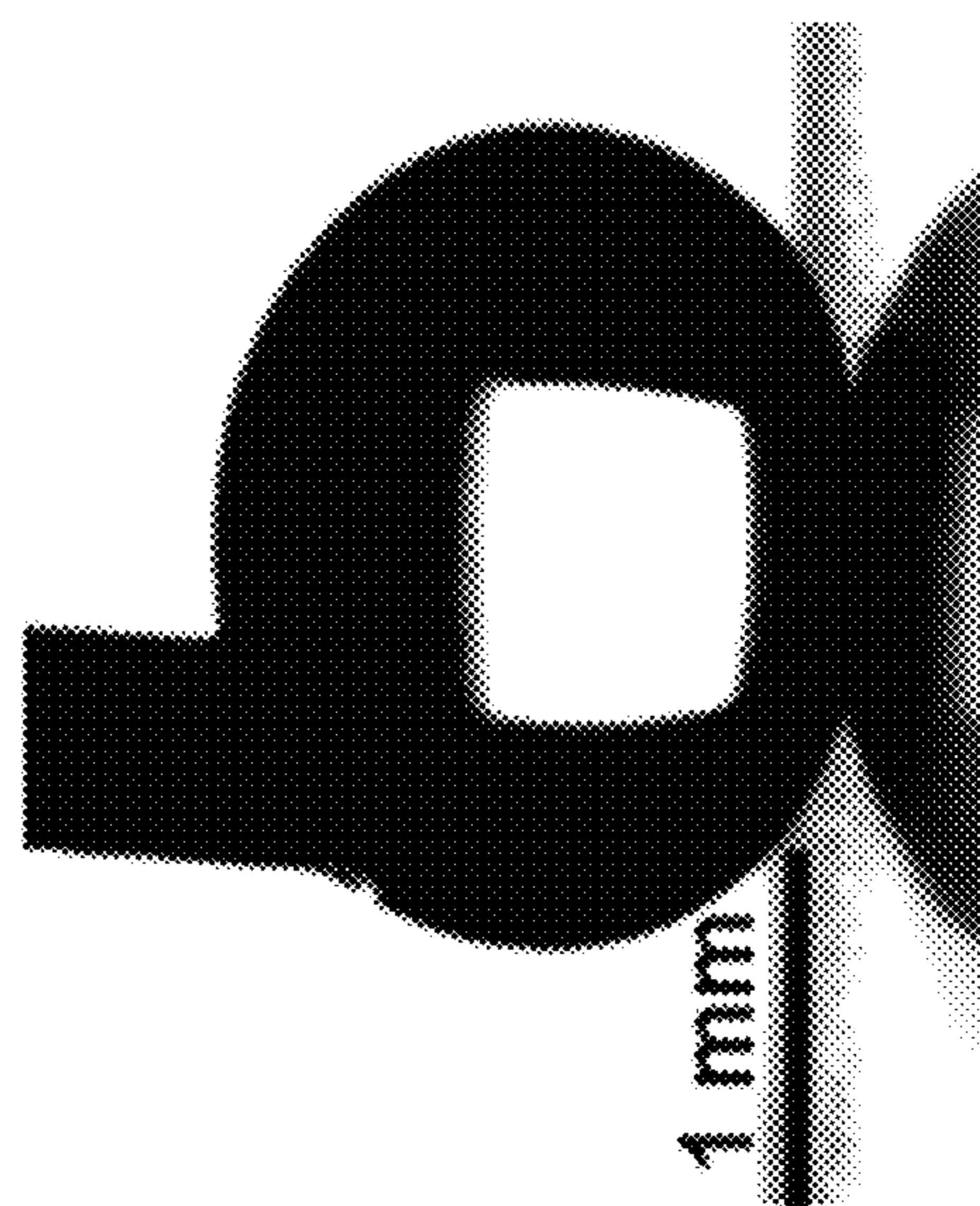


FIG. 12D

FIG. 12E

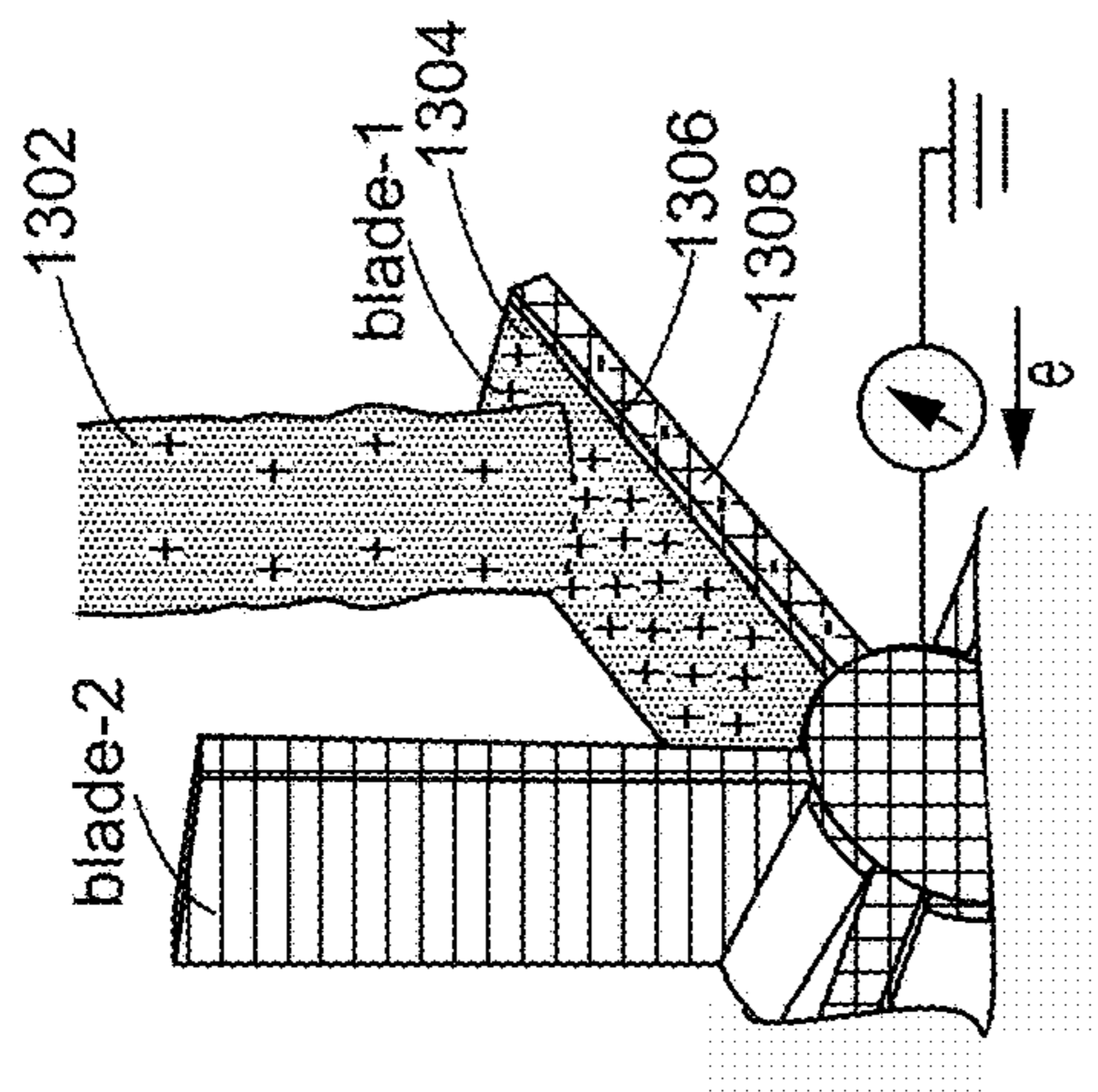


FIG. 13B

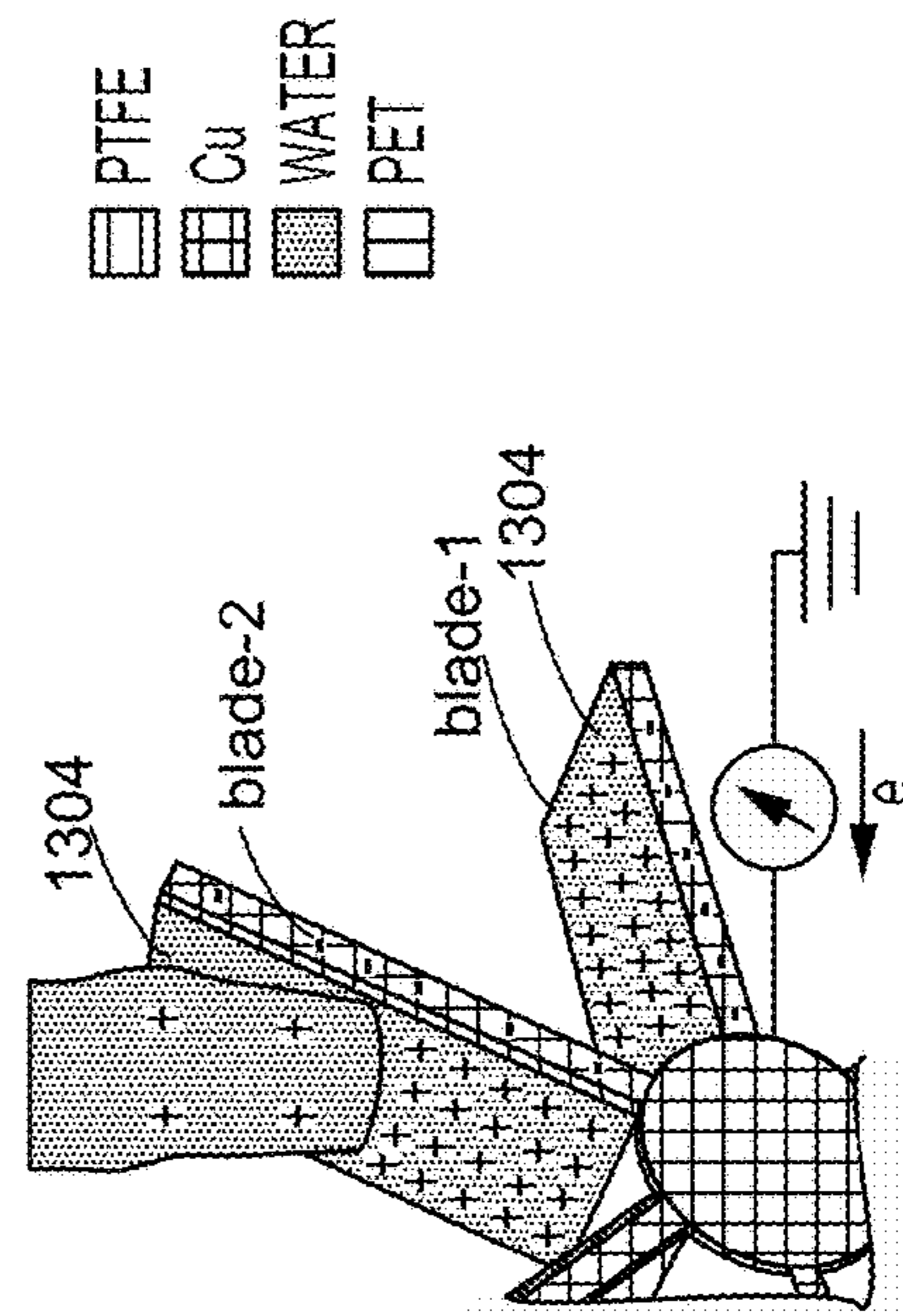


FIG. 13C

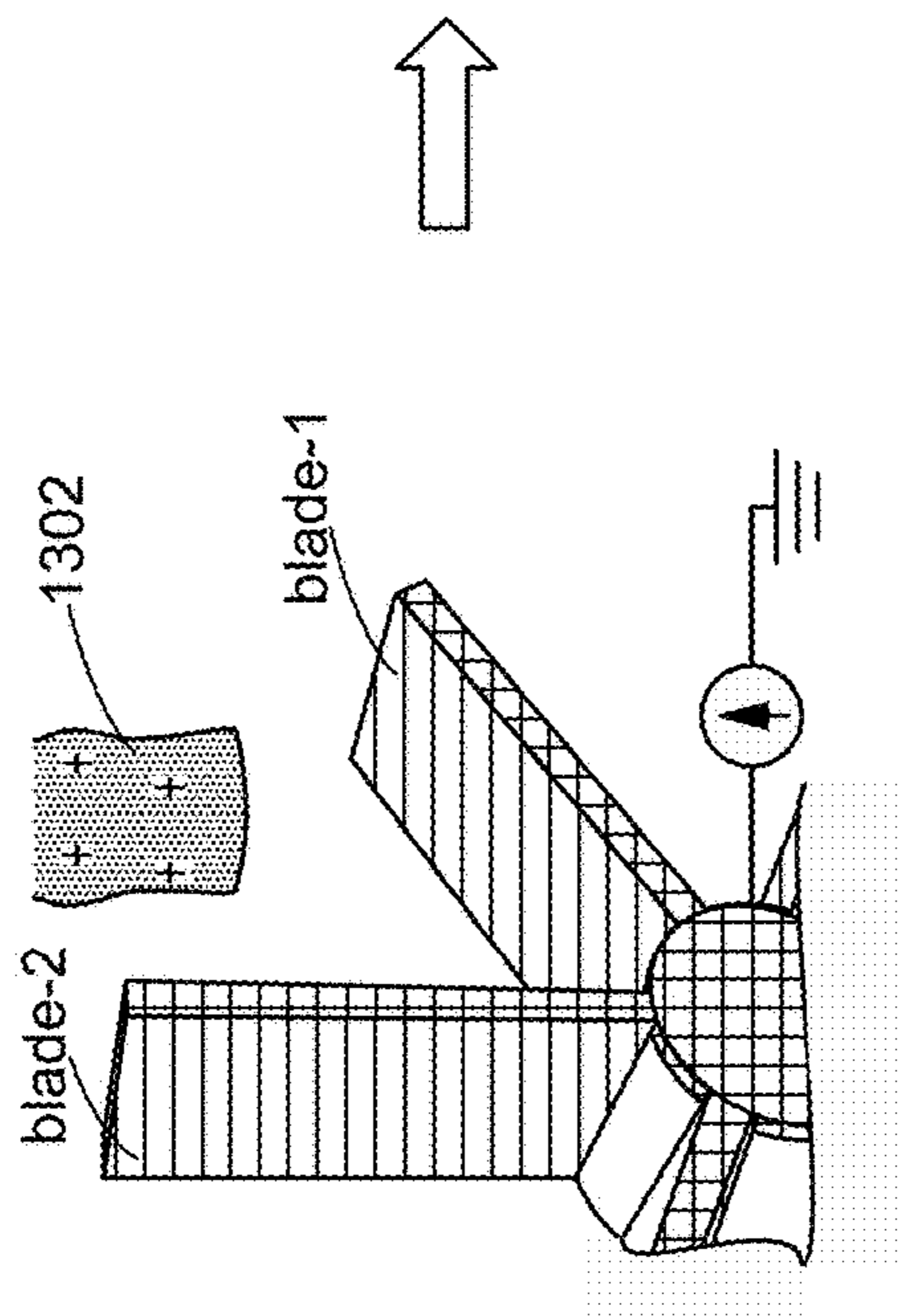


FIG. 13A

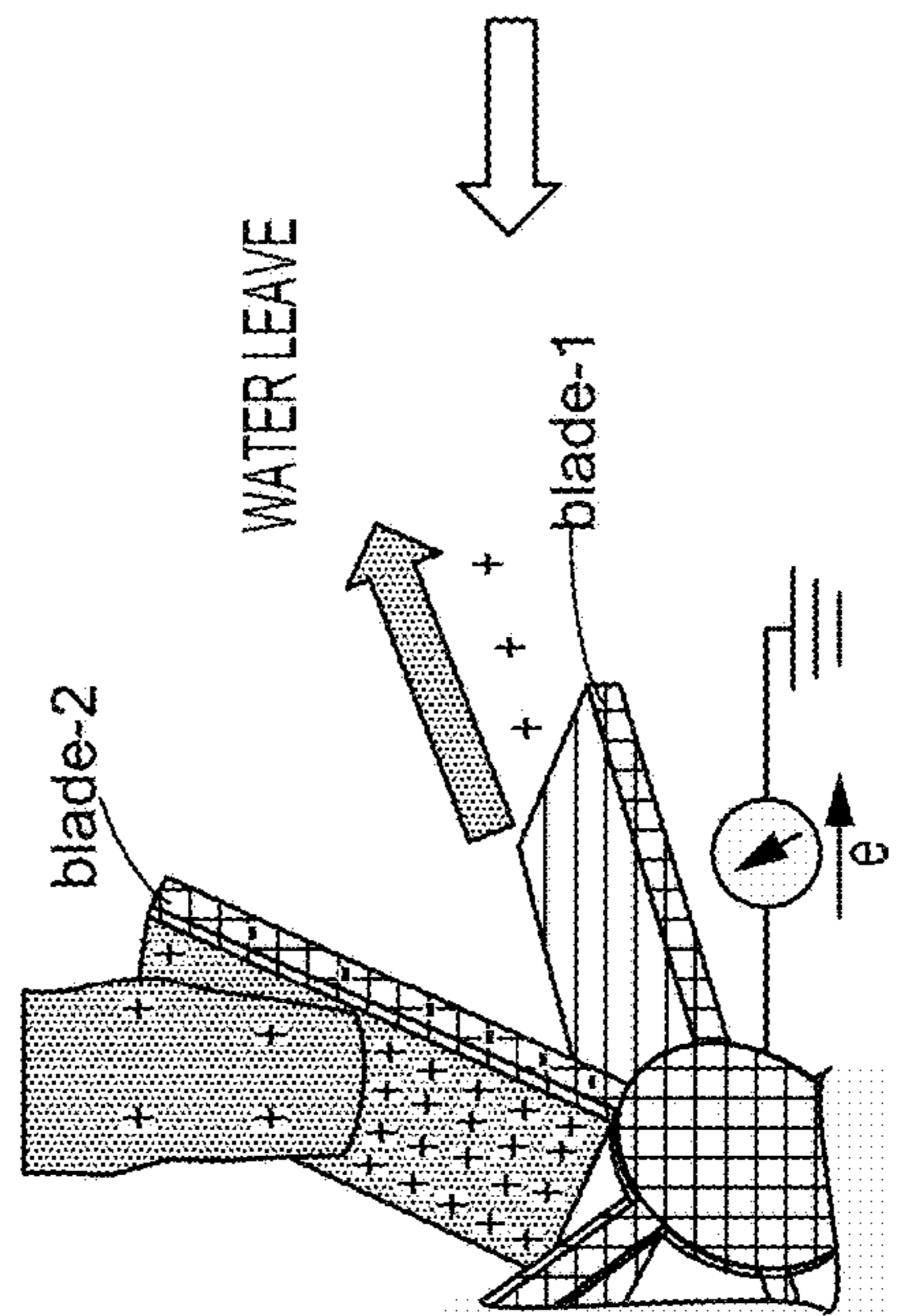


FIG. 13D

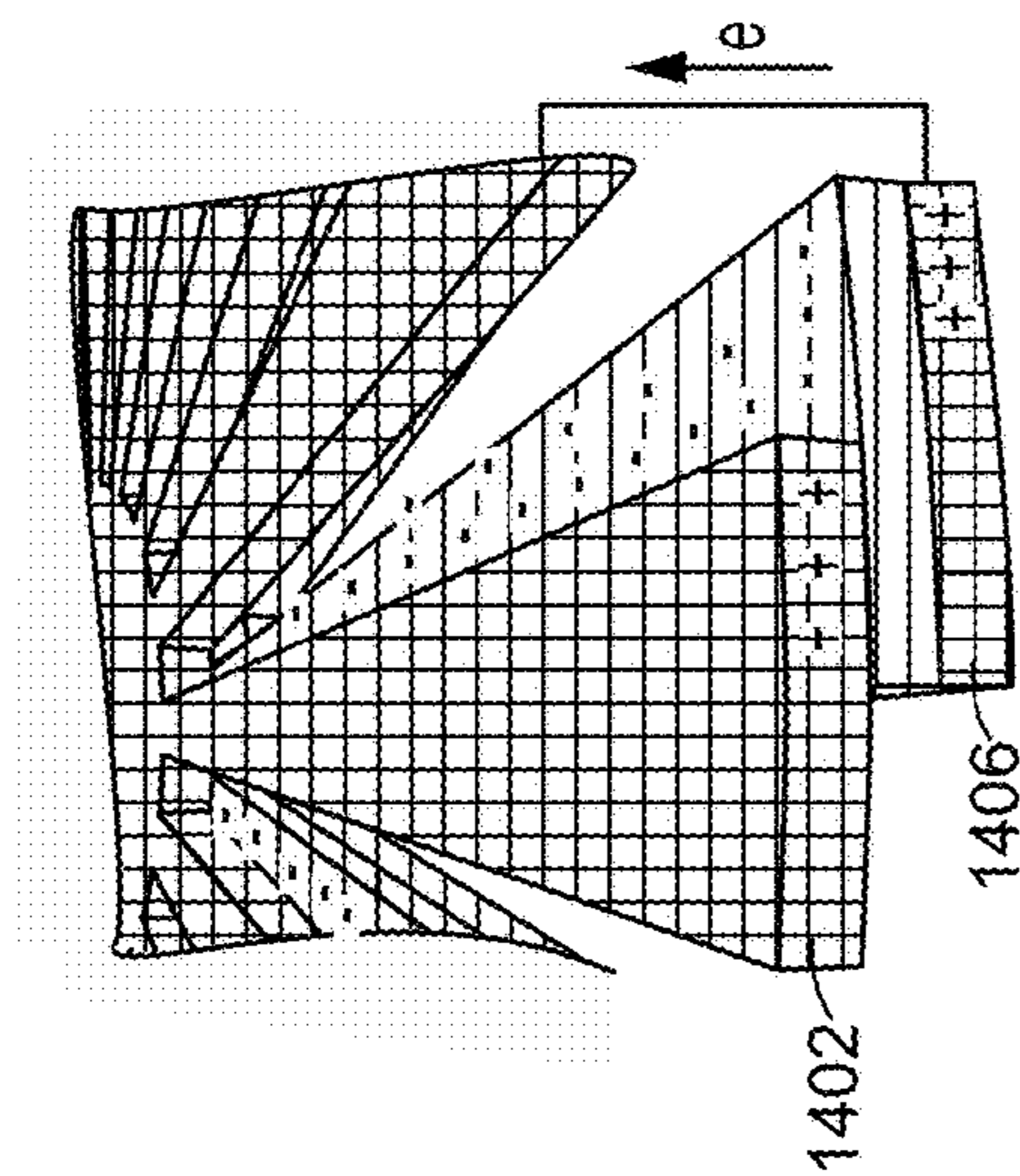


FIG. 14B

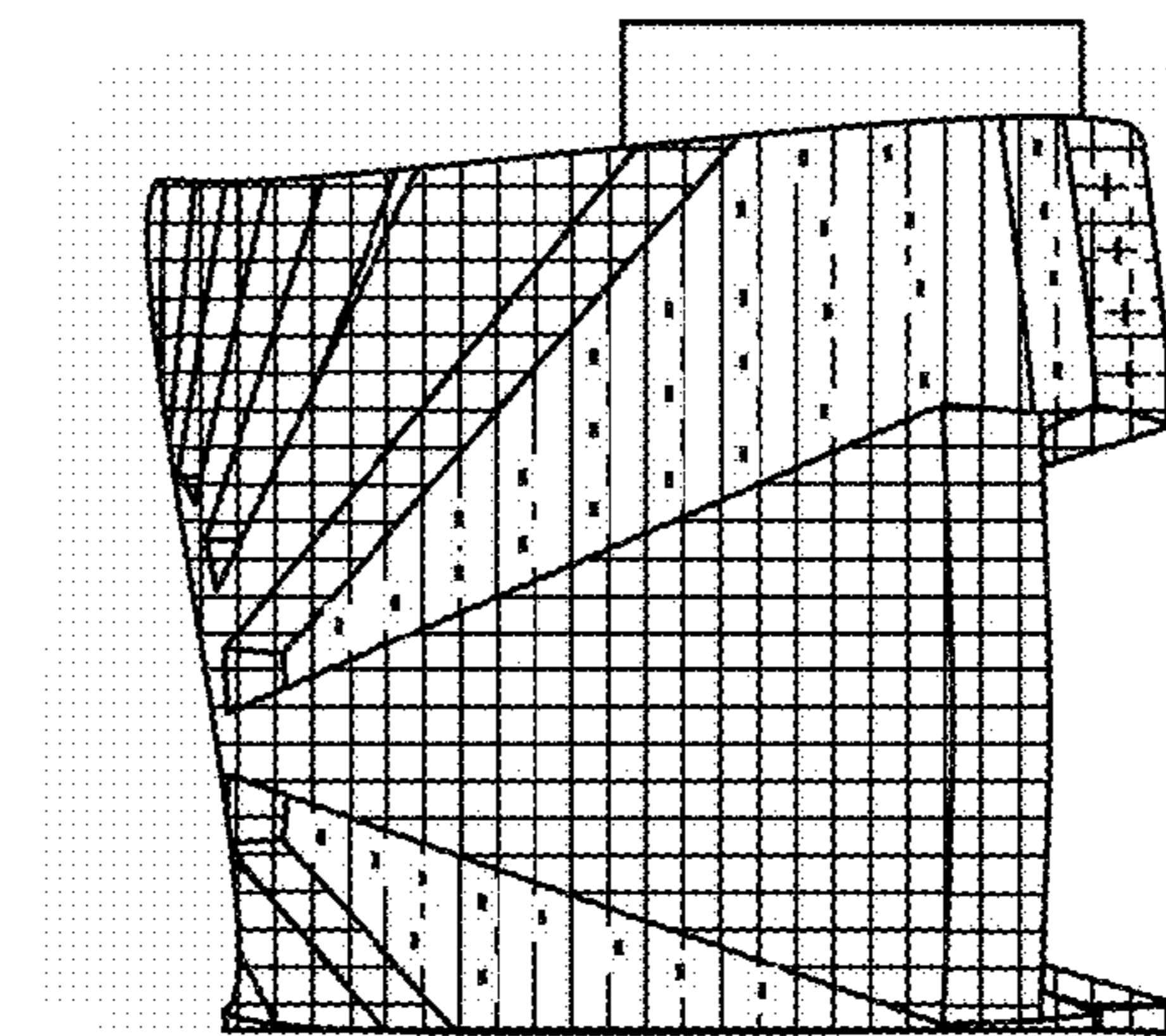


FIG. 14C

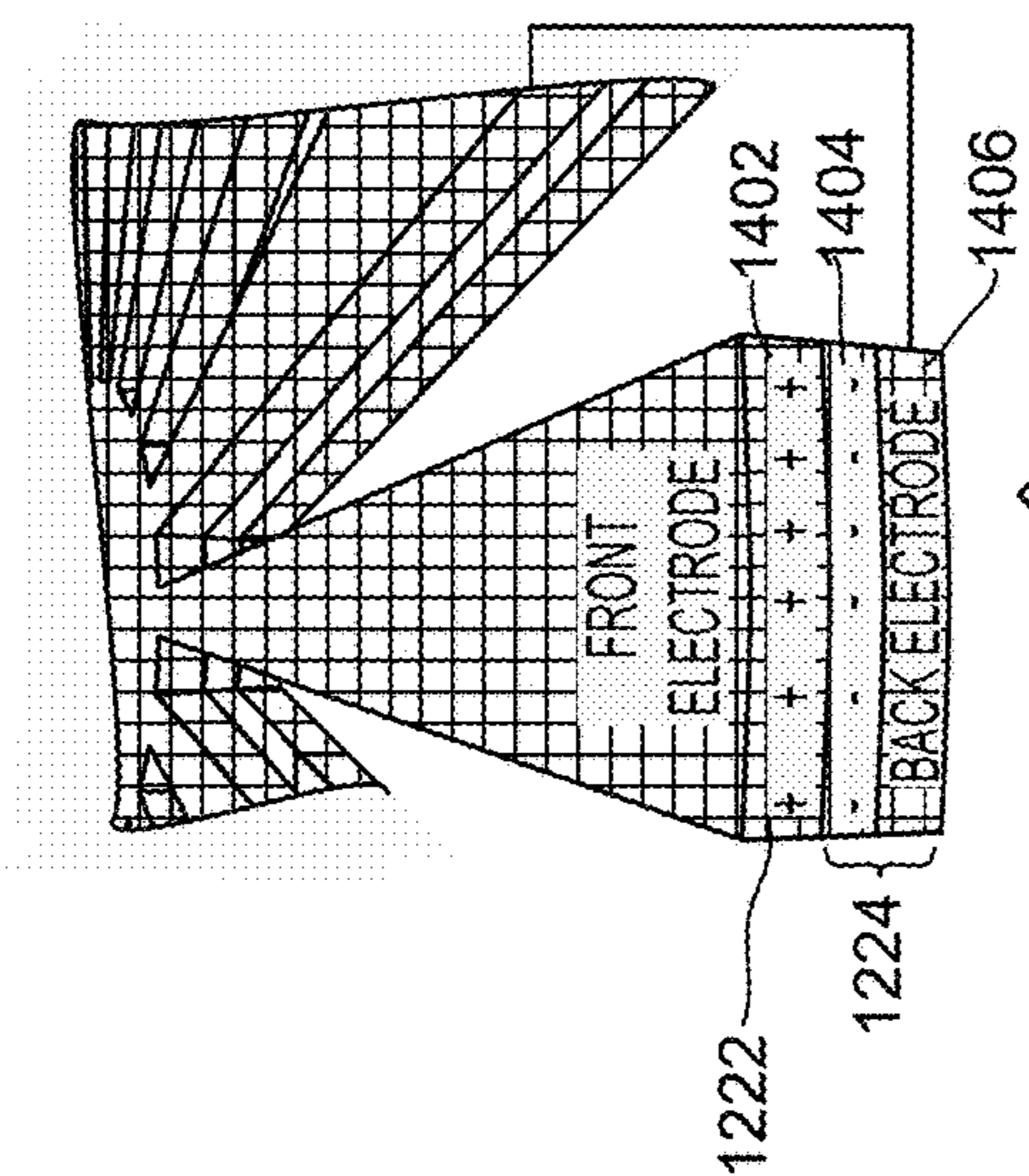


FIG. 14A

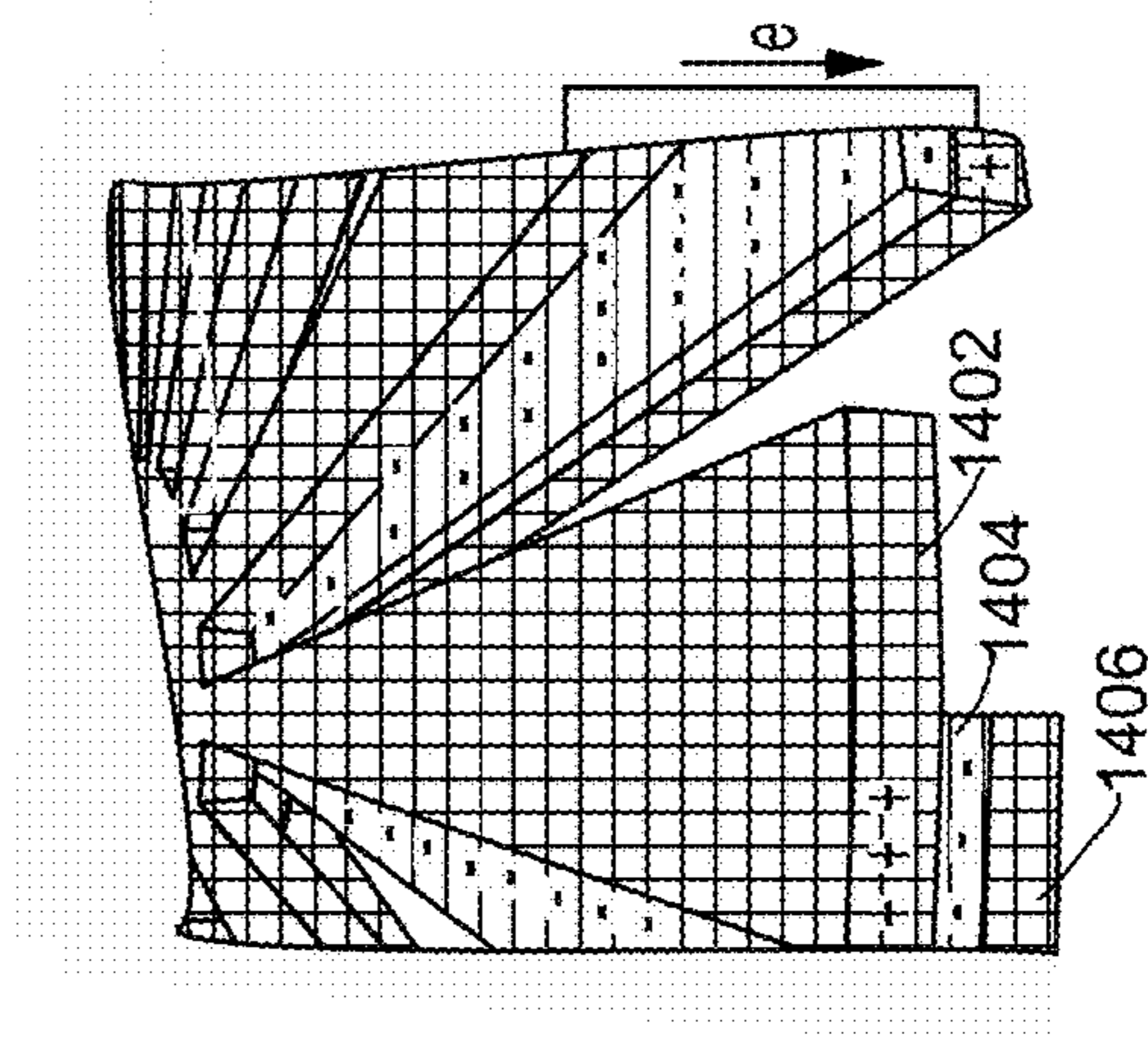


FIG. 14D

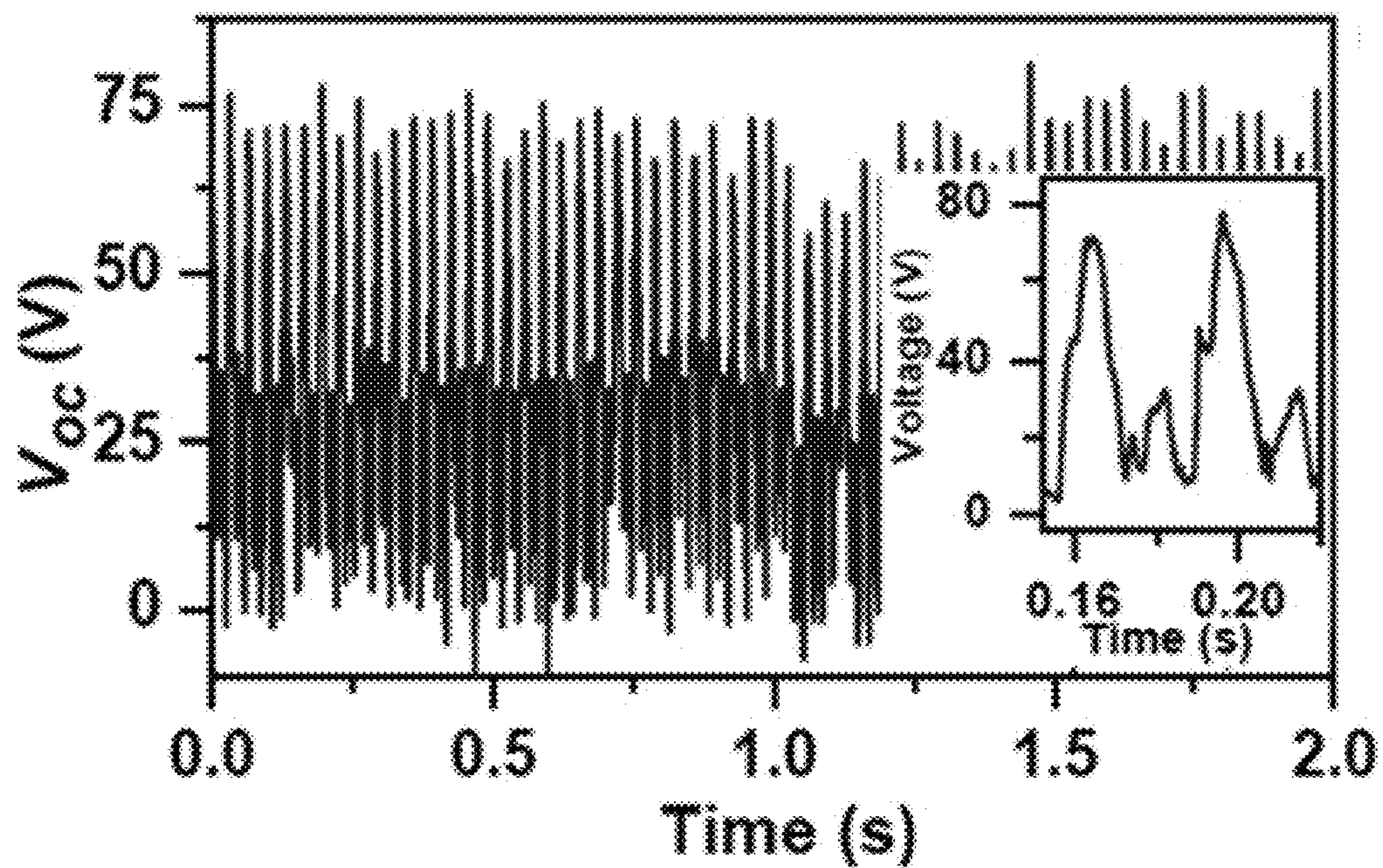


FIG. 15A

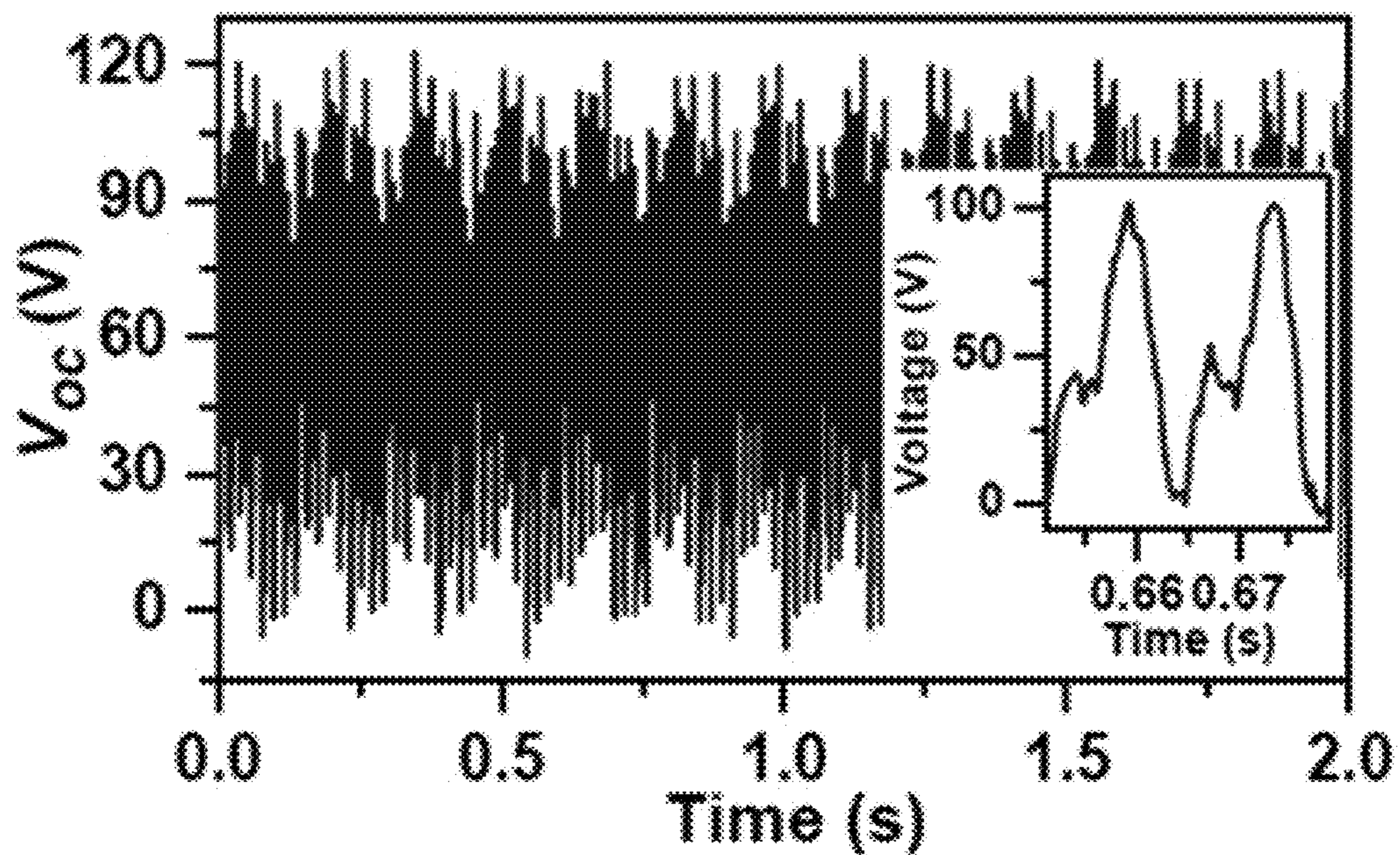


FIG. 15B

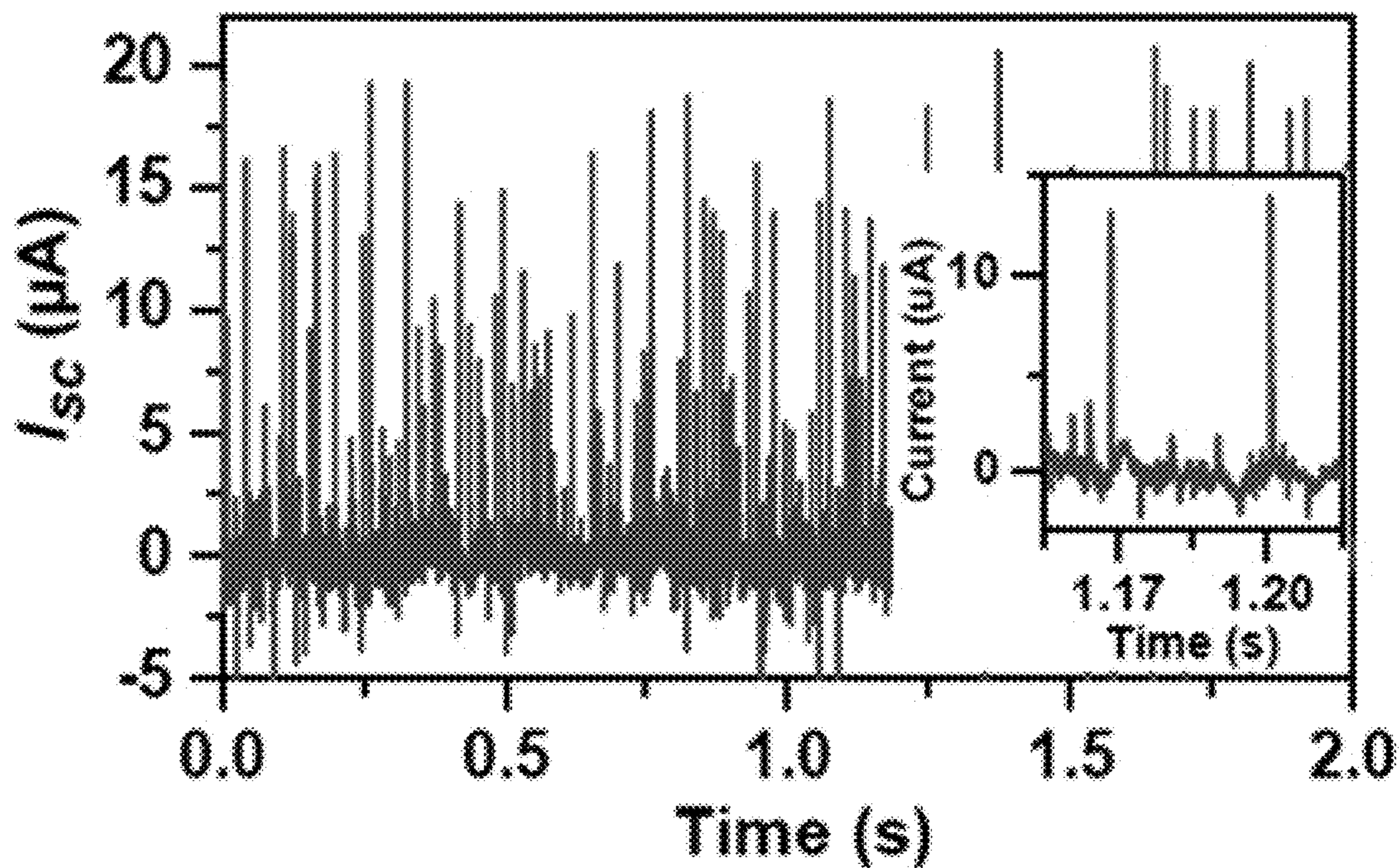


FIG. 15C

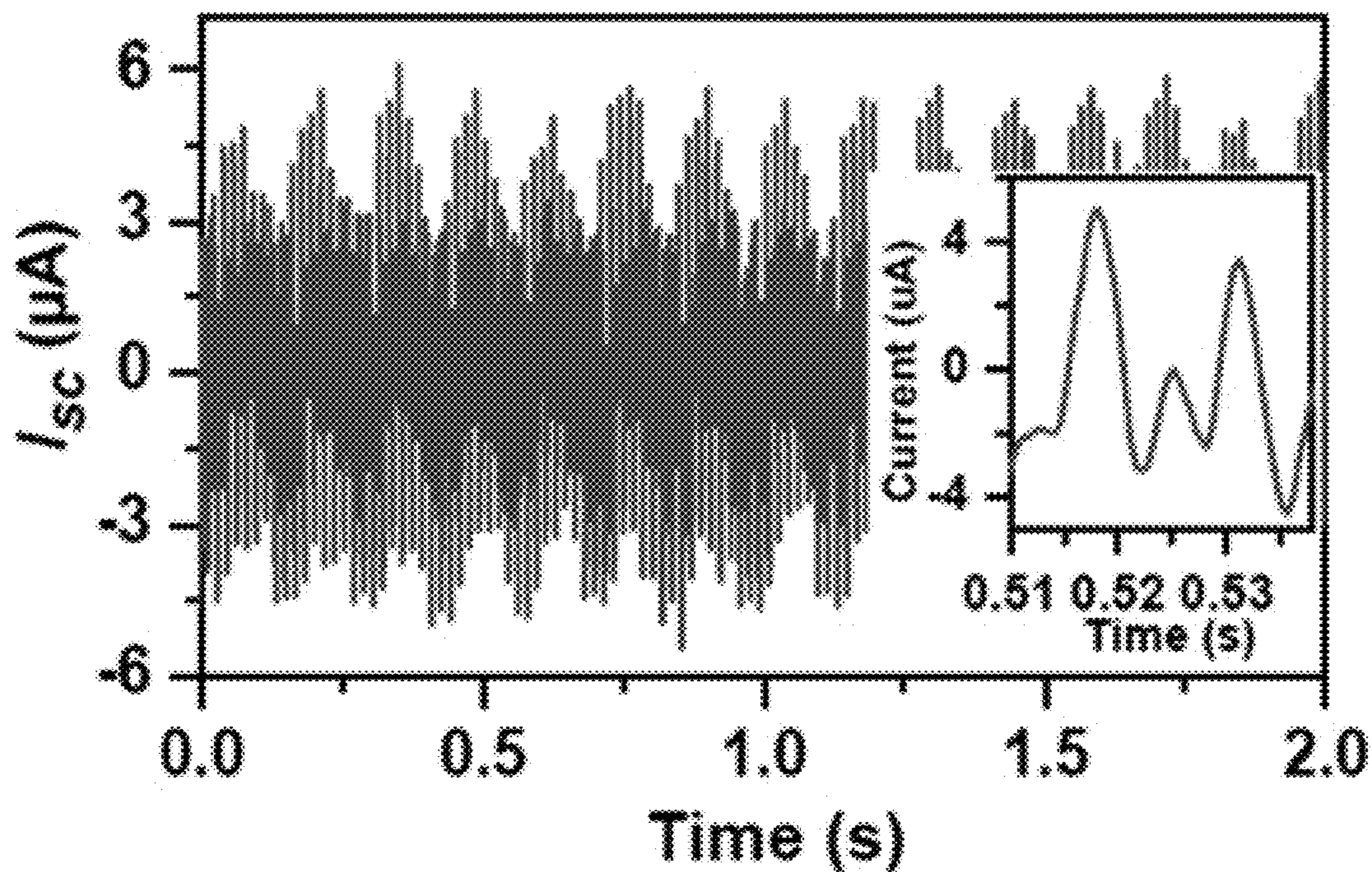


FIG. 15D

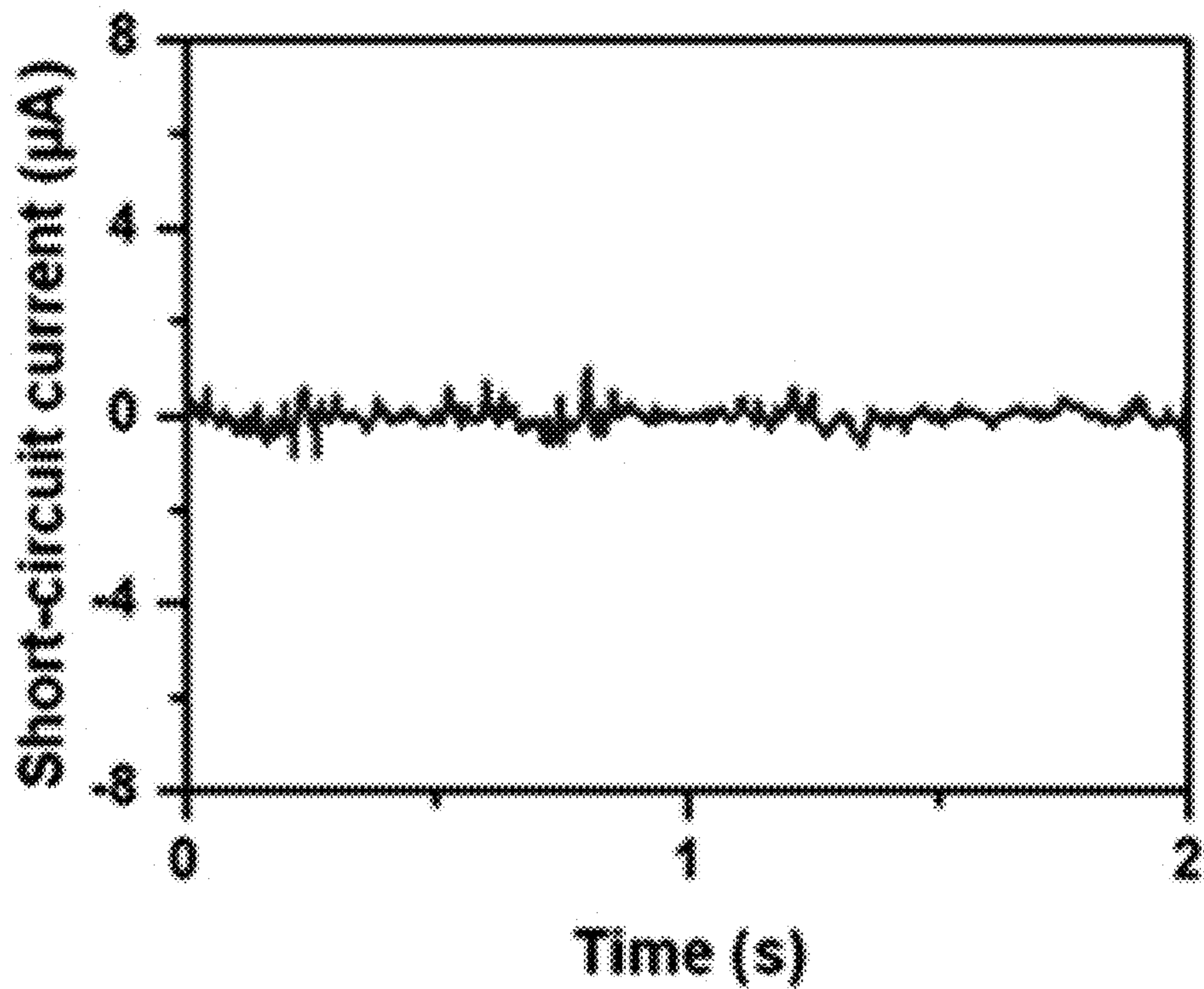


FIG. 16A

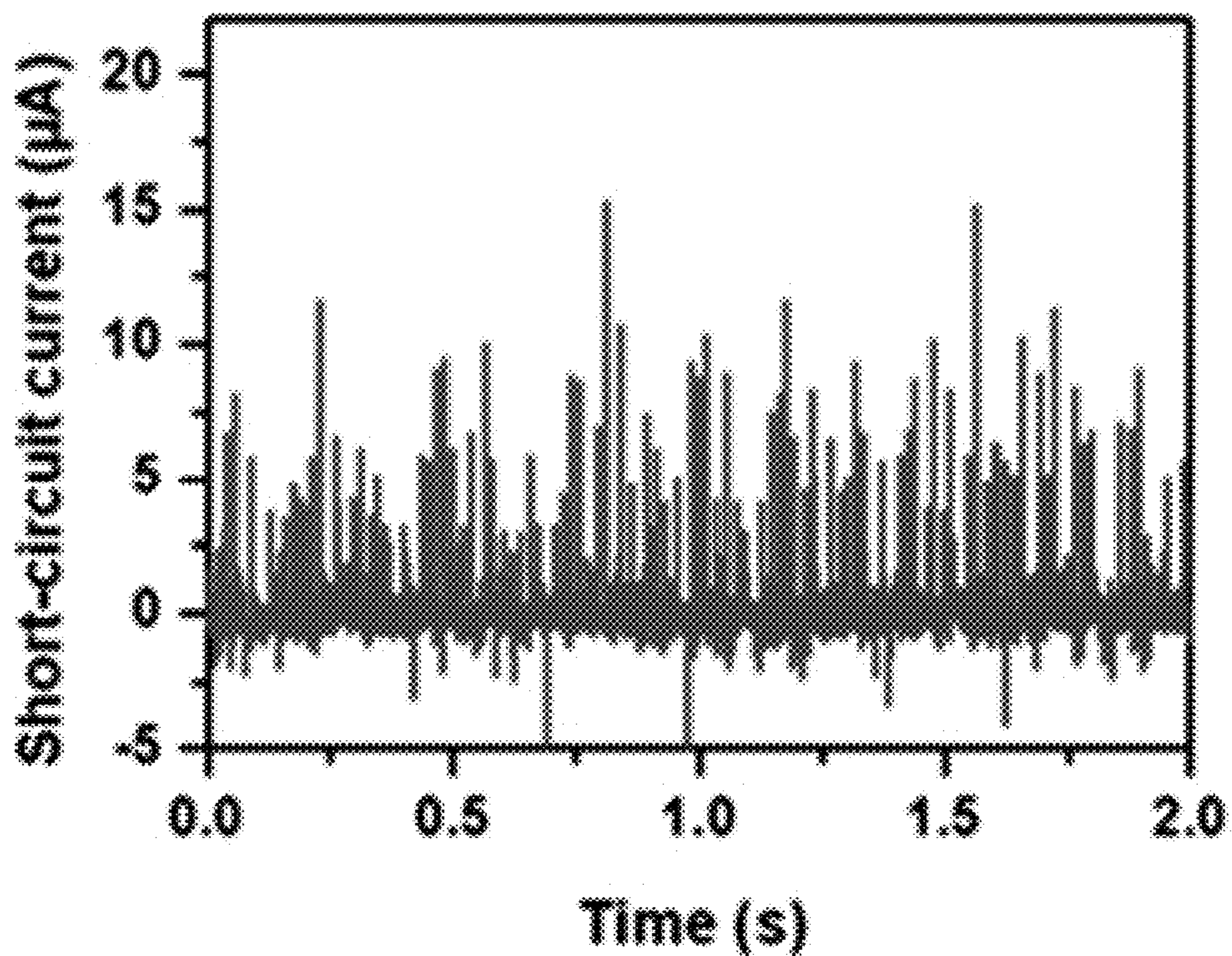


FIG. 16B

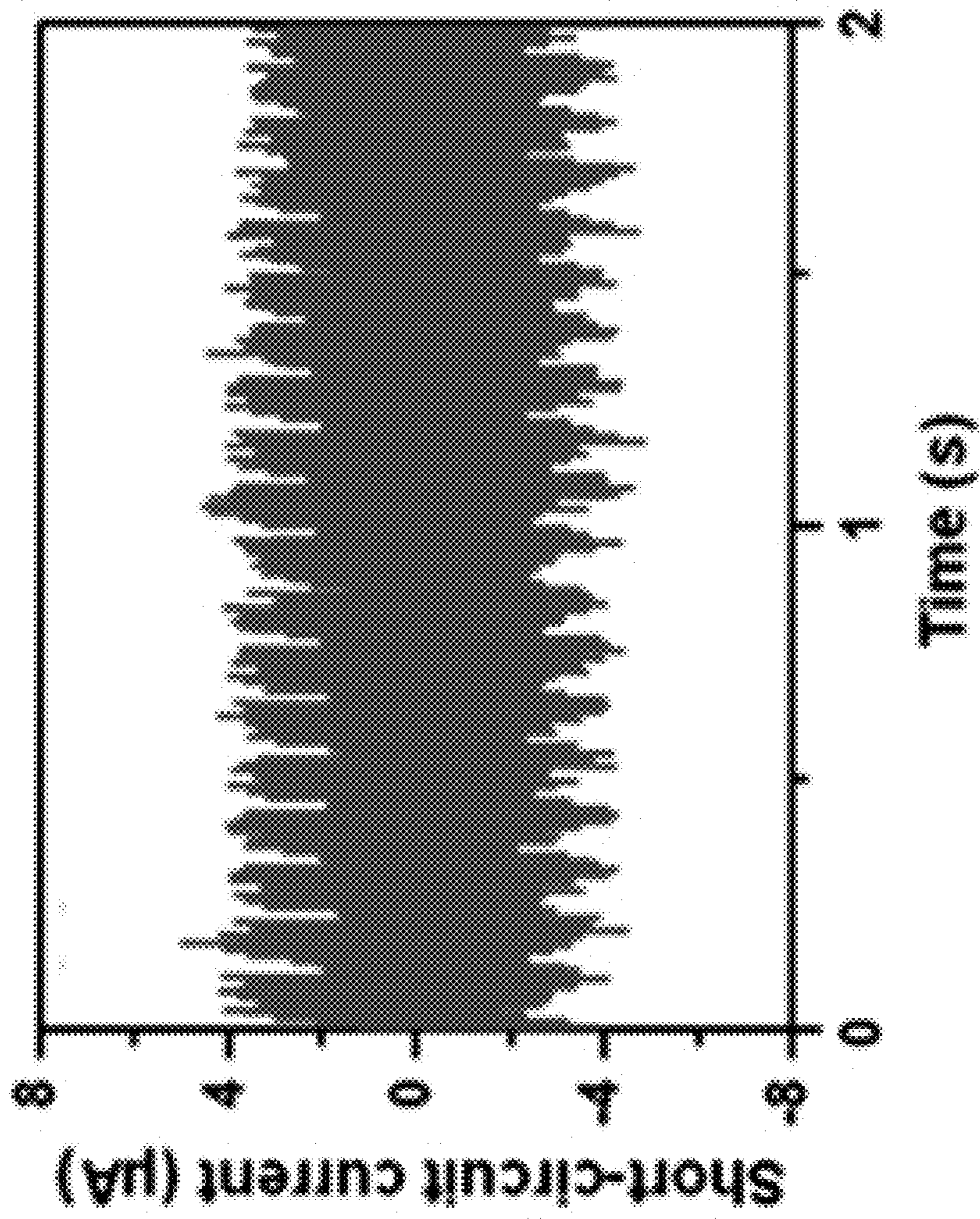


FIG. 16C



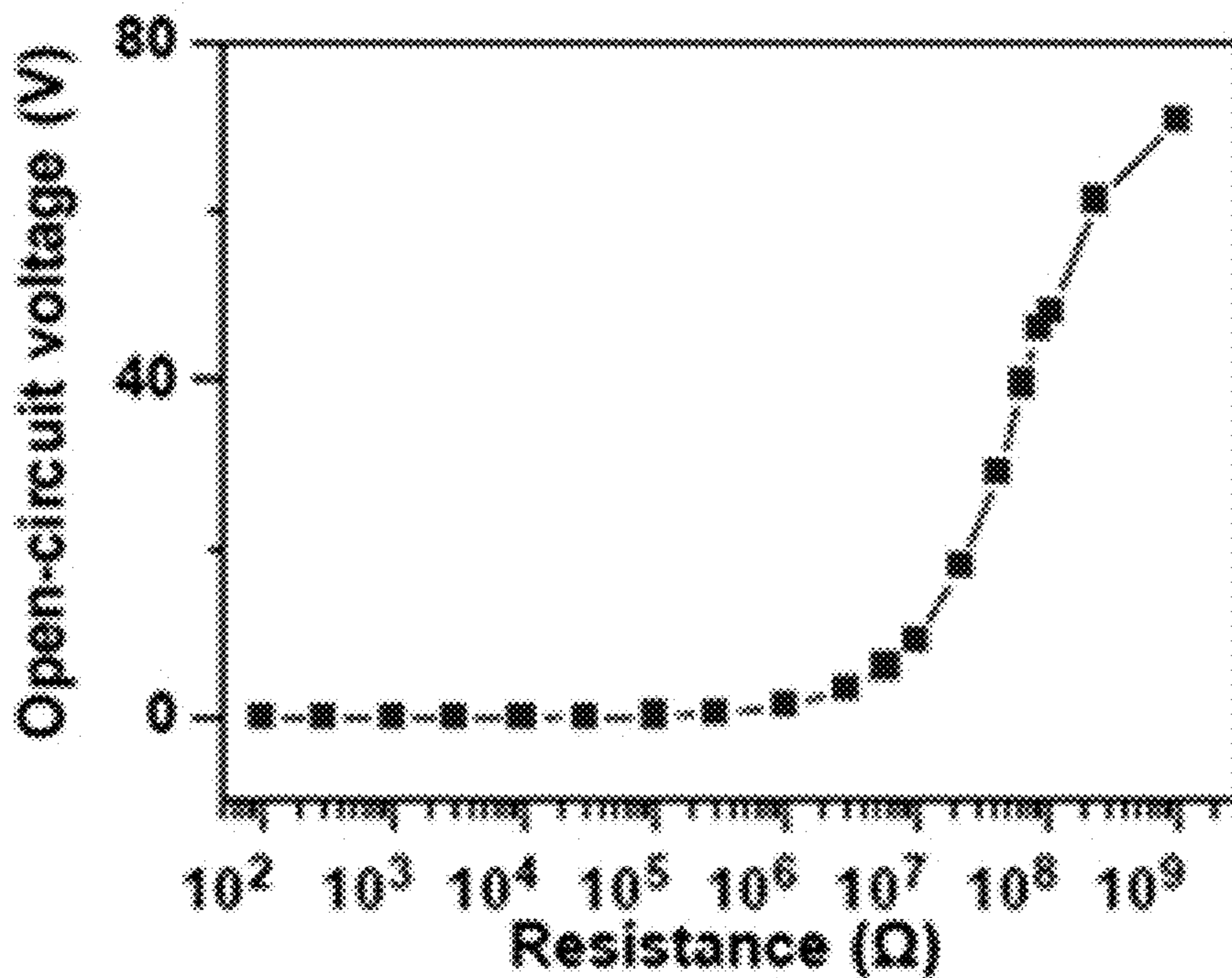


FIG. 17A

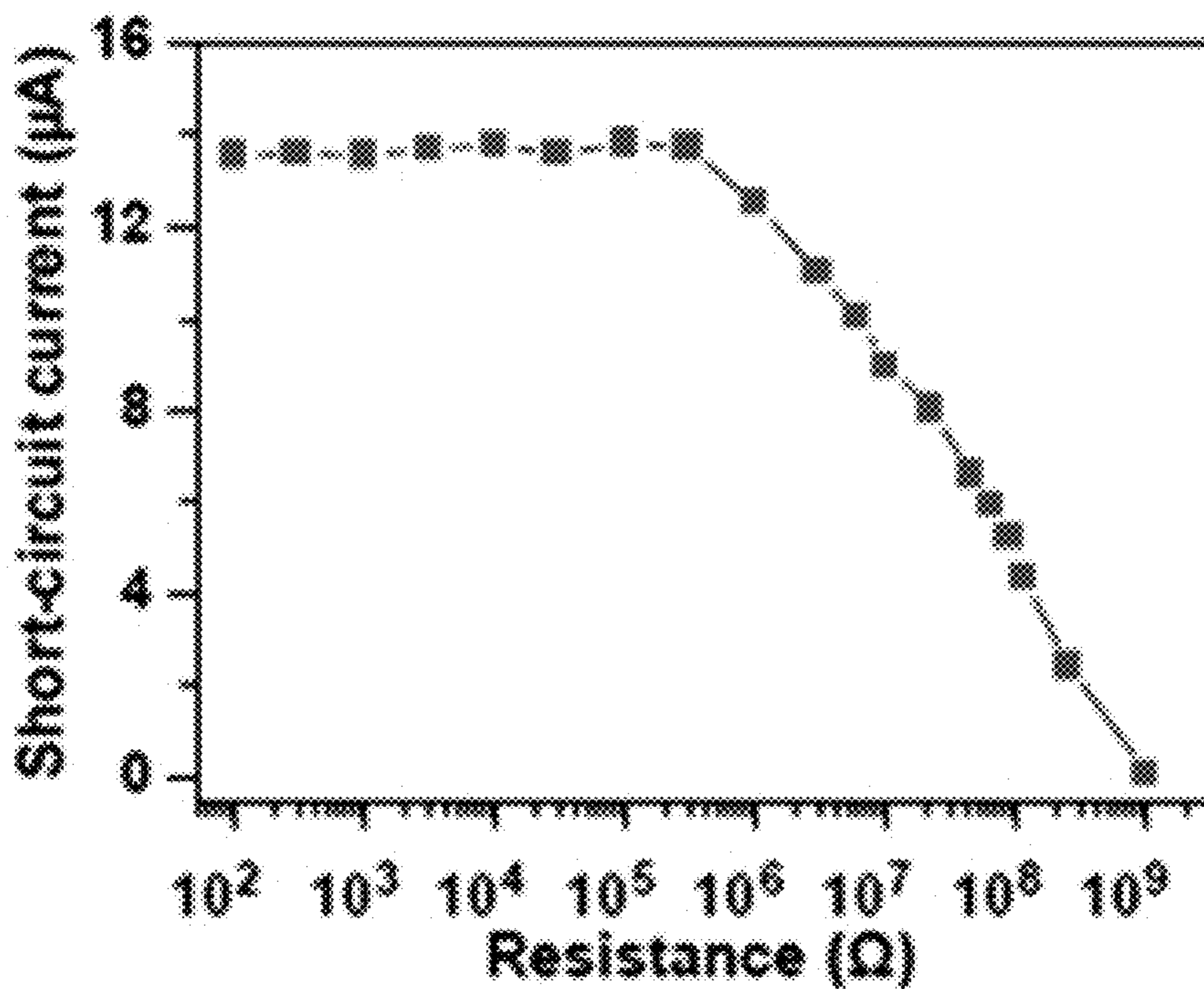


FIG. 17B

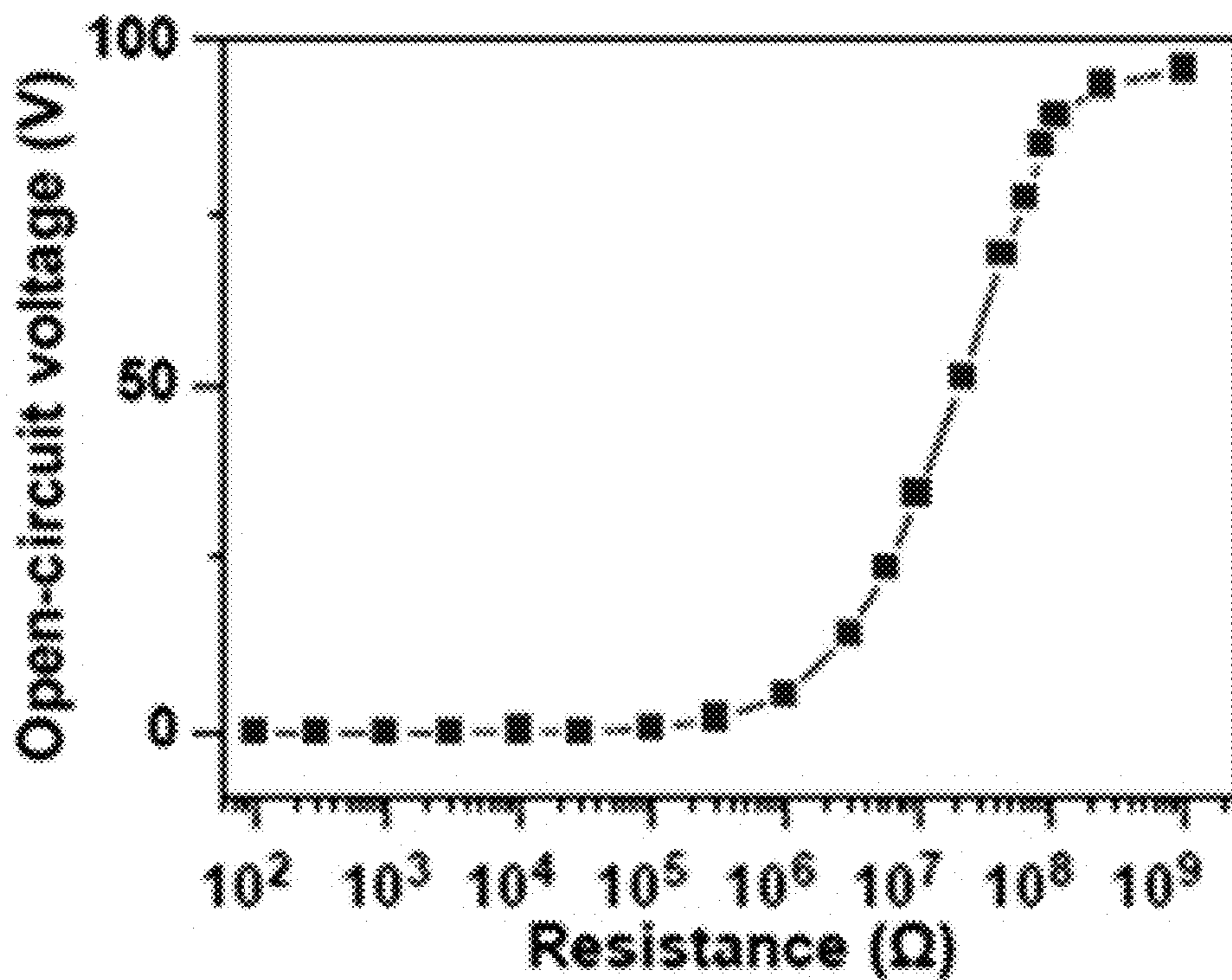


FIG. 17C

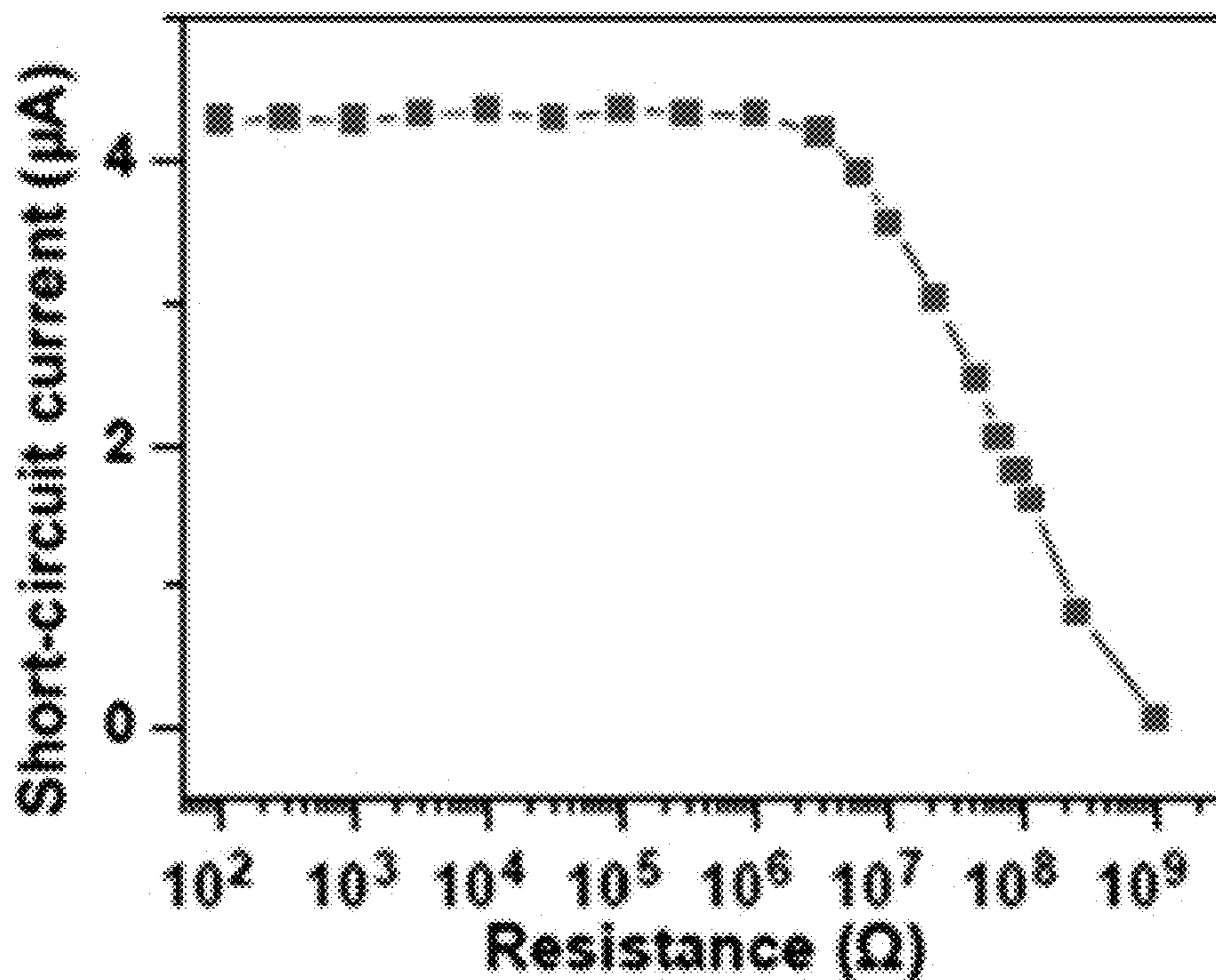


FIG. 17D

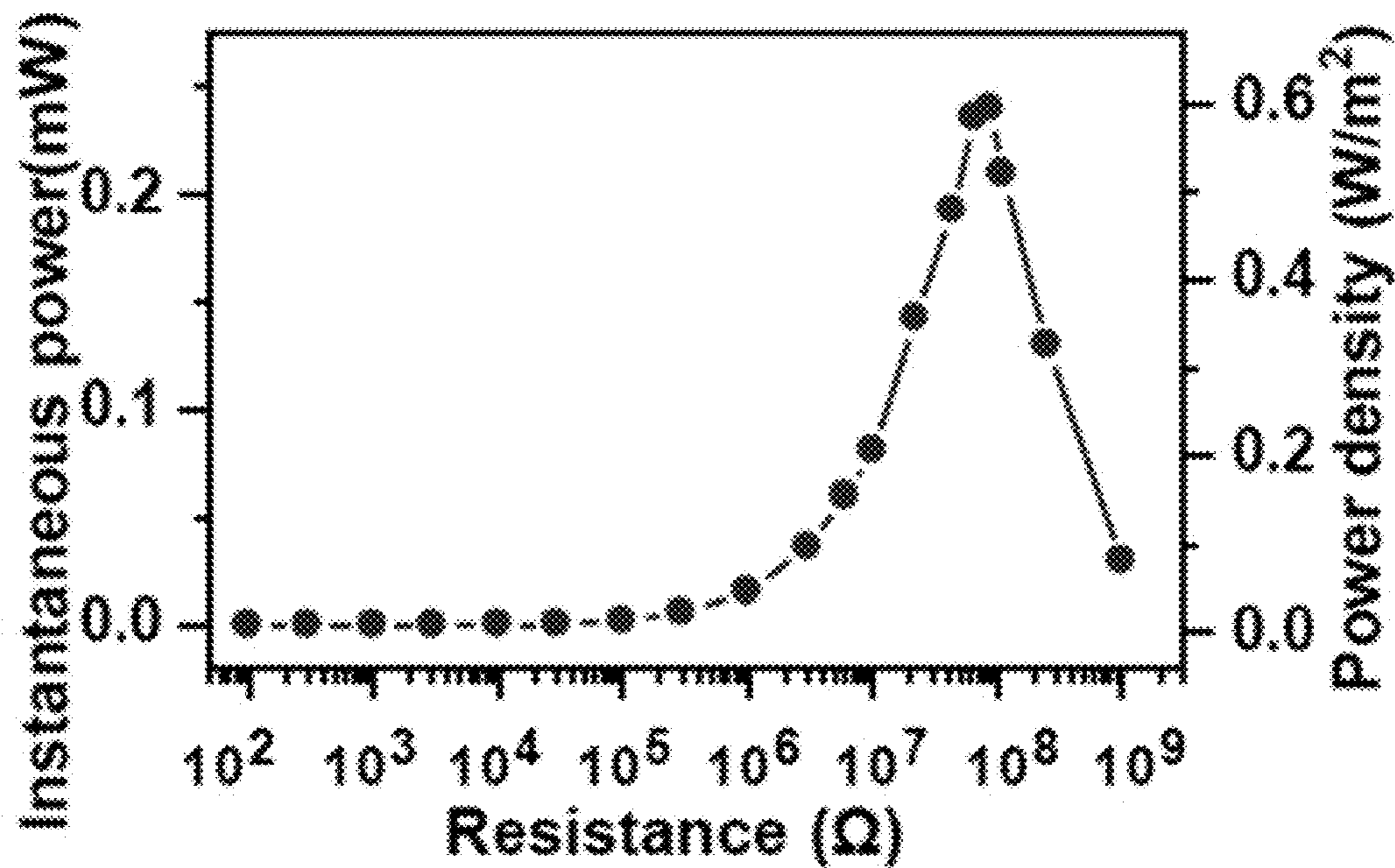


FIG. 18A

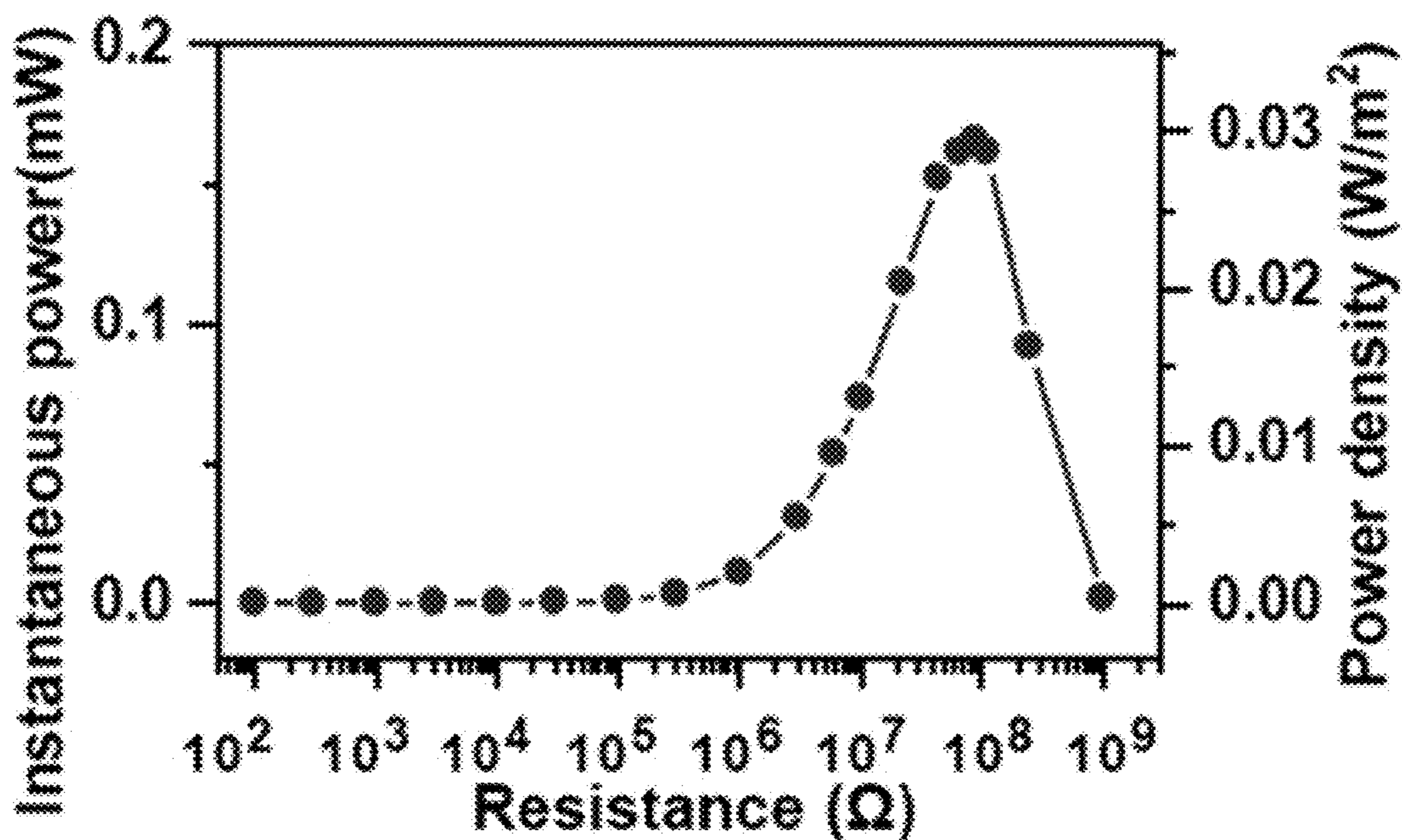


FIG. 18B

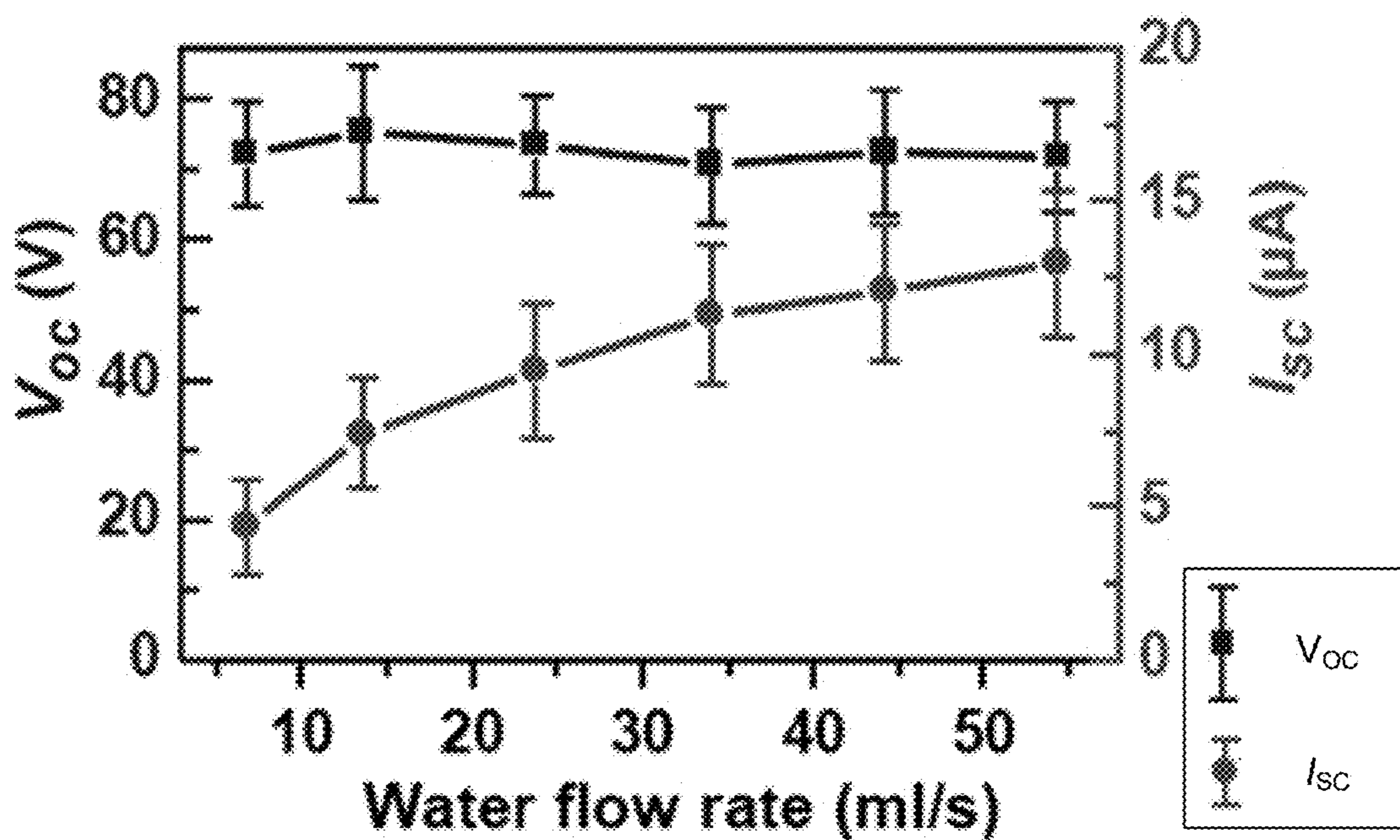


FIG. 18C

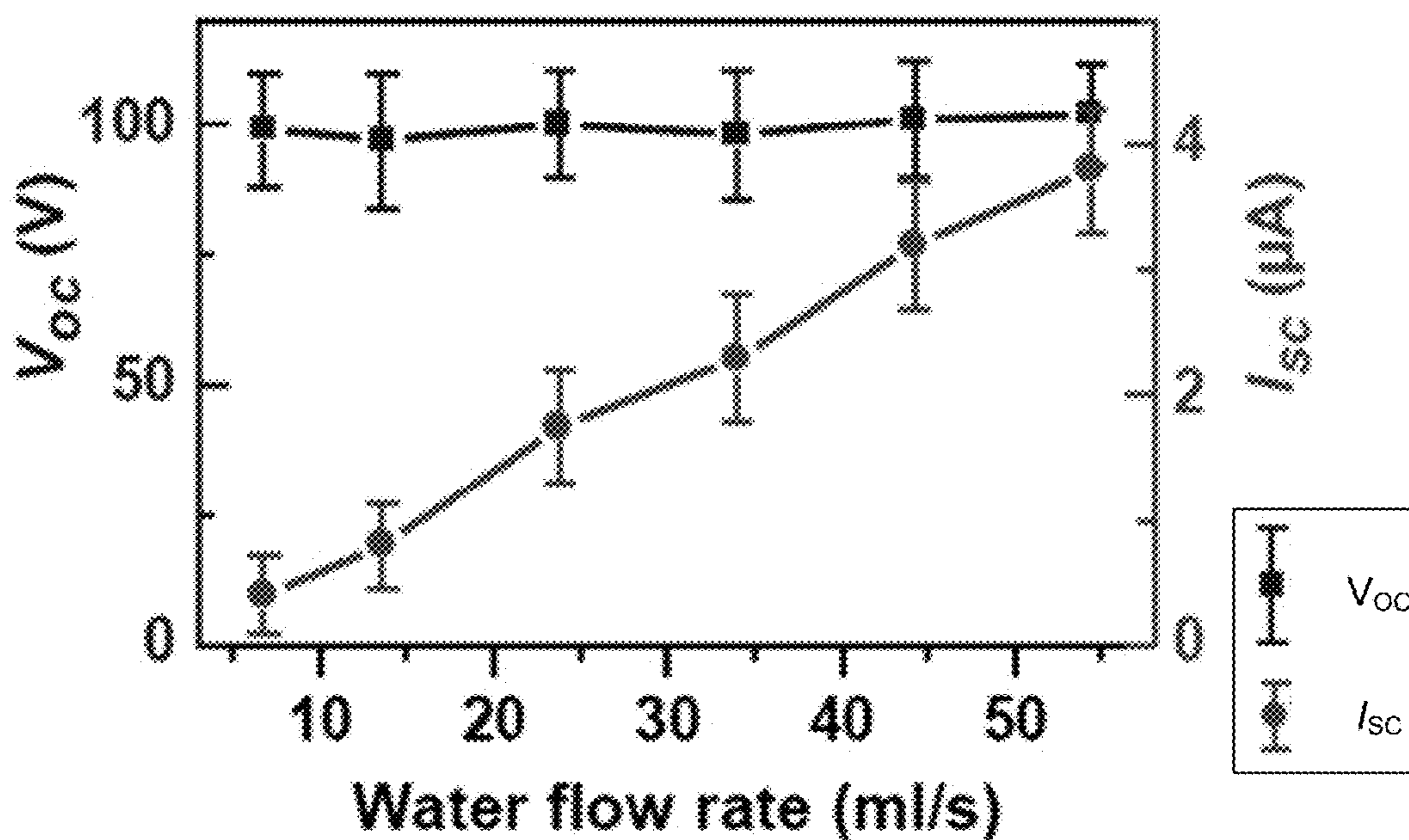


FIG. 18D

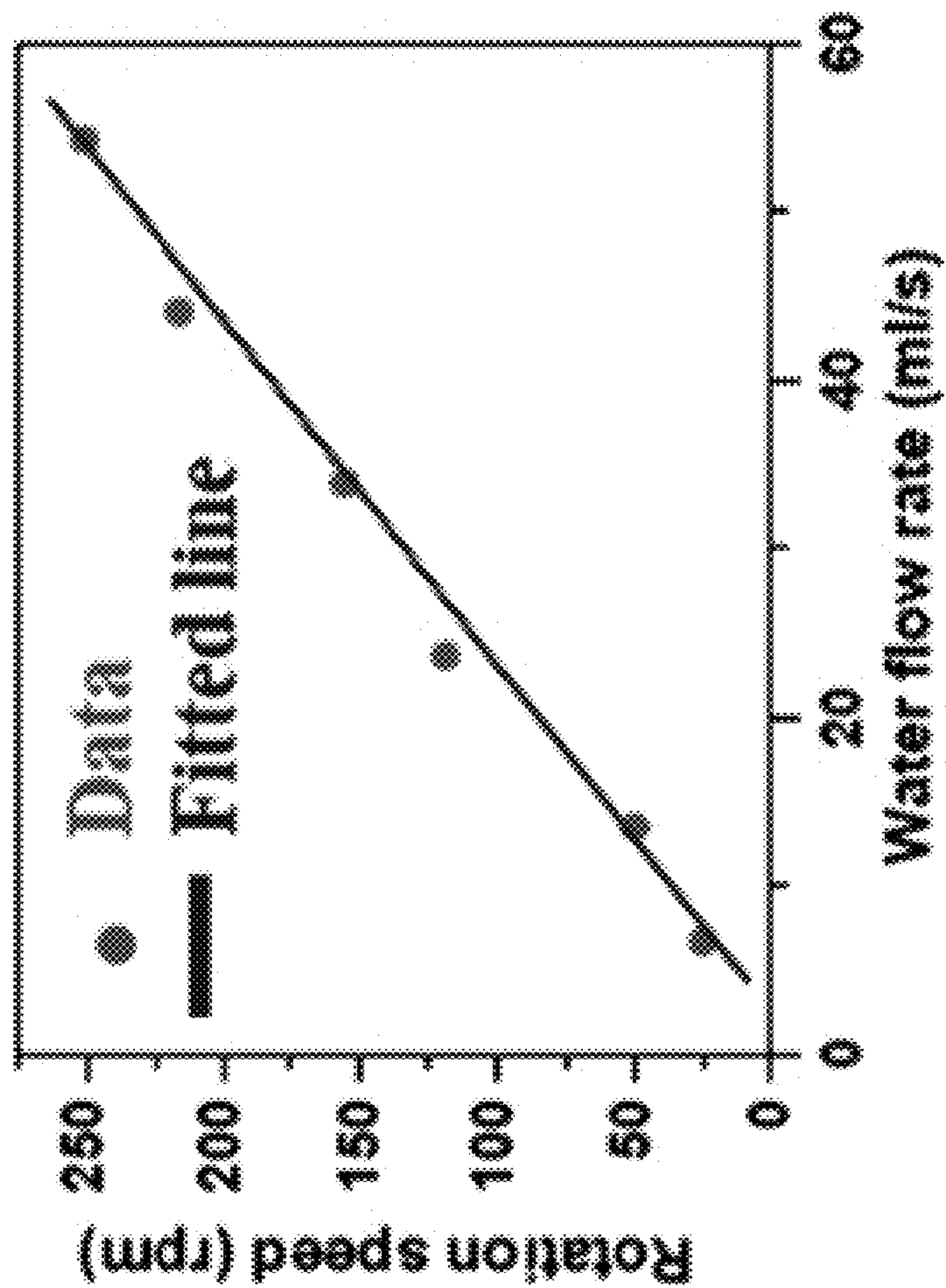


FIG. 19

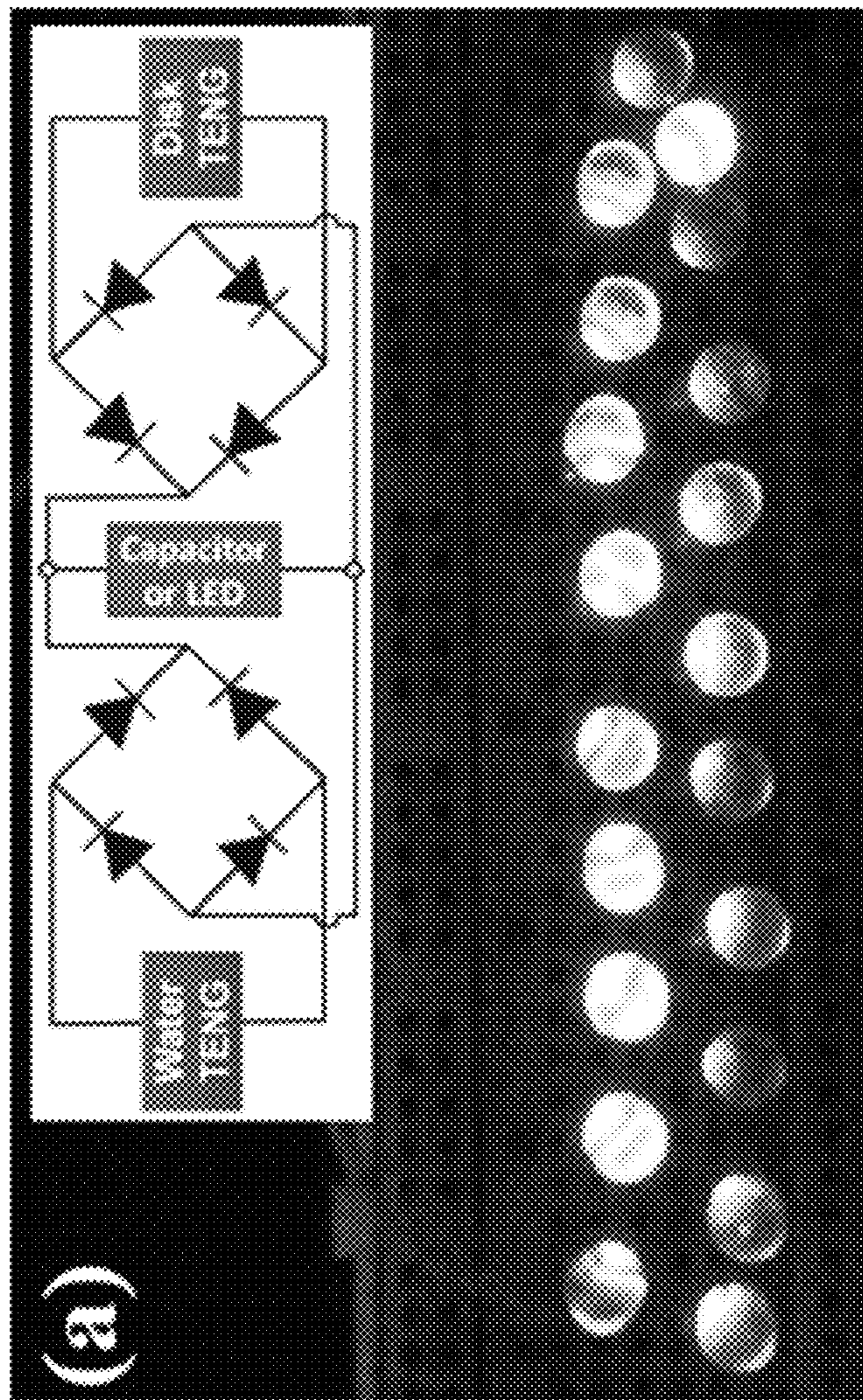


FIG. 20A

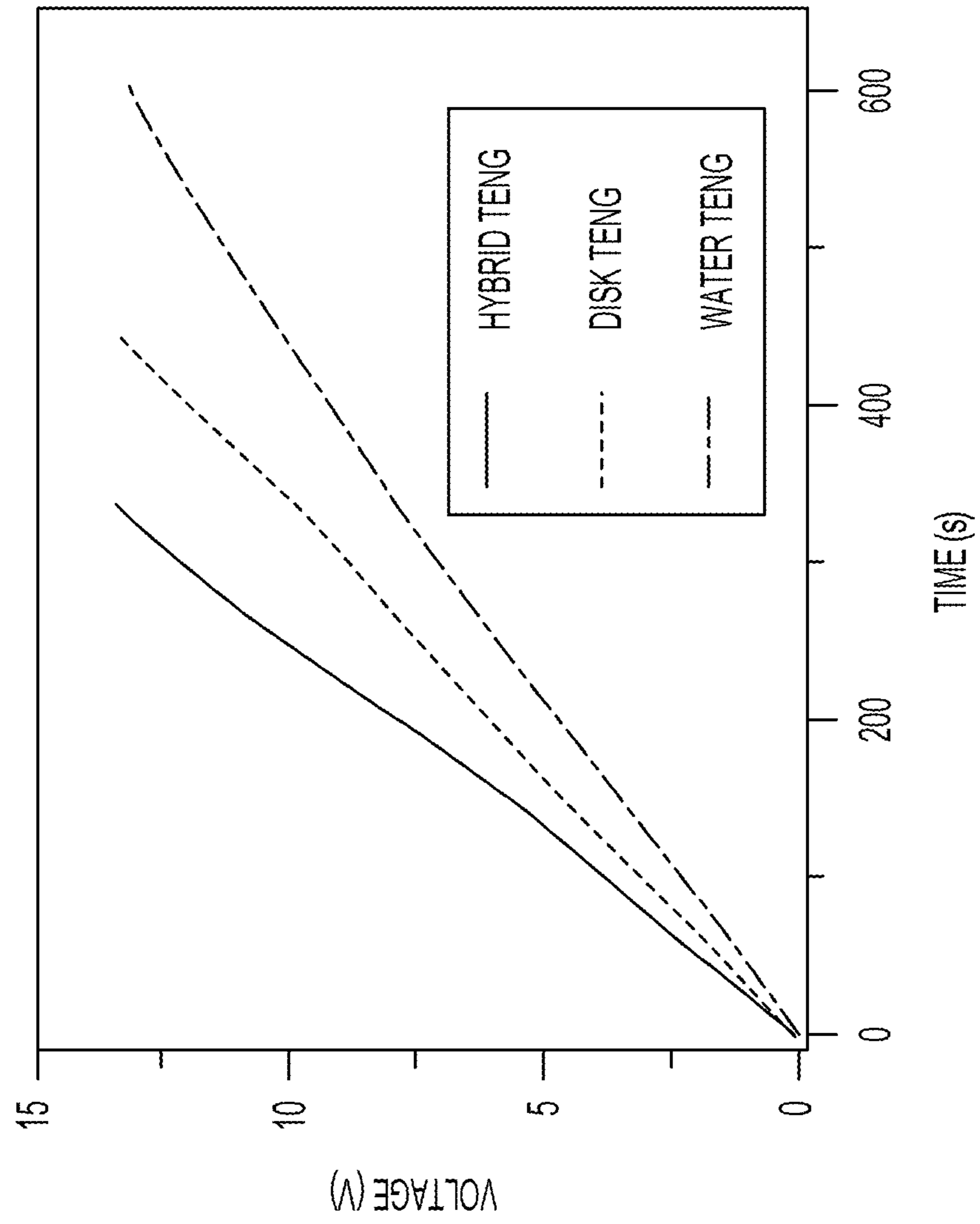


FIG. 20B

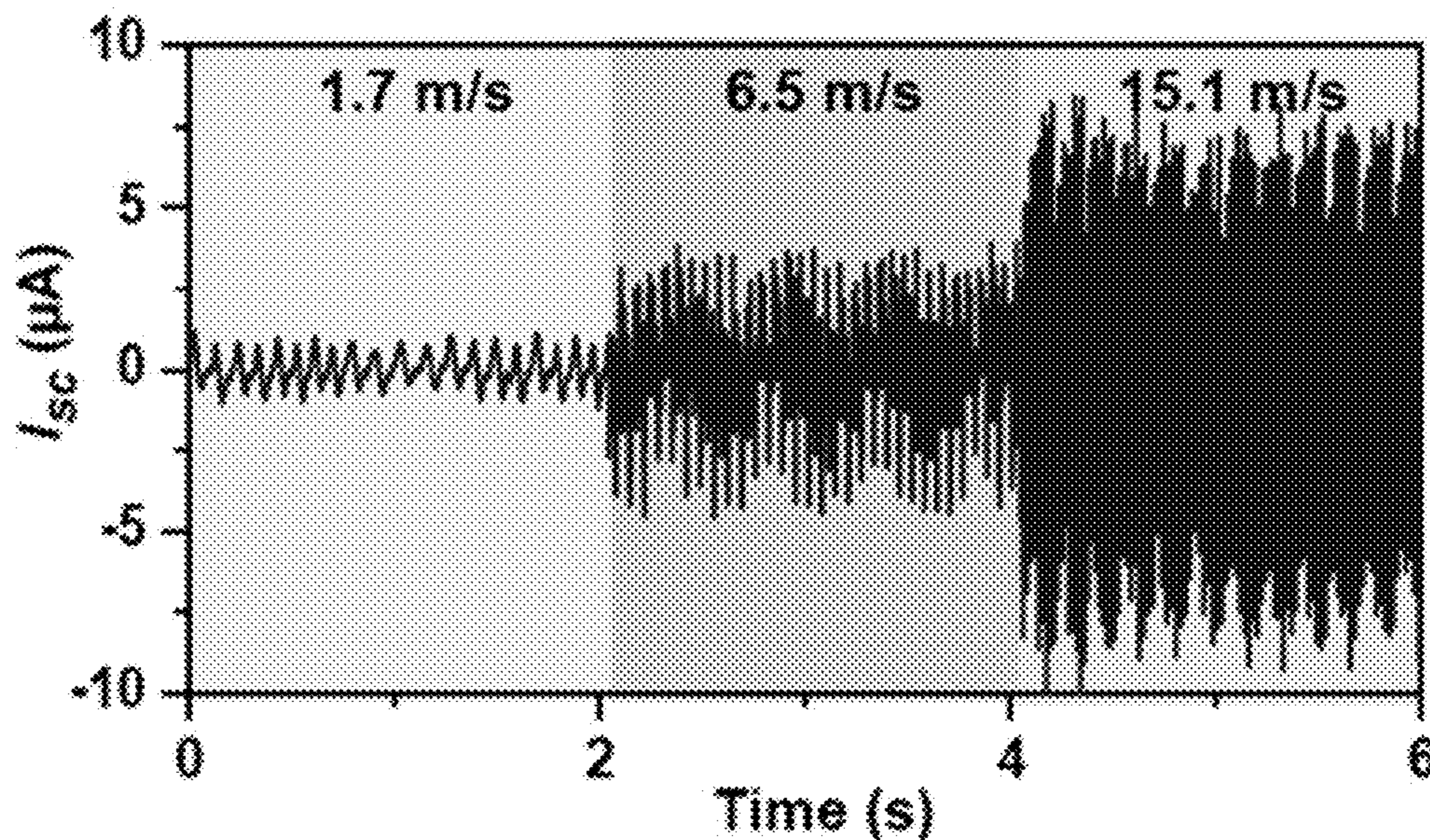


FIG. 21A

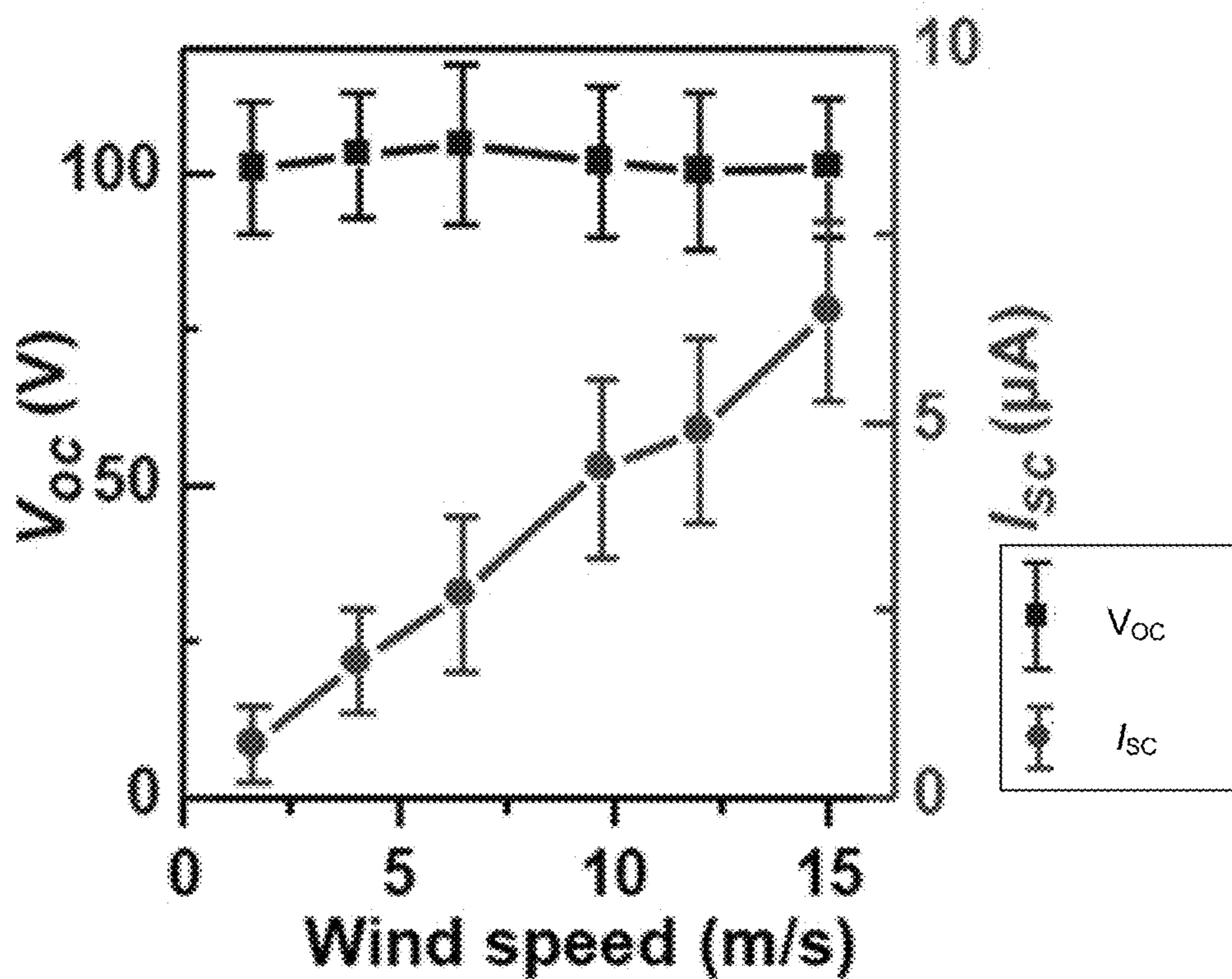


FIG. 21B



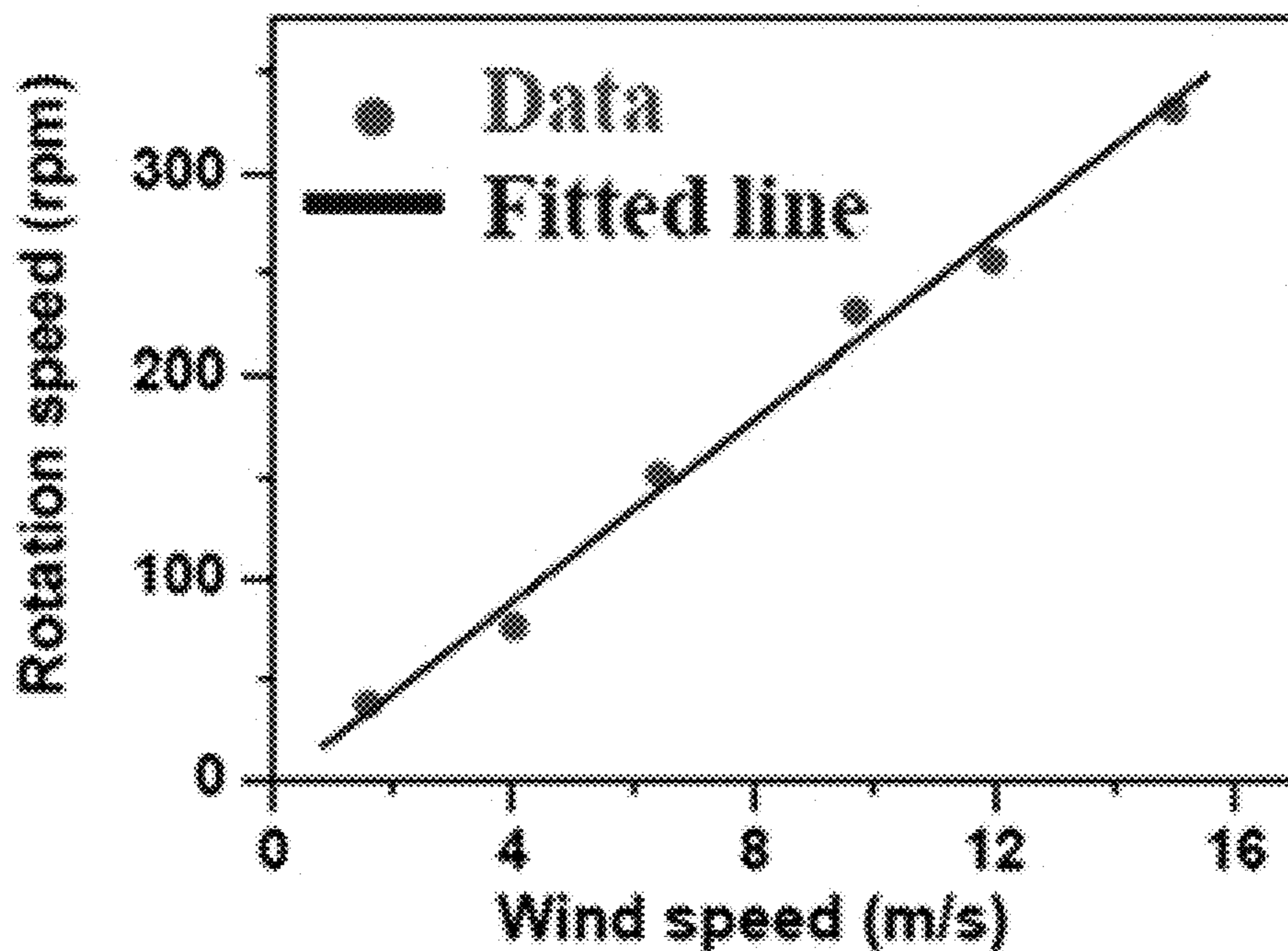


FIG. 22

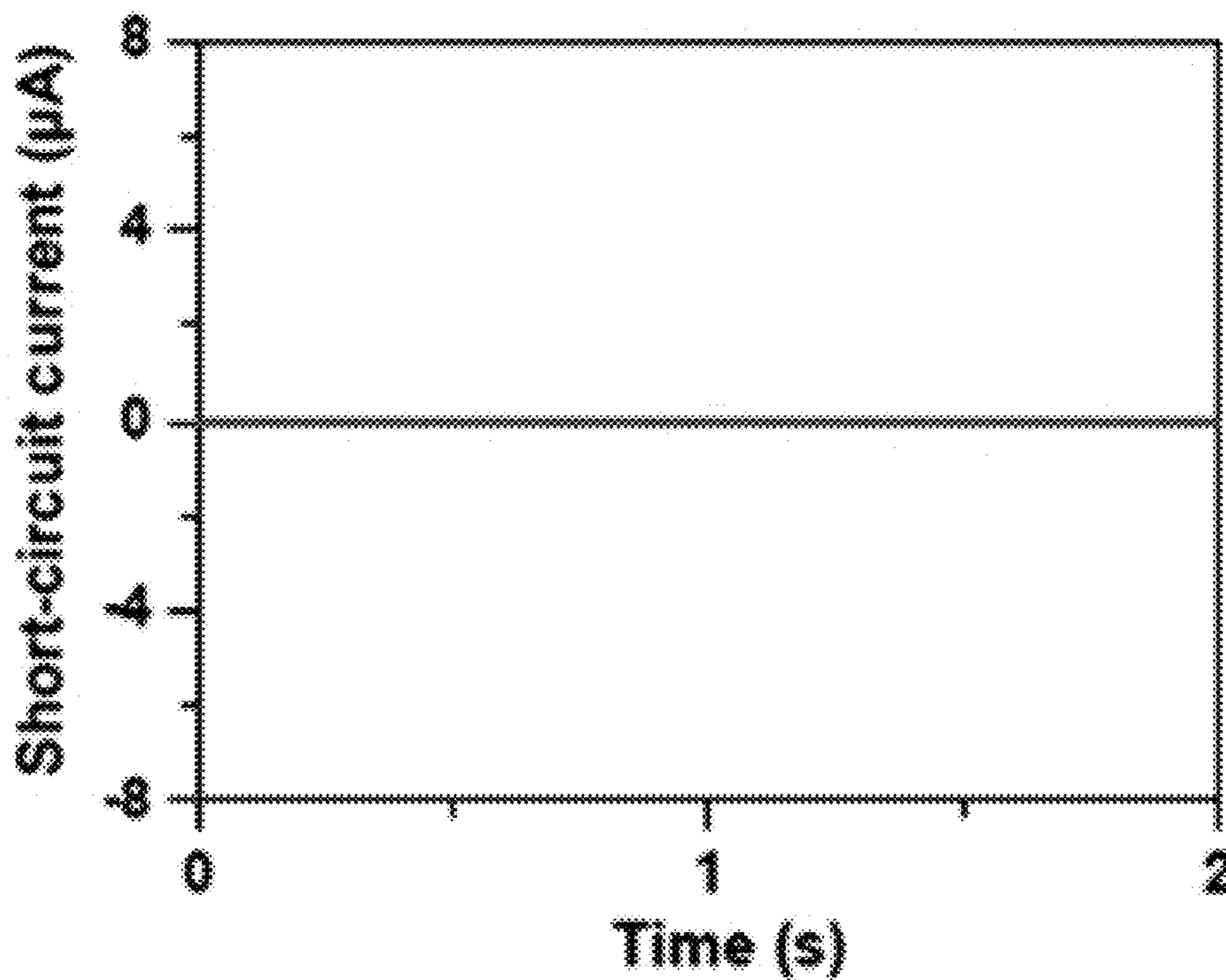


FIG. 23

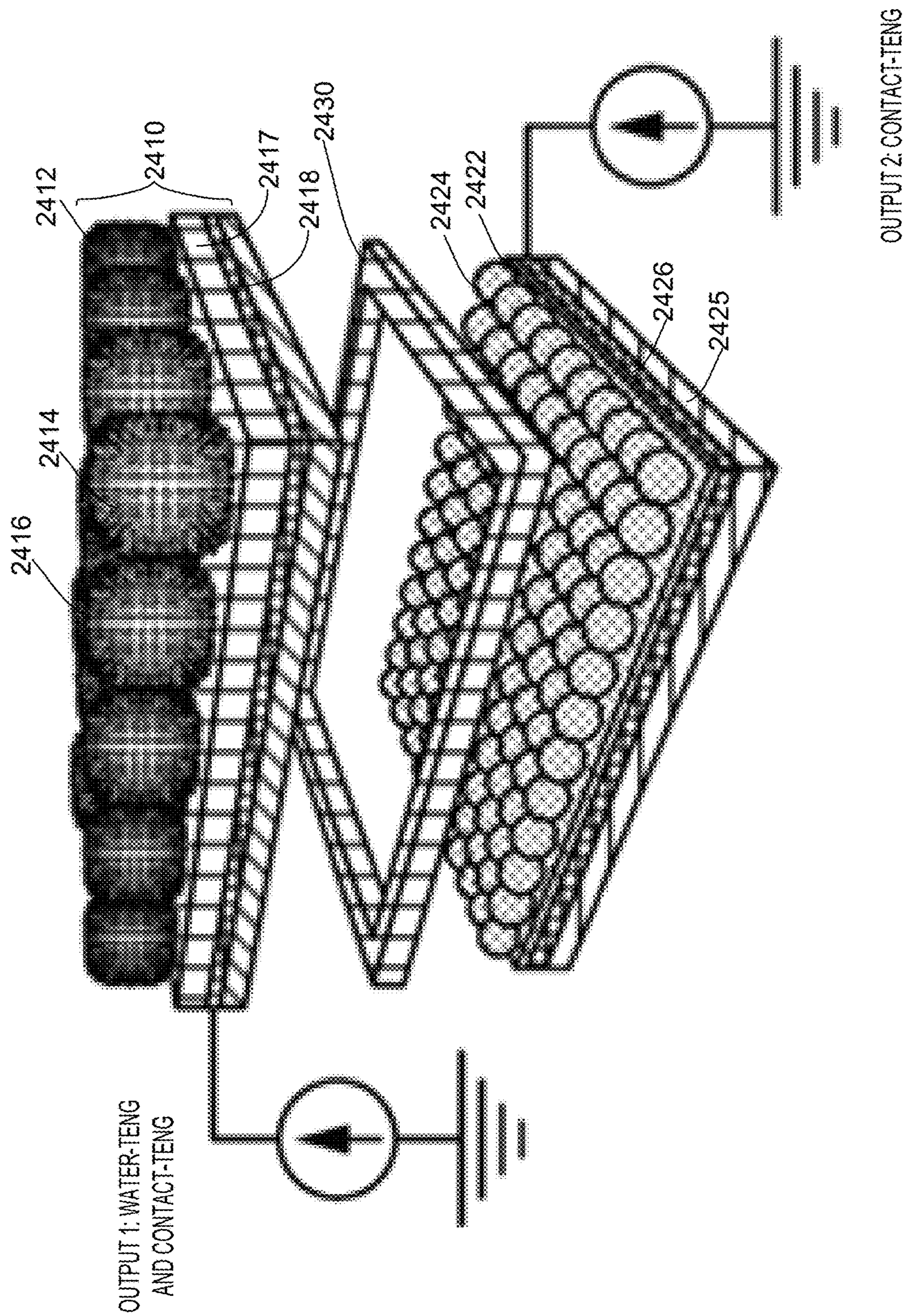


FIG. 24

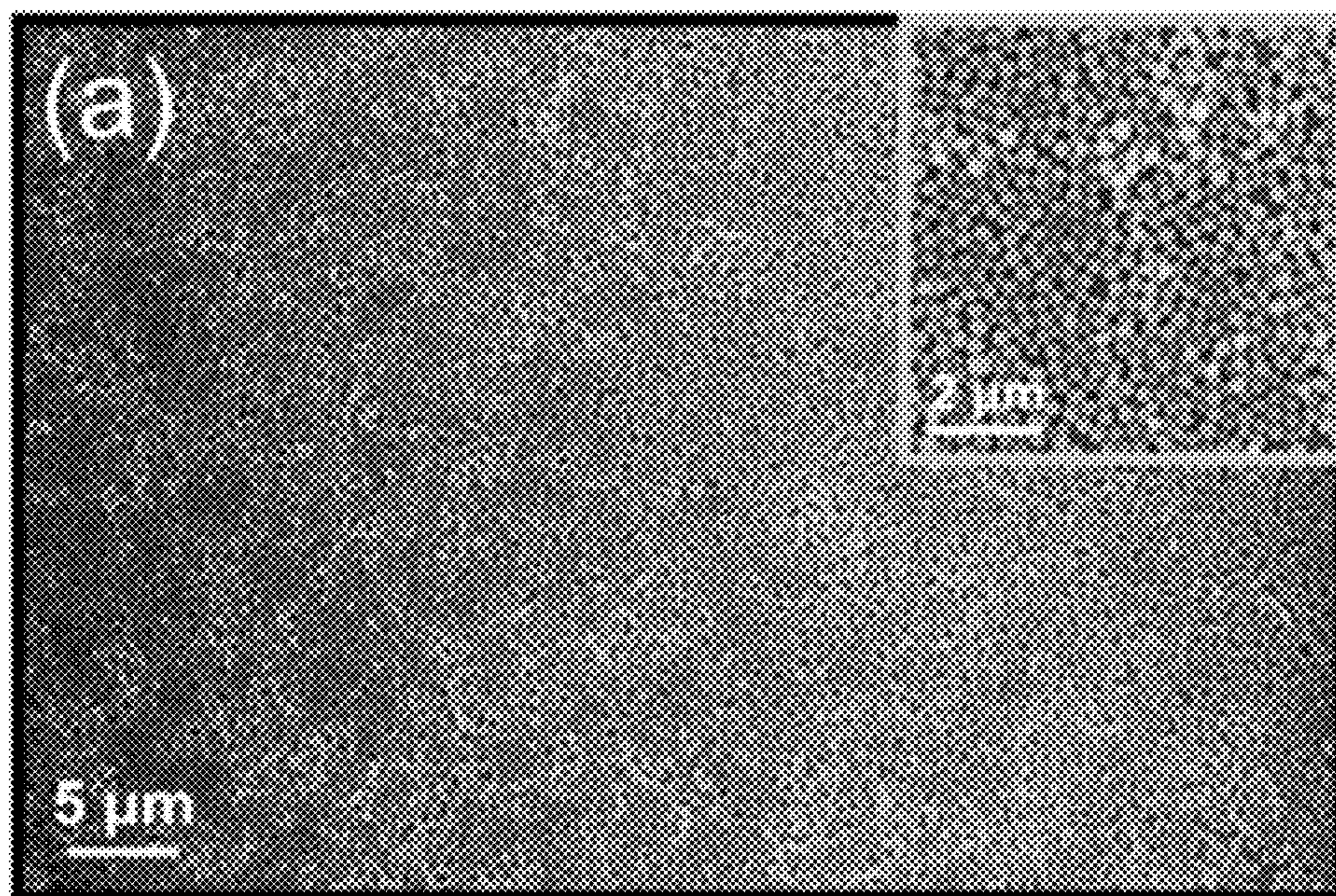


FIG. 25A

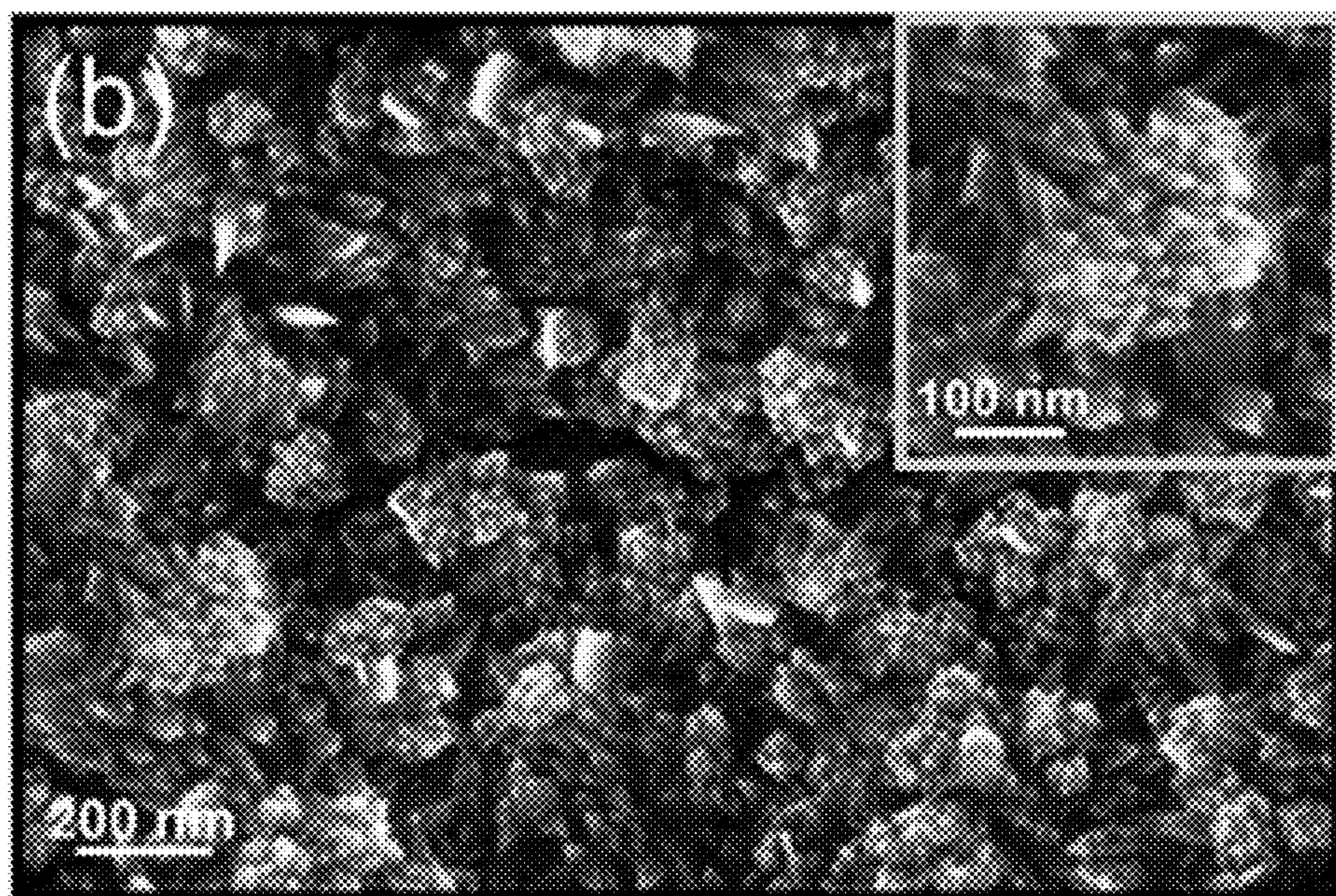


FIG. 25B

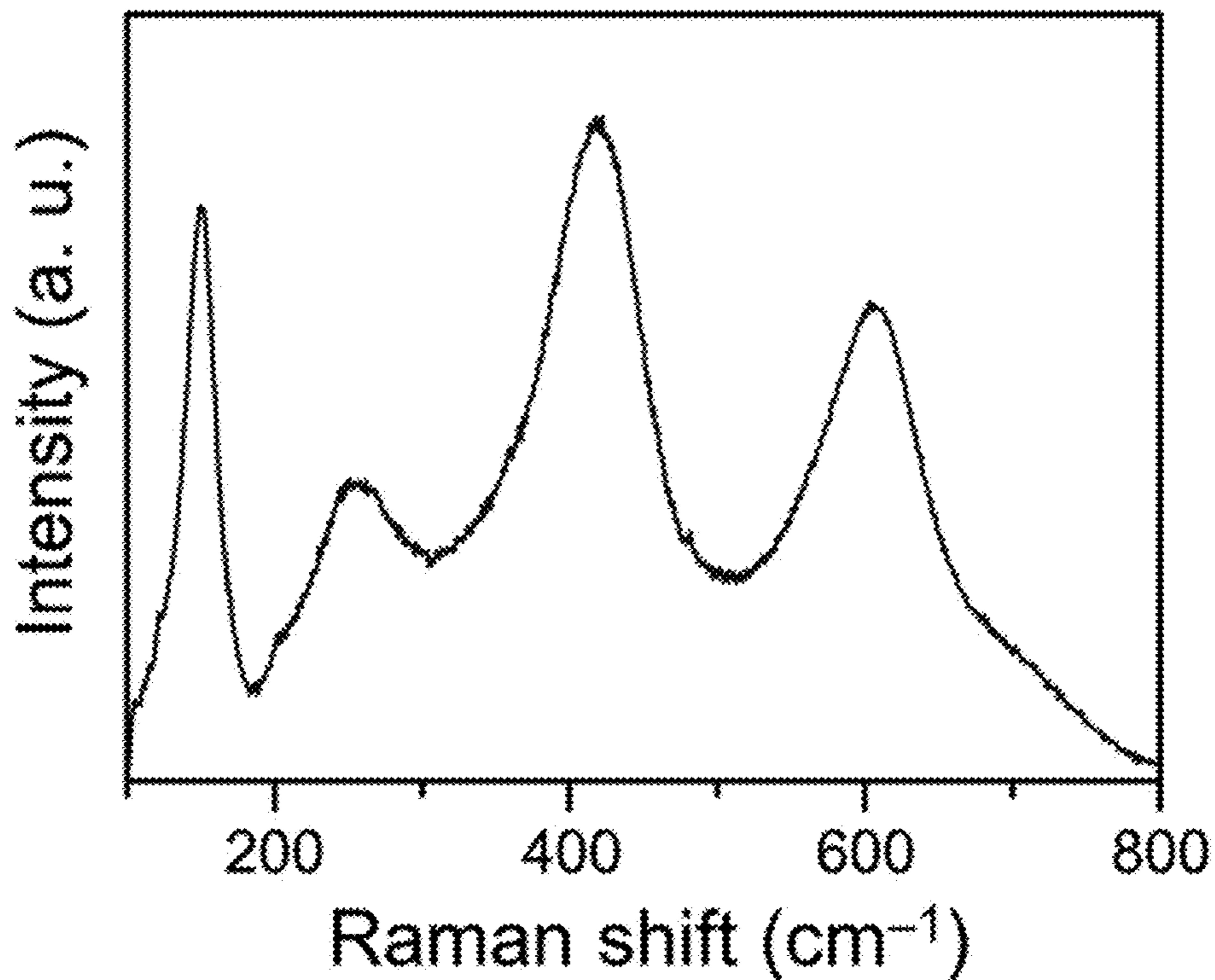


FIG. 26A

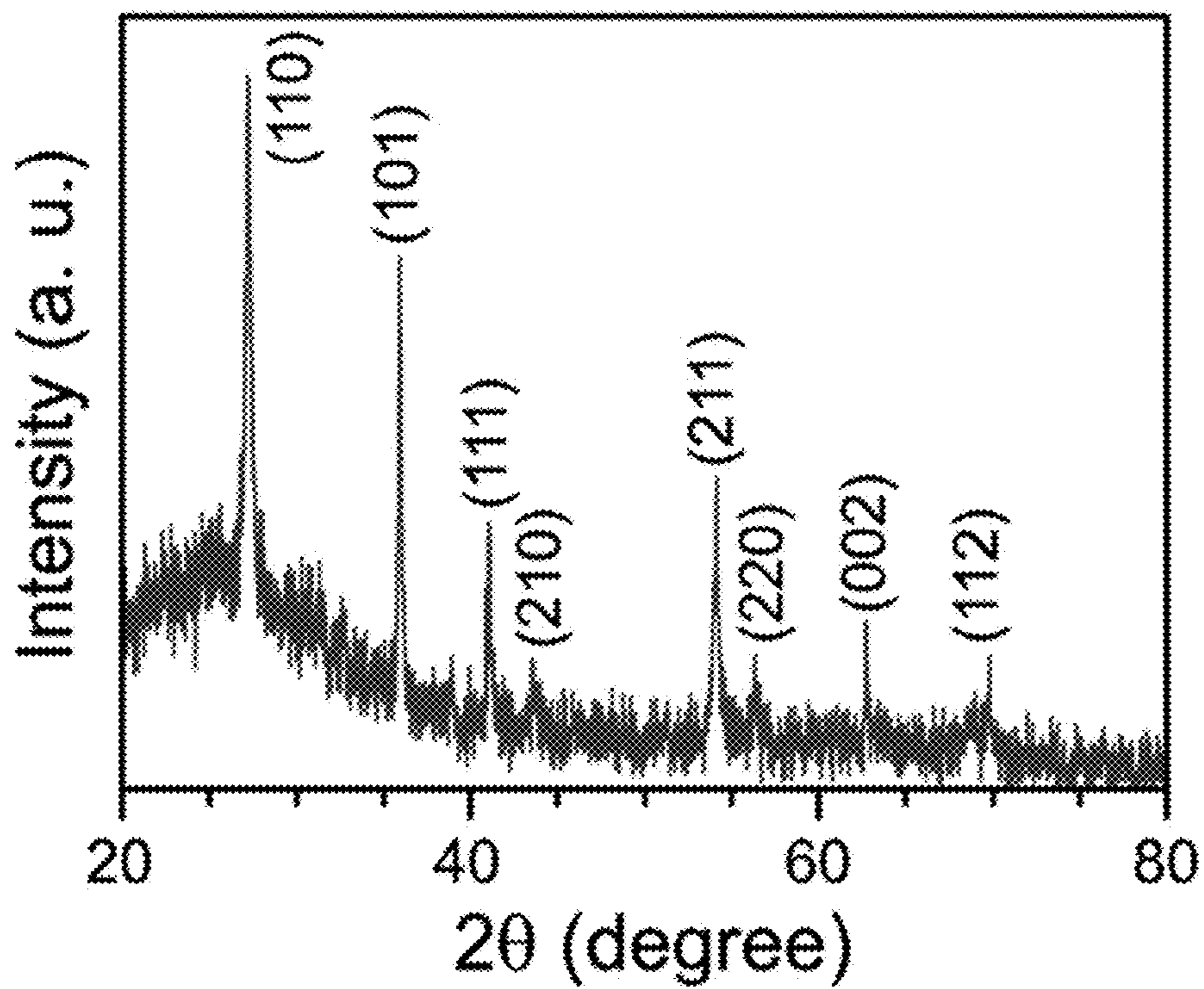


FIG. 26B

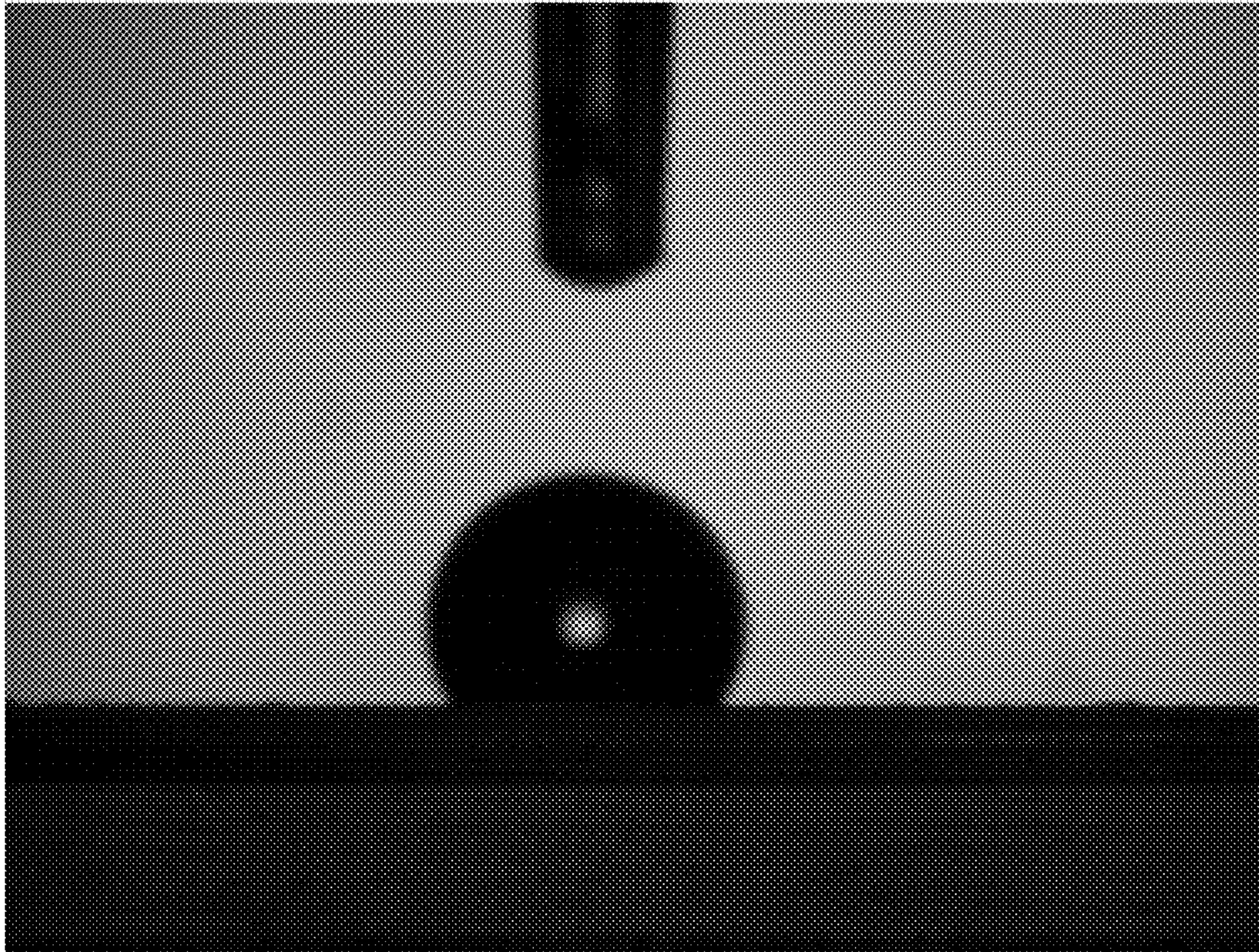


FIG. 27A

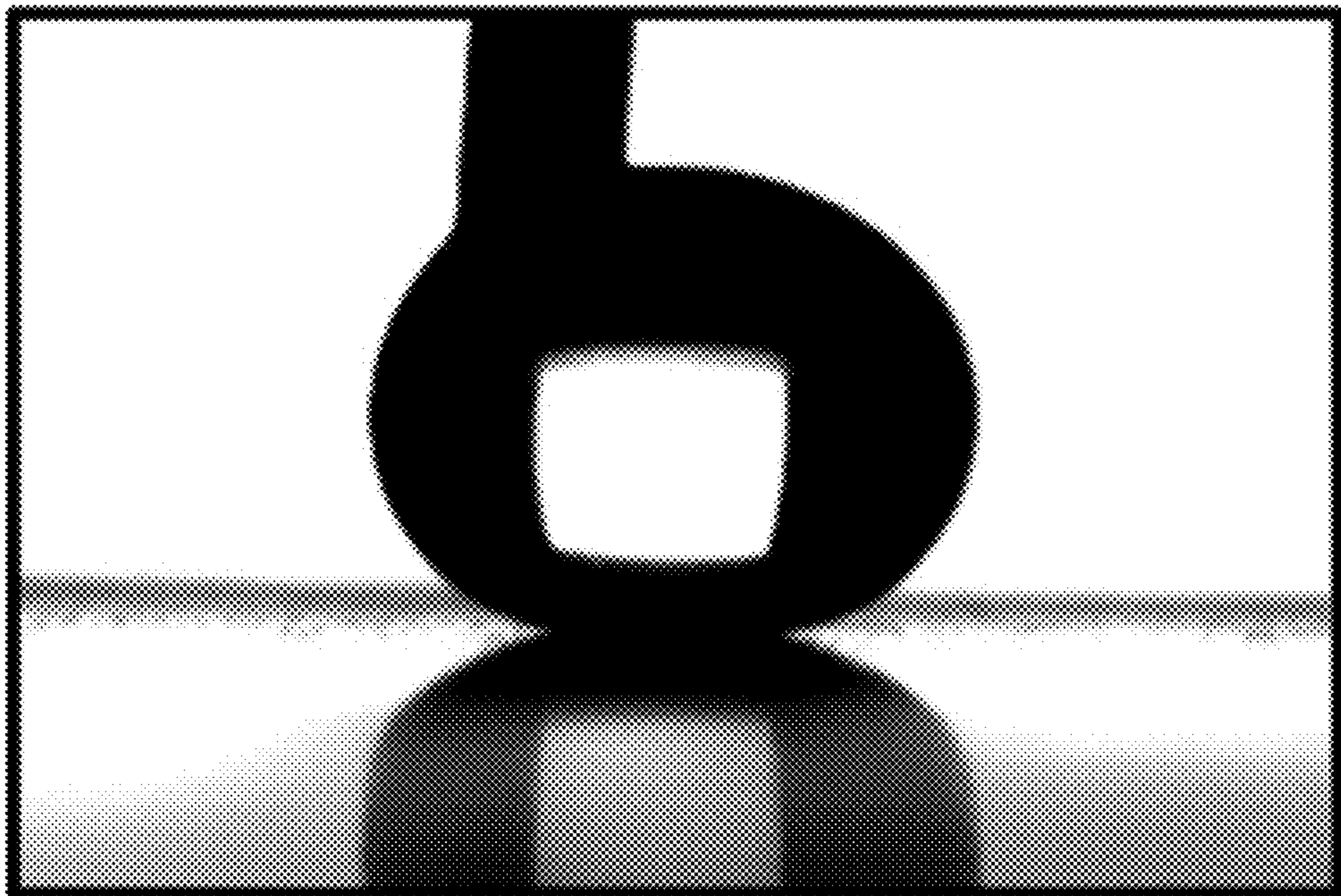


FIG. 27B

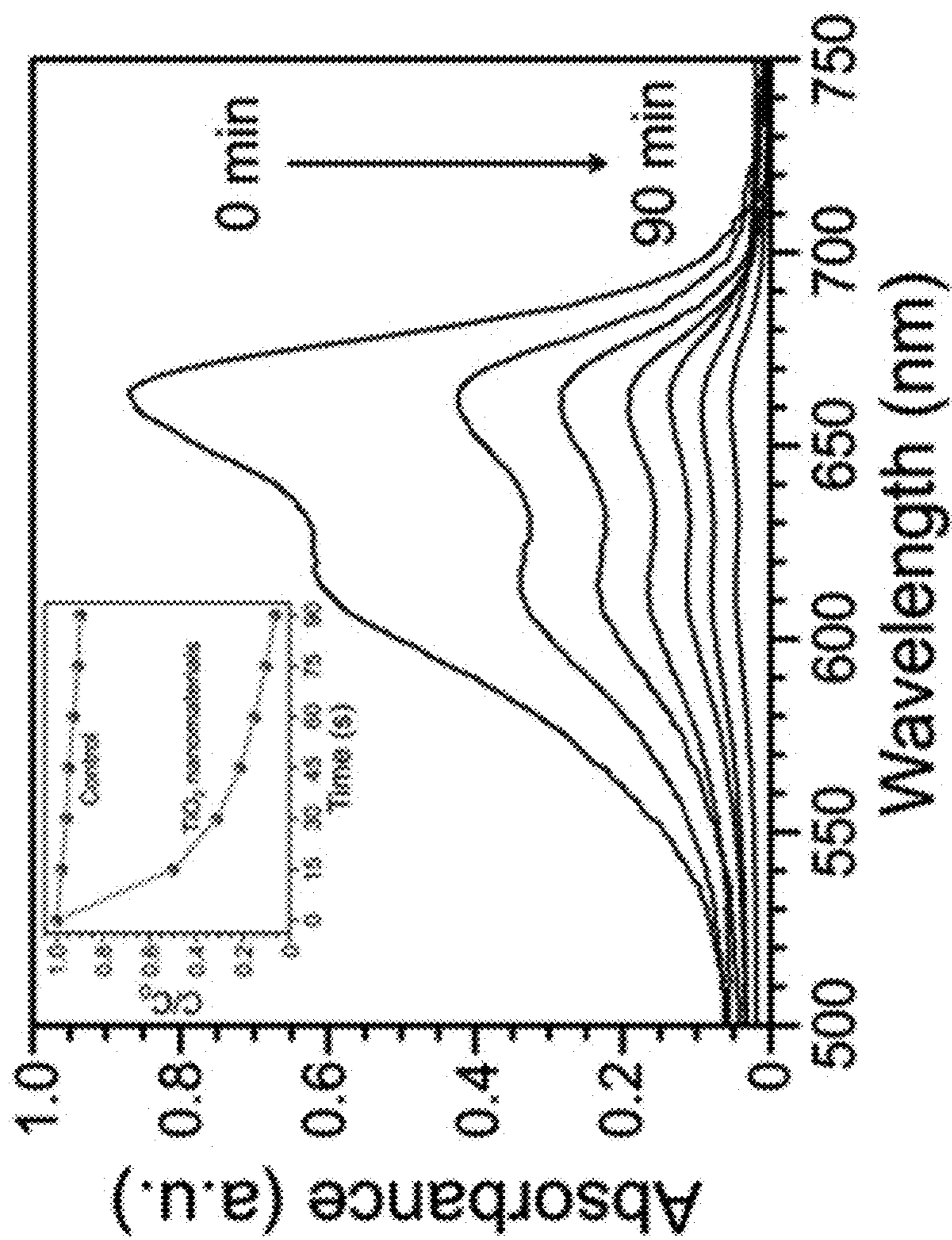


FIG. 28

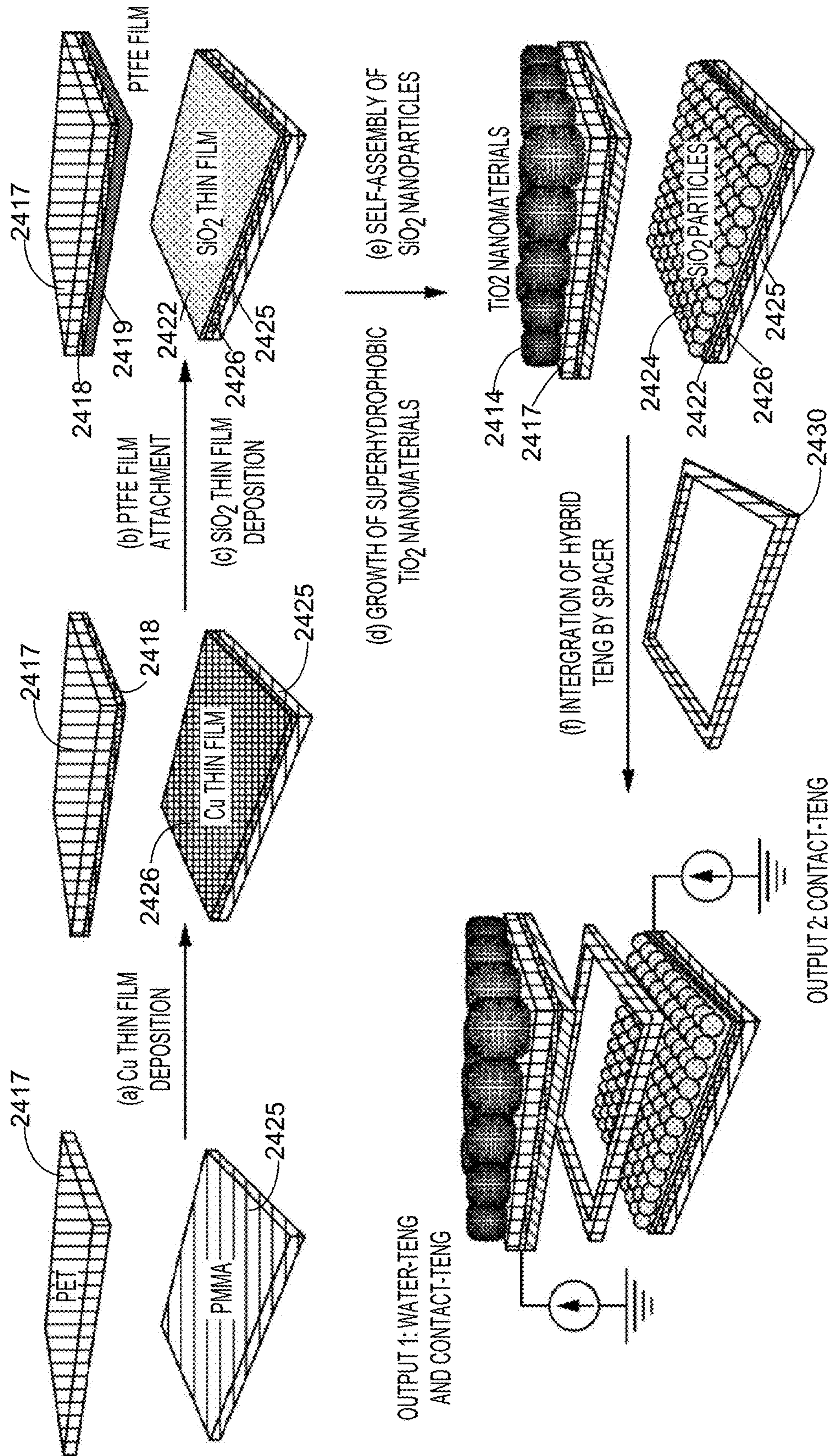


FIG. 29

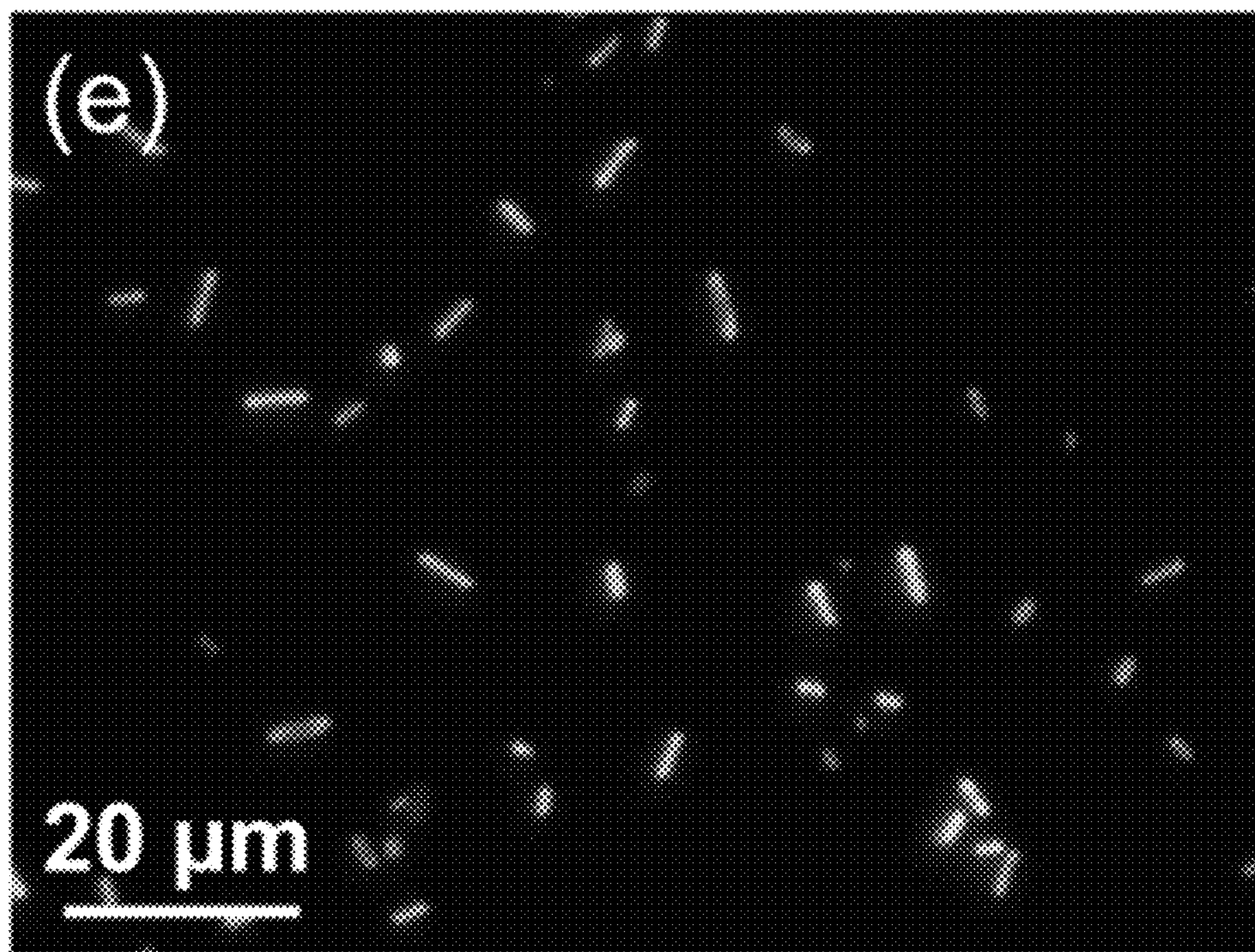


FIG. 30A

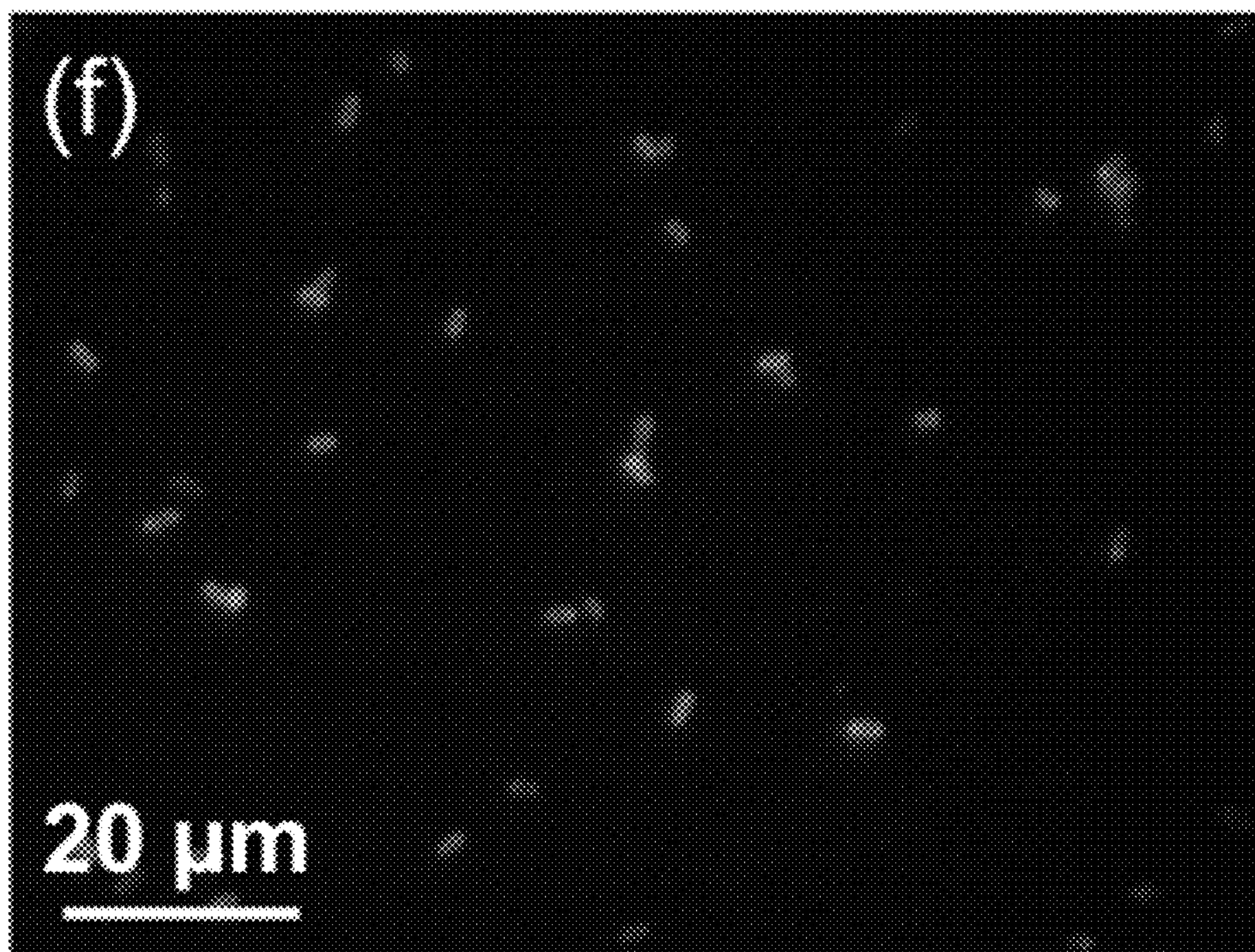


FIG. 30B



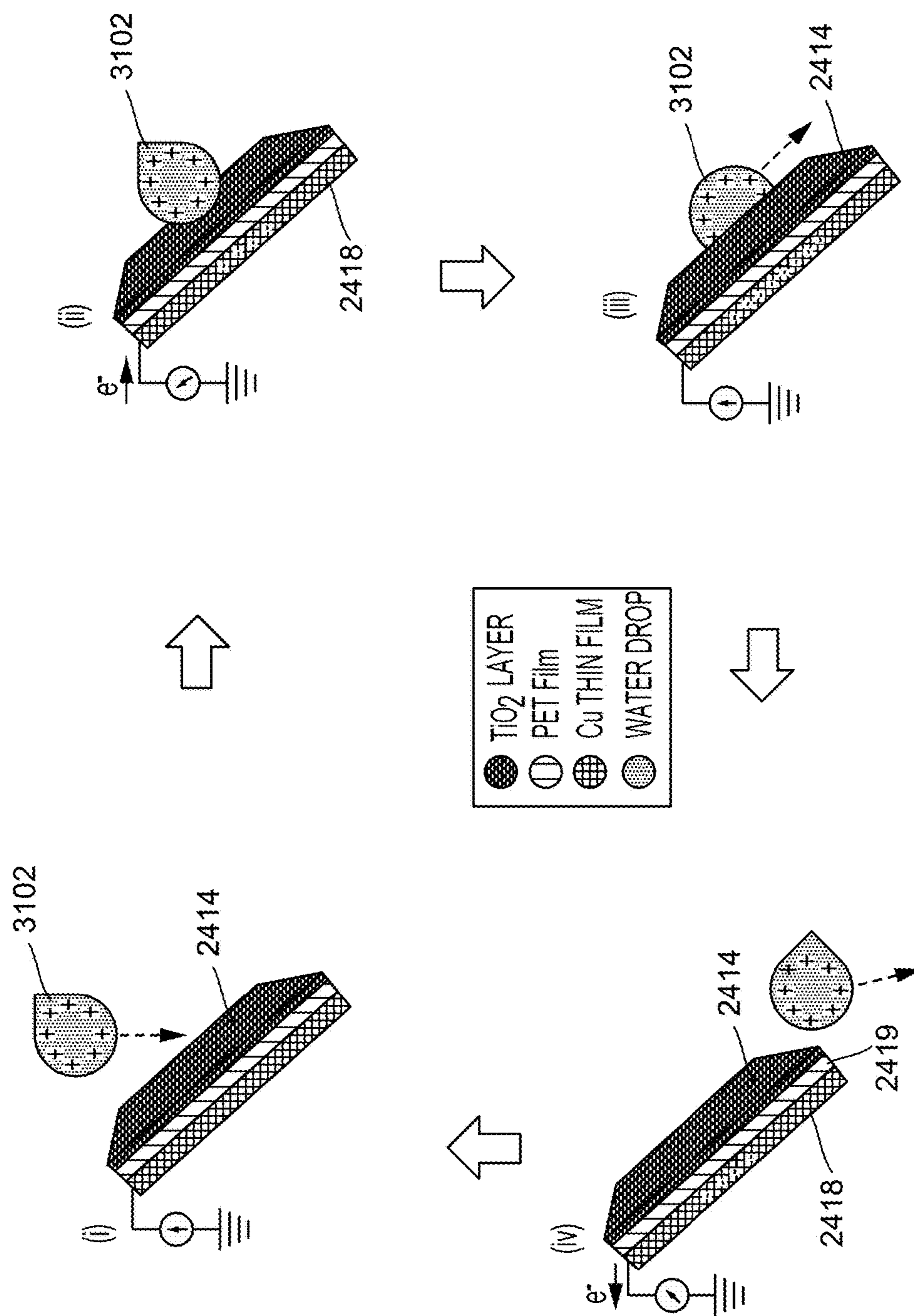


FIG. 31A

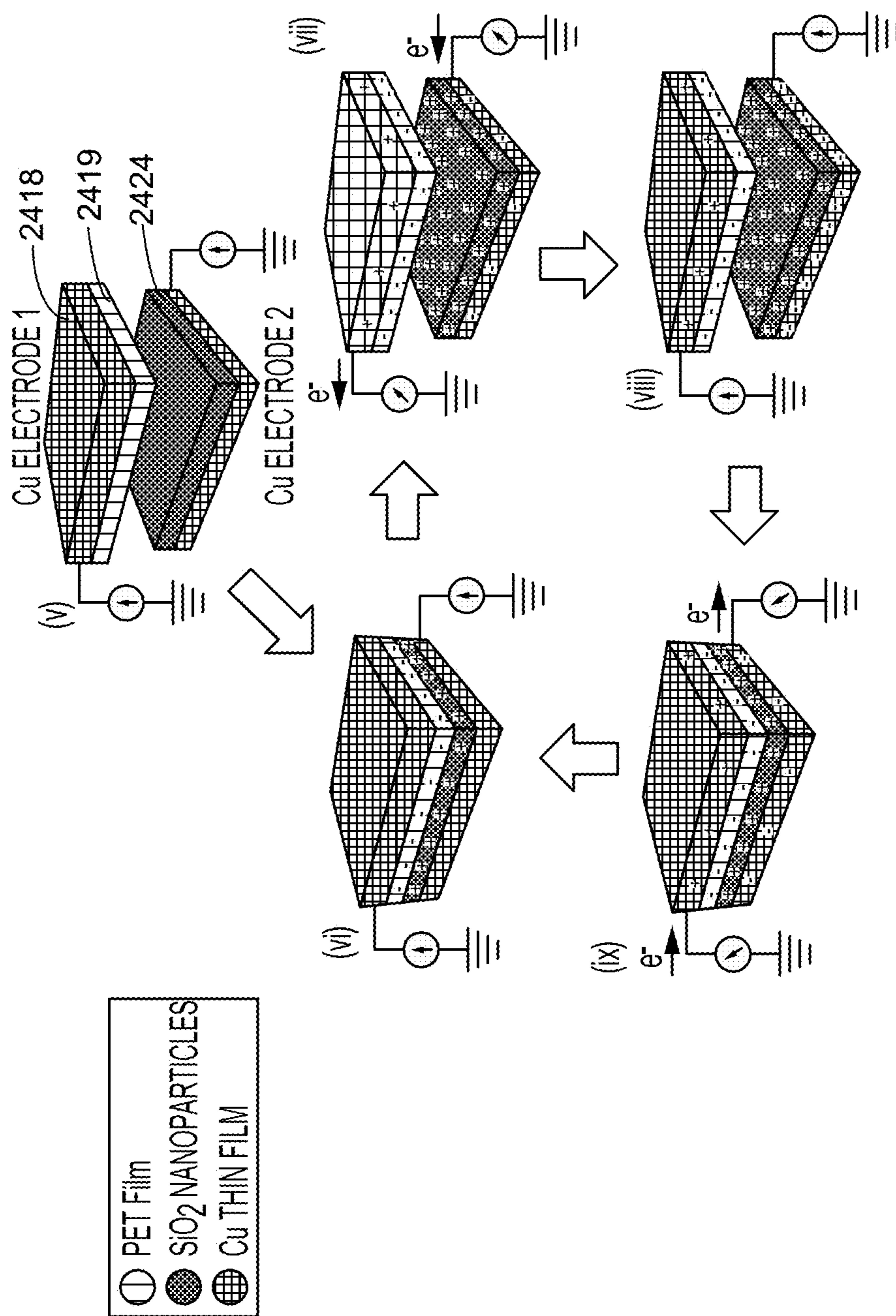


FIG. 31B

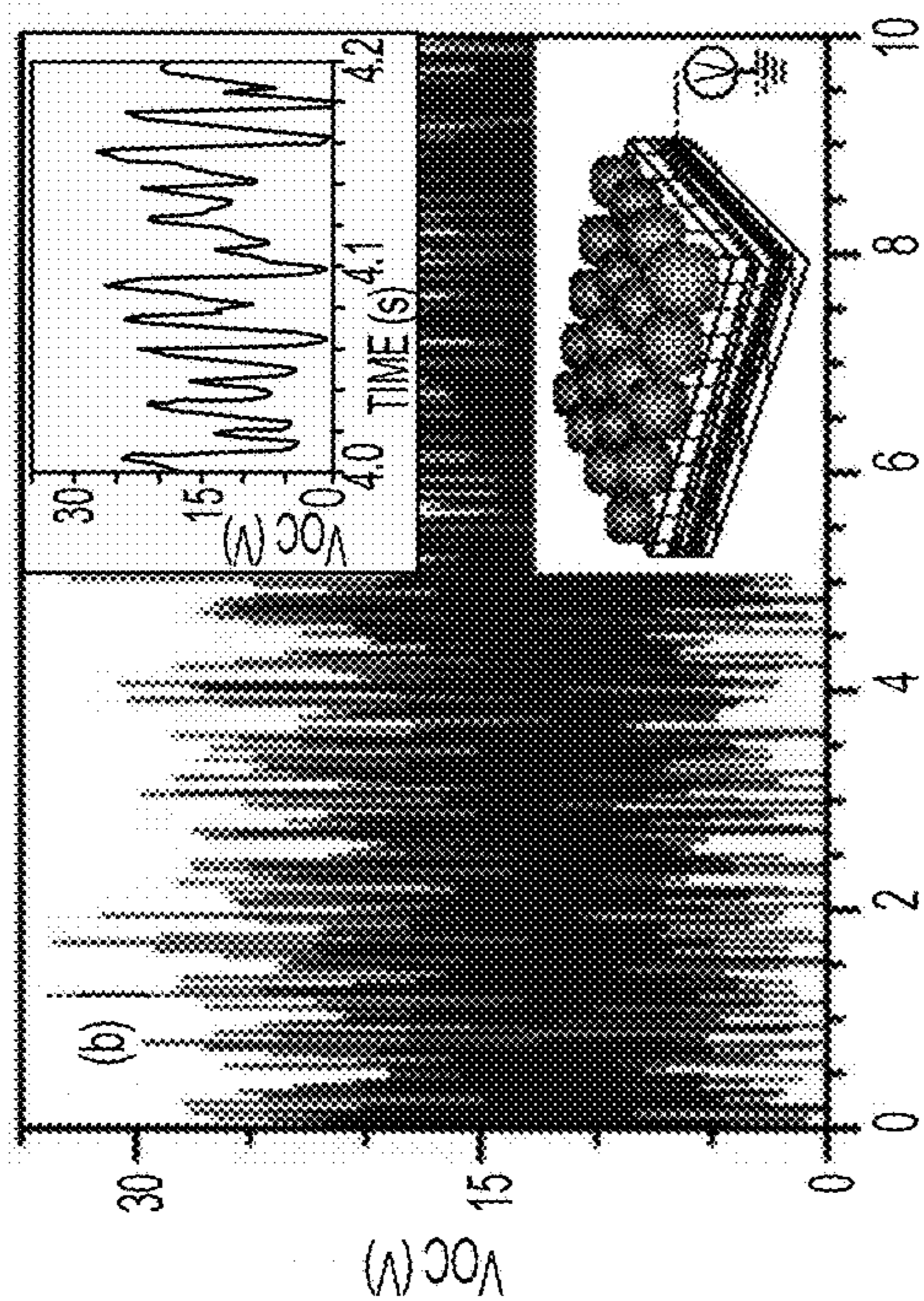


FIG. 32B

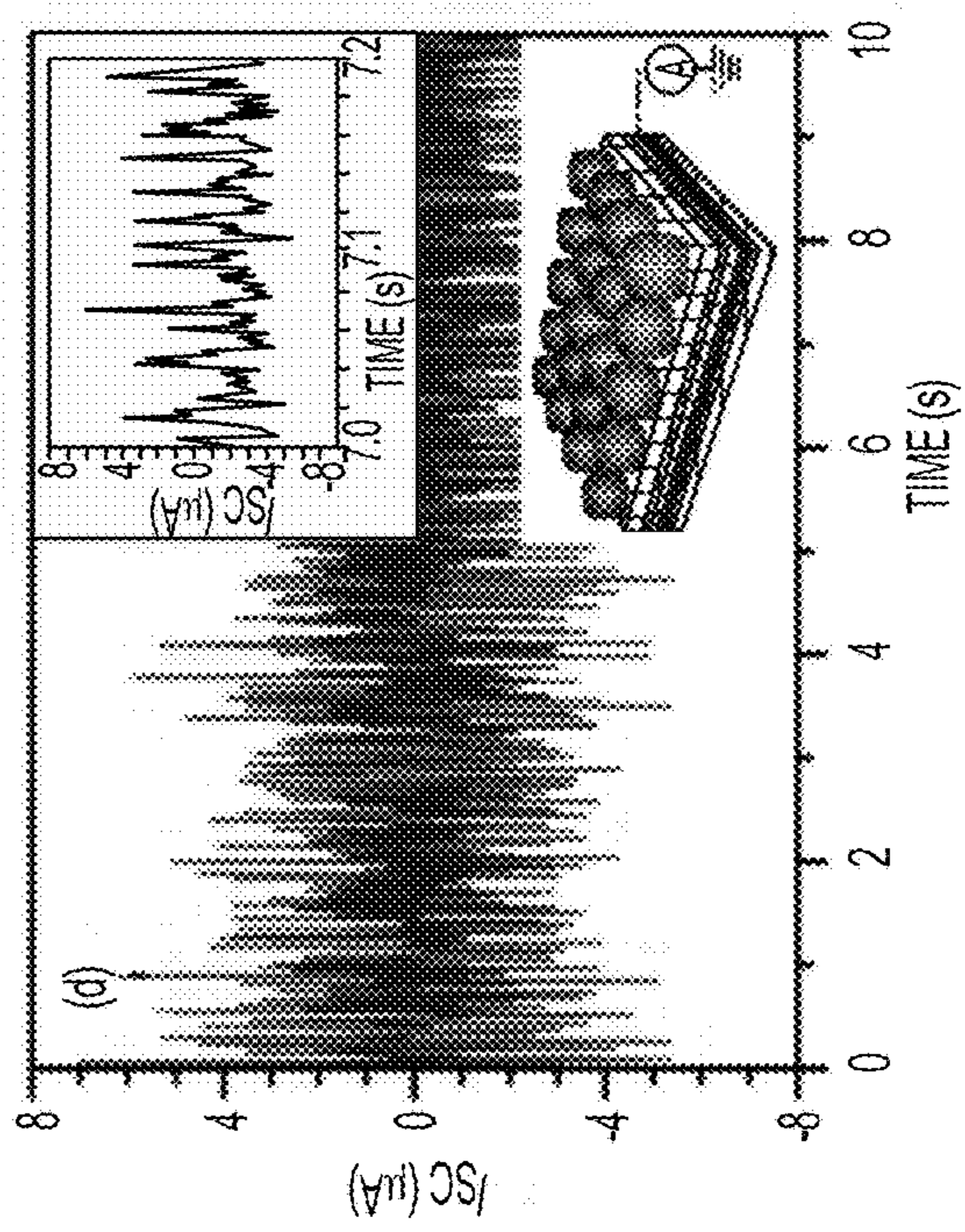


FIG. 32D

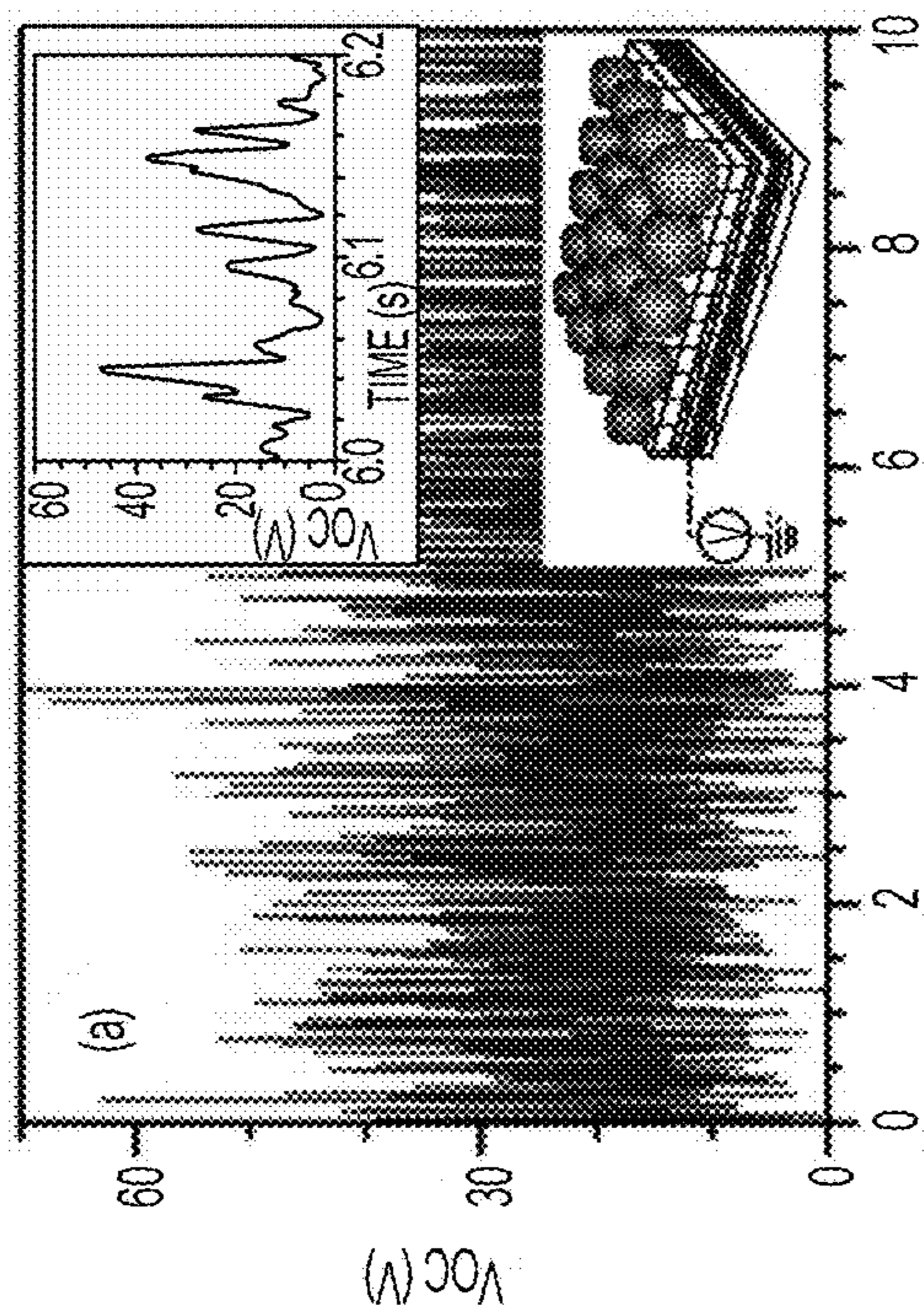


FIG. 32A

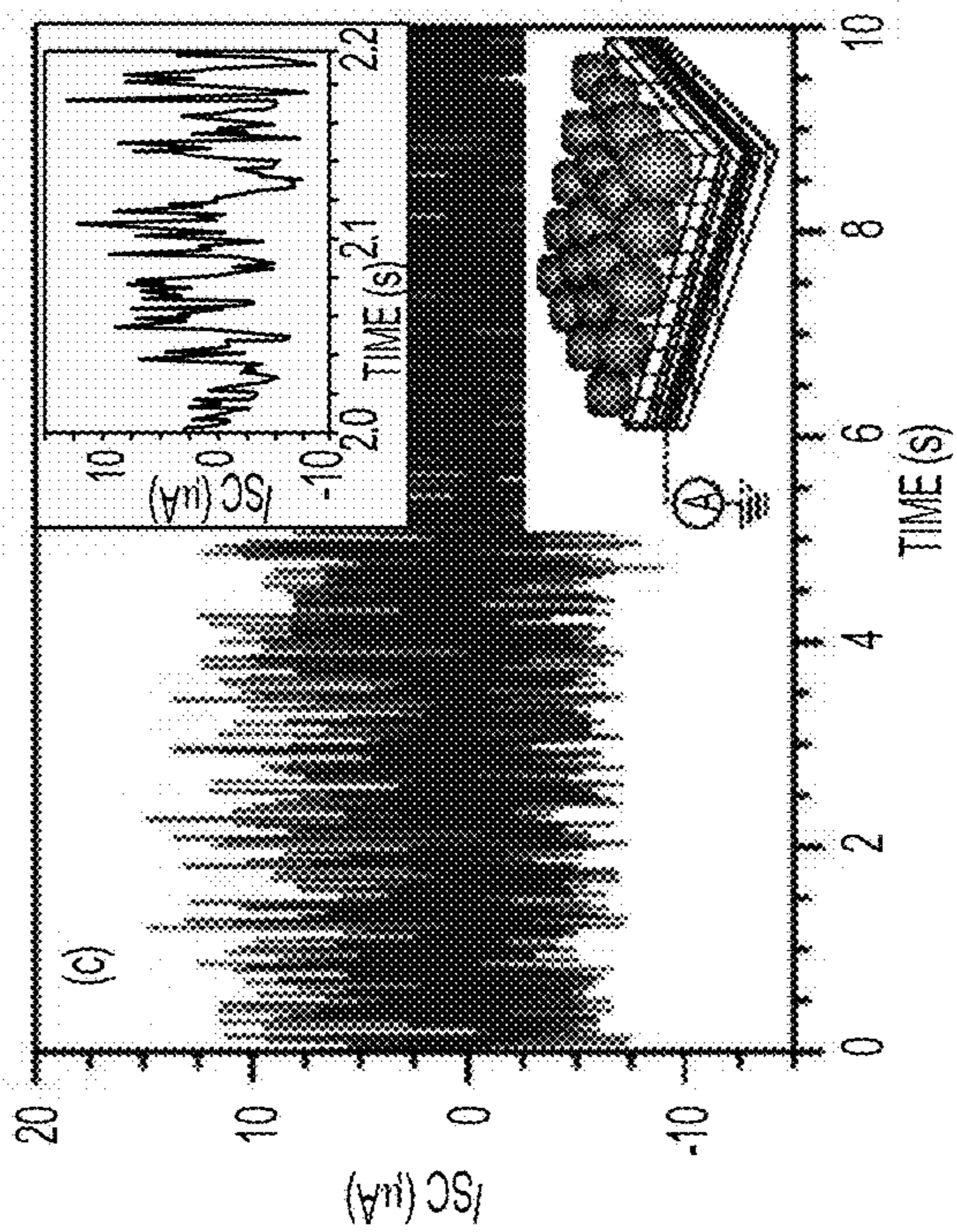


FIG. 32C

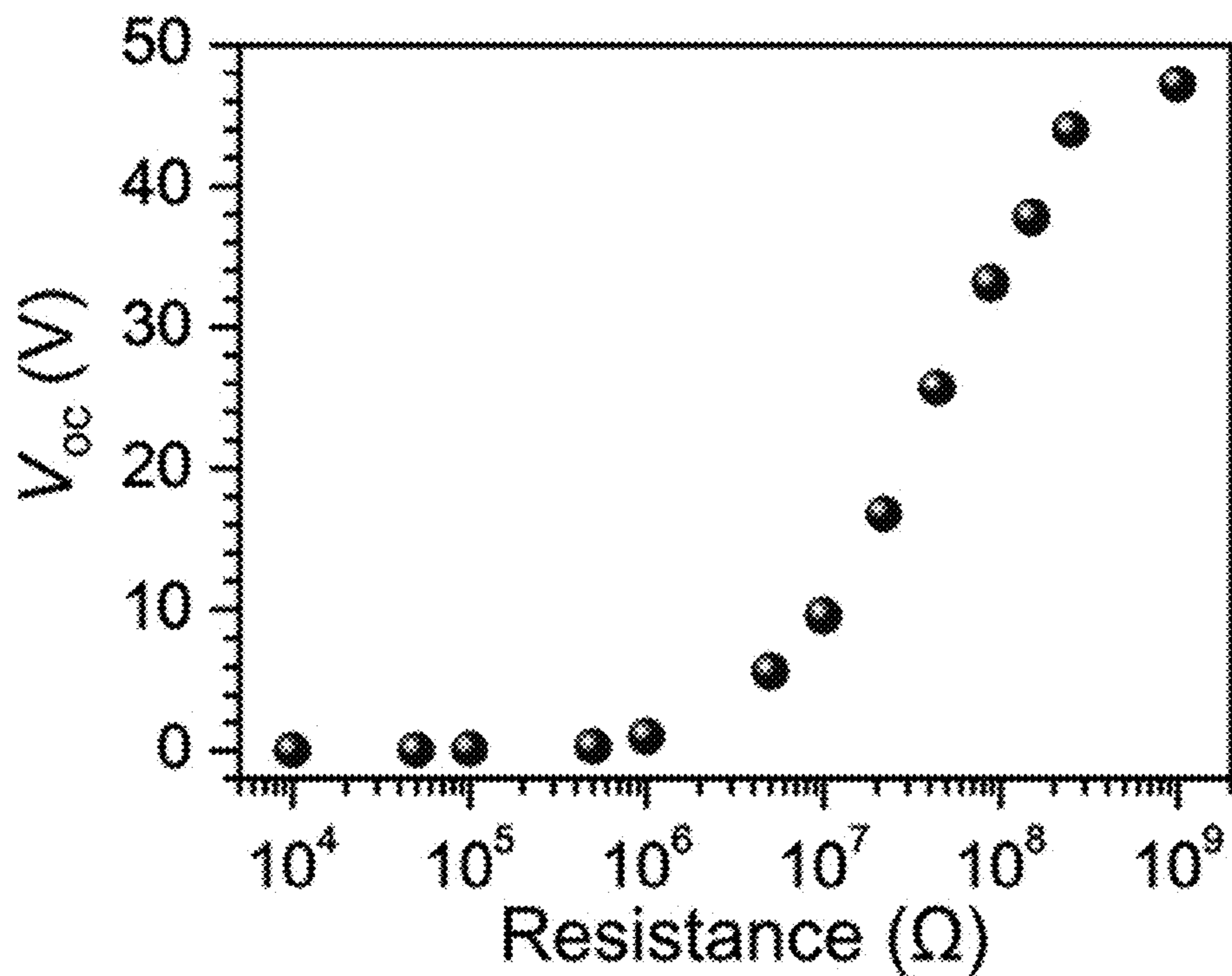


FIG. 33A

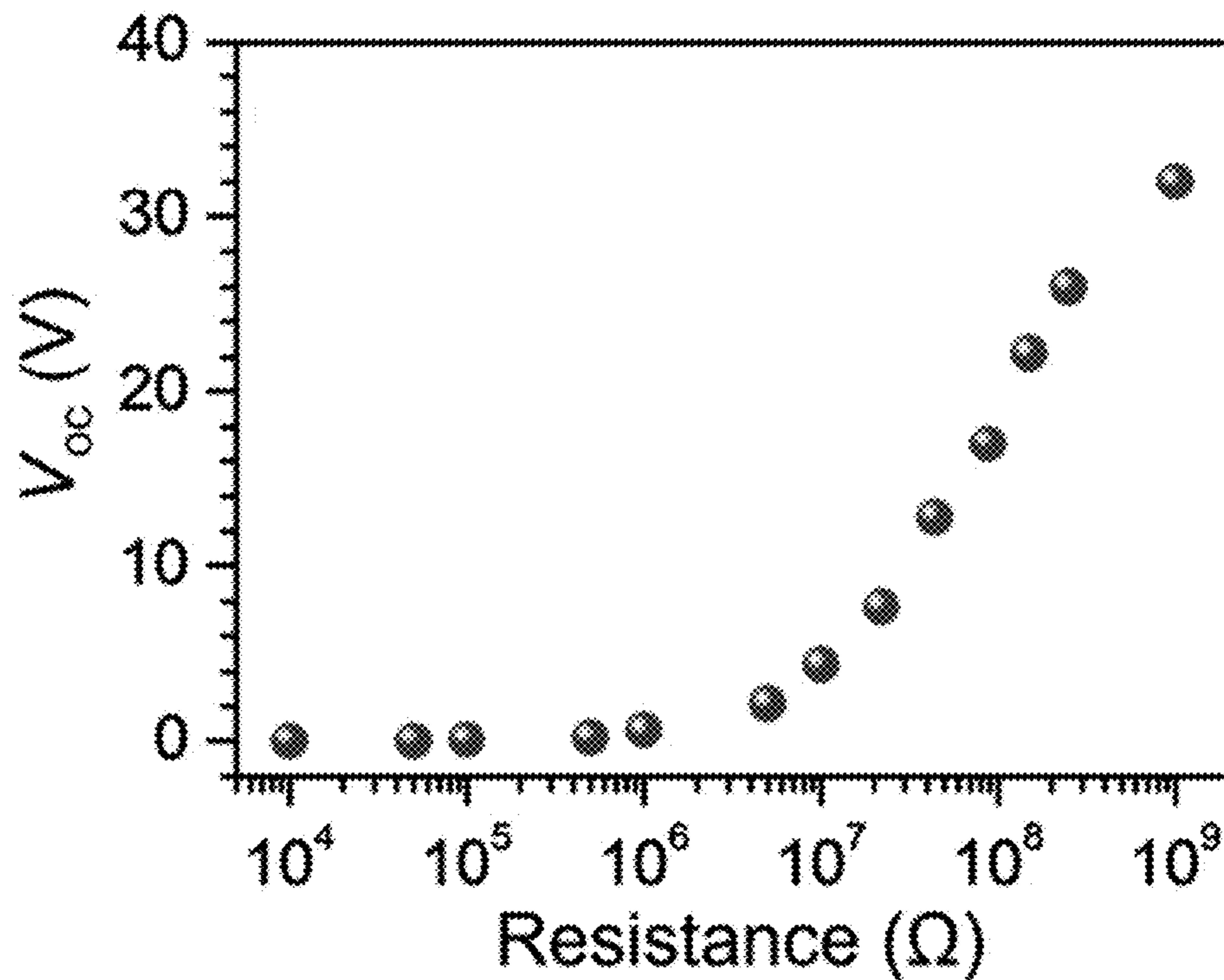


FIG. 33B

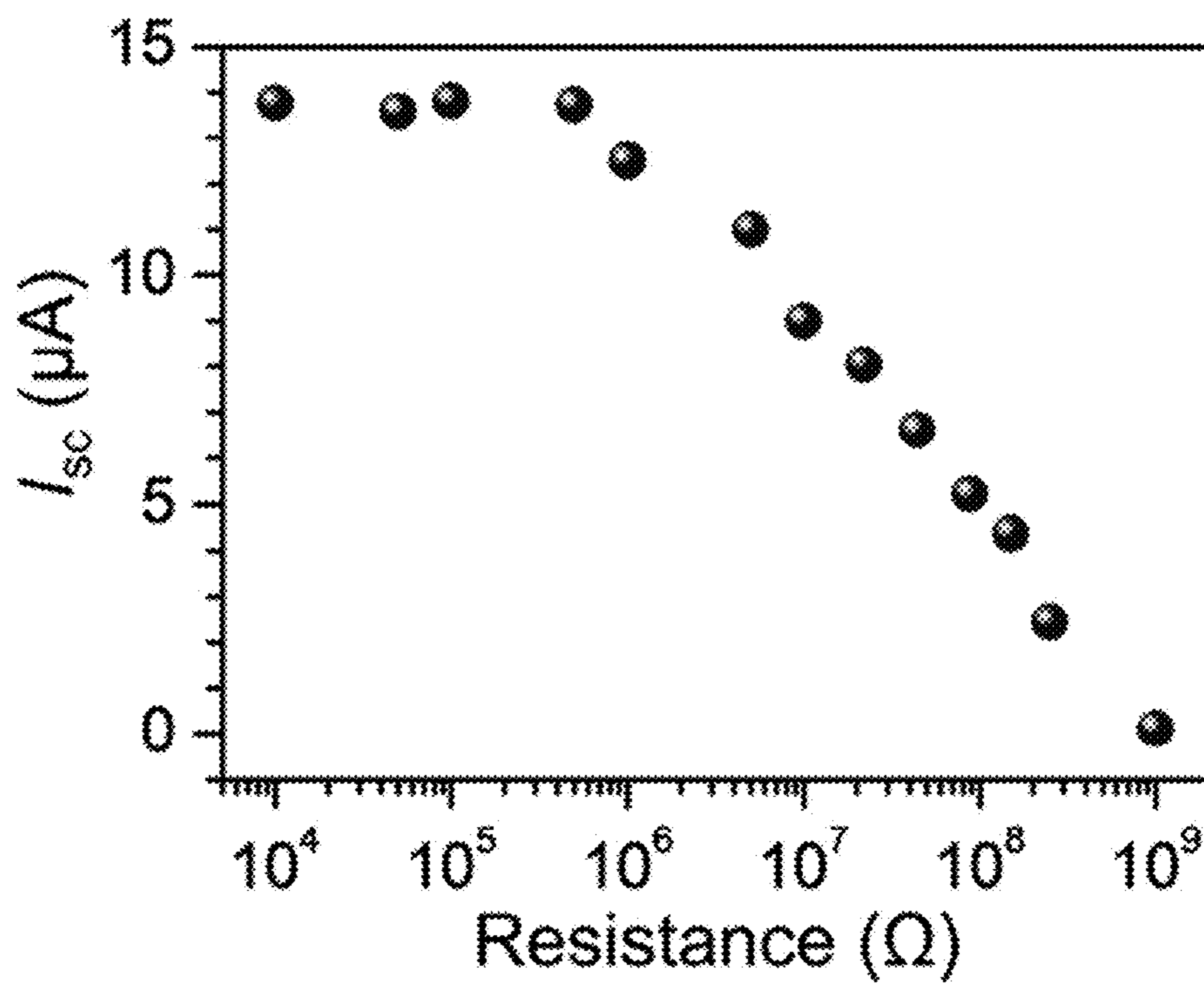


FIG. 33C

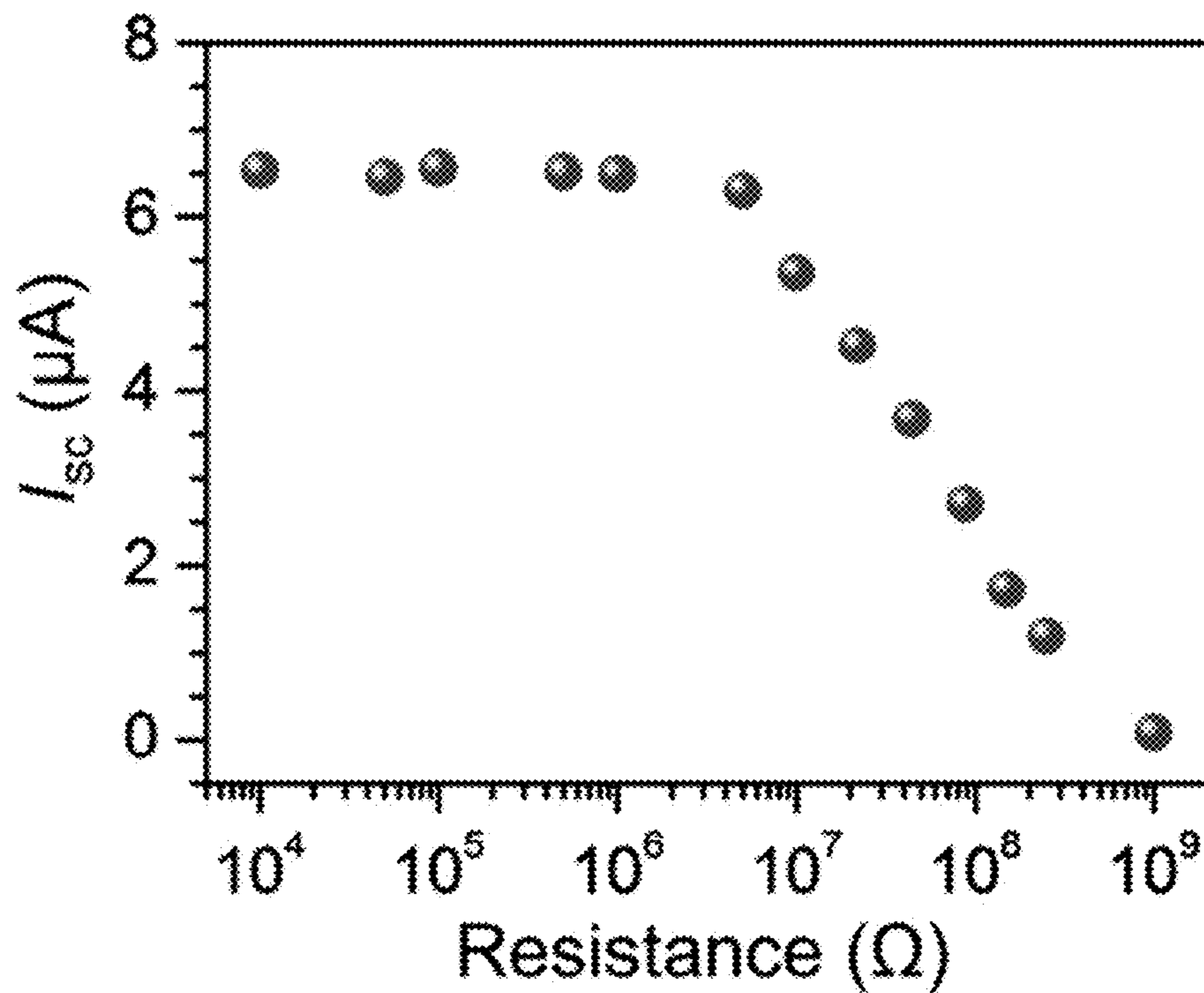


FIG. 33D

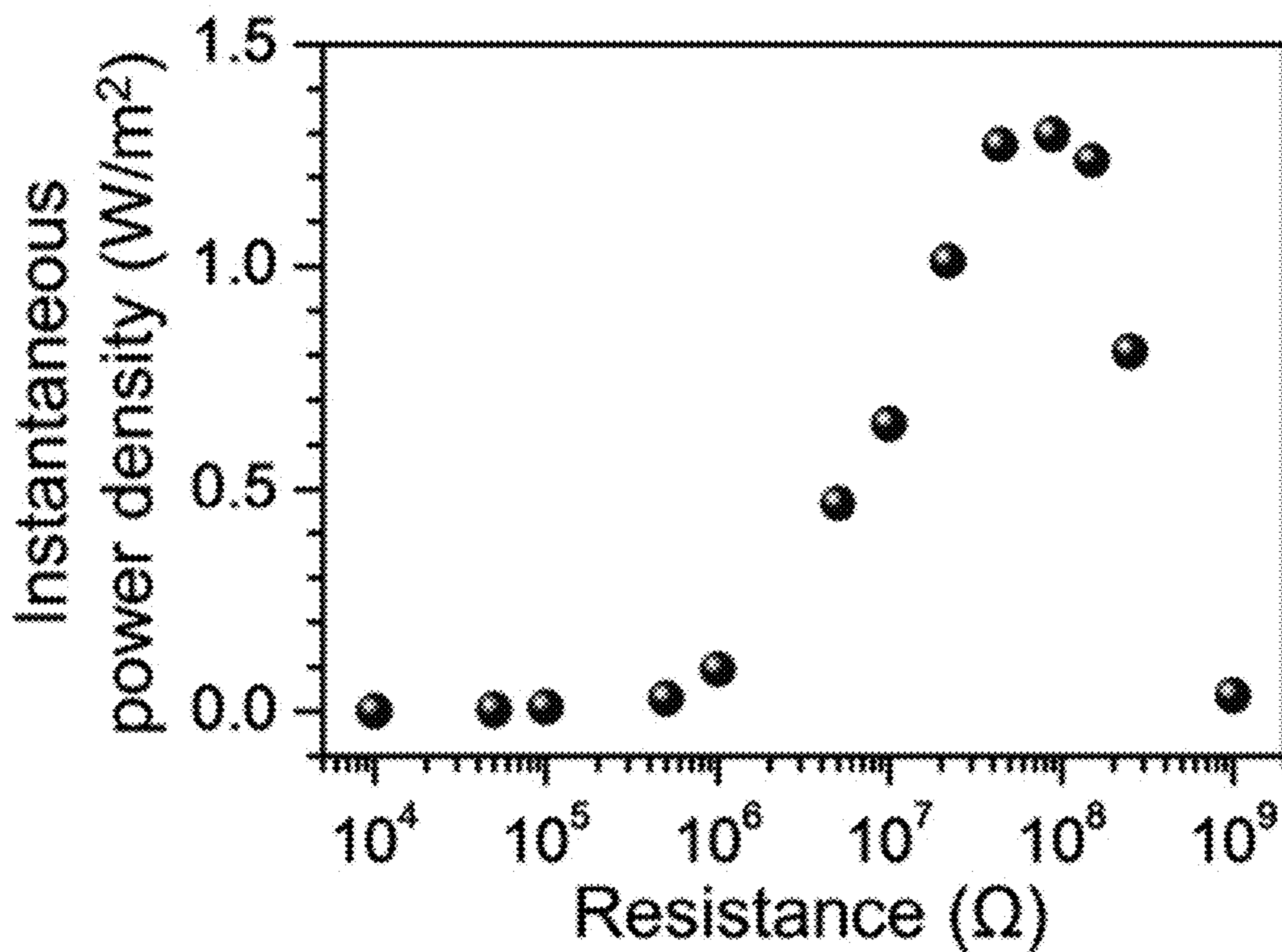


FIG. 33E

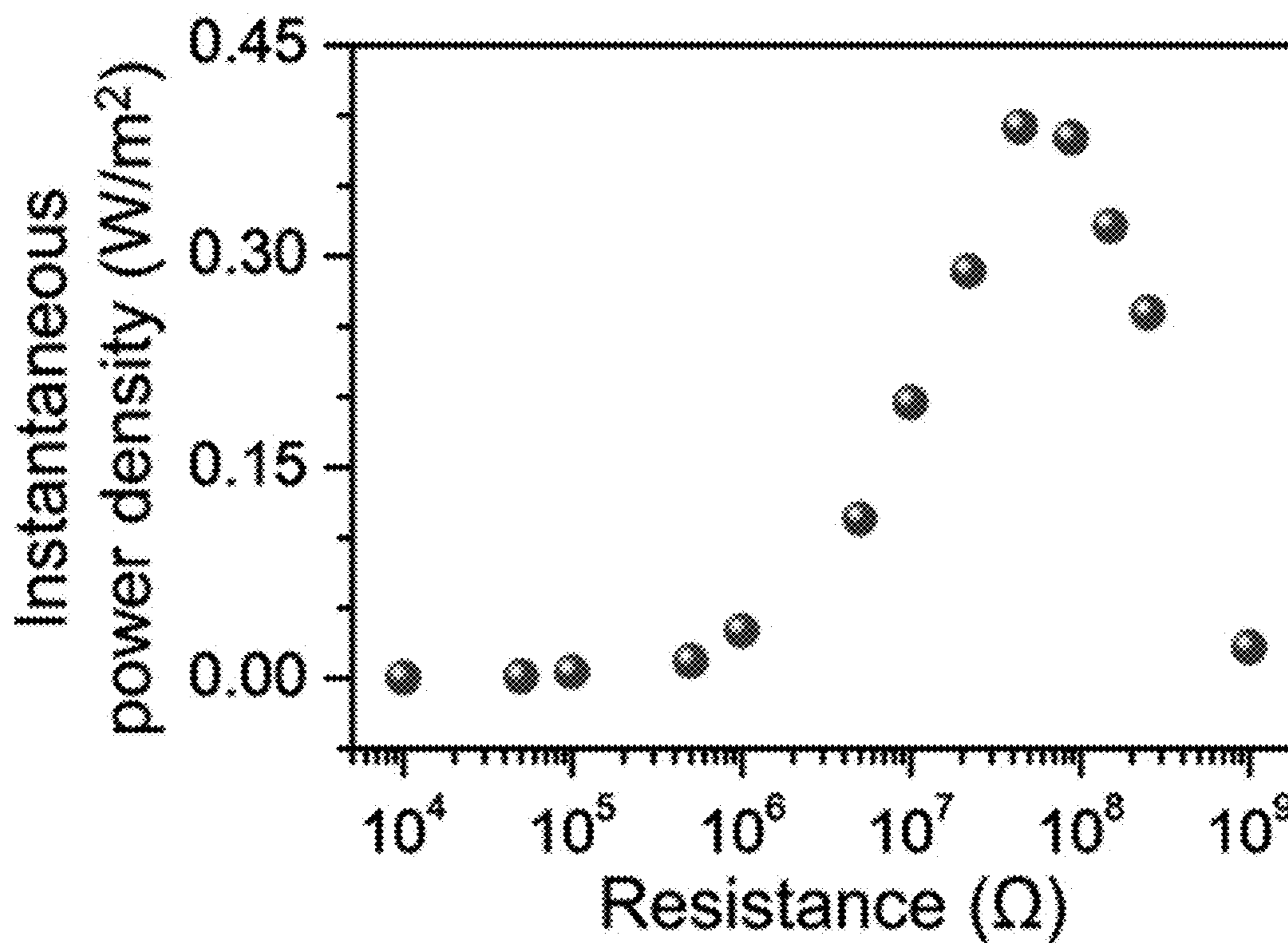


FIG. 33F

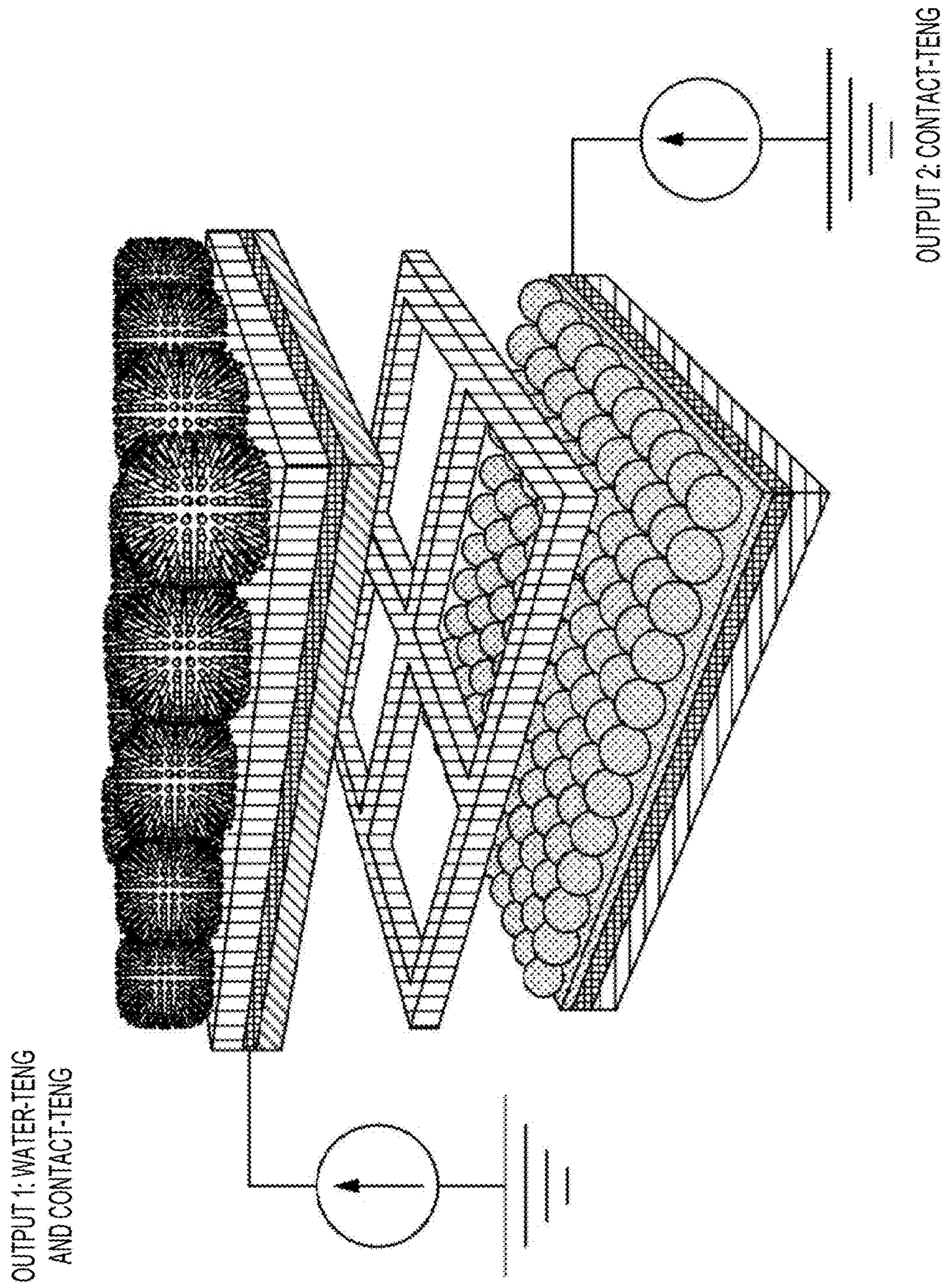


FIG. 34

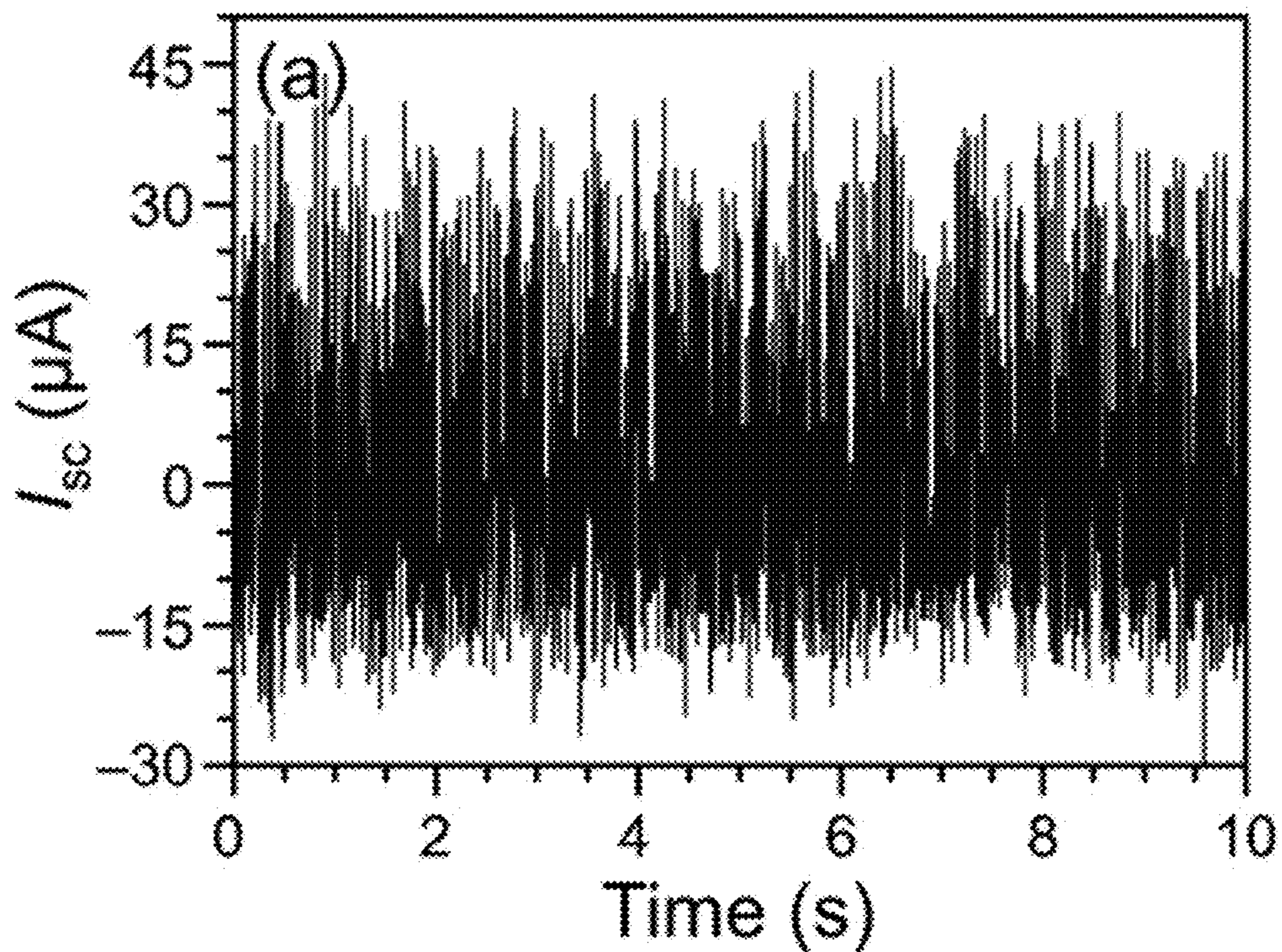


FIG. 35A

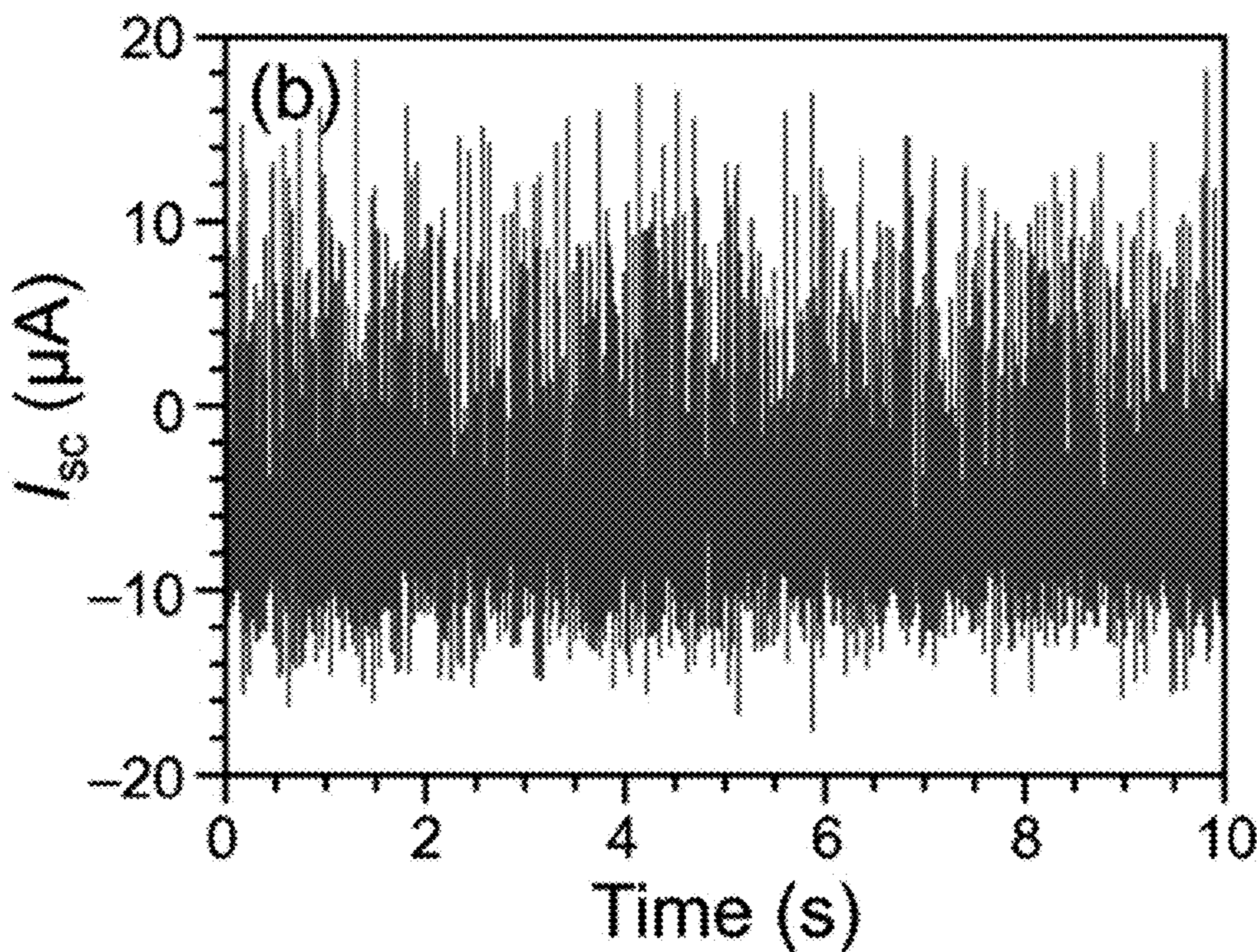


FIG. 35B



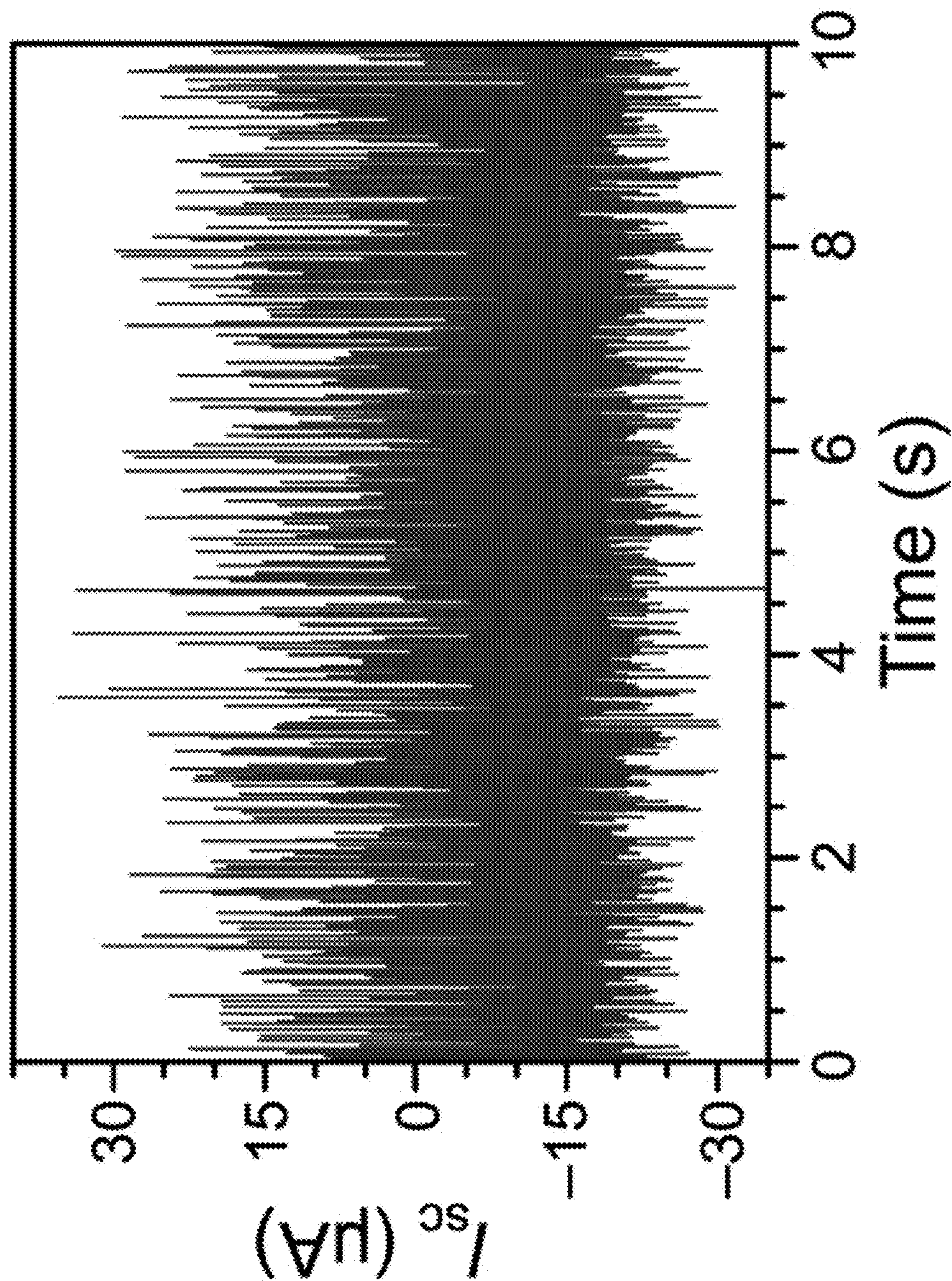


FIG. 36

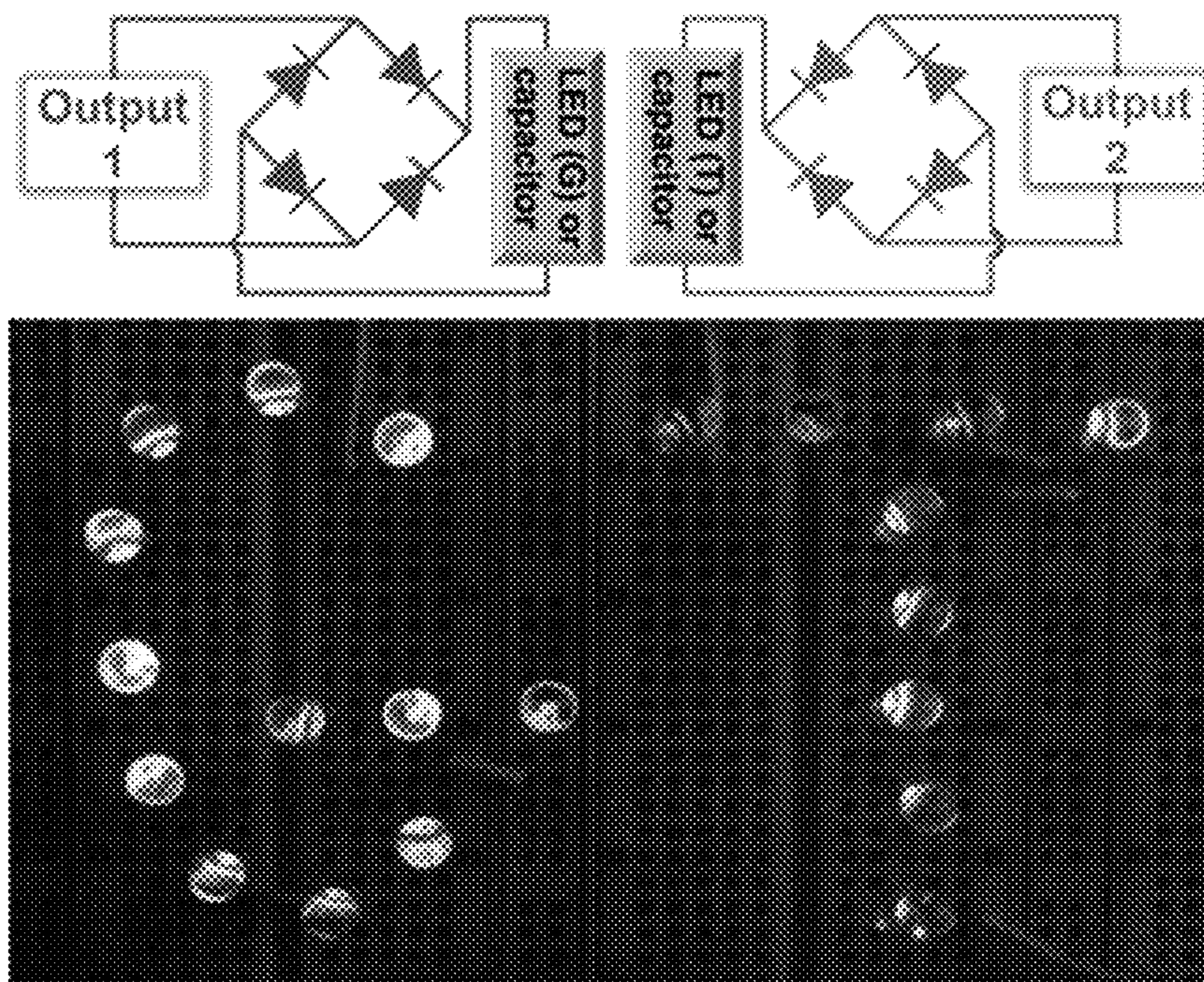


FIG. 37A

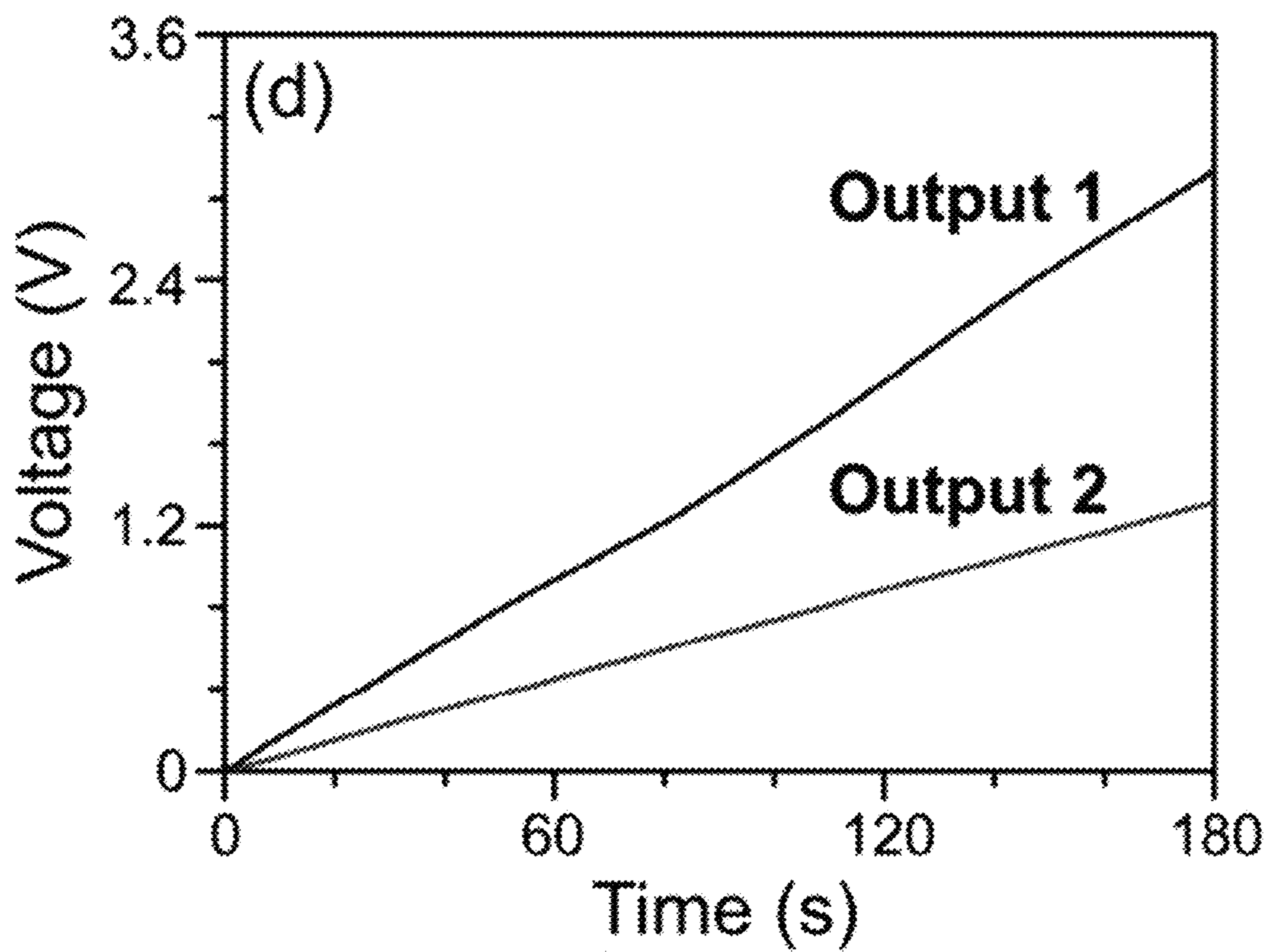


FIG. 37B

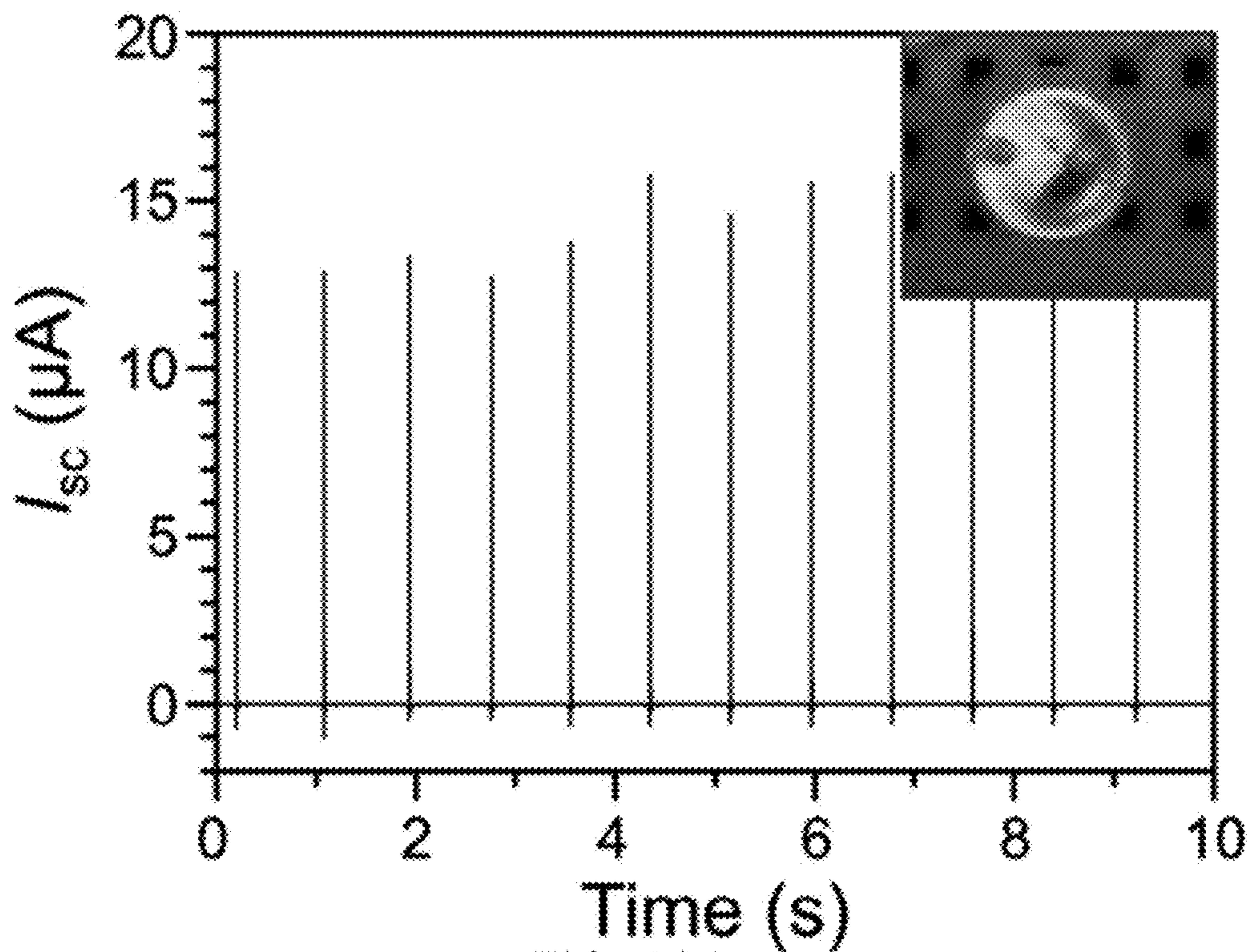


FIG. 38A

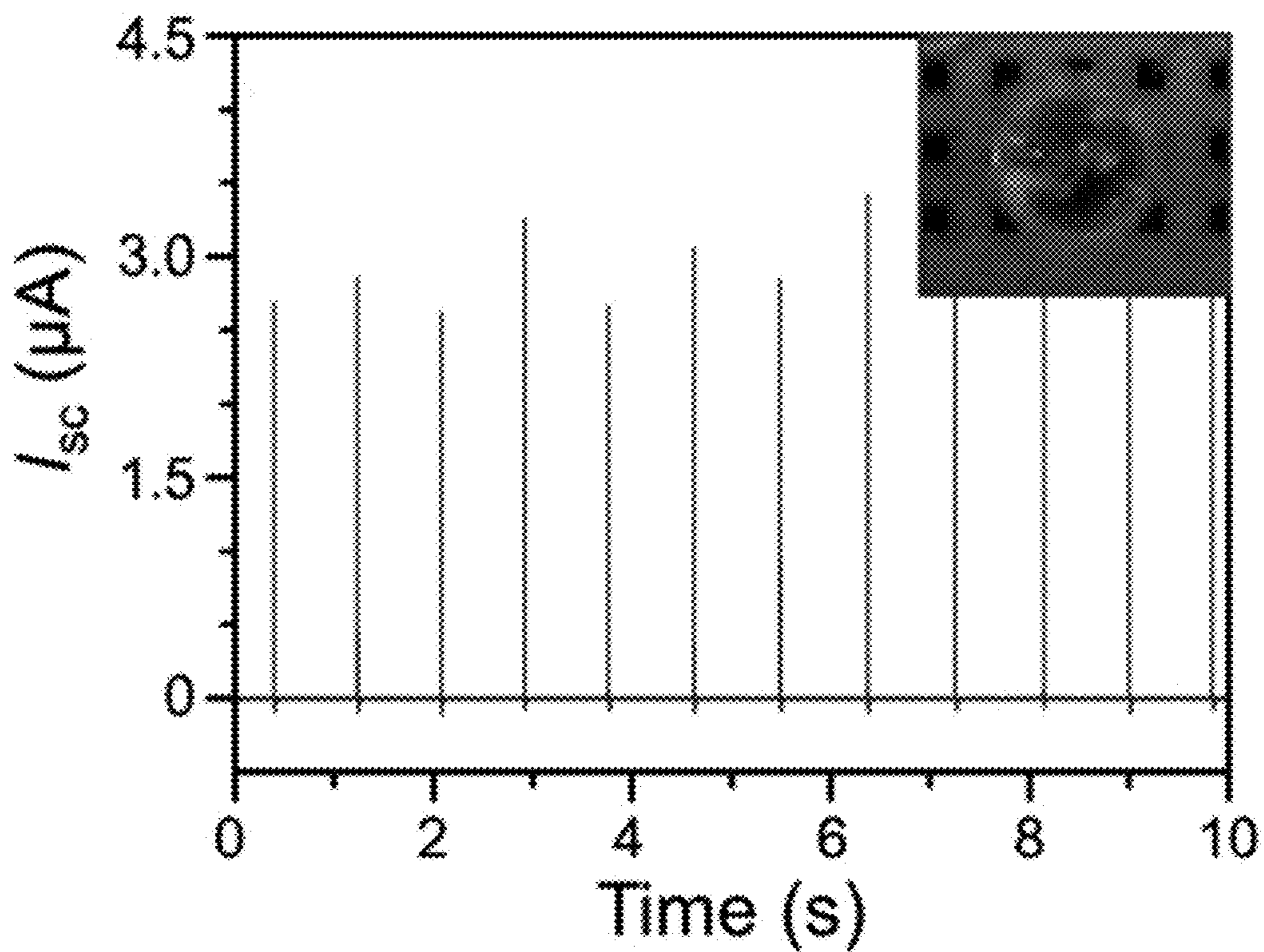
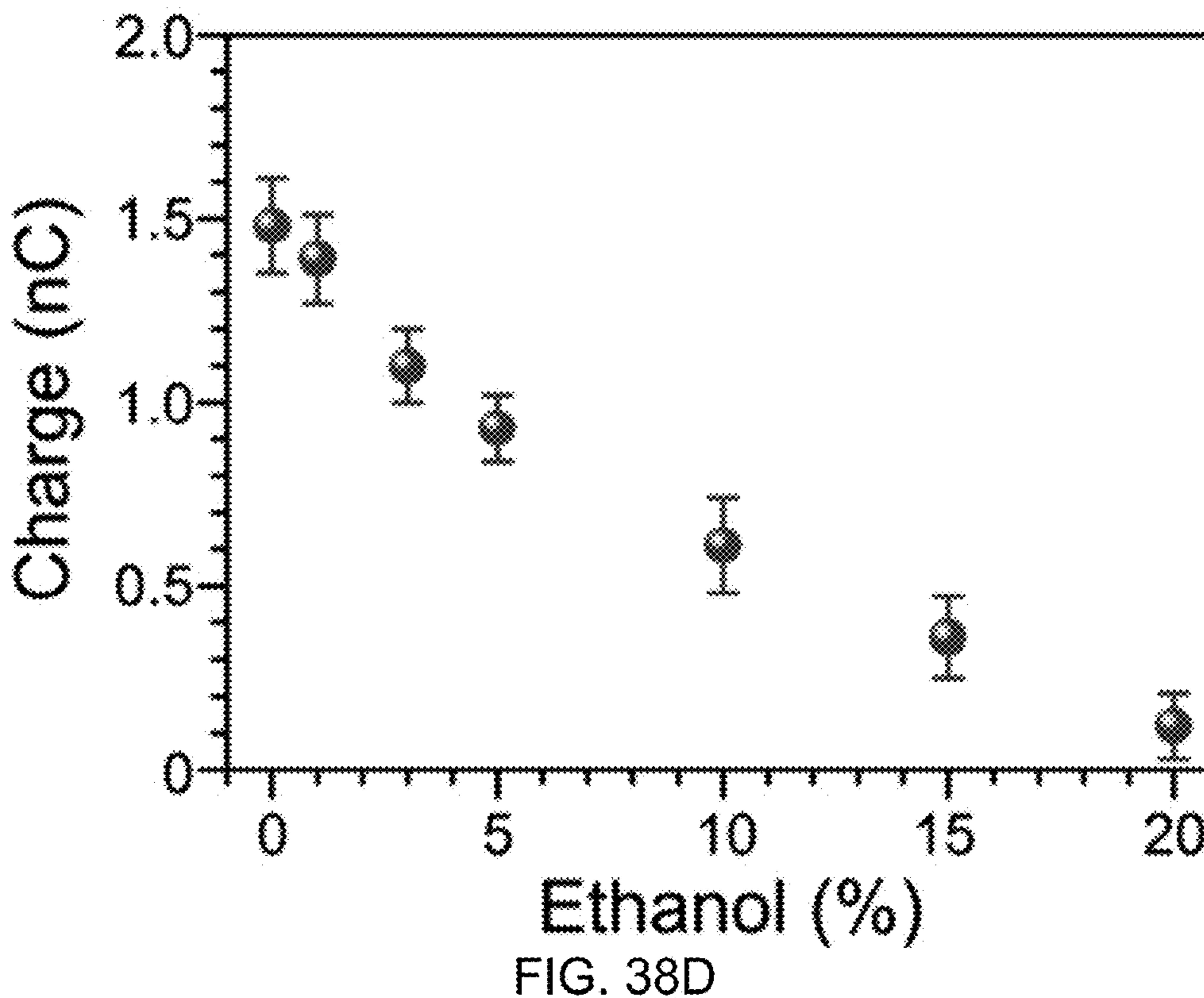
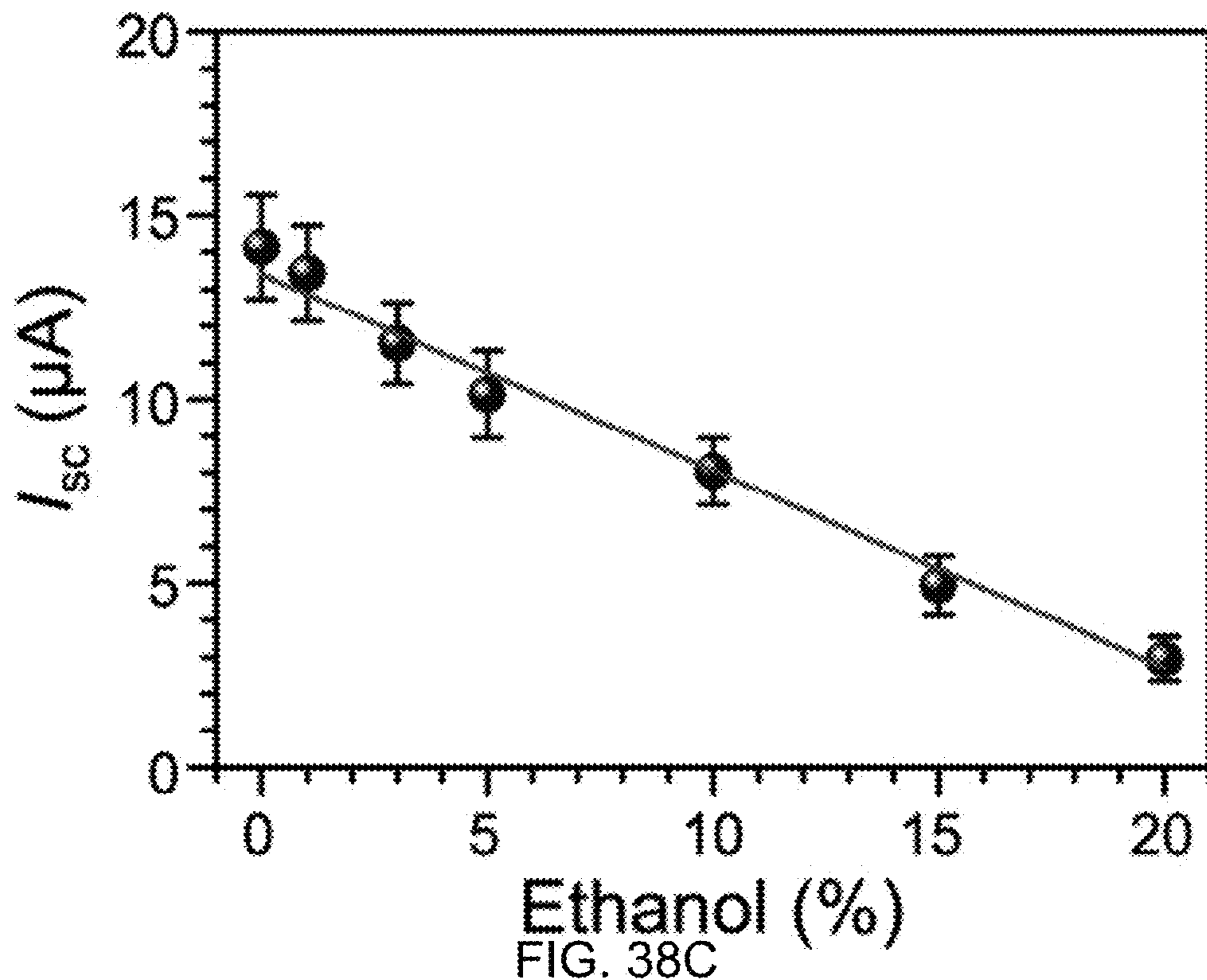


FIG. 38B



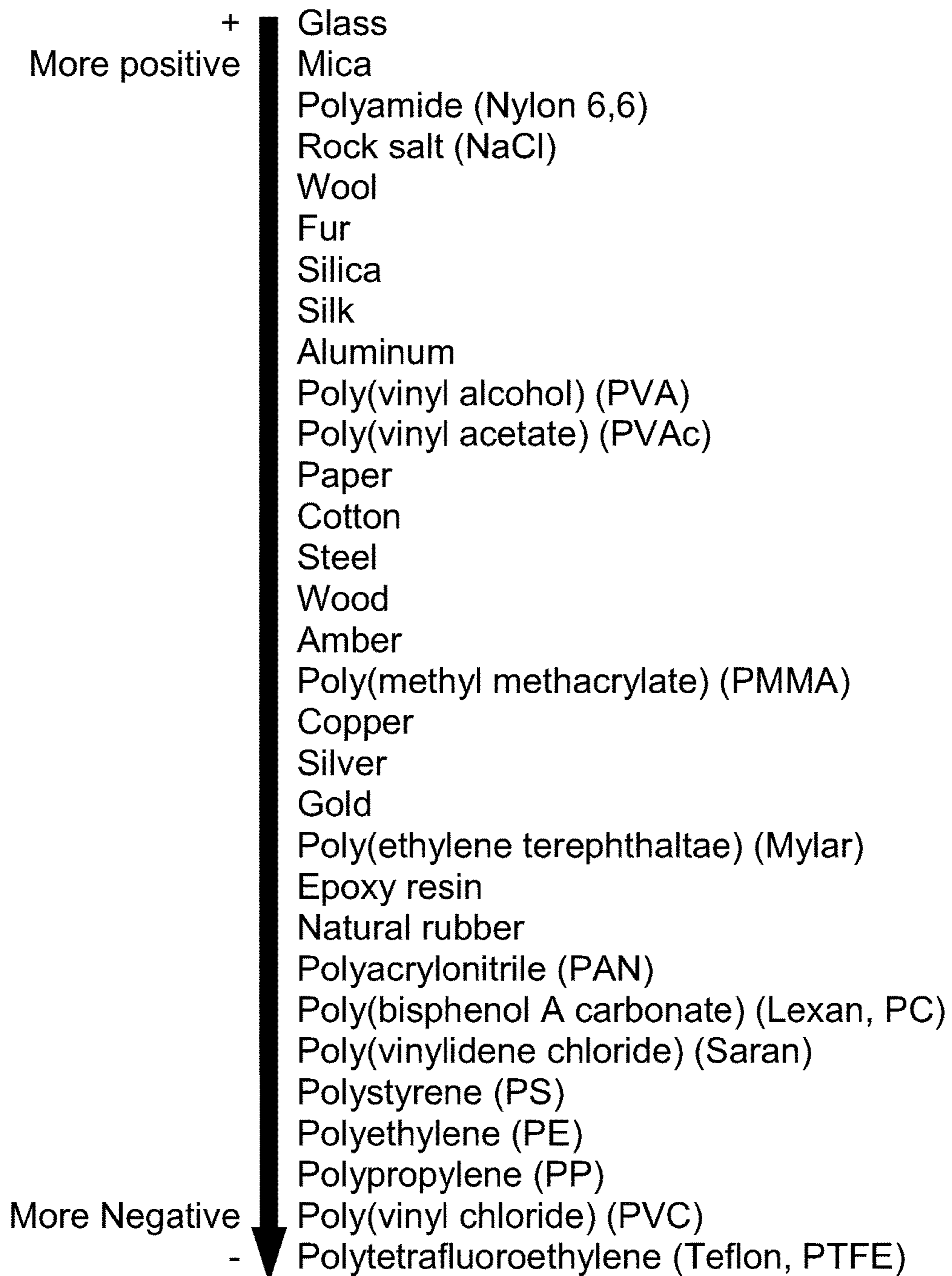


FIG. 39

## TRIBOELECTRIC NANOGENERATOR FOR HARVESTING ENERGY FROM WATER

### CROSS-REFERENCE

This application claims the benefit of U.S. Provisional Patent Application Ser. No. 62/128,757, filed on Mar. 5, 2015, and U.S. Provisional Patent Application Ser. No. 62/107,855, filed on Jan. 26, 2015, all of which are hereby incorporated by reference to their entireties.

### STATEMENT OF GOVERNMENT INTEREST

This invention was made with government support under agreement No. DE-FG02-07ER46394, awarded by the U.S. Department of Energy. The government has certain rights in the invention.

### TECHNICAL FIELD DISCLOSED

Embodiments of the disclosed technology generally relate to triboelectric nanogenerators for harvesting energies from water.

### BACKGROUND DISCLOSED

There are abundant of water-related energy sources in the environment including, for example, ocean wave, tide, waterfall, and rainwater. Each water source may carry multiple types of energy. For example, a single water drop carries two types of energy, including mechanical kinetic energy and electrostatic energy owing to triboelectric charges caused by its contact with surrounding media.

Since 1867, the Kelvin water dropper has been invented to collect the water electrostatic energy and illustrate the natural generation of electricity in atmospheric phenomena such as thunderstorms. The Kelvin water dropper uses falling water to generate a potential difference by electrostatic induction between two interconnected, oppositely charged systems, and it utilizes the initial instantaneous non-equilibrium status of charge distributions in the liquid rather than the friction between the liquid and air.

Recently, triboelectric nanogenerator (TEENG) has been developed to convert mechanical vibration energy into electricity. The working mechanism of TEENG is based on a combination of contact electrification and electrostatic induction. Normally, TEENG needs a relatively dry condition to provide a stable output, because the surface triboelectrification would be largely reduced or totally eliminated owing to the presence of water.

There is a need for a new prototype TEENG to harvest water-related energy. There is also a need to maximize the TEENG's output by converting both mechanical kinetic energy and electrostatic energy from water into electricity.

### BRIEF SUMMARY DISCLOSED

The disclosed technology relates to energy harvesting. One aspect of the disclosed technology relates to a generator. The generator includes a plurality of blades arranged in a radially outward fashion. Each blade includes an electrode and a surface layer for receiving flowing water carrying triboelectric charges. The flowing water affects a flow of electrons between the electrode and ground.

Another aspect of the disclosed technology relates to a generator having a first component for receiving flowing water carrying triboelectric charges. The first component

harvests electrostatic energy from the flowing water. The generator includes a second component coupled to the first component. The second component includes a rotatable disk that rotates when the first component receives the flow water. The second component harvests mechanical kinetic energy from the flowing water during rotation.

Yet another aspect of the disclosed technology relates to a generator for harvesting energy from wind. The generator includes a first member including a first electrode. A second member is coupled to the first member about an axis. The second member includes a second electrode and a surface layer between the first electrode and the second electrode. The second member is rotatable with respect to the axis by wind to change triboelectric charges on the electrodes, and to affect a flow of electrons between the electrodes.

A further aspect of the disclosed technology relates to a self-powered sensor for detecting energy flow rate. The sensor includes a first member including a first electrode. The sensor also includes a second member coupled to the first member about an axis. The second member includes a second electrode and a surface layer between the first electrode and the second electrode. The second member is rotatable with respect to the axis by energy flow to change triboelectric charges on the electrodes, and to affect a flow of electrons between the electrodes. A processor is configured to detect the energy flow rate based on at least one of a measurement of current generated by the flow of electrons and a rotation speed of the second member.

One aspect of the disclosed technology relates to a generator. The generator includes an electrode and a superhydrophobic surface layer for receiving flowing water carrying triboelectric charges. The surface layer includes a TiO<sub>2</sub> layer with nanostructures thereon. The flowing water affects a flow of electrons between the electrode and ground.

Another aspect of the disclosed technology relates to a generator. The generator includes a first component for receiving flowing water carrying triboelectric charges, and harvesting electrostatic energy from the flowing water. A second component is coupled to the first component. The second component harvests mechanical kinetic energy from the flowing water. When the first component receives the flowing water, the first component contacts the second component to affect a flow of electrons at the first component and the second component.

A further aspect of the disclosed technology relates to a self-powered sensor for detecting chemical. The sensor includes a triboelectric generator including an electrode and a superhydrophobic surface layer for receiving a solution containing a chemical and water. The chemical removes at least one triboelectric charge from the water. The sensor also includes a power indicator indicative of whether the chemical is present based on power output of the triboelectric generator.

These and other aspects of the disclosed technology are described in the Detailed Description disclosed below and the accompanying figures. Other aspects and features of embodiments of the disclosed technology will become apparent to those of ordinary skill in the art upon reviewing the following description of specific, exemplary embodiments of the disclosed technology in concert with the figures. While features of the disclosed technology may be discussed relative to certain embodiments and figures, all embodiments of the disclosed technology can include one or more of the features discussed herein. While one or more embodiments may be discussed as having certain advantageous features, one or more of such features may also be used with the various embodiments of the disclosed tech-

nology discussed herein. In similar fashion, while exemplary embodiments may be discussed below as system or method embodiments, it is to be understood that such exemplary embodiments may be implemented in various devices, systems, and methods of the disclosed technology.

#### BRIEF DESCRIPTION OF THE DRAWINGS

The following Detailed Description technology is better understood when read in conjunction with the appended drawings. For the purposes of illustration, there is shown in the drawings exemplary embodiments, but the subject matter is not limited to the specific elements and instrumentalities disclosed.

FIG. 1 provides a schematic illustration of a water-TENG according to one aspect of the disclosed technology.

FIG. 2A provides a SEM image of a prepared PTFE thin film with hierarchical micro-/nanostructures according to one aspect of the disclosed technology.

FIG. 2B is a photograph of a large-sized PTFE thin film with a uniform superhydrophobic property according to one aspect of the disclosed technology.

FIG. 3 illustrates a fabrication process of a superhydrophobic PTFE thin film with hierarchical micro-/nanostructures according to one aspect of the disclosed technology.

FIG. 4 provides a SEM image of an AAO template with irregular microstructures and nanometer-sized holes according to one aspect of the disclosed technology.

FIG. 5 schematically illustrates an operating principle of the water-TENG for harvesting energy from a water drop according to one aspect of the disclosed technology.

FIG. 6 schematically illustrates an operating principle of the water-TENG for harvesting energy from flowing water or continuous water drop according to one aspect of the disclosed technology.

FIG. 7A illustrates output voltage of the water-TENG according to one aspect of the disclosed technology.

FIG. 7B illustrates output current of the water-TENG according to one aspect of the disclosed technology.

FIG. 7C illustrates a relationship between water drop falling height and inductively transferred charges of the water-TENG according to one aspect of the disclosed technology.

FIG. 7D illustrates dependence of output voltage and output current of the water-TENG on the resistance of the external load according to one aspect of the disclosed technology.

FIG. 7E illustrates dependence of output power of the water-TENG on the resistance of the external load according to one aspect of the disclosed technology.

FIG. 7F illustrates dependence of output energy of the water-TENG on the resistance of the external load according to one aspect of the disclosed technology.

FIG. 8A illustrates output current density of a water-TENG having a hydrophilic Nylon film with a smooth surface according to one aspect of the disclosed technology.

FIG. 8B illustrates output current density of a water-TENG having hydrophobic PTFE film with a smooth surface according to one aspect of the disclosed technology.

FIG. 9A illustrates output current density of the water-TENG when harvesting energy from flowing tap water according to one aspect of the disclosed technology.

FIG. 9B illustrates AC output transformed to pulse output in the same direction by a full-wave rectifying bridge according to one aspect of the disclosed technology.

FIG. 9C is a photograph of the water-TENG used as a direct power source to light up 20 LEDs according to one aspect of the disclosed technology.

FIG. 9D illustrates a rectified output of the water-TENG used to charge a commercial capacitor of 33  $\mu$ F.

FIG. 9E illustrates power density of the water-TENG when harvesting energy from flowing tap water according to one aspect of the disclosed technology.

FIG. 10A provides a schematic illustration of a double-layered water-TENG according to one aspect of the disclosed technology.

FIG. 10B illustrates output current density of the double-layered water-TENG when harvesting energy from flowing tap water according to one aspect of the disclosed technology.

FIG. 11A provides a schematic diagram of an integrated TENG system having a water-TENG and a packaged conventional TENG according to one aspect of the disclosed technology.

FIG. 11B provides a SEM image of a patterned PDMS pyramid array according to one aspect of the disclosed technology.

FIG. 11C illustrates output current density of the water-TENG of the integrated TENG system of FIG. 11A according to one aspect of the disclosed technology.

FIG. 11D provides a photograph of the water-TENG used as a direct power source to light up 20 LEDs according to one aspect of the disclosed technology.

FIG. 11E illustrates output current density of the packaged conventional TENG according to one aspect of the disclosed technology.

FIG. 11F illustrates both the rectified outputs from the water-TENG and the packaged TENG used to charge commercial capacitors of 33  $\mu$ F according to one aspect of the disclosed technology.

FIG. 11G illustrates output current density of the water-TENG for harvesting energy from spray water drop at a higher water temperature of 65° C. according to one aspect of the disclosed technology.

FIG. 12A provides a structure diagram of a water wheel hybridized triboelectric nanogenerator according to one aspect of the disclosed technology.

FIG. 12B provides a structure diagram of a PTFE thin film with nanostructures according to one aspect of the disclosed technology.

FIG. 12C provides a SEM image of the PTFE thin film with nanostructures according to one aspect of the disclosed technology.

FIG. 12D illustrates a contact angle of the PTFE thin film with nanostructures according to one aspect of the disclosed technology.

FIG. 12E is a photograph of the generator of FIG. 12A according to one aspect of the disclosed technology.

FIGS. 13A-D illustrate the working mechanism of the water-TENG of the generator of FIG. 12A according to one aspect of the disclosed technology.

FIGS. 14A-D illustrate the working mechanism of the disk-TENG of the generator of FIG. 12A according to one aspect of the disclosed technology.

FIG. 15A illustrates  $V_{oc}$  curve of the water-TENG of the generator of FIG. 12A according to one aspect of the disclosed technology.

FIG. 15B illustrates  $V_{oc}$  curve of the disk-TENG of the generator of FIG. 12A according to one aspect of the disclosed technology.

## 5

FIG. 15C illustrates  $I_{sc}$  curve of the water-TENG of the generator of FIG. 12A according to one aspect of the disclosed technology.

FIG. 15D illustrates  $I_{sc}$  curve of the disk-TENG of the generator of FIG. 12A according to one aspect of the disclosed technology.

FIG. 16A illustrates short-circuit current curve of the water-TENG of the generator of FIG. 12A by using a nylon film according to one aspect of the disclosed technology.

FIG. 16B illustrates short-circuit current curve of the water-TENG of the generator of FIG. 12A by using a smooth PTFE film without nanorods according to one aspect of the disclosed technology.

FIG. 16C illustrates short-circuit current of the disk-TENG of the generator of FIG. 12A with a flowing water rate of 54.4 ml/s, as the superhydrophobic PTFE film of the blades is replaced, according to one aspect of the disclosed technology.

FIG. 17A illustrates dependences of the open-circuit voltage of the water-TENG of the generator of FIG. 12A on the load resistance according to one aspect of the disclosed technology.

FIG. 17B illustrates dependences of the short-circuit current of the water-TENG of the generator of FIG. 12A on the load resistance according to one aspect of the disclosed technology.

FIG. 17C illustrates dependences of the open-circuit voltage of the disk-TENG of the generator of FIG. 12A on the load resistance according to one aspect of the disclosed technology.

FIG. 17D illustrates dependences of the short-circuit current of the disk-TENG of the generator of FIG. 12A on the load resistance according to one aspect of the disclosed technology.

FIG. 18A illustrates dependences of the instantaneously maximum power and power density on the load resistance of the water-TENG of the generator of FIG. 12A according to one aspect of the disclosed technology.

FIG. 18B illustrates dependences of the instantaneously maximum power and power density on the load resistance of the disk-TENG of the generator of FIG. 12A according to one aspect of the disclosed technology.

FIG. 18C illustrates dependences of the  $V_{oc}$  and  $I_{sc}$  values on the flowing water rate of the water-TENG of the generator of FIG. 12A according to one aspect of the disclosed technology.

FIG. 18D illustrates dependences of the  $V_{oc}$  and  $I_{sc}$  values on the flowing water rate of the disk-TENG of the generator of FIG. 12A according to one aspect of the disclosed technology.

FIG. 19 illustrates dependence of the rotation speed of the disk-TENG of the generator of FIG. 12A on the flowing water rate according to one aspect of the disclosed technology.

FIG. 20A is a photograph of 20 commercial LED bulbs driven by the generator of FIG. 12A at a flowing water rate of 54 ml/s according to one aspect of the disclosed technology.

FIG. 20B illustrates measured voltage of a 4.7  $\mu$ F capacitor charged by the generator of FIG. 12A and each component thereof at a flowing water rate of 54 ml/s according to one aspect of the disclosed technology.

FIG. 21A illustrates  $I_{sc}$  curve at various wind speeds of the disk-TENG of the generator of FIG. 12A when it is driven by wind according to one aspect of the disclosed technology.

## 6

FIG. 21B illustrates dependences of  $V_{oc}$  and  $I_{sc}$  values on wind speed of the disk-TENG of the generator of FIG. 12A when it is driven by wind according to one aspect of the disclosed technology.

FIG. 22 illustrates dependence of the rotation speed of the disk-TENG of the generator of FIG. 12A on the wind speed according to one aspect of the disclosed technology.

FIG. 23 illustrates short-circuit current curve of the water-TENG of the generator of FIG. 12A without flowing water as it is driven by wind at a wind speed of 15.1 m/s according to one aspect of the disclosed technology.

FIG. 24 provides a schematic illustration of a generator according to one aspect of the disclosed technology.

FIG. 25A provides a SEM image of assembled  $\text{SiO}_2$  nanoparticles according to one aspect of the disclosed technology.

FIG. 25B provides a SEM image of a prepared  $\text{TiO}_2$  layer with irregular structures according to one aspect of the disclosed technology.

FIG. 26A illustrates a Raman spectrum of the prepared  $\text{TiO}_2$  layer according to one aspect of the disclosed technology.

FIG. 26B illustrates an XRD pattern of the prepared  $\text{TiO}_2$  layer according to one aspect of the disclosed technology.

FIG. 27A illustrates an advancing contact angle of the prepared  $\text{TiO}_2$  layer according to one aspect of the disclosed technology.

FIG. 27B illustrates an advancing contact angle of the prepared  $\text{TiO}_2$  layer after coating with PFTS according to one aspect of the disclosed technology.

FIG. 28 illustrates UV-Vis absorption spectra of the MB solution under the solar light irradiation in the presence of the prepared  $\text{TiO}_2$  layer according to one aspect of the disclosed technology.

FIG. 29 illustrates a fabrication process of the generator of FIG. 24 according to one aspect of the disclosed technology.

FIG. 30A provides a fluorescence image of *E. coli* in LB media under the solar light irradiation for 60 min without the prepared  $\text{TiO}_2$  layer according to one aspect of the disclosed technology.

FIG. 30B provides a fluorescence image of *E. coli* in LB media under the solar light irradiation for 60 min with the prepared  $\text{TiO}_2$  layer according to one aspect of the disclosed technology.

FIG. 31A illustrates working mechanism of the water-TENG of the generator illustrated in FIG. 24 according to one aspect of the disclosed technology.

FIG. 31B illustrates working mechanism of the contact-TENG of the generator illustrated in FIG. 24 according to one aspect of the disclosed technology.

FIG. 32A illustrates generated  $V_{oc}$  from Output 1 of the generator of FIG. 24 under the impact of the flowing water from a household faucet according to one aspect of the disclosed technology.

FIG. 32B illustrates generated  $V_{oc}$  from Output 2 of the generator of FIG. 24 under the impact of the flowing water from a household faucet according to one aspect of the disclosed technology.

FIG. 32C illustrates generated  $I_{sc}$  from Output 1 of the generator of FIG. 24 under the impact of the flowing water from a household faucet according to one aspect of the disclosed technology.

FIG. 32D illustrates generated  $I_{sc}$  from Output 2 of the generator of FIG. 24 under the impact of the flowing water from a household faucet according to one aspect of the disclosed technology.



FIG. 33A illustrates dependence of generated  $V_{oc}$  from Output 1 of the generator of FIG. 24 on the resistance of the external load according to one aspect of the disclosed technology.

FIG. 33B illustrates dependence of generated  $V_{oc}$  from Output 2 of the generator of FIG. 24 on the resistance of the external load according to one aspect of the disclosed technology.

FIG. 33C illustrates dependence of generated  $I_{sc}$  from Output 1 of the generator of FIG. 24 on the resistance of the external load according to one aspect of the disclosed technology.

FIG. 33D illustrates dependence of generated  $I_{sc}$  from Output 2 of the generator of FIG. 24 on the resistance of the external load according to one aspect of the disclosed technology.

FIG. 33E illustrates dependence of instantaneous power density from Output 1 of the generator of FIG. 24 on the resistance of the external load according to one aspect of the disclosed technology.

FIG. 33F illustrates dependence of instantaneous power density from Output 2 of the generator of FIG. 24 on the resistance of the external load according to one aspect of the disclosed technology.

FIG. 34 provides a schematic illustration of a generator according to one aspect of the disclosed technology.

FIG. 35A illustrates generated  $I_{sc}$  from Output 1 of the generator of FIG. 34 under the impact of the flowing water from a household faucet according to one aspect of the disclosed technology.

FIG. 35B illustrates generated  $I_{sc}$  from Output 2 of the generator of FIG. 34 under the impact of the flowing water from a household faucet according to one aspect of the disclosed technology.

FIG. 36 illustrates generated  $I_{sc}$  from a single water-TENG under the impact of the flowing water from a household faucet according to one aspect of the disclosed technology.

FIG. 37A illustrates a diagram of corresponding circuit connection polarities and a photograph of rectified outputs from Output 1 and Output 2 of the generator of FIG. 34 to drive commercial LEDs according to one aspect of the disclosed technology.

FIG. 37B illustrates charging curves of 33  $\mu$ F capacitors by the rectified outputs from Output 1 and Output 2 of the generator of FIG. 34 according to one aspect of the disclosed technology.

FIG. 38A illustrates output  $I_{sc}$  of the water-TENG generated by deionized water drops according to one aspect of the disclosed technology.

FIG. 38B illustrates output  $I_{sc}$  of the water-TENG generated by a solution containing 20% ethanol (percentage by volume) according to one aspect of the disclosed technology.

FIG. 38C illustrates output  $I_{sc}$  value of the water-TENG generated by samples containing different concentration of ethanol according to one aspect of the disclosed technology.

FIG. 38D illustrates inductively transferred charges of the water-TENG generated by samples containing different concentration of ethanol according to one aspect of the disclosed technology.

FIG. 39 illustrates a triboelectric series.

## DETAILED DESCRIPTION

To facilitate an understanding of the principles and features of the various embodiments of the present invention, various illustrative embodiments are explained below.

Although exemplary embodiments of the present invention are explained in detail, it is to be understood that other embodiments are contemplated. Accordingly, it is not intended that the present invention is limited in its scope to the details of construction and arrangement of components set forth in the following description or examples. The present invention is capable of other embodiments and of being practiced or carried out in various ways. Also, in describing the exemplary embodiments, specific terminology will be resorted to for the sake of clarity.

It must also be noted that, as used in the specification and the appended claims, the singular forms “a,” “an” and “the” include plural references unless the context clearly dictates otherwise. For example, reference to a component is intended also to include composition of a plurality of components. References to a composition containing “a” constituent is intended to include other constituents in addition to the one named.

Also, in describing the exemplary embodiments, terminology will be resorted to for the sake of clarity. It is intended that each term contemplates its broadest meaning as understood by those skilled in the art and includes all technical equivalents that operate in a similar manner to accomplish a similar purpose.

Ranges may be expressed herein as from “about” or “approximately” or “substantially” one particular value and/or to “about” or “approximately” or “substantially” another particular value. When such a range is expressed, other exemplary embodiments include from the one particular value and/or to the other particular value.

By “comprising” or “containing” or “including” is meant that at least the named compound, element, particle, or method step is present in the composition or article or method, but does not exclude the presence of other compounds, materials, particles, method steps, even if the other such compounds, material, particles, method steps have the same function as what is named.

It is also to be understood that the mention of one or more method steps does not preclude the presence of additional method steps or intervening method steps between those steps expressly identified. Similarly, it is also to be understood that the mention of one or more components in a composition does not preclude the presence of additional components than those expressly identified. Such other components or steps not described herein can include, but are not limited to, for example, similar components or steps that are developed after development of the disclosed technology.

The materials described as making up the various elements of the present invention are intended to be illustrative and not restrictive. Many suitable materials that would perform the same or a similar function as the materials described herein are intended to be embraced within the scope of the present invention. Such other materials not described herein can include, but are not limited to, for example, materials that are developed after the time of the development of the present invention.

### 1. Water-TENG

#### 1.1 Structure

FIG. 1 is a schematic illustration of a triboelectric nanogenerator 100 according to one embodiment of the disclosed technology. The triboelectric nanogenerator 100 may also be referred to as water-TENG 100. The water-TENG 100 may harvest energy from flowing water such as household waste-

water, spray water drop and ocean wave. For example, the water-TENG **100** may harvest the electrostatic energy from the water drop.

The water-TENG **100** may include a surface layer **102**, an electrode **104**, and a substrate **108**. The surface layer **102** may include a superhydrophobic surface **106**. In one embodiment, the surface layer **102** may include a polytetrafluoroethylene (PTFE) thin film. The superhydrophobic surface **106** may include polytetrafluoroethylene (PTFE) hierarchical micro-/nanostructures **110**.

FIG. **2A** provide a scanning electron microscopy (SEM) image of an exemplary surface layer **102**. The inset of FIG. **2A** illustrates the SEM image at a higher magnification. The surface layer **102** may be prepared on a large scale. For example, FIG. **2B** illustrates a prepared large-sized surface layer with a uniform superhydrophobic property. The large-sized PTFE thin film may have a dimension of 13 cm×33 cm.

As shown in FIG. **2A**, the surface **106** of the surface layer **102** may include irregular microstructures, which may be further covered by high-density nanostructures, such as nanorods. In one embodiment, the mean length and diameter of the nanorods may be about 360 nm and 45 nm, respectively. The hierarchical micro-/nanostructures may contain trapped air, which may reduce the actual contact area between the surface layer **102** and a water drop, consequently strengthening the superhydrophobic ability of the surface layer **102**.

The superhydrophobic property of the hierarchical micro-/nanostructures-composed thin film **102** may be assessed by measuring the contact angle of a water drop. The inset of FIG. **2B** shows the advancing contact angle of the surface layer **102**.

In one embodiment, the average value of the measured contact angle of the surface layer **102** is 169°, which exceeds a minimum requirement for a superhydrophobic surface.

The water-TENG **100** may have any effective dimension, including but not limited to, 4 cm×4 cm and 15 cm×15 cm, among many other possibilities.

The surface layer **102** may have triboelectric characteristics, a triboelectric series rating, a triboelectric polarity, or a charge affinity different from that of water. FIG. **39** provides a triboelectric series.

In one example, the surface layer **102** may include a material with a relatively less negative triboelectric series rating. Examples of suitable materials for the surface layer **102** may include, but not limited to, anyone or a combination of the following materials: polyethylene terephthalate (PET), poly (methyl methacrylate) (PMMA), polydimethylsiloxan (PDMS), polytetrafluoroethylene (PTFE), fluorinated ethylene propylene (FEP), poly (vinyl chloride) (PVC), polyimide, metal and alloy, among many other possibilities.

The electrode **104** may include, but not limited to, anyone or a combination of the following materials: metal such as copper, gold, silver and aluminum, indium tin oxide (ITO) and conductive polymer, among many other possibilities.

The substrate **108** may include anyone or a combination of the following materials: PMMA and PET, among other possibilities.

## 1.2 Fabrication and Assembly

### 1.2.1 Fabricate Surface Layer

The fabrication process of water-TENG may start from the preparation of the surface layer **102** with superhydro-

phobic hierarchical structures. FIG. **3** describes a process for fabricating a PTFE thin film which may serve as the surface layer **102**.

First, microstructures may be fabricated by blasting an Al foil **302** with sand particles (diameter around 30 μm) using compressed air (4 kgf/cm<sup>2</sup>). The sand-blasted Al foil **304** may be further anodizing in a 0.3 M oxalic acid solution to obtain an anodic Al oxide (AAO) template **306** with nanometer-sized holes **308**. Specifically, the sand-blasted Al foil **304** may be put into the oxalic acid solution and acting as the anode. Another flat Al sheet may be used as the cathode. The distance between those two electrodes may be 5 cm. The operating voltage may be set up at 40 V by using a computer-interfaced power supply. During the anodization process, the solution may be maintained at a temperature of 15° C. by a circulator. As a result, the AAO template **306** with nanometer-sized holes **308** may be obtained. A Hitachi SU8010 field emission scanning electron microscope (SEM) may be used to measure the size and shape of PTFE hierarchical micro-/nanostructures and the pore diameter of AAO template. FIG. **4** provides an exemplary SEM image of the AAO template **306** with irregular microstructures and nanometer-sized holes.

Next, after cleaning the AAO template **306** with water, a commercial PTFE precursor (AF 601S2, 6 wt %, DuPont) may be poured into the AAO template. A conventional vacuum process may be applied to remove the air remaining in the nanoholes.

After the curing at ambient temperature for one day, the solvent may evaporate, leaving behind a PTFE thin film **311** with hierarchical micro-/nanostructures. Finally, the PTFE thin film **311** may be peeled off from the AAO template by using a double-sided tape **312**.

### 1.2.2 Fabricate Electrode on Substrate

In one embodiment, the electrode **104** of the water-TENG may include a Cu thin film. The Cu thin film may have a thickness about 100 nm. In one embodiment, Cu thin films may be deposited on PMMA substrates by a RF magnetron sputtering deposition system. Conducting wires may be connected to the Cu thin films as leads for subsequently electrical measurements.

### 1.2.3 Assembly

Once the PTFE thin film **311** is peeled off from the AAO template by using the double-sided tape **312**, the double-sided tape **312** may then be attached to the Cu electrode **104** deposited poly(methyl methacrylate) (PMMA) substrate to form the complete water-TENG **100**.

## 1.3 Operating Principle

The water-TENG **100** works substantially different from the working mechanism of the Kelvin water dropper. The working mechanism of the water-TENG **100** may include a sequential contact-electrification and electrostatic-induction process.

### 1.3.1 Single Water Drop

FIG. **5** schematically illustrates the working mechanism of a single-electrode-based water-TENG **100**. As shown in step (i), when the water drop **502** falls from the sky or flows through an insulating tube, triboelectricity is created and causes the surface of the water drop **502** to be positively or

negatively charged. In one example, each water drop **502** may have a surface charge density of  $4.5 \mu\text{C}/\text{m}^2$ . The charge on the water drop surface may be positive or negative depending on the counterpart that the drop interacts with. For simplicity purposes, positive charges on the water drop surface are used in FIG. 5 to illustrate the process of converting the electrostatic energy to electricity.

With continued reference to FIG. 5, at step (ii), as the positively charged water drop **502** reaches the surface layer **102**, a positive electric potential difference may be established between the water drop **502** and ground. In the short-circuit case, the electrons may transfer from ground to the electrode **104** to balance the potential from the water drop **502** and finally reach an equilibrium condition at step (iii). This contributes to an instantaneously positive current. The charge density on the water drop surface and the contact area between the water drop **502** and the surface layer **102** may affect the inductively transferred charges on the electrode **104**, which, in turn, may affect the magnitude of the generated current.

At step (iv), once the water drop moves off the surface layer **102**, it causes a negative electric potential difference and therefore, the electrons may flow from the electrode **104** to ground, until achieving a new equilibrium at step (i). This process corresponds to another instantaneously negative current. If the water drops and contacts the surface layer **102** periodically, an AC output may be continuously generated. To obtain the maximum electricity output, the water drop should be completely off after contacting the surface layer **102** to keep the surface layer **102** clean for the next cycle. When the surface layer **102** is superhydrophobic, the electricity output may be improved.

### 1.3.2 Flowing Water and Continuous Water Drop

FIG. 6 illustrates working mechanism of the water-TENG **100** in case of flowing water or continuous water drops such as raindrop. Again, a sequential process of contact electrification and electrostatic induction is involved.

As shown in FIG. 6(b), once water is left on the surface layer **102**, a thin water layer **604** may be formed on the surface layer **102** during the energy harvesting process. The water layer **604** may be a positively charged thin layer. As shown in FIG. 6(c), a positive electric potential difference may occur, causing the electrons to transfer from ground to the electrode **104** to balance the potential difference and reach equilibrium. As positively charged water drops **602** fall on the thin water layer **604**, another positive electric potential difference may occur between the water drops and ground. Then, electrons may transfer from ground to the electrode **104** to balance the potential difference and achieve equilibrium, as shown in FIG. 6(d). This contributes to an instantaneously positive current.

As shown in FIG. 6(e), once the water drops move off the water thin layer **604**, a negative electric potential difference occurs. As a result, the electrons may flow from the electrode **104** to ground, until achieving a new equilibrium as illustrated in FIG. 6(b). This process corresponds to another instantaneously negative current. If the water drops fall on the thin layer-remained water-TENG periodically, continuous outputs may be generated and collected.

## 1.4 Output Performance

### 1.4.1 Output Voltage and Output Current

In one experiment, to measure the electrical output of the water-TENG **100**, a programmable syringe pump (PHD

2000, Harvard Apparatus) is applied to control the volume and dropping speed of each water drop. In the experiment, the volume of each water drop is fixed at  $30 \mu\text{L}$ , the dropping speed is around  $1 \text{ m/s}$  when the water drop falls from a height of  $90 \text{ cm}$ , and the tap water is chosen as the water source. In the experiment, the electrical outputs of water-TENG are measured using a programmable electrometer (Keithley Model 6514) and a low-noise current preamplifier (Stanford Research System Model SR570).

From a  $30\text{-}\mu\text{L}$  water drop, the water-TENG **100** may generate a peak voltage of  $9.3 \text{ V}$ . FIG. 7A illustrates that the output voltage of  $9.3 \text{ V}$  is switched between zero and a pinnacle value, which correspond to the separated and contacted status.

From a  $30\text{-}\mu\text{L}$  water drop, the water-TENG **100** may generate a peak current of  $17 \mu\text{A}$ . FIG. 7B illustrates that the output current reaches a value of  $17 \mu\text{A}$  and exhibits AC behavior, with an equal amount of electrons flowing in opposite directions within one cycle. The inset of FIG. 7B is the magnified output curve in one cycle. The inset of FIG. 7B illustrates that the current peak corresponding to separating has a smaller magnitude but lasts longer than that for contacting. This observation may be explained by the fact that separating corresponds to a slower process and thus a smaller but wider current signal.

### 1.4.2 Water Falling Distance

The output performance of the water-TENG **100** may depend upon the water falling distance. Specifically, the charge density on the water drop surface may impact the generated output. FIG. 7C illustrates a relationship between the triboelectricity and the water falling distance. The inductively transferred charges on the electrode may be deduced by integrating the current peak of the water-TENG obtained at different falling heights from the contact surface. The inductively transferred charges on the electrode may be proportional to the charge density of water drop. As shown in FIG. 7C, the inductively transferred charges are increased when enlarging the falling height, and finally saturated at a falling height of  $20 \text{ cm}$ , corresponding to the maximum charges that a water drop can hold. FIG. 7C verifies that the triboelectricity does exist when the water drop falls through the air, and also indicates that the concept may be applied to harvest the raindrop energy from the environment.

### 1.4.3 Load Resistance

The output performance of the water-TENG **100** may depend upon the load resistance. In one experiment, the electrical output of the water-TENG **100** is measured by connecting the water-TENG **100** directly to loads of various resistances at a falling height of  $90 \text{ cm}$ . As shown in FIG. 7D, when the resistance is below  $0.1 \text{ M}\Omega$ , the voltage remains close to 0 and the current density almost has no change. When the resistance increases from  $0.1 \text{ M}\Omega$  to  $1 \text{ G}\Omega$ , the voltage through the load generally increases, but the current across the load follows an opposite trend. Therefore, as illustrated in FIG. 7E, the instantaneous power on the load remains small with the resistance below  $0.1 \text{ M}\Omega$  and reaches the maximum value of  $145 \mu\text{W}$  at a resistance of  $5 \text{ M}\Omega$ . The generated output here is from a single water drop. The output energy is also calculated by the time integral of  $I^2R$ , as illustrated in FIG. 7F. As shown in FIG. 7F, the curve exhibits that the output energy increases as the resistance

increases, and gradually saturates at a resistance of 22 M $\Omega$  (30 nJ), which is 3 orders of magnitude larger than that of 1 K $\Omega$  (0.03 nJ).

#### 1.4.4 Superhydrophobicity

The output performance of the water-TENG **100** may depend upon the superhydrophobic nature of the surface layer **102**. In one experiment, the water-TENG **100** is modified by removing the superhydrophobic nature, for example by replacing the superhydrophobic PTFE film **102** with hydrophilic Nylon film and hydrophobic PTFE film with a smooth surface. FIGS. **8A** and **8B** respectively illustrate the output performance of the two modified water-TENG generators. Both of the results clearly show the importance of superhydrophobic surface.

#### 1.4.5 Output Current Density and Instantaneous Power Density

The water-TENG **100** may be used to collect the energy of a continuously flowing tap water from a kitchen faucet. The output current density and instantaneous power density may reach 15 mA/m<sup>2</sup> and 0.2 W/m<sup>2</sup>, respectively, when considering the water-TENG dimensions. The output may directly drive 20 light-emitting diodes (LEDs) instantaneously.

In one experiment, the flowing rate of tap water is set up at around 30 mL/s and the distance between the water-TENG and faucet is 20 cm. To highlight the potential application, the generated output is divided by the water-TENG dimensions (4 cm $\times$ 4 cm). FIG. **9A** displays the output current density of the water-TENG. It is noticed that the maximum output current density may reach 15 mA/m<sup>2</sup> and the signal varies due to the unstable flowing of tap water from the faucet. The output signal becomes zero after the faucet is turned off, revealing that the output is generated from the faucet flowing water. As shown in FIG. **9B**, the AC output may be transformed to pulse output in the same direction simply by a full-wave rectifying bridge. The inset of FIG. **9B** provides a sketch of exemplary circuit connection polarities. The rectified output may be utilized to drive 20 commercial LEDs instantaneously as illustrated FIG. **9C**, and charge a 33- $\mu$ F capacitor as illustrated in FIG. **9D**. The inset of FIG. **9D** illustrates a sketch of exemplary circuit connection polarities.

As shown in FIG. **9E**, the instantaneous peak to peak power density is determined about 0.2 W/m<sup>2</sup> when the water-TENG is connected to a 5 M $\Omega$  load resistor.

## 2. Double-Layered Water-TENG

FIG. **10A** illustrates a multilayer-based device **1000** to harvest energy from water according to one aspect of the disclosed technology. The device **1000** may include multiple layers of the water-TENG **100** described earlier. In one example, the device **1000** may be a double-layered water-TENG. The double-layered water-TENG **1000** may be more effective than the single-layered water-TENG **100** in harvesting energy from faucet flowing water. FIG. **10B** shows that the double-layered water-TENG **1000** may provide twice generated output as compared to that of single-layered water-TENG as illustrated in FIG. **9A**.

## 3. Hybrid Generator

Flowing water carries two types of energies. One type of energy is electrostatic energy due to the existence of tribo-

electric charges on its surface as a result of contact with surrounding media due to the contact electrification, such as contact with air/solid surface during its traveling processes in pipe and/or air. The other type of energy is mechanical kinetic energy.

The disclosed technology includes various embodiments of a hybrid triboelectric nanogenerator designed to simultaneously harvest the electrostatic and mechanical kinetic energies of flowing water. Detailed discussions with respect to these alternative embodiments are provided herein.

## 3.1 Water-TENG and Packaged TENG

### 3.1.1 Structure

FIG. **11A** illustrates an integrated energy collection system **1100** including a water-TENG **100** (also denoted by (i) in the figure) and a packaged TENG **1110** (also denoted by (ii) in the figure) according to one aspect of the disclosed technology. The water-TENG **100** may harvest the electrostatic energy, whereas the packaged TENG **1110** may harvest the mechanical energy. The system **1100** may effectively collect, including but not limited to, the spray water drop energy as well as the raindrop energy, among other possibilities.

### 3.1.2 Fabrication of Packaged TENG

#### 3.1.2.1 Fabricate PDMS Film

Fabrication of the packaged TENG **1110** may start from the design of PDMS film with patterned pyramid array as illustrated in FIG. **11B**. The inset of FIG. **11B** is a SEM image at a higher magnification.

At first, a Si wafer may be molded using photolithography. Then, the wafer may be etched through a dry etching process, resulting in the Si wafer mold with a notched pyramid feature. After a clean wash by acetone and ethanol, the prepared Si wafer mold may be treated with chlorotrimethylsilane to avoid the adhesion between PDMS and Si in the next step. A PDMS mixture may be spin-coated (1000 rpm, 1 min) on the Si wafer mold and then incubated at 60 $^{\circ}$  C. The PDMS may include PDMS elastomer and cross-linker in a ratio of 5:1. After 24 hours, a uniform PDMS film with patterned pyramid array may be formed.

#### 3.1.2.2 Fabricate Electrode on Substrate

100 nm of Cu thin films may be deposited on two Kapton substrates (127  $\mu$ m, DuPont) by a RF magnetron sputtering deposition system. Conducting wires may be connected to the Cu thin films as leads for subsequently electrical measurements.

#### 3.1.2.3 Assembly

The formed PDMS film with patterned pyramid array may be peeled from Si wafer mold and then placed onto a Cu thin film-deposited Kapton substrate with uncured PDMS mixture on the top, then incubating at 60 $^{\circ}$  C. for another 24 hours. Finally, those two Kapton substrates may be assembled by using a 60- $\mu$ m-thick hot-melt ionomer film (Surlyn 1702, DuPont) under heating at 150 $^{\circ}$  C. for 10 min and a fully packaged TENG is obtained.

### 3.1.3 Output Performance

In one experiment, to measure the output performance of the system **1100**, the water-TENG **100** is configured to

dimensions of 15 cm×15 cm. In the experiment, a household shower jet system is used for the demonstration of the spray water drop. FIG. 11C illustrates that the water-TENG 100 of the system 1100 may achieve a maximum output current density of 1.5 mA/m<sup>2</sup>. The water-TENG 100 may be the primary source for harvesting energy from the spray water drop. The rectified output may successfully power 20 commercial LEDs instantaneously as illustrated in FIG. 11D.

Also from FIGS. 11E and 11F, the packaged TENG 1110 may also successfully collect the mechanical energy of spray water drop. The packaged TENG 1110 may act as the secondary source for harvesting energy from the spray water drop.

The rectified outputs of the system 1100 including the water-TENG 100 and the packaged TENG 1110 may charge a 33-μF capacitor as illustrated in FIG. 11F. The generated output of the water-TENG 100 may not be impacted by a higher water temperature of 65° C., as illustrated in FIG. 11G.

### 3.2 Water-TENG and Disk-Teng

#### 3.2.1 Structure

FIG. 12A illustrates a structure diagram of a water wheel hybridized triboelectric nanogenerator 1200. The generator 1200 may include a first component 1210 for receiving flowing water carrying triboelectric charges and harvesting electrostatic energy from the flowing water. The first component may be referred to as a water-TENG 1210. The generator 1200 may include a second component 1220 coupled to the first component for harvesting mechanical kinetic energy from the flowing water. The second component may be referred to as a disk-TENG 1220.

The water-TENG 1210 may include a plurality of wheel blades 1212. The plurality of blades 1212 may be arranged in a radially outward fashion. The plurality of blades 1212 may exhibit a wheel-like structure 1214. In one example, the water-TENG 1210 may include 8 blades and operate as a single-electrode-based triboelectric nanogenerator to harvest the electrostatic energy from flowing water.

Each blade 1212 may have a surface layer 1306 for receiving flowing water. The surface layer 1306 may be superhydrophobic. The surface layer 1306 may include a plurality of nanostructures thereon. In one example, the surface layer 1306 may include a material with a relatively less negative triboelectric series rating. Examples of suitable materials for the surface layer 102 may include, but not limited to, anyone or a combination of the following materials: polyethylene terephthalate (PET), poly (methyl methacrylate) (PMMA), polydimethylsiloxan (PDMS), polytetrafluoroethylene (PTFE), fluorinated ethylene propylene (FEP), poly (vinyl chloride) (PVC), polyimide, metal and alloy, among many other possibilities.

Each blade 1212 may include an electrode 1308. An electrical channel may be formed between the electrode on each blade and ground. The electrode 1308 may include, but not limited to, anyone or a combination of the following materials: metal such as copper, gold, silver and aluminum, indium tin oxide (ITO) and conductive polymer, among many other possibilities.

The electrode 1308 may be deposited on a substrate 1310. The substrate 1310 may include anyone or a combination of the following materials: PMMA and PET, among other possibilities.

The flowing water that falls upon each blade 1212 may carry triboelectric charges. The flowing water may affect a

flow of electrons between the electrode 1308 and ground. The flowing water impacted on the blades 1212 may induce rotation of the disk-TENG 1220.

The disk-TENG 1220 may have a disk configuration. The disk-TENG 1220 may include two disks, a front disk 1222 and a back disk 1224. Each disk may exhibit a segmented disk profile. For example, each disk may include 16 segments as illustrated in FIG. 12A. Each disk may include an electrode. For example, as illustrated in FIG. 12A, the front disk 1222 may include a front electrode 1402, and the back disk 1224 may include a back electrode 1406. Each electrode may include, but not limited to, anyone or a combination of the following materials: metal such as copper, gold, silver and aluminum, indium tin oxide (ITO) and conductive polymer, among many other possibilities.

The back disk 1224 may include a surface layer 1404 over the electrode 1406. The surface layer 1404 may be superhydrophobic. The surface layer 1404 may include a plurality of nanostructures thereon. The surface layer 1404 may include anyone or a combination of the following materials: polyethylene terephthalate (PET), poly (methyl methacrylate) (PMMA), polydimethylsiloxan (PDMS), polytetrafluoroethylene (PTFE), fluorinated ethylene propylene (FEP), poly (vinyl chloride) (PVC), polyimide, metal and alloy, among many other possibilities.

A smooth metal rod 1230 may travel through the centers of the wheel-like structure 1214 and the two disks along the rotation axis "A".

The front disk 1222 may be fixed on the rotation axis and stays motionless during the whole process. A screw behind the back disk 1224 may be used to adjust the distance between the two disks. A closer contact can induce higher effective contact area, tribo-charge density,  $V_{oc}$ , and  $I_{sc}$ , while largely increasing the rotation resistance between the two disks. In one embodiment, the two disks may moderately contact in a low rotation resistance status, as seen in FIG. 14A. In FIG. 14A, the surface layer 1404 of the back disk 1224 is positioned between the back electrode 1406 and the front electrode 1402. The disk-TENG 1220 may harvest the mechanical energy of the water, in which an electrical channel is formed between the electrodes of the two disks.

The back disk 1224 may be rotatable with respect to the rotation axis "A" by energy flow, such as flowing water or wind, to change triboelectric charges on the front electrode 1402 and the back electrode 1406. Rotation of the back disk 1224 may affect a flow of electrons between the electrodes 1402 and 1406.

The back disk 1224 may be connected to the wheel-like structure 1214. The back disk 1224 may be rotatable such that it may rotate when the water-TENG 1210 receives the flowing water. For example, when a blade 1212 receives the flowing water, the blade 1212 may gather the flowing water force. The blade 1212 may induce rotation of the water-TENG 1210 and the back disk 1224 about a rotation axis "T" as depicted in FIG. 12A. The blade 1212 may gather the flowing water force to drive the rotation of the wheel-like structure 1214 and the back disk 1224.

The back disk 1224 may rotate together with the blades 1212 under the impact of flowing water. The disk-TENG 1220 may harvest mechanical kinetic energy from the flowing water during rotation.

In one example, each blade 1212 as well as the back disk 1224 may include a superhydrophobic surface layer. The surface layer may include high-density PTFE nanostructures 1240 as illustrated in FIG. 12B. In one embodiment, the surface layer may include a PTFE film. FIG. 12 C provides a SEM image of the surface layer. In one embodiment, the

mean length and diameter of the PTFE nanostructures **1240** may be 360 nm and 45 nm. The contact angle of the surface layer may be 162°, as illustrated in FIG. **12D**. The high-density nanostructures **1240** covered on the surface layer may contain trapped air and reduce the actual contact area between the surface layer and water droplets, which increases the superhydrophobic ability. The nanostructures **1240** on the surface layer may increase the effective contact area of two tribo-surfaces and enhance the electrical output of the disk-TENG **1220**.

FIG. **12E** is a photograph of the generator **1200**. In one embodiment, the generator **1200** may include a PET sheet between the blades **1212** and the back disk **1224** to prevent the disk-TENG **1220** from water when the generator is at work. However, for the purpose of clearly showing the structure of the generator **1200**, the PET sheet is not shown in the structure diagram FIG. **12A** nor the photograph FIG. **12E** of the generator **1200**.

### 3.2.2 Fabrication

The generator **1200** may be fabricated according to the following exemplary process. To fabricate the blades **1212**, a 100-nm-thin Cu film may be deposited on a square Polyethylene terephthalate (PET) sheet to serve as the electrode layer. The PET sheet may have a thickness of 0.5 mm. The PET sheet may be processed by laser cutting (e.g., PLS6.75, Universal Laser Systems) to serve as the substrate of the blades. A Cu film, e.g., of thickness of 100 nm, may be deposited on the substrate by e-beam evaporator. A PTFE film with nanostructures fabricated by using porous anodic Al oxide (AAO) as template may be attached onto the Cu electrode by using a double-sided tape. The Cu electrodes of the 8 blades may be electrically connected together.

To fabricate the disks **1222** and **1224**, two Poly(methyl methacrylate) (PMMA) sheets may be first processed by laser cutting to form the 16-segment-structured circle disks as the substrates of the disks **1222** and **1224**. The PMMA sheets may have a thickness of 3 mm. For the back disk, a 100-nm thin Cu film may be deposited on one PMMA substrate by e-beam evaporator. Then, a PTFE film with nanostructures may be attached onto the Cu electrode by using a double-sided tape. For the front disk, another 100-nm thin Cu film may be deposited on the other PMMA substrate and directly used as the contact material. The PTFE layer of the back disk and the Cu layer of the front disk may be brought to a face-to-face intimate contact to form a sliding TENG operating at a rotation disk mode.

The smooth metal rod **1230** may be used as a rotation axis to assemble the generator **1200** through the centers of the blades **1212** and the two disks **1222** and **1224**.

### 3.2.3 Operating Principle

#### 3.2.3.1 Operating Principle of Water-TENG

FIGS. **13A-D** schematically illustrate the working mechanism of the water-TENG **1210** of the generator **1200**.

As shown in FIG. **13A**, flowing water **1302** may have positive tribo-charges due to the contact electrification between the water and the pipe/air during its traveling processes. As the flowing water reaches the blade-1, a positively charged water film **1304** may be formed on the surface layer **1306** of the blade-1, because of the tribo-charges created between the water and the water pipe. As a result, a positive potential difference may be created between the electrode **1308** of the blade-1 and ground,

which may drive the electrons to transfer from ground to the electrode **1308** of the blade-1 and generate a positive current until the potential difference is decreased to zero. Because the flowing water impacted on the blade-1 may also cause the rotation of wheel, the flowing water may next contact the blade-2 as illustrated in FIG. **13C**. Then, another positively charged water film **1304** may form on the PTFE surface of the blade-2, consequently, another positive potential difference may be created between the electrode **1308** of the blade-2 and ground, attributing a positive current until the potential difference is decreased to zero. After this, as illustrated in FIG. **13D**, the water film with its positive charges may move off the surface layer, e.g., the PTFE film, of blade-1 due to the continuous rotation of blades and the superhydrophobic property of the surface. With continued reference to FIG. **13D**, with the removal of the water film from the blade-1, a negative potential difference may be generated between the electrode of blade-1 and ground because of the negative charges on the electrode, which drives the electrons to transfer from the electrode to ground and generates a negative current until the potential difference becomes zero. With the continuous rotation of the blades, the water reaches different blades in sequence. Alternative positive and negative current may be generated with similar processes as shown in FIGS. **13C-D**.

The superhydrophobicity of the surface layer on the blades plays a key role for the removal of the water film. As a result, the superhydrophobicity enhances the electrical output of the water-TENG.

#### 3.2.3.2 Operating Principle of Disk-TENG

FIGS. **14A-14D** schematically illustrate the working mechanism of the disk-TENG **1220** of the generator **1200**. In the initial stage, the front disk **1222** and the back disk **1224** may fully contact each other. As illustrated in FIG. **14A**, the positive and negative tribo-charges may be generated on the Cu electrode surface **1402** of the front disk **1222** and the PTFE surface **1404** of the back disk **1224**, respectively, since PTFE has stronger tendency to gain electrons than Cu in the triboelectric series. At the initial stage, the positive and negative charges may fully overlap with each other, and thus there is no potential difference between the Cu electrodes of the two disks and no current is generated. With the rotation of the back disk, the two disks are partly separated as shown in FIG. **14B**, and a positive potential difference on the front electrode **1402** is formed, which drives the electrons to flow from the back electrode **1406** to the front electrode **1402** and generates a positive current. As the two disks are fully separated as shown in FIG. **14C**, the induced positive charges on the back electrode **1406** may reach its maximum value, and the net charges on the front electrode **1402** may decrease to zero. As the back disk **1224** continues rotating, the front electrode **1402** begins to contact the PTFE film **1404** of another adjacent segment of the back disk as shown in FIG. **14D**, and then a negative potential difference is formed on the front electrode **1402**, which drives the electrons to flow from the front electrode **1402** to the back electrode **1406** and generates a negative current. Next, the two disks fully contact with each other again as shown in FIG. **14A**, the induced charges in the back electrodes **1406** fully flow to the front electrode **1402**. With the further rotation of the back disk **1224**, another cycle similar to the processes from FIG. **14A** to **14D** will start.

## 3.2.4 Output Performance

## 3.2.4.1 Output Voltage and Output Current

In an experiment to measure electrical output properties of the generator **1200**, tap water flowing from a household faucet at a flow rate of 54 ml/s is used to drive the generator **1200**, and the vertical distance between the water outlet of the faucet and the rotation axis of the generator **1200** is around 25 cm. In the experiment, current meter (SR570 low noise current amplifier, Stanford Research System) and voltage meter (6514 system electrometer, Keithley) are used to measure the electric outputs of the generator **1200**.

FIG. **15A** and FIG. **15B** illustrate curves of open-circuit voltage,  $V_{oc}$ , of the water-TENG **1210** and the disk-TENG **1220**, respectively. Their magnification curves are shown in the insets. As illustrated, at a flowing water rate of 54 ml/s, the open-circuit voltage  $V_{oc}$  of the water-TENG **1210** and the disk-TENG **1220** may be about 72 and 102 V, respectively. The positive  $V_{oc}$  value of the water-TENG **1210** indicates the positive tribo-charges in the flowing water from the household faucet.

FIGS. **15C-D** illustrate curves of the short-circuit current ( $I_{sc}$ ) of the water-TENG **1210** and the disk-TENG **1220**. Their magnification curves are shown in the insets. As illustrated, at a flowing water rate of 54 ml/s, the short-circuit current  $I_{sc}$  of the water-TENG **1210** and the disk-TENG **1220** may reach 12.9 and 3.8  $\mu\text{A}$ , respectively.

By integrating the absolute values of the  $I_{sc}$  curve of the water-TENG **1210**, the collected charge in a unit time is 0.68  $\mu\text{Q/s}$ . Therefore, the carried tribo-charge in the flowing water in a unit time is 0.34  $\mu\text{Q/s}$ , and the corresponding tribo-charge density in the flowing water from faucet is 6.3 nQ/ml. The mean interval time between two positive current peaks of the water-TENG **1210** and the disk-TENG **1220** are around 0.03 and 0.015 s, respectively, and the corresponding output frequencies are 33.3 and 66.7 Hz, respectively. The output frequency of the TENG with multiple segments may be expressed by  $f=nN/60$ , where  $n$  is the number of the divided segments in the generator **1200** and  $N$  is the rotation speed in a unit of rounds per minute (rpm). According to this equation, the rotation speed of the generator **1200** at a flowing water rate of 54 ml/s is around 249 rpm. Since the two components **1210** and **1220** of the generator **1200** have the same rotation speed and the segment number of the disk-TENG **1220** (16) is two times of that of the water-TENG **1210** (8), the output frequency of the disk-TENG **1220** is two times of that of the water-TENG **1210**. Increasing the segment number in the disk and the blades number in the blades can increase the output frequency of the disk-TENG **1220** and the water-TENG **1210**, respectively.

For the water-TENG **1210**, the positive and negative current peaks correspond to the processes of the formation and the removal of the positively charged water film on the blade surface, respectively. As shown in FIG. **15C**, the positive current peak of the water-TENG **1210** is remarkably higher than the negative current peak, which indicates that the removal process of the water film requires longer time than the formation process.

## 3.2.4.2 Superhydrophobicity

In another experiment, the superhydrophobic PTFE film on the blades is replaced by a hydrophilic nylon film and a hydrophobic smooth PTFE film without nanorods to test the effect of the superhydrophobicity on the output performance of the generator **1200**. With the use of a nylon film in the

blade surface and the same experiment conditions, the periodically sharp current peaks disappear and only some irregular peaks around 0.4  $\mu\text{A}$  are present as shown in FIG. **16A**. With the use of a smooth PTFE film of contact angle about  $120^\circ$  and the same experiment conditions, the  $I_{sc}$  peaks of the water-TENG **1210**, as illustrated in FIG. **16B**, decrease about 60% compared to that using superhydrophobicity PTFE film with nanorods. As shown in FIG. **16C**, the  $I_{sc}$  curve of the disk-TENG **1220** stays almost the same as that using the superhydrophobicity PTFE film with nanorods in the blades. The comparison result indicates that superhydrophobic surface of the blades plays a critical role for the removal of the water film on the blade surface and is helpful for enhancing the output performance of the water-TENG **1210**. Since the disk-TENG **1220** is designed to harvest the mechanical energy of the flowing water, its output performance is independent of the hydrophobic property of the blades surface.

## 3.2.4.3 Load Resistance

In order to investigate the output power of the generator **1200** at an external load resistor, the output voltage and output current of the water-TENG and the disk-TENG at various load resistances ranging from  $100\Omega$  to  $1\text{ G}\Omega$  are measured, and the corresponding output power value at each resistance is calculated by using  $P=IV$ . FIGS. **17A-D** illustrate dependences of the output voltage and output current of the water-TENG **1210** and the disk-TENG **1220** on the load resistance. FIGS. **18A** and **18B** show dependences of the instantaneously maximum output power and the corresponding power density (the output power per contact area of the generator) of the water-TENG **1210** and the disk-TENG **1220**, respectively. For the water-TENG **1210**, the instantaneously maximum power of 0.24 mW appears at a load of 88 M $\Omega$ , and the corresponding instantaneously maximum power density is 0.59 W/m<sup>2</sup>. For the disk-TENG **1220**, the instantaneously maximum power of 0.17 mW appears at a load of 88 M $\Omega$ , and the corresponding instantaneously maximum power density is 0.03 W/m<sup>2</sup>. The  $V_{oc}$  and  $I_{sc}$  of the water-TENG **1210** and the disk-TENG **1220** at various flowing water rates ranging from 7 to 54 ml/s are measured. The dependences of  $V_{oc}$  and  $I_{sc}$  on the flowing water rate for the water-TENG **1210** are shown in FIG. **18C**, in which  $V_{oc}$  values stay almost constant at about 72 V for various flow rates, and the  $I_{sc}$  value increases from 4.3 to 12.9  $\mu\text{A}$  as the flowing water rate increases from 7 to 54 ml/s. The increase of the  $I_{sc}$  is caused by more tribo-charges carried in the flowing water in a unit time at a higher flowing rate. The dependences of  $V_{oc}$  and  $I_{sc}$  on the flowing water rate for the disk-TENG **1220** are shown in FIG. **18D**, in which  $V_{oc}$  values stay almost constant at about 101 V for various flowing rates, and the  $I_{sc}$  value increases almost in a linear fashion with respect to the flowing water rate. For the generator **1200** operating at the rotation disk mode, the  $I_{sc}$  values may increase linearly with respect to the rotation speed of the disk. As shown in FIG. **19**, the rotation speed of the generator **1200** increases linearly with the flowing water rate, which is the reason for the linear increase of the  $I_{sc}$  values of the disk-TENG **1220**. This linear dependence of the  $I_{sc}$  value on the flowing water rate demonstrates its potential application as a self-powered sensor for detecting flowing water rate. In one example, the self-powered sensor may detect energy flow rate, including but not limited flowing water rate and wind speed, among other possibilities. The self-powered sensor may include a processor configured to detect the energy flow rate. In one embodi-

ment, the processor may detect the energy flow rate based on a measurement of current generated by the flow of electrons. In addition or as an alternative, the processor may detect the energy flow rate based on a rotation speed of the back disk **1224**.

### 3.2.5 Application

#### 3.2.5.1 LEDs

For practical applications in driving LEDs or charging a capacitor, the electrical output of the water-TENG **1210** and the disk-TENG **1220** may be connected in parallel after they are converted to pulse output in the same directions by using two full-wave rectifying bridges, as shown in the inset of FIG. **20A**. As the generator **1200** is driven by water at a flow rate of 54 ml/s, 20 commercial green LEDs may light up, as shown in FIG. **20A**. The generator **1200** may charge a capacitor of 4.7  $\mu\text{F}$  at a flowing water rate of 54 ml/s. FIG. **20B** illustrates the voltage curves of the capacitor. When the capacitor is charged by the rectified output of the water-TENG **1210** and the rectified output of the disk-TENG **1220**, respectively, it takes about 596 s and 435 s to charge the capacitor to a voltage of 13 V, respectively. When using the generator **1200** as a whole, it takes 326 s to charge the capacitor to a voltage of 13 V.

#### 3.2.5.2 Wind

The generator **1200** may harvest wind energy and act as a self-powered sensor to detect the flowing water rate and wind speed.

Since the rotation of the blades **1212** may be driven by wind, the generator **1200** may harvest the wind energy. The wind with various speeds may drive the rotation of the disk-TENG **1220**. The back disk **1224** may rotate with respect to the rotation axis "A" under the influence of the wind. As a result, the triboelectric charges on the front and back electrodes **1402** and **1406** may change during this process, and affect a flow of electrons between the electrodes **1402** and **1406**.

FIG. **21A** illustrates the measured  $I_{sc}$  curve of the disk-TENG **1220**. With the increase of the wind speed, the output frequency and  $I_{sc}$  value remarkably increase. FIG. **21B** illustrates dependences of the  $V_{oc}$  and  $I_{sc}$  values of the disk-TENG **1220** on the wind speed ranging from 1.7 to 15.1 m/s, in which the  $V_{oc}$  value stays almost constant at about 101 V for various wind speeds, and the  $I_{sc}$  value increases almost in a linear fashion with respect to the wind speed. As shown in FIG. **22**, the rotation speed of the disk-TENG **1220** increases linearly with the wind speed, and this causes the linear increase of the  $I_{sc}$  value based on the similar reason discussed in FIG. **18D**. The linear dependence of the  $I_{sc}$  values on the wind speed demonstrates its potential application as a self-powered sensor for detecting wind speed. When the generator **1200** is used to harvest wind energy, only the disk-TENG **1220** can generate electric energy, and the function of the blades **1212** of the water-TENG **1210** is converting the wind energy to the mechanical rotation motion of the back disk **1224**. In this case, there is no electrical output for the water-TENG **1210** as shown in FIG. **23**, because the flowing water with tribo-charges is a necessary condition to generate electrical output for the water-TENG **1210**.

## 3.3 Water-TENG and Contact-TENG

### 3.3.1 Structure

FIG. **24** illustrates a generator **2400** for harvesting energy from flowing water according to one aspect of the disclosed

technology. The generator **2400** may include a water-TENG **2410** to collect the electrostatic energy of water and a contact-TENG **2420** to collect the mechanical/kinetic energy of water. Both the water-TENG **2410** and the contact-TENG **2420** may operate in a single-electrode mode.

Output **1** of the generator **2400** may include power generated from both the water-TENG **2410** and the contact-TENG **2420**, whereas Output **2** of the generator **2400** may only include power generated from the contact-TENG **2420**. Therefore, the power generated by the water-TENG **2410** is the difference between Output **1** and Output **2**.

#### 3.3.1.1 Water-TENG

The water-TENG **2410** may include a surface layer **2412**. The surface layer **2412** may be superhydrophobic to enhance the electrostatic induction effect. In one example, the surface layer **2412** may include a  $\text{TiO}_2$  layer **2414** with hierarchical micro-/nanostructures **2416** thereon.

The water-TENG **2410** may include an electrode **2418**. The electrode **2418** may include, but not limited to, anyone or a combination of the following materials: metal such as copper, gold, silver and aluminum, indium tin oxide (ITO) and conductive polymer, among many other possibilities.

The surface layer **2412** may receive flowing water carrying triboelectric charges. The flowing water may affect a flow of electrons between the electrode and ground.

FIG. **25A** displays a SEM image of assembled  $\text{SiO}_2$  nanoparticles on the  $\text{SiO}_2$  thin film. The inset of FIG. **25A** shows that the nanoparticles are uniformly distributed on the surface. By contrast, FIG. **25B** illustrates a prepared  $\text{TiO}_2$  layer on a PET film with irregular structures. As illustrated in the inset of FIG. **25B**, the irregular structures may be dendrite-like particles made of nanoplatelets. In one embodiment, the particles may have an average size of 180 nm and composed by nanoplatelets with an average width of 5 nm and length of 70 nm, respectively.

FIG. **26A** illustrates the crystal phase of  $\text{TiO}_2$  layer as identified by Raman spectroscopy. The Raman bands appearing at 137, 254, 430, and 605  $\text{cm}^{-1}$  can be assigned to the  $B_{1g}$ , two-phonon scattering,  $E_g$ , and  $A_{1g}$  modes of rutile phase, indicating that the dendrite-like particles are formed by rutile  $\text{TiO}_2$  nanoplatelets. FIG. **26B** illustrates the crystal phase of  $\text{TiO}_2$  layer as identified by X-ray diffraction (XRD). The XRD pattern shows the characteristic diffraction peaks of rutile phase, which also validates the Raman spectroscopy result.

The  $\text{TiO}_2$  layer with hierarchical micro-/nanostructures increases hydrophobicity of the water-TENG **2410**. The hydrophobicity of the  $\text{TiO}_2$  layer is assessed by measuring the contact angle of water drops. FIG. **27A** illustrates that the measured contact angle of the  $\text{TiO}_2$  layer is about  $130^\circ$ . Compared to the rutile form of smooth  $\text{TiO}_2$  surface with a contact angle less than  $80^\circ$ , the increased contact angle in the  $\text{TiO}_2$  layer is attributed to the hierarchical micro-/nanostructures that trap air, which, in turn, reduce the actual contact area between the surface and water drops. After a monolayer coating of 1H,1H,2H,2H-perfluorooctyltrichlorosilane (PFTS) on the  $\text{TiO}_2$  layer, the measured contact angle of  $\text{TiO}_2$  layer may be enhanced to  $156^\circ$  as illustrated in FIG. **27B**, which may be referred to as superhydrophobic.

$\text{TiO}_2$  is selected due to its low cost, high chemical stability, excellent photocatalytic activity, and broad-spectrum antibacterial property. The use of  $\text{TiO}_2$  nanomaterials in the water-TENG **2410** may not only harvest the electrostatic



energy of water, but also provide the advantages of photocatalytic activity and antibacterial property for water purification.

#### 3.3.1.1.1 Photocatalytic Activity of TiO<sub>2</sub>

In one experiment, the photocatalytic activity of the TiO<sub>2</sub> layer **2414** is evaluated by the photodegradation of methylene blue (MB) under the solar light irradiation (intensity 100 mW cm<sup>-2</sup>), as illustrated in FIG. **28**. The inset of FIG. **28** provides a comparison of photocatalytic activity without and with the prepared TiO<sub>2</sub> layer **2414**.

In a typical experiment, the TiO<sub>2</sub> layer on PET film is dipped into a MB solution (10 mL, 20 μM). Prior to the irradiation, the solution is kept in the dark for 20 min to achieve the adsorption-desorption equilibrium between the TiO<sub>2</sub> nanomaterials and MB. Then, at certain time interval (every 15 min) during the irradiation process, the solution is analyzed with a UV-Vis spectrophotometer to measure the concentration change of MB. After the light irradiation for 90 min, almost all MB is photodegraded as compared to the control experiment in the absence of TiO<sub>2</sub> layer.

In the experiment, a 450-W xenon arc lamp (Oriental, Stratford, Conn.) equipped with an AM 1.5 filter is used as a solar irradiation source. A commercially available silicon-based reference cell is employed to examine the light intensity (100 mW cm<sup>-2</sup>).

#### 3.3.1.1.2 Antibacterial Property of TiO<sub>2</sub>

The antibacterial property of the TiO<sub>2</sub> layer **2414** against *E. coli* is also assessed. In one experiment, *E. coli* (DH5α) is grown in sterile LB medium. The medium is prepared by dissolving bacto-tryptone, bacto-yeast extract, and NaCl in deionized water. The solution is adjusted to pH 7.0 by adding NaOH. The *E. coli* is controlled to grow until the absorbance of the solution at wavelength 600 nm reached 1.0. A portion of the solution is centrifuged and washed with 0.85% NaCl to remove the matrix. Cells diluted to 4.0×10<sup>6</sup> CFU mL<sup>-1</sup> are incubated in LB medium with and without the prepared TiO<sub>2</sub> layer under the solar light irradiation (intensity 100 mW cm<sup>-2</sup>). The viability assay is calculated by using SYTO 9 and propidium iodide (PI) dyes. The *E. coli* treated with the prepared TiO<sub>2</sub> layer is subject to three centrifugation/wash cycles and washed with 0.85% NaCl to remove the matrix. Then the suspension is mixed with the dyes. The mixtures are incubated for 15 min at 25° C. Fluorescence intensities of SYTO 9 (excitation wavelength of 475 nm, emission wavelength of 530 nm, green) and PI (excitation wavelength of 475 nm, emission wavelength of 640 nm, red) are recorded. The fluorescence intensity ratio of 530 nm/640 nm is used to calculate the percentage of live/dead cell population.

FIGS. **30A-B** provide representative microscopic images of *E. coli* in LB media incubating without and with the TiO<sub>2</sub> layer under the light irradiation for 30 min. Fluorescent stains in FIG. **30A** represent live cells, whereas fluorescent stains in FIG. **30B** represent dead cells. The viability values of *E. coli* in the presence of the TiO<sub>2</sub> layer without and with the light irradiation are 84% and 17%, respectively.

#### 3.3.1.2 Contact-TENG

The contact-TENG **2420** may be coupled to the water-TENG **2410**. The contact-TENG **2420** may include a negative triboelectric charging material **2422** and a positive triboelectric charging material **2424**. In one example, the

negative triboelectric charging material **2422** may include but not limited to a PTFE layer. The positive triboelectric charging material **2424** may include but not limited to a layer of SiO<sub>2</sub> nanoparticles. SiO<sub>2</sub> nanoparticles **2424** may provide the advantage of larger contact surface area and enhance the electric output of the contact-TENG **2420**.

When the water-TENG **2410** receives the flowing water, the water-TENG **2410** may contact the contact-TENG **2420** to affect a flow of electrons at the water-TENG **2410** and the contact-TENG **2420**.

#### 3.3.2 Fabrication

FIG. **29** illustrates an exemplary fabrication process of the generator **2400**.

##### 3.3.2.1 Fabricate Water-TENG

The water-TENG **2410** may use a polyethylene terephthalate (PET) film **2417**. The PET film **2417** may have a thickness of 0.1mm.

Before the growth of TiO<sub>2</sub> layer with hierarchical micro-/nanostructures, the PET film may be ultrasonically cleaned in ethanol and water for 30 min, respectively. Then, the PET film may be placed in a glass bottle filled with TiCl<sub>3</sub> solutions (0.1 M). After 10 min, the glass bottle may be heated in an oven at 80° C. for 6 h and cooled in air. The growth cycle need to repeat 2 times to make sure the PET film surface is coated with a uniform TiO<sub>2</sub> layer.

During the growth of TiO<sub>2</sub> crystal, Ti(III) species may be gradually oxidized to Ti(IV) species by the dissolved O<sub>2</sub> and then hydrolyzed to form TiO<sub>2</sub>. By increasing the reaction time and growth cycle, a TiO<sub>2</sub> layer **2414** with hierarchical micro-/nanostructures **2416** instead of vertically aligned TiO<sub>2</sub> nanoplatelet arrays is formed.

The TiO<sub>2</sub> layer **2414** coated PET film may be rinsed with water to remove the non-adsorbed TiO<sub>2</sub> nanomaterials and dried at ambient temperature. After that, the TiO<sub>2</sub> layer **2414** may be further coated with 1H,1H,2H,2H-perfluorooctyltrichlorosilane (PFTS) to increase the hydrophobicity. Specifically, the TiO<sub>2</sub> layer coated PET film may be immersed in 0.5% 1H,1H,2H,2H-perfluorooctyltrichlorosilane (PFTS) in hexane for 10 min, and washed with hexane to remove residual PFTS. After further drying at ambient temperature, the TiO<sub>2</sub> layer coated PET film may be treated in a vacuum oven at 110° C. for 1 h.

A Cu thin film **2418** (e.g., 100 nm) may be firstly deposited on the other side of the PET film **2417** as the electrodes for the water-TENG **2410**. The Cu thin film **2418** may be connected with Output 1 of the generator **2400**, including power generated from both the water-TENG **2410** and the contact-TENG **2420**.

A commercial polytetrafluoroethylene (PTFE) film **2419** (e.g., 25 μm) may cover the top of the deposited Cu thin film **2418**. On the other side of PET film, a TiO<sub>2</sub> layer **2414** with hierarchical micro-/nanostructures **2416** may grow directly through a facile, scalable, and low cost chemical bath method.

##### 3.3.2.2 Fabricate Contact-TENG

The contact-TENG **2420** may use a poly(methyl methacrylate) (PMMA) sheet **2425**. A Cu thin film **2426** may be deposited on one side of the PMMA sheet **2425** as the electrodes for the contact-TENG **2420**. The Cu thin film **2426** may have a thickness of approximately 100 nm. The

Cu thin film **2426** is the Output **2** of the generator **2400**, which may only include the power generated from the contact-TENG **2420**.

For purposes of generating triboelectric charges with a high density on the surface, silica ( $\text{SiO}_2$ ) may be selected because it is positioned extremely positive in the triboelectric series. A  $\text{SiO}_2$  thin film **2422** (e.g., 20 nm) may be deposited on top of the Cu thin film **2426**. Then, a layer of  $\text{SiO}_2$  nanoparticles **2424** may be assembled on the deposited  $\text{SiO}_2$  thin film **2422** to increase the contact area.  $\text{SiO}_2$  nanoparticles **2424** with an average size of 250 nm may be synthesized according to the Stober method. Typically, concentrated ammonia (28%, 3 mL) is added rapidly to the solution containing absolute ethanol (99.9%, 50 mL) and tetraethyl orthosilicate (99%, 1.5 mL). The mixture is reacted at ambient temperature for 24 h.

### 3.3.2.3 Assembly

A spacer **2430** may combine all parts of the generator **2400**. For example, the spacer **2430** may be applied to maintain a gap distance between the PTFE film **2419** of the water-TENG **2410** and the  $\text{SiO}_2$  nanoparticles **2424** of the contact-TENG **2420**. The spacer **2430** may include a PET film. The spacer **2430** may have a thickness of about 0.5 mm.

### 3.3.3 Operating Principle

Both the water-TENG **2410** and the contact-TENG **2420** may operate in a single-electrode mode. FIG. **31A** illustrates the working mechanism of the water-TENG **2410** of the generator **2400**. When a water drop **3102** carrying positive charges contacts the  $\text{TiO}_2$  layer **2414** as shown in step (ii), a positive electric potential difference may occur between the charged water drop **3102** and ground. This may cause the electrons to flow from ground to the electrode **2418** and generate an instantaneously opposite potential to balance the electric field, finally reaching equilibrium at step (iii). Once the charged water drop **3102** leaves the  $\text{TiO}_2$  layer **2414**, a negative electric potential difference may occur, forcing the electrons to flow from the electrode **2418** to ground at step (iv), until achieving another equilibrium at step (i).

FIG. **31B** illustrates the working mechanism of the contact-TENG **2420** of the generator **2400**. The impact force from the water drop may also drive the contact-TENG **2420** to work. The impact force from the water drop can overcome the resistance from the spacer **2430** to make the PTFE film **2419** of the water TENG **2410** contact the  $\text{SiO}_2$  nanoparticles **2424** at step (vi), causing the electrons to transfer from the  $\text{SiO}_2$  nanoparticles **2424** to the PTFE film surface **2419** and leaving the  $\text{SiO}_2$  nanoparticles **2424** a positively charged surface. As the water drop leaves the  $\text{TiO}_2$  layer **2414**, the contacted surfaces are separated, then a positive electric potential difference between the  $\text{SiO}_2$  nanoparticles **2424** and ground and a negative electric potential difference between ground and the PTFE film **2419** are established at step (vii). This causes the electrons flowing from ground to the electrode **2424** and from the electrode **2418** to ground, finally reaching equilibrium at step (viii). This contributes to instantaneously positive and negative currents from the Output **2** and Output **1** of the generator **2400**. Once another charged water drop falls on the generator **2400**, and makes the PTFE film **2419** contact the  $\text{SiO}_2$  nanoparticles **2424** again, a negative electric potential difference between the  $\text{SiO}_2$  nanoparticles and ground and a positive electric potential difference between ground and the PTFE film **2419** may

occur. This causes the electrons to flow from the electrode **2424** to ground and from ground to the electrode **2418** at step (ix), until achieving equilibrium at step (vi). This process corresponds to instantaneously negative and positive currents from the Output **2** and Output **1** of the generator **2400**. So from the working mechanism of the generator **2400**, when a charged water drop falls on the generator **2400**, the generated outputs of the water-TENG **2410** and the contact-TENG **2420** may be simultaneous and in the same direction. If the charged water drop or flowing water contact and leave the generator **2400** periodically, both the outputs of the water-TENG **2410** and the contact-TENG **2420** may be continuously generated.

### 3.3.4 Output Performance

The measured signal of the Output **1** of the generator **2400** may contain the power generated from both the water-TENG **2410** and the contact-TENG **2420**, while the measured signal of the Output **2** of the generator **2400** represents the power from the contact-TENG **2420**.

In one experiment, the performance of the generator **2400** may be tested by using the flowing water from a household faucet. The flowing rate of water is controlled at  $20 \text{ mL s}^{-1}$  and the distance between the generator **2400** and the outlet of faucet is 25 cm. The impact angle is optimized at  $30^\circ$ . The effective dimensions of the generator **2400** are  $1.2 \text{ cm} \times 1.2 \text{ cm}$ . The open-circuit voltage ( $V_{oc}$ ) and  $I_{sc}$  are measured to evaluate the performance of the generator **2400**. FIGS. **32A-B** illustrate typical  $V_{oc}$  and  $I_{sc}$  curves generated from the Output **1** and Output **2** of the generator **2400**. FIG. **32A** illustrates that the  $V_{oc}$  values of the Output **1** achieve 52 V. FIG. **32B** illustrates that the  $V_{oc}$  values of the Output **2** achieve 35 V. FIG. **32C** illustrates that the  $I_{sc}$  values of the Output **1** exceed  $14 \mu\text{A}$ . FIG. **32D** illustrates that the  $I_{sc}$  values of the Output **2** exceed  $6.7 \mu\text{A}$ .

To investigate the output power density of the generator **2400**, the generated  $V_{oc}$  and  $I_{sc}$  from the Output **1** and Output **2** of the generator **2400** when connected to an external load resistor are also measured. The resistance varies from  $0.01 \text{ M}\Omega$  to  $1 \text{ G}\Omega$ . As illustrated in FIGS. **33A-B**, when the resistance is below  $0.1 \text{ M}\Omega$ , the generated  $V_{oc}$  from the Output **1** (as illustrated in FIG. **33A**) and Output **2** (as illustrated in FIG. **33B**) of the generator **2400** is close to 0. Similarly, as illustrated in FIGS. **33C-D**, when the resistance is below  $0.1 \text{ M}\Omega$ , the generated  $I_{sc}$  from the Output **1** (as illustrated in FIG. **33C**) and Output **2** (as illustrated in FIG. **33D**) of the generator **2400** has only little changes. However, when the resistance is raised from  $0.1 \text{ M}\Omega$  to  $1 \text{ G}\Omega$ , the generated  $I_{sc}$  from the Output **1** and Output **2** of the generator **2400** through the load generally increases, but the generated  $I_{sc}$  from the Output **1** and Output **2** of the generator **2400** across the load decreases. As a result, the instantaneous power density generated from the Output **1** of the generator **2400** as illustrated in FIG. **33E** and the instantaneous power density generated from the Output **2** of the generator **2400** as illustrated in FIG. **33F** remain small with the resistance below  $0.1 \text{ M}\Omega$  and achieve the maximum values of  $1.31 \text{ W m}^{-2}$  and  $0.38 \text{ W m}^{-2}$  at a resistance of  $44 \text{ M}\Omega$ , respectively.

For the measurement of electrical outputs of the generator **2400**, a programmable electrometer (Keithley Model 6514) and a low-noise current preamplifier (Stanford Research System Model SR570) are used.

## 3.3.5 Application

## 3.3.5.1 LED

In one experiment, to address the potential applications of the generator **2400**, the generator **2400** is configured to have an increased effective dimension of 3.3 cm×3.3 cm as illustrated in FIG. **34**. The flowing rate of water is raised to 40 mL s<sup>-1</sup>. The distance between the generator **2400** and the outlet of faucet is 25 cm. FIG. **35A** illustrates that the generated  $I_{sc}$  from the Output **1** of the generator **2400** may reach 43 μA. FIG. **35B** illustrates that the generated  $I_{sc}$  from the Output **2** of the generator **2400** may reach 18 μA.

FIG. **36** illustrates the generated  $I_{sc}$  from a single water-TENG. As shown in FIG. **36**, the value of the generated  $I_{sc}$  is 30 μA, which is smaller than the Output **1** of the generator **2400**. By integrating the  $I_{sc}$  peak, collected charges from the Output **1** and Output **2** of the generator **2400** in a unit time may be determined as 3.3 μQ s<sup>-1</sup> and 1.4 μQ s<sup>-1</sup>, respectively. A full-wave rectifying bridge may be applied to further transform the AC outputs to pulse outputs in the same direction. The rectified outputs from the Output **1** and Output **2** of the generator **2400** may drive commercial LEDs as illustrated in FIG. **37A** and charge 33-μF capacitors as illustrated in FIG. **37B**. The effective dimensions of the generator may be 3.3 cm×3.3 cm.

## 3.3.5.2 Self-Powered Nanosensor for Ethanol Detection

The water-TENG may be used as a self-powered nanosensor for ethanol detection. In one experiment to realize the concept, a programmable syringe pump (PHD 2000, Harvard Apparatus) is applied to control the volume each sample drop (30 μL). The sample drop is set up to fall from a height of 50 cm. FIG. **38A** displays the output  $I_{sc}$  of the water-TENG generated by deionized water drops. As illustrated in FIG. **38A**, the output  $I_{sc}$  reaches a value of 14 μA. The inset of FIG. **38A** shows that the generated output is capable of turning on a commercial LED as indicator.

However, as shown in FIG. **38B**, when the sample is changed from deionized water to a solution containing 20% ethanol (percentage by volume), the generated  $I_{sc}$  of the water-TENG is decreased to 3 μA. FIG. **38C** illustrates the relationship between the generated  $I_{sc}$  and ethanol concentration. By connecting the water-TENG with a LED (indicator), a stand-alone and self-powered ethanol nanosensor may be formed. The inset of FIG. **38B** reveals that the LED powers off when detecting the 20% ethanol solution. In other words, the generated output in FIG. **38B** cannot drive the LED.

The decrease in the generated  $I_{sc}$  may be caused by the reduced charges on the sample drop. By integrating the  $I_{sc}$  peak of water-TENG generated at different ethanol concentration, the inductively transferred charges on the Cu electrode may be deduced, which may be proportional to the triboelectric charges on sample drop. FIG. **38D** illustrates that the triboelectric charges on a sample drop decrease when raising ethanol concentration.

Ethanol is capable of removing the triboelectric charges. Hence, the presence of ethanol may reduce the triboelectric charges on sample drop surface and decrease the electrical output of water-TENG. Compared to another self-powered ethanol sensor based on the contact electrification of hydrophobic polymer film and sample, the as-developed water-TENG is not only a new design but also has the advantage of minimizing the sample volume.

The combination of a commercial LED with water-TENG indicates that the sensing system toward ethanol detection may be simplified by replacing the electrometer with an LED.

In one embodiment, the generator **2400** as shown in FIG. **24** may be coupled to a power indicator. The surface layer **2412** may receive a solution containing a chemical and water, where the chemical may remove at least one triboelectric charge from the water. The power indicator may indicate whether the chemical is present based on power output of the triboelectric generator. In one example, the chemical is ethanol. The power indicator may be an LED.

## 4. Summary

The disclosed technology provides a green and sustainable solution for harvesting multiple types of energies from the environment, including but not limited to, energies from water flow such as tap water flowing from a household faucet, raindrop, ocean wave and wind. Types of water which the energies may be harvested from include deionized, tap and salt water, among many other possibilities.

The disclosed technology may have many applications, including, but not limited to, powering low power applications including but not limited to light emitting diodes, sensors and portable electronics, and charging capacitors. The disclosed technology may be adapted to many applications, including but not limited to, self-powered sensors for detecting flowing water rate, wind speed, chemicals such as ethanol, temperature, and water/liquid leakage from a container/pipe.

Numerous characteristics and advantages have been set forth in the foregoing description, together with details of structure and function. While the invention has been disclosed in several forms, it will be apparent to those skilled in the art that many modifications, additions, and deletions, especially in matters of shape, size, and arrangement of parts, can be made therein without departing from the spirit and scope of the invention and its equivalents as set forth in the following claims. Therefore, other modifications or embodiments as may be suggested by the teachings herein are particularly reserved as they fall within the breadth and scope of the claims here appended. The term “exemplary” used herein does not mean best mode, but rather, example.

Accordingly, those skilled in the art will appreciate that the conception upon which the application and claims are based may be readily utilized as a basis for the design of other structures, methods, and systems for carrying out the several purposes of the embodiments and claims disclosed in this application. It is important, therefore, that the claims be regarded as including such equivalent constructions.

Furthermore, the purpose of the foregoing Abstract is to enable the public generally, and especially including the practitioners in the art who are not familiar with patent and legal terms or phraseology, to determine quickly from a cursory inspection the nature and essence of the technical disclosure of the application. The Abstract is neither intended to define the claims of the application, nor is it intended to be limiting to the scope of the claims in any way.

The invention claimed is:

1. A generator comprising:

blades arranged in a radially outward fashion, each blade including:

an electrode; and

a surface layer for receiving flowing water carrying triboelectric charges, the flowing water affecting a flow of electrons between the electrode and ground.

29

2. The generator of claim 1, wherein the blades exhibit a wheel-like structure.

3. The generator of claim 1, wherein the surface layer is superhydrophobic.

4. The generator of claim 1, wherein the surface layer includes nanostructures thereon.

5. The generator of claim 1, wherein the surface layer includes at least one material selected from the group consisting of polyethylene terephthalate, poly(methyl methacrylate), polydimethylsiloxan, polytetrafluoroethylene, fluorinated ethylene propylene, poly(vinyl chloride), polyimide, metal and alloy.

6. The generator of claim 1, wherein the electrode includes at least one material selected from the group consisting of metal, indium tin oxide and conductive polymer.

7. The generator of claim 1 further comprising and a rotatable disk that rotates when the blades receive the flow water;

30

wherein the rotatable disk harvests mechanical kinetic energy from the flowing water during rotation.

8. The generator of claim 7, wherein the rotatable disk comprises two segmented disks; and

wherein each segmented disk includes an electrode.

9. A generator comprising:

an electrode; and

a superhydrophobic surface layer for receiving an energy flow carrying triboelectric charges, the surface layer including a  $\text{TiO}_2$  layer with nanostructures thereon, the energy flow affecting a flow of electrons.

10. The generator of claim 9, wherein the energy flow is water flow; and

wherein the water flow affects a flow of electrons between the electrode and ground.

\* \* \* \* \*